The Development and Characterisation of a Pyruvate Biosensor for Real-Time Neurochemical Monitoring of Brain Extracellular Pyruvate

A thesis submitted by

Jason P. Branigan B.Sc. (Hons.)

to

Maynooth University

For the degree of Doctor of Philosophy

Maynooth University
National University of Ireland Maynooth

Based on the research carried out in the

Department of Chemistry, Faculty of Science and Engineering,

Maynooth University, Maynooth.

Under the supervision of

Prof. John P. Lowry

And direction of

Head of Department: Prof. Denise Rooney

November 2021

Table of Contents

Declaration

This thesis has not been submitted before, in whole or in part, to this or any other university for any degree, and except where otherwise stated, is the original work of the author. The research on the development and characterisation of a pyruvate biosensor was supervised by Prof. John P. Lowry.

Signed: _____

Jason Branigan

Acknowledgements

This work has emanated from research conducted with the financial support of Science Foundation Ireland (SFI) under Grant Number 15/IA/3176.

First and foremost, I would like to thank my supervisor Prof. John Lowry. Thank you for providing me with such an amazing opportunity to be part of your research group and thank you for having faith in my ability when even I didn't. Your support, guidance, encouragement, patience and, most importantly, friendship over the last four years is massively appreciated and means I will only ever look back on this with the fondest of memories. It has truly been a privilege to be part of your research group and I will be forever grateful.

A massive thank you to all the members of the Lowry research group. The coffee breaks, lunches, conference trips and "surprise" birthdays have really been a highlight of the last four years. The laughs and constant slagging provided a massive boost and ensured the work atmosphere was an enjoyable place to be. A special thank you to Gama, not only for all the help over the years but for introducing me to the world of scientific research and starting this whole journey for me. To "princess" Michelle D, thank you for all your help, guidance and putting up with my endless questions, stupid or otherwise, over the past four years. Even though you had a colossal amount of your own work to do there was never a moment where you weren't available to help and I don't think I would be where I am today without you. To Sean, thank you, not only for all the help with my studies but also for being a friend. Being able to call over to Auxilia just to get out of the lab and have a chat about running, football or whatever was very much appreciated. Thank you also to Kobi and Caytlin, our corridor and writing room conversations, arguments and laughs were fantastic. At times the whole task could seem overwhelming but it was a great comfort to have you guys there to support and help me, or even just struggle with me! Best of luck with the remainder of your projects, I know it hasn't been the easiest of journeys but the finish line is in sight. A special thanks to Michelle S, the backbone of the group, your help has made the whole experience as smooth as possible. There was never a request too awkward or trivial you couldn't solve, with ruthless efficiency might I add, and your words of advice along the way were also much appreciated.

Thank you to all the academic staff, technicians, Noel, Carol and Donna for all your help and support over the last four years. Thank you to Luke, I'm so glad you were finally allowed to talk to me, it's been a brilliant four years and I'm delighted we've shared this experience together. To Amanda, thank you for all the laughs over the years, particularly during the buckminsterfullerene's lab. I'm happy I was able to remember your name all those years ago, and I'm glad you didn't hold it against me (for too long anyway). To Steve, Harlei, Colm and all the post grads and post docs, past and present, in the department, thank you for all the times spent in the tearoom chatting, laughing and venting it definitely helped me keep my sanity. I'm extremely fortunate to have met you all and I wish you every success and happiness wherever life may take you in the future.

To my friends Dave, John Mc, Brian, Jamie, Mathew, Kerrie and Ciara thank you for always being there for me. The opportunity to switch off, chill out and have a laugh with all of you provided a great distraction throughout my studies. Thank you also to Shane and my brother Mathew, it cannot be understated how lucky I am to have the two of you in my life. It is a privilege to call the two of you my best friends, and as always WCCFL.

To all the members of my family that have supported me on this journey I was to extend a special thank you, especially to my grandparents, who still don't quite understand what I've been doing for the last four years but still brag about it to anybody who will listen. I hope I've done you proud, your unfaltering love and support is something I cherish dearly. To Collie, Madge, Chris, Dario, Danny, Louise, Lilly and Rob thank you all for being there for the laughs, dinners and sessions along the way it was a great help and distraction from all that was going on.

Mam and dad, words will never quantify the levels of gratitude, admiration and love I have for you. None of this would have been possible if it wasn't for your guidance, encouragement and love. Your endless determination and hard work ensured I had every opportunity to succeed. The sacrifices you've made are too numerous to list and more than what was required of you as parents yet there was never a moment's hesitation when I was in need. This thesis is the culmination of all those sacrifices and hard work and while I know there is no way to repay you for everything you have done for me, I hope this is a start.

Finally, to Rachel your never ending love and belief in me throughout this whole experience has been immense, you are the foundation on which all of this has been built. You were aware of the limitations undertaking a project like this would put on us but you never once offered anything other than complete dedication and support. Knowing you were there to come home to at the end of the day made even the darkest days good ones in the end. Thank you for everything I love you.

Jason P. Branigan

Abbreviations

3,4-methylenedioxymethamphetamine	MDMA
5-hydroxyindolacetic acid	5-HIAA
5-hydroxytryptomine	5-HT
Acetaminophen	AAP
Acetyl coenzyme A	acetyl-CoA
Adenosine triphosphate	ATP
Aerococcus viridians pyruvate oxidase	*Av*POx
Analogue-to-digital	ADC
Artificial cerebrospinal fluid	aCSF
Ascorbic acid	AA
Astrocyte-neuron-lactate shuttle	ANLS
Bioresource unit	BRU
Blood brain barrier	BBB
Bilayer lipid membrane	BLM
Bovine serum albumin	BSA
Calcium chloride	$CaCl_2$
Carbon paste electrode	CPE
Central nervous system	CNS
Cerebrospinal fluid	CSF
Constant potential amperometry	CPA
Cyclic voltammetry	CV

Dehydroascorbic acid	DHAA
Dementia of Alzheimer's type	DAT
Dichloroacetate	DCA
Differential pulse amperometry	DPA
Digital-to-analogue	DAC
Dihydroxyphenylacetic acid	DOPAC
Dopamine	DA
Electroencephalography	EEG
Extracellular fluid	ECF
Fast scan cyclic voltammetry	FSCV
Flavin adenine dinucleotide	FAD
Foreign body response	FBR
Functional magnetic resonance imaging	fMRI
Glassy carbon electrode	GCE
Glutaraldehyde	GA
Gold disc electrode	GDE
Highest occupied molecular orbital	HOMO
Homovanillic acid	HVA
Horse radish peroxidase	HRP
Hydrogen peroxide	H_2O_2
Ideal polarisable electrode	IPE
Lactate to pyruvate ratio	L/P
Lactobacillus plantarum pyruvate oxidase	*Lp*POx

Limit of detection	LOD
Linear region slope	LRS
Long term in-vivo electrochemistry	LIVE
Lowest unoccupied molecular orbital	LUMO
Magnesium	Mg^{2+}
Magnesium chloride	$MgCl_2$
Magnetoencephalography	MEG
Methyl methacrylate	MMA
Microdialysis	MD
Mitochondrial pyruvate carrier	MPC
Monocarboxylate transporters	MCT
Nitrogen gas	N_2
o-Phenylenediamine	*o*-PD
One-way analysis of variance	ANOVA
Overoxidized polypyrrole	PPYox
Oxygen	O_2
Pediococcus sp. pyruvate oxidase	*Ps*POx
Phosphate buffer saline	PBS
Platinum/iridium	Pt/Ir
Polymer composite	PC
Poly-*o*-phenylenediamine	PPD
Polyethyleneimine	PEI
Polyurethane	PU

Polyvinyl alcohol	PVA
Polyvinyl alcohol containing styryl pyridine groups	PVA-SbQ
Positron emission tomography	PET
Potassium chloride	KCl
Potassium phosphate dibasic	K_2HPO_4
Potassium phosphate monobasic	KH_2PO_4
Pyruvate dehydrogenase complex	PDHC
Pyruvate dehydrogenase complex deficiency	PDCD
Pyruvate kinase deficiency	PKD
Pyruvate oxidase	POx
Regional cerebral blood flow	rCBF
Saturated calomel electrode	SCE
Self-assembled monolayer	SAM
Sodium chloride	NaCl
Tetracyanoquinodimethane	TCNQ
Tetrathiafulvalene	TTF
Thiamine pyrophosphate	TPP
Traumatic brain injury	TBI
Tricarboxylic acid	TCA
Uric acid	UA
Zero-net-flux	ZNF
Zinc oxide	ZnO

Abstract

This thesis presents research on the development and characterisation of a pyruvate biosensor for the study of brain energy metabolism. The aim of the project was to utilise a pyruvate oxidase enzyme to develop the biosensor *in-vitro*, followed by a detailed *in-vitro* characterisation study. Finally, the developed biosensor was deployed in the *in-vivo* environment and a detailed *in-vivo* validation study was carried out.

Three results chapters are presented in this thesis. The first of these, Chapter 4 details the development of the biosensor. The finalised design was comprised of 15 layers of an enzyme solution (800 U/mL + 80 µM flavin adenine dinucleotide (FAD)) immobilised on a Pt/Ir disc micro-electrode using styrene. Cross-linkers and stabilisers were also introduced (1 % bovine serum albumin (BSA), 0.25 % glutaraldehyde (GA) and 2 % polyethyleneimine (PEI)) as a final layer to further increase sensitivity and reproducibility. Chapter 5 discusses the detailed *in-vitro* characterisation study carried out to determine the potential viability of use of the developed biosensor in the *in-vivo* environment. Temperature dependence issues were resolved by the introduction of 200 mM sucrose into the enzyme solution and the addition of the cross-linkers and stabilisers to every layer of the design. The best design was found to be:

$$Pt/Ir\ (disc) - PPD - \{Sty - ([POx\ (800\ U/mL) + FAD\ (80\ \mu M) + Sucrose\ (200\ mM)] + BSA\ (1\ \%) + GA\ (0.25\ \%) + PEI\ (2\ \%))_{15}\}$$

It showed excellent sensitivity (9.66 ± 0.08 pA/µM, n = 10) and was highly selective towards pyruvate due to the incorporated poly-phenylenediamine (PPD) layer's ability to reject endogenous electroactive species present in the brain. It was also sufficiently independent of changes in oxygen levels within the relevant physiological range. The limit of detection (LOD) was determined to be 0.33 ± 0.172 µM with an *in-vitro* response time of *ca.* 10 s (n = 4), which was within the mixing time.

Chapter 6 details the *in-vivo* validation of the biosensor signal. This initially involved investigating the possibility of cross-talk between the pyruvate biosensor and a composite blank electrode bi-laterally implanted. Correlation analysis showed that cross-talk was negligible. This was followed by determining the circadian/diurnal changes for pyruvate over a 60 hr recording period. Using *in-vitro* calibration data the basal extracellular concentration

of pyruvate was estimated to be 197 ± 18 µM, which is within the expected concentration range reported in the literature. The biosensor was sufficiently oxygen independent and highly selective toward pyruvate. Finally, confirmation that the sensor responds to changes in extracellular pyruvate was achieved using local perfusions of 500 mM pyruvate which resulted in an increase in signal. These were also used to confirm that the biosensors remained viable for at least 2 weeks and were thus deemed suitable for chronic *in-vivo* recording.

Chapter 1:

Introduction

1.1 Introduction

The aim of this thesis was the development and characterisation of a biosensor which can detect, with appropriate sensitivity and selectivity, pyruvate in the mammalian brain. It is hoped that the development of such a device will provide an invaluable tool to help bring a degree of clarity to some of the major discussions presently ongoing about the role of pyruvate in the processes of energy metabolism in the intact living brain, as well as its role in some of the major neurodegenerative diseases currently afflicting the human race.

The human brain is a highly complex organ which relies on glucose and pyruvate metabolism to generate cellular energy which in turn supports a wide range of functions. As a result, the brain requires between 20 % and 25 % of the body's daily glucose consumption (Gray, Tompkins and Taylor, 2014). The brain is comprised of two different types of matter, grey and white, and two types of cells, neurons and glial cells (Watson, Kirkcaldie and Paxinos, 2010). It contains approximately 10^{12} neurons and between 10 to 50 times more glial cells (Lewine, 1995). The neurons are comprised of three main parts; dendrites, axons and cell bodies, which are shown below in Figure 1.1.

Neurons function by sending and receiving signals to and from other nerve cells through synaptic contacts. Synapses are comprised of three main parts: the axon terminal, the synaptic cleft and the membrane encasing the tip of the dendritic spine. Synaptic transmission involves the releases of a neurotransmitter, which in turn carries information from the presynaptic cell to the postsynaptic cell (Hammond and Esclapez, 2015). The release of neurotransmitters at a synapse is caused by an action potential, which is created when an initial stimulus causes an electrical impulse. The electrical impulse is a result of changes in the concentration of K^+ or Na^+ ions. This impulse travels down the axon of the neuron to the axon terminal where a neurotransmitter is released from the presynaptic cell. It then diffuses, by exocytosis, across the synaptic cleft and binds to the transmitter-activated receptors of a postsynaptic cell (Hammond and Esclapez, 2015). This stimulation can either lead to an action potential in the postsynaptic neuron, or it can be inhibitory and thus prevents any further signal transmission.

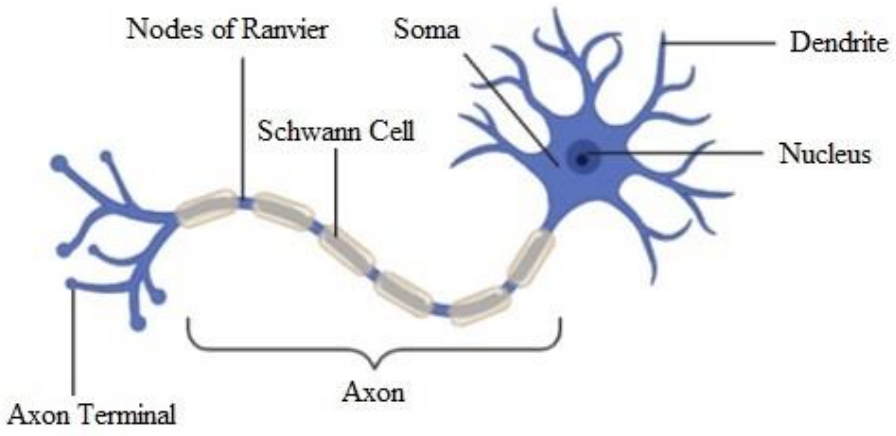

Figure 1.1: A neuron (created using BioRender.com).

Neurons however, would not be able to function without the glial cells as they are the major support structures in the brain (Jessen, 2004). Glial cells can be separated into macroglia and microglia. Macroglia include astrocytes, oligodendrocytes and ependymal cells and these are the major supporting cells, while microglia are phagocytic cells which are activated after injury or infection (Johnston, 2006). Astrocytes are the most common glial cell and their role is to support neuronal function by producing antioxidants, maintaining the blood-brain barrier (BBB) and recycling of neurotransmitters such as glutamate and GABA (Snyder *et al.*, 2018). Oligodendrocytes form and produce myelin sheaths that envelops the axons which significantly increases the efficiency and speed of the signal transmission (Snyder *et al.*, 2018). Ependymal cells line the surface of all brain ventricles in a single layer or cuboidal to columnar cells, the function of these cells is to circulate cerebrospinal fluid (CSF) from the brain through the ventricular system (Snyder *et al.*, 2018).

The largest component of the brain is the cerebrum (Figure 1.2) and its functions are critical for survival as it is responsible for processing information related to memory, learning, movement, communication, language, sensory perception and smell (Willerth, 2017). The outer layer of the cerebrum is known as the cerebral cortex and is made up of four lobes: the frontal lobe, the parietal lobe, the temporal lobe and the occipital lobe. While other important

structures such as the hippocampus, basal ganglia and olfactory bulb are located in deeper regions of the cerebrum. The brain is a highly complex system and trying to understand the mechanisms and functions at play still remains a challenge to this day. The next section discusses some of the different methodologies employed to study the neurochemical phenomena of the living brain.

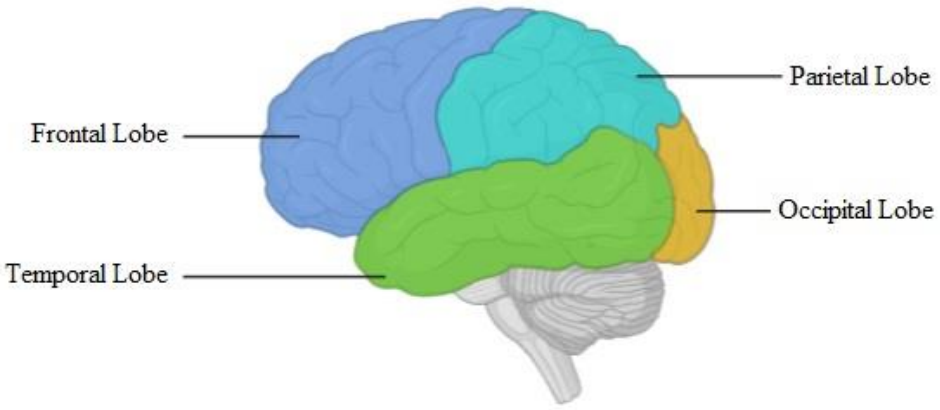

Figure 1.2: The lobes of the cerebrum (created using BioRender.com).

1.2 Neurochemical Analysis

Due to the complex nature of the brain, it is clear that it cannot be treated as a uniform unit, this is due to the different regions being responsible for different processes and functions. As a result, a number of techniques have been developed and utilised to analyse the structure, metabolism and the role of neurochemicals in the *in-vivo* environment. These include both non-invasive and invasive techniques. There are a number of non-invasive techniques such as Electroencephalography (EEG) (İnce, Adanır and Sevmez, 2020), Magnetoencephalography (MEG) (Cohen, 1972), positron emission tomography (PET) (Wagner, 1998) and functional magnetic resonance imaging (fMRI) (Glover, 2011). Along with these techniques there has also been developments in two surgically invasive techniques - microdialysis (MD)

(Ungerstedt and Pyock, 1974; Schulz *et al.*, 2000) and long term *in-vivo* electrochemistry (LIVE) (O'Neill, Lowry and Mas, 1998). As there are a lot of interesting processes occurring in the synaptic cleft these two methods allow neuroscientists to sample overflow chemicals found in the extracellular fluid (ECF). LIVE is the primary technique employed for the *in-vivo* validation (Chapter 6) in this research project.

While the first reports of voltammetry in the living brain date back to 1958 when Leland C. Clark used voltammetry to monitor oxygen (O_2) (Clark, Misrahy and Fox, 1958; Clark and Lyons, 1962), it did not become a mainstream neuroanalytical technique until 1973 when work by Ralph N. Adams *et al.* established the techniques and methodologies that are currently used in research today (Kissinger, Hart and Adams, 1973). LIVE involves the insertion of an electrode into the brain and the application of a specific potential, or potential profile, to the electrode which gives rise to a current as the analyte of interest is either oxidised or reduced at the electrode surface. Various different electrochemical techniques have utilised a varying potential such as linear sweep voltammetry, cyclic voltammetry (CV), fast scan cyclic voltammetry (FSCV), while fixed potentials have also been employed in techniques such as constant potential amperometry (CPA) or differential pulse amperometry (DPA). These techniques have been utilised in combination with a wide range of sensors capable of detecting several electroactive species found in the ECF, such as; ascorbic acid (AA) (Ewing *et al.*, 1983; Ormonde and O'Neill, 1990), oxygen (O_2) (Bolger and Lowry, 2005), uric acid (UA) (Sun *et al.*, 2011), dopamine (Lyne and O'Neill, 1990; Robinson *et al.*, 2003) and nitric oxide (NO) (Brown, Finnerty and Lowry, 2009; Meiller, Sequeira and Marinesco, 2020). However, the detection of important electroinactive species such as amino acids, glucose, pyruvate or lactate, requires the incorporation of a biorecognition element into the sensor design.

1.3 Biosensors

Biosensors provide a mediated system for the detection of electroinactive species in the brain. A biosensor is defined as "a self-contained integrated device, which is capable of providing specific quantitative or semi-quantitative analytical information using a biological recognition element (biochemical receptor) which is retained in direct spatial contact with an electrochemical transduction element" (Thvenot *et al.*, 1999). There are three main parts to a

biosensor; the biological recognition element, the transducer and the signal processing system (Ronkainen, Halsall and Heineman, 2010). The biological recognition element has many forms such as, enzyme, tissue, microbe or organelle (Liu *et al.*, 2018) and translates the biological information into a chemical output signal. The biological recognition element is immobilised on the transducer which converts the output signal into a measurable signal which is then converted into a readable form by the signal processing system (Thvenot *et al.*, 1999). Noble metal-based transducers such as, platinum, platinum/iridium (Pt/Ir), gold and silver are excellent for developing *in-vivo* biosensors. This is due to their small size, biocompatibility and easy accessibility for modification (Geddes and Roeder, 2003; Choi *et al.*, 2021). A Pt/Ir (90%/10%) electrode was used throughout this research project. Iridium is much harder than platinum therefore its inclusion increases the robustness of the electrode material (Geddes and Roeder, 2003). The process of immobilising the enzyme component onto the electrode surface is achieved by utilising various different strategies such as physical adsorption, entrapment and chemical bonding (Thvenot *et al.*, 1999).

There are three types of biosensors: first, second and third generation. First generation biosensors directly monitor the production of O_2 or the consumption of hydrogen peroxide (H_2O_2) (Clark and Lyons, 1962; Lowry *et al.*, 1994). These sensors are limited by both O_2 dependence and the large over-potential required for the oxidation of H_2O_2 which allows for high levels of interference from electroactive species that are also oxidisable at this potential, most notably AA. Second generation biosensors incorporate a mediator species into the electrode design which acts as an electron transfer agent which replaces the reliance on O_2 in the enzymatic reaction and effectively lowers the over-potential required (Frew and Hill, 1987; El Atrash and O'Neill, 1995). Problems associated with second generation biosensors include leaching of the mediator from the enzyme layer as well as toxicity in biological tissue (McMahon *et al.*, 2007). Finally, there are third generation biosensors which involve direct electron transfer between the active centre of the redox enzyme and the electrode (Allen and Hill, 1987; Putzbach and Ronkainen, 2013). Examples of these biosensors include hemeprotein entrapped in recombinant silk films for NO detection (Musameh *et al.*, 2018) and hydrothermally grown zinc oxide (ZnO) nanorods for glucose detection (Ridhuan, Abdul Razak and Lockman, 2018).

One of the main challenges facing biosensors for use in the *in-vivo* environment, regardless of generation, is the electroactive interference from endogenous molecules. Even with the use of a second generation biosensor with its lower operating potential the issue is still not fully mitigated (Lowry and O'Neill, 1992). To overcome this issue an interference rejection layer, e.g., a polymer, is deposited on the electrode surface. The polymer layer must have sufficiently low permeability to the interferants while still retaining a high permeability to H_2O_2. The electropolymerisation of a poly-*o*-phenylenediamine (PPD) is a much cited polymer that meets this criteria (Lowry *et al.*, 1994; Garjonyte and Malinauskas, 1999; Turkmen *et al.*, 2014; Baker *et al.*, 2019). This polymer is used throughout the course of this thesis and is described in more detail in Section 2.6.5. Polymers play an important role in the fabrication of biosensors with polymers such as polypyrrole (Ozoner, Yalvac and Erhan, 2010; Nezhadali, Mehri and Shadmehri, 2012) and polyaniline (Granot *et al.*, 2006; Solanki *et al.*, 2011) being extensively used. This is due to their excellent electrochemical properties and long term stability as well as functionally rich chemical structure. As mentioned previously, polymers are utilised for interference rejection but they are also used for immobilisation and stabilisation (Losic *et al.*, 2001; Baker, Bolger and Lowry, 2015; Knyzhnykova *et al.*, 2018). The enzyme immobilisation technique utilised can vary whether it be physisorption, entrapment in/behind a membrane, crosslinking or a mixture of these techniques (Pantano and Kuhr, 1995), these are discussed in more detail in Chapter 4 Section 4.3.4.

The implantation of biosensors in the living brain leads to a certain degree of tissue damage and as a result has driven the field of biosensors towards the goal of miniaturisation. The Pt/Ir electrode used throughout the development of this biosensor has quite a small diameter (127-µm uncoated, 200-µm coated). This is below the threshold value for cellular damage *in-vivo* as measured by uric acid release as a result of the glial reaction to the perturbation of the tissue (Duff and O'Neill, 1994). More recently, no glial response at the site of a choline biosensor implantation, similar to the design presented in this thesis, has been reported (Teles-Grilo Ruivo *et al.*, 2017).

1.4 Microdialysis

Microdialysis (MD) is generally ascribed to have been first carried out by Prof. Urban Ungerstedt in the Karolinska Institute in Sweden in 1974 (Ungerstedt and Pyock, 1974). This technique involved the implantation of a probe into the living brain. A perfusion fluid (perfusate) is then passed into the probe via an inlet tube at a constant flow rate (0.5 – 5 µL/min), it passes through a semi-permeable membrane at the probe tip and is then transported through the outlet tubing and collected (dialysate) for further analysis (Figure 1.3) (Plock and Kloft, 2005). The perfusion of molecules through the membrane allows for sampling of neurotransmitters, metabolites and other analytes of interest in the brain. The perfusate is an aqueous solution, usually artificial cerebrospinal fluid (aCSF), that mimics the ionic concentration of the surrounding ECF and equilibrates with the ECF by osmotic diffusion across the membrane. The membrane allows molecules up to a certain molar mass (< 20 kDa) diffuse into (recovery) or out of (delivery) the perfusion fluid (Shippenberg and Thompson, 1997; Plock and Kloft, 2005).

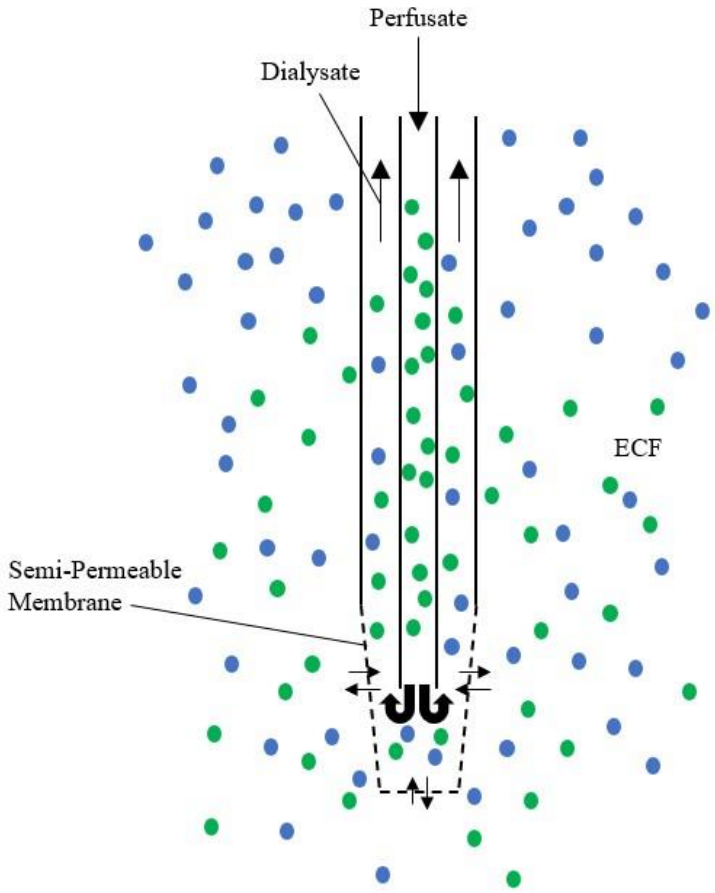

Figure 1.3: A microdialysis probe showing the flow of molecules out of the perfusate into the ECF and vice versa.

MD has been used to study a number of compounds *in-vivo* including ascorbate (Hallström *et al.*, 1989), GABA (Bourdelais and Kalivas, 1992) dopamine, dihydroxyphenylacetic acid (DOPAC) (Zetterström *et al.*, 1988) glucose, pyruvate and lactate (Yao, Yano and Nishino, 2004). While MD is considered the gold standard for *in-vivo* neurochemical monitoring it does suffer from drawbacks. Due to the relatively large probe size (~ 300 µm), in comparison to microelectrodes (defined by at least one dimension < 100 µm) and ultra-microelectrodes (defined by at least one critical dimension below 10 µm down to around 100 nm) (Compton *et al.*, 2008), tissue trauma is expected from the insertion of the probe. Gliosis around the MD probe, which can lead to a blockage of the membrane, have been reported previously (Qu *et al.*, 2001). MD also suffers from poor temporal resolution, while sample times can be as low as less than a minute more typically five to ten minute collection periods are used. Therefore,

MD does not provide real time information with regard to changes in the neurochemical environment which can be achieved using electrochemical techniques such as FSCV and CPA (Chefer *et al.*, 2009). For this project microdialysis was used simply for the delivery of substances into the environment of a biosensor, this is known as retrodialysis (Chefer *et al.*, 2009).

1.5 Pyruvate

According to the classical model for brain energy metabolism, glucose is the main source of energy for both neurons and glial cells under normal physiological conditions, with a lesser contribution from ketone bodies and monocarboxylic acids such as pyruvate and lactate (Vannucci, Maher and Simpson, 1997). These ketone bodies are of great importance during early development but pyruvate and lactate also seem to have a role in the adult brain (Vannucci and Simpson, 2003). Concentrations of pyruvate in the human body have been reported in the range of 40-120 µM for blood (Arai *et al.*, 1999) and 120-300 µM for basal brain levels (Reinstrup *et al.*, 2000; Zetterling *et al.*, 2009; Cordeiro *et al.*, 2015).

Pyruvate is produced in the cytosol by a process known as glycolysis (Figure 1.4), which is a series of enzyme catalysed reactions that break down glucose and other sugars to give pyruvate or lactate (Kumar Jha, Jeon and Suk, 2012). Pyruvate is transported into the mitochondria by the mitochondrial pyruvate carrier (MPC) where it then enters the citric acid cycle to produce acetyl coenzyme A (acetyl-CoA) (Gray, Tompkins and Taylor, 2014). The translocation of pyruvate across the inner mitochondrial membrane via the MPC is directly proton-coupled (Papa *et al.*, 1971). Pyruvate is formed under aerobic conditions while lactate is formed under anaerobic conditions and as a result are of great interest in metabolic disorders such as cerebral ischemia (Yao, Yano and Nishino, 2004). It is possible for the brain to temporarily maintain function during periods of oxygen deprivation by anaerobically producing lactate from glycolysis (Skjøth-Rasmussen *et al.*, 2004). However, as the supply of glucose often decreases with the reduced supply of oxygen there will be a decrease in pyruvate concentration and an increase in lactate concentration and the ratio of lactate to pyruvate (L/P) measured via microdialysis has been seen as an indicator of cerebral ischemia (Skjøth-Rasmussen *et al.*,

2004). Concentrations of lactate *in-vivo* have been reported to be between 0.45 – 0.84 mM (Demestre, Boutelle and Fillenz, 1997; Bazzu *et al.*, 2011; Rocchitta *et al.*, 2013) while, as previously stated, the concentration of pyruvate *in-vivo* has been reported to be 120 – 300 µM. A L/P ratio greater than 25 is interpreted to be the result of high glycolytic activity which is indicative of either mitochondrial dysfunction or hypoxia (Timofeev *et al.*, 2011). High lactate concentrations and as a result a high L/P ratio in the ECF, is one of the best known metabolic characteristics of traumatic brain injury (TBI) (Carpenter, Jalloh and Hutchinson, 2015).

Pyruvate has also shown promise as a neuroprotective agent and the administration of exogenous pyruvate has been seen to mitigate nerve cell damage in rat models of reversible cerebral and retinal ischemia (Lee, Kim and Koh, 2001; Yoo *et al.*, 2004). However, pyruvate had an adverse effect on neuronal survival when administered in a model of irreversible cerebral ischemia (González-Falcón *et al.*, 2003). This may be due to administration causing increased neuronal excitability and stimulating peri-infarct depolarisation which possibly explains the increase in infarct size that was observed (Gonzalez *et al.*, 2005). However, there is little doubt that pyruvate is an important neurochemical that has been somewhat neglected compared to glucose and lactate.

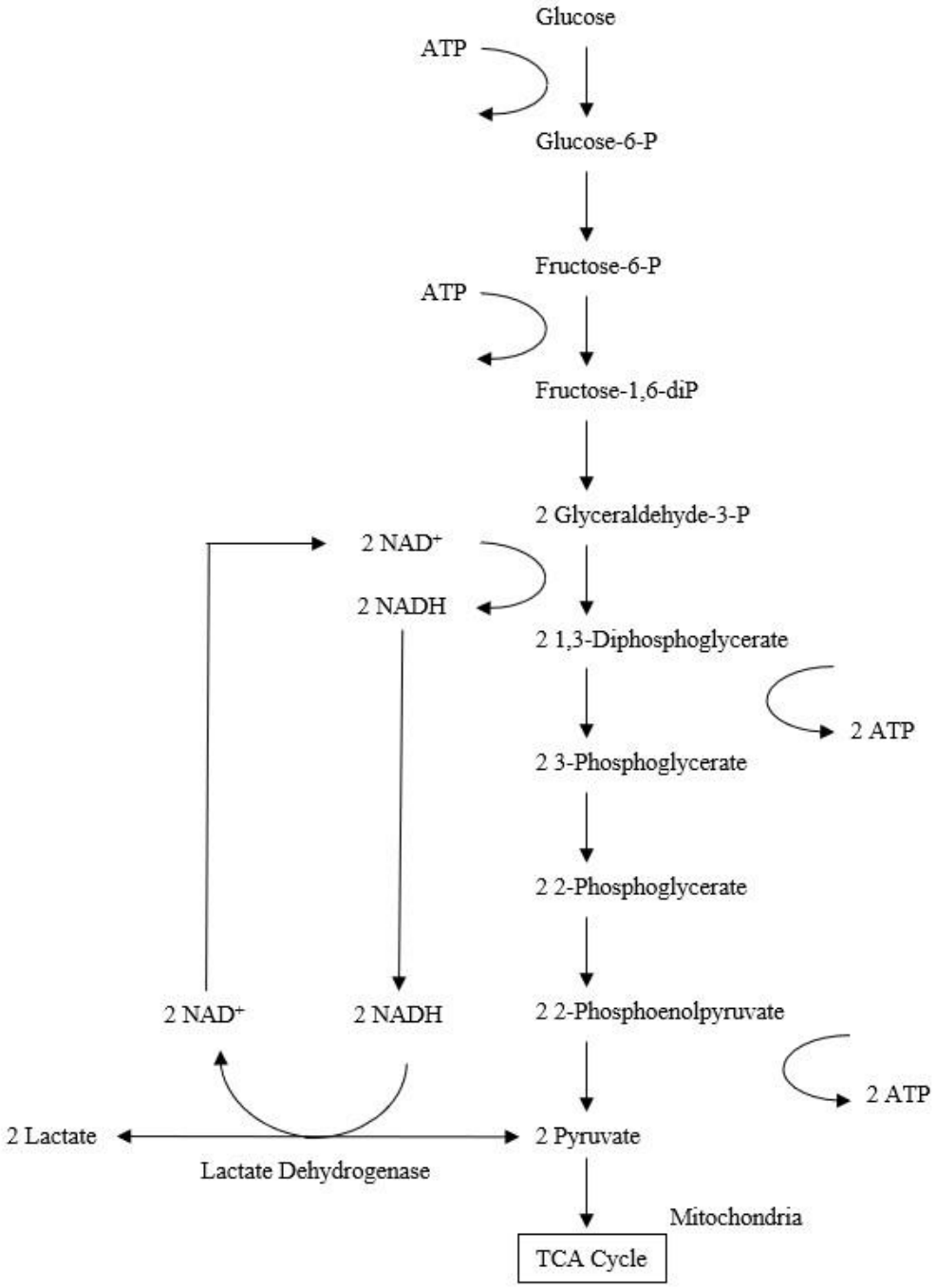

Figure 1.4: The metabolic pathway of glycolysis in which glucose is converted to pyruvate.

1.6 Pyruvate Oxidase

Pyruvate oxidase (POx) was first discovered in 1957 by Lowell P. Hager (Hager, 1957). It is a flavo-protein which catalyses the oxidative decarboxylation of pyruvate and is unique in the fact that it requires both TPP and FAD for catalytic turnover at a single active centre (Mather and Gennis, 1985). As described in the work of Muller and Schulz, POx is a homotetramer with D_2 symmetry with each monomer divided into three domains. Each of the domains contain a six-stranded parallel *β*-sheet surrounded by α-helices. The first domain forms the core of the tetramer and is linked by a chain segment, which lacks secondary structure, to the FAD-binding domain, while the third domain binds TPP. This third domain includes a long α-helix which connects it to the FAD domain. These domains are closely packed at the intersection of the three molecular two-fold axes at the tetramer centre, while there is only a small amount of remaining free space (~100 $Å^3$) (Muller and Schulz, 1993). Shown below in Figure 1.5 is the mechanism of elementary catalytic steps of POx as described by Tittmann *et al.* (Tittmann *et al.*, 2000). The 1st step shows the 4′-imino function of the enzyme bound TPP deprotonating the C2-TPP, which forms an ylide species. In step 2 this ylide attacks the carbonyl group of the substrate pyruvate in a nucleophilic manner. Lactyl-TPP is then decarboxylated to hydroxyethyl-TPP in step 3 which is subsequently oxidised by FAD, leading to formation of acetyl-TPP and $FADH_2$ in step 4. The reduced flavin transfers two electrons to O_2, regenerating FAD and releasing H_2O_2 in step 5 and finally, acetyl-TPP is cleaved phosphorolytically to give acetyl phosphate and regenerate TPP.

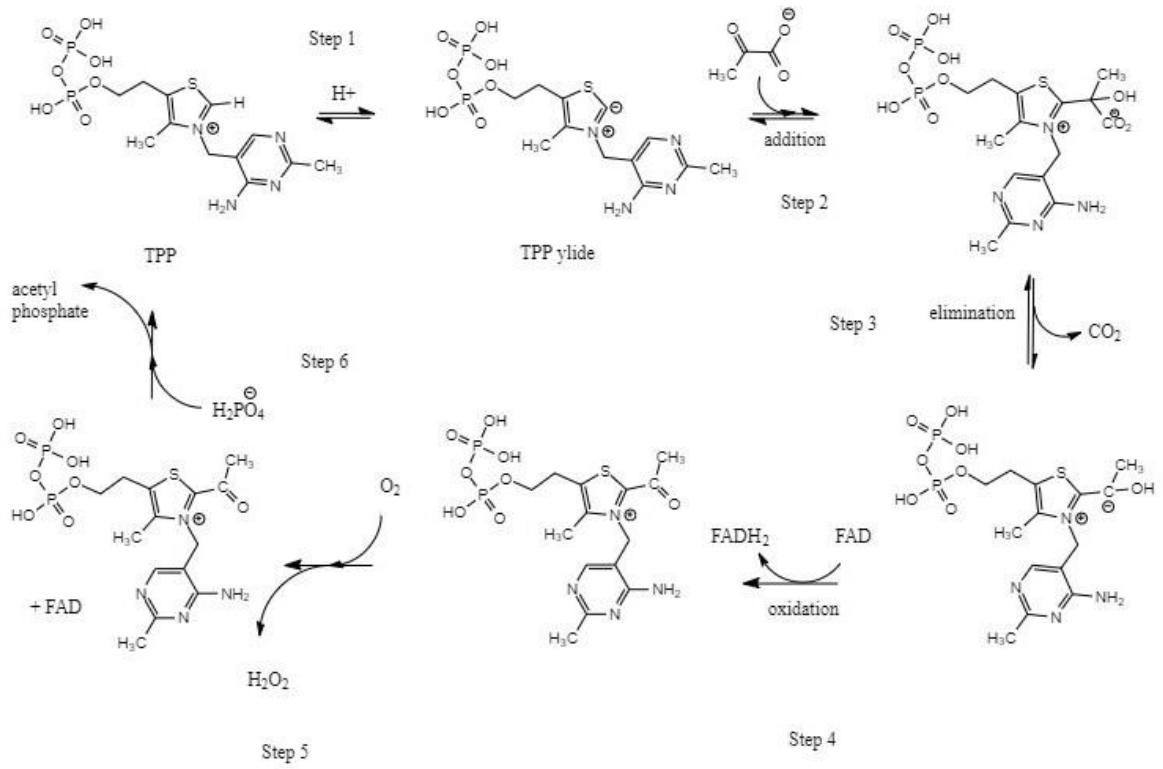

Figure 1.5: Reaction mechanism for the elementary catalytic steps of pyruvate oxidase.

There are multiple sources of POx which have been utilised in various biosensor designs in the past. Bergmann *et al.*, developed a bienzyme-modified carbon paste electrode with pyruvate oxidase from *Lactobacillus plantarum* (*Lp*POx) and pyruvate oxidase from *Pediococcus sp.* (*Ps*POx) (Bergmann, Rudolph and Spohn, 1999). While, Cordeiro *et al.*, utilised pyruvate oxidase from microorganisms (POx) in their multiplex design for *in-vivo* monitoring (Cordeiro *et al.*, 2015). It is also worth noting that Gowers *et al.*, constructed an online microdialysis probe using pyruvate oxidase from *Aerococcus viridans* (*Av*POx) (Gowers *et al.*, 2019). While there is a large variety in terms of enzyme sources it was decided to only focus on ones that have successfully been employed in *in-vivo* monitoring (Cordeiro *et al.*, 2015; Gowers *et al.*, 2019).

The *Av*POx enzyme is a 266 kDa homotetramer with 589 residues and 222 symmetry (Juan *et al.*, 2007), while the *Lp*POx is also a homotetrameric enzyme, it has a total molecular mass of 266 kDa composed of 603 residues (Wille *et al.*, 2005). Each subunit contains one tightly and

noncovalently bound FAD and TPP as well as Mg^{2+} for anchoring the diphosphate moiety of the TPP (Tittmann *et al.*, 2000). The two flexible regions which occupy the walls of the tunnel leading to the active site of both enzyme sources have several differences in the confirmation of their flexible regions. In *Lp*POx structures these regions are more compact in comparison to the same regions in the *Av*POx enzyme. This is due to more extensive contacts in the residues which occupy the base of the flexible regions in the *Lp*POx enzyme which may lead to an increase in stability (Juan *et al.*, 2007). As well as this there is also additional contact between the Glu483 side chain and the thiazolium moiety of TPP. In the *Lp*POx enzyme Glu483 adopts an extended confirmation and as a result appears close to the active site. While in the *Av*POx the main chain of the Lys478 residue occupies a similar position to the Glu483 of the *Lp*POx, but it is not capable of forming interactions with TPP as its side chain is bent (Juan *et al.*, 2007). It is thought that the added stability seen in the *Lp*POx means there is less of a reliance on the addition of extra TPP and it is possible to remove it from the bulk solution with no detrimental effect on the reaction. However, this may not be possible for the *Av*POx and as a result the research conducted in this project only focused on the use of POx from microorganisms.

1.7 Existing Work (Literature Review)

Due to the importance of pyruvate, as outlined above, the need for rapid reliable detection in the *in-vivo* environment is required. Current published biosensors are overviewed below in Table 1.1. It can be seen that while there are a range of pyruvate biosensors that have been developed the majority suffer from either a lack of sensitivity, selectivity or in some cases both. It is also worth noting that the majority of these sensors were developed for other applications and are mainly macro-electrodes which are not ideal for *in-vivo* use due to the substantial tissue damage they would cause. As a result of this there have been few recorded instances where a pyruvate biosensor has been employed in the *in-vivo* environment. The research carried out by Cordeiro *et al.* in 2015 produced an implantable multiplex micro-biosensor for simultaneous detection of glucose lactate and pyruvate. The pyruvate biosensor in this multiplex system was fabricated using a 1 mm length, 0.2 mm diameter platinum cylinder, which had a pre-implantation sensitivity of 25.92 nA. μM^{-1}. cm^{-2}. and there was no response to any interferants (Cordeiro *et al.*, 2015). While this research demonstrated that it is possible to develop and

deploy a pyruvate biosensor in the *in-vivo* environment, it was only a preliminary study in anesthetised animals focusing on the development of a multiplex biosensor. The main technique that has been used to examine extracellular pyruvate has been brain microdialysis with various different research groups publishing work on this as recently as 2019 (Reinstrup *et al.*, 2000; Schulz *et al.*, 2000; Yao, Yano and Nishino, 2004; Gowers *et al.*, 2019). However, there are certain issues with microdialysis such as poor temporal resolution coupled with a large and invasive probe size which limits this technique somewhat (Chefer *et al.*, 2009).

Sensitivity (nA. μM^{-1}. cm^{-2}.)*	Selectivity	Transducer	Active surface size	Immobilisation technique	*In-vivo* viability	Reference
6.23	AA sensitive	Carbon paste electrode (CPE)	3 mm diameter	POx co-immobilised with horse radish peroxidase (HRP)	Not viable	(Bergmann, Rudolph and Spohn, 1999)
51.7	AA, UA, L-Cystine, acetaminophen (AAP) sensitive	Gold disc electrode (GDE)	1.6 mm diameter	POx immobilised on a polyion complex membrane	Not viable	(Mizutani *et al.*, 2000)
0.13	Not determined	Gold micro-electrode array	50-500 µm diameter	Entrapment within an electrostatically complexed monolayer	Possible, interference study required	(Revzin *et al.*, 2002)
8.46	No response to interferants	GCE	2.98 mm diameter	Covalent immobilisation of POx onto nano conducting polymers	Feasible, for phosphate ion detection	(Rahman *et al.*, 2006)
1.66 mg/l µM	Glucose, Lactate, AA sensitive	Dissolved Oxygen probe	Not specified	POx immobilised with gelatin and crosslinked via glutaraldehyde (GA)	Not viable	(Akyilmaz and Yorganci, 2007)
0.08 µA µM	Not determined	GDE	Not specified	POx immobilised via GA cross-linked with β-cyclodextrin	Not viable	(Tu, Long and Deng, 2008)
12389	Not Determined	GDE	2 mm diameter	POx immobilised via GA cross-linking	Not viable	(Bayram and Akyilmaz, 2014)
25.9	No response to interferants	Platinum cylinder micro-electrode	0.2 mm diameter 1 mm height	POx immobilised via GA cross-linking	Utilised *in-vivo*	(Cordeiro *et al.*, 2015)
15.8	No response to interferants	Platinum disc electrode	0.5 mm diameter	Photo-polymerisation of POx in polyvinyl alcohol containing styryl pyridine groups (PVA-SbQ)	Feasible	(Knyzhnykova *et al.*, 2018)

Table 1.1: A selection of published work on pyruvate biosensors highlighting selectivity and sensitivity issues along with a lack of *in-vivo* viability. * Unless otherwise stated.

1.8 Thesis Overview

This thesis describes the development and characterisation of a new biosensor for the amperometric detection of pyruvate *in-vivo* which aims to address issues of both sensitivity and selectivity seen in previously published designs and highlighted above. The current chapter, Chapter 1, presents an introduction to the area of neurochemical monitoring with a particular focus on the detection of pyruvate and its importance in brain energy metabolism. Chapter 2 gives a detailed account of the theory relevant to the study undertaken in this thesis. Chapter 3 provides a detailed description of the experimental techniques and equipment utilised in the development and characterisation of the new pyruvate biosensor *in-vitro*, as well as experimental techniques and equipment used in the application of the biosensor *in-vivo*. Chapter 4 describes the *in-vitro* development of a new pyruvate biosensor while Chapter 5 details its characterisation under conditions mimicking the *in-vivo* environment. Chapter 6 describes the *in-vivo* validation of the newly developed pyruvate biosensor and Chapter 7 presents an overall conclusion to this body of work.

1.9 References

Akyilmaz, E. and Yorganci, E. (2007) 'Construction of an amperometric pyruvate oxidase enzyme electrode for determination of pyruvate and phosphate', *Electrochimica Acta*, 52(28), pp. 7972–7977. doi:10.1016/j.electacta.2007.06.058.

Allen, H. and Hill, O. (1987) 'Bio-electrochemistry', *Pure and Applied Chemistry*, 59(6), pp. 743–748. doi:10.1351/pac198759060743.

Arai, G., Noma, T., Habu, H. and Yasumori, I. (1999) 'Pyruvate sensor based on pyruvate oxidase immobilized in a poly(mercapto-p-benzoquinone) film', *Journal of Electroanalytical Chemistry*, 464(2), pp. 143–148. doi:10.1016/S0022-0728(99)00011-X.

El Atrash, S.S. and O'Neill, R.D. (1995) 'Characterisation in vitro of a naphthoquinone-mediated glucose oxidase-modified carbon paste electrode designed for neurochemical analysis in vivo', *Electrochimica Acta*, 40(17), pp. 2791–2797. doi:10.1016/0013-4686(95)00260-L.

Baker, K.L., Bolger, F.B., Doran, M.M. and Lowry, J.P. (2019) 'Characterisation of a Platinum-based Electrochemical Biosensor for Real-time Neurochemical Analysis of Choline', *Electroanalysis*, 31(1), pp. 129–136. doi:10.1002/elan.201800642.

Baker, K.L., Bolger, F.B. and Lowry, J.P. (2015) 'A microelectrochemical biosensor for real-time in vivo monitoring of brain extracellular choline', *Analyst*, 140(11), pp. 3738–3745. doi:10.1039/c4an02027h.

Bayram, E. and Akyilmaz, E. (2014) 'A new pyruvate oxidase biosensor based on 3-mercaptopropionic acid/6-aminocaproic acid modified gold electrode', *Artificial Cells, Nanomedicine and Biotechnology*, 42(6), pp. 418–422. doi:10.3109/21691401.2013.815626.

Bazzu, G., Biosa, A., Farina, D., Spissu, Y., Dedola, S., Calia, G., Puggioni, G., Rocchitta, G., Migheli, R., Desole, M.S. and Serra, P.A. (2011) 'Dual asymmetric-flow microdialysis for in vivo monitoring of brain neurochemicals', *Talanta*, 85(4), pp. 1933–1940. doi:10.1016/j.talanta.2011.07.018.

Bergmann, W., Rudolph, R. and Spohn, U. (1999) 'A bienzyme modified carbon paste

electrode for amperometric detection of pyruvate', *Analytica Chimica Acta*, 394(2–3), pp. 233–241. doi:10.1016/S0003-2670(99)00296-2.

Bolger, F. and Lowry, J. (2005) 'Brain Tissue Oxygen: In Vivo Monitoring with Carbon Paste Electrodes', *Sensors*, 5(11), pp. 473–487. doi:10.3390/s5110473.

Bourdelais, A.J. and Kalivas, P.W. (1992) 'Modulation of Extracellular γ-Aminobutyric Acid in the Ventral Pallidum Using In Vivo Microdialysis', *Journal of Neurochemistry*, 58(6), pp. 2311–2320. doi:10.1111/j.1471-4159.1992.tb10979.x.

Brown, F.O., Finnerty, N.J. and Lowry, J.P. (2009) 'Nitric oxide monitoring in brain extracellular fluid: Characterisation of Nafion®-modified Pt electrodes in vitro and in vivo', *Analyst*, 134(10), pp. 2012–2020. doi:10.1039/b909005c.

Carpenter, K.L.H., Jalloh, I. and Hutchinson, P.J. (2015) 'Glycolysis and the significance of lactate in traumatic brain injury', *Frontiers in Neuroscience*, 9(APR), p. 112. doi:10.3389/fnins.2015.00112.

Chefer, V.I., Thompson, A.C., Zapata, A. and Shippenberg, T.S. (2009) 'Overview of brain microdialysis', *Current Protocols in Neuroscience*, Chapter 7(SUPPL. 47), p. Unit7.1-Unit7.1. doi:10.1002/0471142301.ns0701s47.

Choi, H.K., Lee, M.J., Lee, S.N., Kim, T.H. and Oh, B.K. (2021) 'Noble Metal Nanomaterial-Based Biosensors for Electrochemical and Optical Detection of Viruses Causing Respiratory Illnesses', *Frontiers in Chemistry*, 9. doi:10.3389/fchem.2021.672739.

Clark, L.C. and Lyons, C. (1962) 'Electrode Systems for Continuous Monitoring in Cardiovascular Surgery', *Annals of the New York Academy of Sciences*, 102(1), pp. 29–45. doi:10.1111/j.1749-6632.1962.tb13623.x.

Clark, L.C., Misrahy, G. and Fox, R.P. (1958) 'Chronically implanted polarographic electrodes.', *Journal of applied physiology*, 13(1), pp. 85–91. doi:10.1152/jappl.1958.13.1.85.

Cohen, D. (1972) 'Magnetoencephalography: Detection of the Brain's Electrical Activity with a Superconducting Magnetometer', *Science*, 175(4022), pp. 664–666. doi:10.1126/science.175.4022.664.

Compton, R.G., Wildgoose, G.G., Rees, N. V., Streeter, I. and Baron, R. (2008) 'Design, fabrication, characterisation and application of nanoelectrode arrays', *Chemical Physics Letters*, 459(1–6), pp. 1–17. doi:10.1016/j.cplett.2008.03.095.

Cordeiro, C.A., de Vries, M.G., Ngabi, W., Oomen, P.E., Cremers, T.I.F.H. and Westerink, B.H.C. (2015) 'In vivo continuous and simultaneous monitoring of brain energy substrates with a multiplex amperometric enzyme-based biosensor device', *Biosensors and Bioelectronics*, 67, pp. 677–686. doi:10.1016/j.bios.2014.09.101.

Demestre, M., Boutelle, M. and Fillenz, M. (1997) 'Stimulated release of lactate in freely moving rats is dependent on the uptake of glutamate', *Journal of Physiology*, 499(3), pp. 825–832. doi:10.1113/jphysiol.1997.sp021971.

Duff, A. and O'Neill, R.D. (1994) 'Effect of Probe Size on the Concentration of Brain Extracellular Uric Acid Monitored with Carbon Paste Electrodes', *Journal of Neurochemistry*, 62(4), pp. 1496–1502. doi:10.1046/j.1471-4159.1994.62041496.x.

Ewing, A.G., Alloway, K.D., Curtis, S.D., Dayton, M.A., Wightman, R.M. and Rebec, G. V. (1983) 'Simultaneous electrochemical and unit recording measurements: Characterization of the effects of d-amphetamine and ascorbic acid on neostriatal neurons', *Brain Research*, 261(1), pp. 101–108. doi:10.1016/0006-8993(83)91288-X.

Frew, J.E. and Hill, H.A. (1987) 'Electron-transfer biosensors.', *Philosophical transactions of the Royal Society of London. Series B, Biological sciences*, 316(1176), pp. 95–106. doi:10.1098/rstb.1987.0020.

Garjonyte, R. and Malinauskas, A. (1999) 'Amperometric glucose biosensor based on glucose oxidase immobilized in poly(o-phenylenediamine) layer', *Sensors and Actuators B: Chemical*, 56(1), pp. 85–92. doi:https://doi.org/10.1016/S0925-4005(99)00163-X.

Geddes, L.A. and Roeder, R. (2003) 'Criteria for the selection of materials for implanted electrodes', *Annals of Biomedical Engineering*, 31(7), pp. 879–890. doi:10.1114/1.1581292.

Glover, G.H. (2011) 'Overview of functional magnetic resonance imaging', *Neurosurgery clinics of North America*, 22(2), pp. 133–vii. doi:10.1016/j.nec.2010.11.001.

González-Falcón, A., Candelario-Jalil, E., García-Cabrera, M. and León, O.S. (2003) 'Effects

of pyruvate administration on infarct volume and neurological deficits following permanent focal cerebral ischemia in rats', *Brain Research*, 990(1–2), pp. 1–7. doi:10.1016/S0006-8993(03)03378-X.

Gonzalez, S.V., Nguyen, N.H.T., Rise, F. and Hassel, B. (2005) 'Brain metabolism of exogenous pyruvate', *Journal of Neurochemistry*, 95(1), pp. 284–293. doi:10.1111/j.1471-4159.2005.03365.x.

Gowers, S.A.N., Rogers, M.L., Booth, M.A., Leong, C.L., Samper, I.C., Phairatana, T., Jewell, S.L., Pahl, C., Strong, A.J. and Boutelle, M.G. (2019) 'Clinical translation of microfluidic sensor devices: focus on calibration and analytical robustness', *Lab Chip*, 19(15), pp. 2537–2548. doi:10.1039/C9LC00400A.

Granot, E., Basnar, B., Cheglakov, Z., Katz, E. and Willner, I. (2006) 'Enhanced bioelectrocatalysis using single-walled carbon nanotubes (SWCNTs)/polyaniline hybrid systems in thin-film and microrod structures associated with electrodes', *Electroanalysis*, 18(1), pp. 26–34. doi:10.1002/elan.200503403.

Gray, L.R., Tompkins, S.C. and Taylor, E.B. (2014) 'Regulation of pyruvate metabolism and human disease', *Cellular and Molecular Life Sciences*, 71(14), pp. 2577–2604. doi:10.1007/s00018-013-1539-2.

Hager, L.P. (1957) 'Trypsin activation of a ferricyanide-linked pyruvic acid oxidation', *The Journal of biological chemistry*, 229(1), pp. 251–263. doi:10.1016/s0021-9258(18)70613-3.

Hallström, Å., Carlsson, A., Hillered, L. and Uncerstedt, U. (1989) 'Simultaneous determination of lactate, pyruvate, and ascorbate in microdialysis samples from rat brain, blood, fat, and muscle using high-performance liquid chromatography', *Journal of Pharmacological Methods*, 22(2), pp. 113–124. doi:10.1016/0160-5402(89)90040-5.

Hammond, C. and Esclapez, M. (2015) 'The chemical synapses', in Hammond, C. (ed.) *Cellular and Molecular Neurophysiology: Fourth Edition*. Fourth Edi. Boston: Academic Press, pp. 121–144. doi:10.1016/B978-0-12-397032-9.00006-6.

İnce, R., Adanır, S.S. and Sevmez, F. (2020) 'The inventor of electroencephalography (EEG): Hans Berger (1873–1941)', *Child's Nervous System* [Preprint]. doi:10.1007/s00381-020-

04564-z.

Jessen, K.R. (2004) 'Glial cells', *International Journal of Biochemistry and Cell Biology*, 36(10), pp. 1861–1867. doi:10.1016/j.biocel.2004.02.023.

Johnston, M. V. (2006) 'Development, Structure, and Function of the Brain and Neuromuscular Systems', in Fuhrman, B.P. and Zimmerman, J.J. (eds) *Pediatric Critical Care*. Third Edit. Philadelphia: Mosby, pp. 767–779. doi:10.1016/B978-032301808-1.50051-1.

Juan, E.C.M., Hoque, M.M., Hossain, M.T., Yamamoto, T., Imamura, S., Suzuki, K., Sekiguchi, T. and Takénaka, A. (2007) 'The structures of pyruvate oxidase from Aerococcus viridans with cofactors and with a reaction intermediate reveal the flexibility of the active-site tunnel for catalysis', *Acta Crystallographica Section F: Structural Biology and Crystallization Communications*, 63(11), pp. 900–907. doi:10.1107/S1744309107041012.

Kissinger, P.T., Hart, J.B. and Adams, R.N. (1973) 'Voltammetry in brain tissue - a new neurophysiological measurement', *Brain Research*, 55(1), pp. 209–213. doi:10.1016/0006-8993(73)90503-9.

Knyzhnykova, D. V., Topolnikova, Y. V., Kucherenko, I.S. and Soldatkin, O.O. (2018) 'Development of pyruvate oxidase-based amperometric biosensor for pyruvate determination', *Biopolymers and Cell*, 34(1), pp. 14–23. doi:10.7124/bc.00096C.

Kumar Jha, M., Jeon, S. and Suk, K. (2012) 'Pyruvate Dehydrogenase Kinases in the Nervous System: Their Principal Functions in Neuronal-glial Metabolic Interaction and Neuro-metabolic Disorders', *Current Neuropharmacology*, 10(4), pp. 393–403. doi:10.2174/157015912804143586.

Lee, J.Y., Kim, Y.H. and Koh, J.Y. (2001) 'Protection by pyruvate against transient forebrain ischemia in rats.', *The Journal of neuroscience : the official journal of the Society for Neuroscience*, 21(20), pp. RC171--RC171. doi:10.1523/jneurosci.21-20-j0002.2001.

Lewine, J.D. (1995) 'Introduction to Functional Neuroimaging: Functional Neuroanatomy', in Orrison, W.W., Lewine, J.D., Sanders, J.A., and Hartshorne, M.F. (eds) *Functional Brain Imaging*. Mosby, pp. 13–95. doi:10.1016/b978-0-8151-6509-5.50006-0.

Liu, H., Ge, J., Ma, E. and Yang, L. (2018) 'Advanced biomaterials for biosensor and

theranostics', in Yang, L., Bhaduri, S.B., and Webster, T.J. (eds) *Biomaterials in Translational Medicine: A Biomaterials Approach*. Academic Press (Woodhead Publishing Series in Biomaterials), pp. 213–255. doi:10.1016/B978-0-12-813477-1.00010-4.

Losic, D., Gooding, J.J., Shapter, J.G., Hibbert, D.B. and Short, K. (2001) 'The influence of the underlying gold substrate on glucose oxidase electrodes fabricated using self-assembled monolayers', *Electroanalysis*, 13(17), pp. 1385–1393. doi:10.1002/1521-4109(200111)13:17<1385::AID-ELAN1385>3.0.CO;2-L.

Lowry, J.P., McAteer, K., El Atrash, S.S., Duff, A. and O'Neill, R.D. (1994) 'Characterization of Glucose Oxidase-Modified Poly(phenylenediamine)-Coated Electrodes in Vitro and in Vivo: Homogeneous Interference by Ascorbic Acid in Hydrogen Peroxide Detection', *Analytical Chemistry*, 66(10), pp. 1754–1761. doi:10.1021/ac00082a025.

Lowry, J.P. and O'Neill, R.D. (1992) 'Strategies for reducing ascorbate interference at glucose oxidase modified conducting organic salt electrodes', *Journal of Electroanalytical Chemistry*, 334(1), pp. 183–194. doi:https://doi.org/10.1016/0022-0728(92)80570-T.

Lyne, P.D. and O'Neill, R.D. (1990) 'Stearate-Modified Carbon Paste Electrodes for Detecting Dopamine in Vivo: Decrease in Selectivity Caused by Lipids and Other Surface-Active Agents', *Analytical Chemistry*, 62(21), pp. 2347–2351. doi:10.1021/ac00220a016.

Mather, M.W. and Gennis, R.B. (1985) 'Kinetic studies of the lipid-activated pyruvate oxidase flavoprotein of Escherichia coli', *Journal of Biological Chemistry*, 260(30), pp. 16148–16155.

McMahon, C.P., Rocchitta, G., Kirwan, S.M., Killoran, S.J., Serra, P.A., Lowry, J.P. and O'Neill, R.D. (2007) 'Oxygen tolerance of an implantable polymer/enzyme composite glutamate biosensor displaying polycation-enhanced substrate sensitivity', *Biosensors and Bioelectronics*, 22(7), pp. 1466–1473. doi:https://doi.org/10.1016/j.bios.2006.06.027.

Meiller, A., Sequeira, E. and Marinesco, S. (2020) 'Electrochemical Nitric Oxide Microsensors Based on a Fluorinated Xerogel Screening Layer for in Vivo Brain Monitoring', *Analytical Chemistry*, 92(2), pp. 1804–1810. doi:10.1021/acs.analchem.9b03621.

Mizutani, F., Yabuki, S., Sato, Y., Sawaguchi, T. and Iijima, S. (2000) 'Amperometric determination of pyruvate, phosphate and urea using enzyme electrodes based on pyruvate

oxidase-containing poly(vinyl alcohol)/polyion complex-bilayer membrane', *Electrochimica Acta*, 45(18), pp. 2945–2952. doi:10.1016/S0013-4686(00)00373-X.

Muller, Y.A. and Schulz, G.E. (1993) 'Structure of the thiamine- and flavin-dependent enzyme pyruvate oxidase', *Science*, 259(5097), pp. 965–967. doi:10.1126/science.8438155.

Musameh, M.M., Dunn, C.J., Uddin, M.H., Sutherland, T.D. and Rapson, T.D. (2018) 'Silk provides a new avenue for third generation biosensors: Sensitive, selective and stable electrochemical detection of nitric oxide', *Biosensors and Bioelectronics*, 103, pp. 26–31. doi:https://doi.org/10.1016/j.bios.2017.12.019.

Nezhadali, A., Mehri, L. and Shadmehri, R. (2012) 'Determination of benzimidazole in biological model samples using electropolymerized-molecularly imprinted polypyrrole modified pencil graphite sensor', *Sensors and Actuators, B: Chemical*, 171–172, pp. 1125–1131. doi:10.1016/j.snb.2012.06.043.

O'Neill, R.D., Lowry, J.P. and Mas, M. (1998) 'Monitoring brain chemistry in vivo: Voltammetric techniques, sensors, and behavioral applications', *Critical Reviews in Neurobiology*, 12(1–2), pp. 69–127. doi:10.1615/CritRevNeurobiol.v12.i1-2.40.

Ormonde, D.E. and O'Neill, R.D. (1990) 'The oxidation of ascorbic acid at carbon paste electrodes. Modified response following contact with surfactant, lipid and brain tissue', *Journal of Electroanalytical Chemistry*, 279(1–2), pp. 109–121. doi:10.1016/0022-0728(90)85170-A.

Ozoner, S.K., Yalvac, M. and Erhan, E. (2010) 'Flow injection determination of catechol based on polypyrrole-carbon nanotube-tyrosinase biocomposite detector', *Current Applied Physics*, 10(1), pp. 323–328. doi:10.1016/j.cap.2009.06.017.

Pantano, P. and Kuhr, W.G. (1995) 'Enzyme-modified microelectrodes for in vivo neurochemical measurements', *Electroanalysis*, 7(5), pp. 405–416. doi:10.1002/elan.1140070502.

Papa, S., Francavilla, A., Paradies, G. and Meduri, B. (1971) 'The transport of pyruvate in rat liver mitochondria', *FEBS Letters*, 12(5), pp. 285–288. doi:10.1016/0014-5793(71)80200-4.

Plock, N. and Kloft, C. (2005) 'Microdialysis - Theoretical background and recent

implementation in applied life-sciences', *European Journal of Pharmaceutical Sciences*, 25(1), pp. 1–24. doi:10.1016/j.ejps.2005.01.017.

Putzbach, W. and Ronkainen, N.J. (2013) 'Immobilization techniques in the fabrication of nanomaterial-based electrochemical biosensors: A review', *Sensors (Switzerland)*, 13(4), pp. 4811–4840. doi:10.3390/s130404811.

Qu, Y., Van der Gucht, E., Massie, A., Vandenbussche, E., Vandesande, F. and Arckens, L. (2001) 'In vivo microdialysis in the visual cortex of awake cat III: Histological verification', *Brain Research Protocols*, 7(1), pp. 52–60. doi:10.1016/S1385-299X(00)00062-3.

Rahman, M.A., Park, D.S., Chang, S.C., McNeil, C.J. and Shim, Y.B. (2006) 'The biosensor based on the pyruvate oxidase modified conducting polymer for phosphate ions determinations', *Biosensors and Bioelectronics*. 2005/05/17, 21(7), pp. 1116–1124. doi:10.1016/j.bios.2005.04.008.

Reinstrup, P., Ståhl, N., Mellergård, P., Uski, T., Ungerstedt, U. and Nordström, C.H. (2000) 'Intracerebral microdialysis in clinical practice: Baseline values for chemical markers during wakefulness, anesthesia, and neurosurgery', *Neurosurgery*, 47(3), pp. 701–710. doi:10.1227/00006123-200009000-00035.

Revzin, A.F., Sirkar, K., Simonian, A. and Pishko, M. V. (2002) 'Glucose, lactate, and pyruvate biosensor arrays based on redox polymer/oxidoreductase nanocomposite thin-films deposited on photolithographically patterned gold microelectrodes', *Sensors and Actuators, B: Chemical*, 81(2–3), pp. 359–368. doi:10.1016/S0925-4005(01)00982-0.

Ridhuan, N.S., Abdul Razak, K. and Lockman, Z. (2018) 'Fabrication and Characterization of Glucose Biosensors by Using Hydrothermally Grown ZnO Nanorods', *Scientific Reports*, 8(1), p. 13722. doi:10.1038/s41598-018-32127-5.

Robinson, D.L., Venton, B.J., Heien, M.L.A. V and Wightman, R.M. (2003) 'Detecting Subsecond Dopamine Release with Fast-Scan Cyclic Voltammetry in Vivo', *Clinical Chemistry*, 49(10), pp. 1763–1773. doi:10.1373/49.10.1763.

Rocchitta, G., Secchi, O., Alvau, M.D., Farina, D., Bazzu, G., Calia, G., Migheli, R., Desole, M.S., O'Neill, R.D. and Serra, P.A. (2013) 'Simultaneous telemetric monitoring of brain

glucose and lactate and motion in freely moving rats', *Analytical Chemistry*, 85(21), pp. 10282–10288. doi:10.1021/ac402071w.

Ronkainen, N.J., Halsall, H.B. and Heineman, W.R. (2010) 'Electrochemical biosensors', *Chemical Society Reviews*, 39(5), pp. 1747–1763. doi:10.1039/b714449k.

Schulz, M.K., Wang, L.P., Tange, M. and Bjerre, P. (2000) 'Cerebral microdialysis monitoring: Determination of normal and ischemic cerebral metabolisms in patients with aneurysmal subarachnoid hemorrhage', *Journal of Neurosurgery*, 93(5), pp. 808–814. doi:10.3171/jns.2000.93.5.0808.

Shippenberg, T.S. and Thompson, A.C. (1997) 'Overview of Microdialysis', *Current Protocols in Neuroscience*, 00(1), p. Unit7.1-Unit7.1. doi:10.1002/0471142301.ns0701s00.

Skjøth-Rasmussen, J., Schulz, M., Kristensen, S.R. and Bjerre, P. (2004) 'Delayed neurological deficits detected by an ischemic pattern in the extracellular cerebral metabolites in patients with aneurysmal subarachnoid hemorrhage', *Journal of Neurosurgery*, 100(1), pp. 8–15. doi:10.3171/jns.2004.100.1.0008.

Snyder, J.M., Hagan, C.E., Bolon, B. and Keene, C.D. (2018) '20 - Nervous System', in Treuting, P.M., Dintzis, S.M., and Montine, K.S. (eds) *Comparative Anatomy and Histology (Second Edition)*. Second Edi. San Diego: Academic Press, pp. 403–444. doi:https://doi.org/10.1016/B978-0-12-802900-8.00020-8.

Solanki, P.R., Kaushik, A., Ansari, A.A., Sumana, G. and Malhotra, B.D. (2011) 'Horse radish peroxidase immobilized polyaniline for hydrogen peroxide sensor', *Polymers for Advanced Technologies*, 22(6), pp. 903–908. doi:10.1002/pat.1594.

Sun, C.L., Lee, H.H., Yang, J.M. and Wu, C.C. (2011) 'The simultaneous electrochemical detection of ascorbic acid, dopamine, and uric acid using graphene/size-selected Pt nanocomposites', *Biosensors and Bioelectronics*, 26(8), pp. 3450–3455. doi:10.1016/j.bios.2011.01.023.

Teles-Grilo Ruivo, L.M., Baker, K.L., Conway, M.W., Kinsley, P.J., Gilmour, G., Phillips, K.G., Isaac, J.T.R., Lowry, J.P. and Mellor, J.R. (2017) 'Coordinated Acetylcholine Release in Prefrontal Cortex and Hippocampus Is Associated with Arousal and Reward on Distinct

Timescales', *Cell Reports*, 18(4), pp. 905–917. doi:https://doi.org/10.1016/j.celrep.2016.12.085.

Thvenot, D.R., Toth, K., Durst, R.A. and Wilson, G.S. (1999) 'Electrochemical biosensors: Recommended definitions and classification (Technical Report)', *Pure and Applied Chemistry*, 71(12), pp. 2333–2348. doi:10.1351/pac199971122333.

Timofeev, I., Carpenter, K.L.H., Nortje, J., Al-Rawi, P.G., O'Connell, M.T., Czosnyka, M., Smielewski, P., Pickard, J.D., Menon, D.K., Kirkpatrick, P.J., Gupta, A.K. and Hutchinson, P.J. (2011) 'Cerebral extracellular chemistry and outcome following traumatic brain injury: A microdialysis study of 223 patients', *Brain*, 134(2), pp. 484–494. doi:10.1093/brain/awq353.

Tittmann, K., Golbik, R., Ghisla, S. and Hubner, G. (2000) 'Mechanism of elementary catalytic steps of pyruvate oxidase from Lactobacillus plantarum.', *Biochemistry*, 39(35), pp. 10747–10754. doi:10.1021/bi0004089.

Tu, Y., Long, Y. and Deng, K. (2008) 'Study on a pyruvate oxidase biosensor based on (β-cyclodextrin included ferrocene as electron-transfer mediator', *Proceedings of the 3rd International Conference on Sensing Technology, ICST 2008*, 42(2), pp. 403–408. doi:10.1109/ICSENST.2008.4757136.

Turkmen, E., Bas, S.Z., Gulce, H. and Yildiz, S. (2014) 'Glucose biosensor based on immobilization of glucose oxidase in electropolymerized poly(o-phenylenediamine) film on platinum nanoparticles-polyvinylferrocenium modified electrode', *Electrochimica Acta*, 123, pp. 93–102. doi:https://doi.org/10.1016/j.electacta.2013.12.189.

Ungerstedt, U. and Pyock, C. (1974) 'Functional correlates of dopamine neurotransmission', *Bulletin der Schweizerischen Akademie der Medizinischen Wissenschaften*, 30(1–3), pp. 44–55.

Vannucci, S.J., Maher, F. and Simpson, I.A. (1997) 'Glucose transporter proteins in brain: Delivery of glucose to neurons and glia', *Glia*, 21(1), pp. 2–21. doi:10.1002/(SICI)1098-1136(199709)21:1<2::AID-GLIA2>3.0.CO;2-C.

Vannucci, S.J. and Simpson, I.A. (2003) 'Developmental switch in brain nutrient transporter expression in the rat', *American Journal of Physiology - Endocrinology and Metabolism*, 285(5

48-5), pp. E1127–E1134. doi:10.1152/ajpendo.00187.2003.

Wagner, H.N. (1998) 'A brief history of positron emission tomography (PET)', *Seminars in Nuclear Medicine*, 28(3), pp. 213–220. doi:https://doi.org/10.1016/S0001-2998(98)80027-5.

Watson, C., Kirkcaldie, M. and Paxinos, G. (2010) *The Brain: An Introduction to Functional Neuroanatomy*.

Wille, G., Ritter, M., Weiss, M.S., König, S., Mäntele, W. and Hübner, G. (2005) 'The role of val-265 for flavin adenine dinucleotide (FAD) binding in pyruvate oxidase: FTIR, kinetic, and crystallographic studies on the enzyme variant V265A', *Biochemistry*, 44(13), pp. 5086–5094. doi:10.1021/bi047337o.

Willerth, S. (2017) 'Introduction to the nervous system', in Willerth, S. (ed.) *Engineering Neural Tissue from Stem Cells*. Academic Press, pp. 17–38. doi:10.1016/b978-0-12-811385-1.00002-9.

Yao, T., Yano, T. and Nishino, H. (2004) 'Simultaneous in vivo monitoring of glucose, L-lactate, and pyruvate concentrations in rat brain by a flow-injection biosensor system with an on-line microdialysis sampling', *Analytica Chimica Acta*, 510(1), pp. 53–59. doi:10.1016/j.aca.2003.12.062.

Yoo, M.H., Lee, J.Y., Lee, S.E., Koh, J.Y. and Yoon, Y.H. (2004) 'Protection by pyruvate of rat retinal cells against zinc toxicity in vitro, and pressure-induced ischemia in vivo', *Investigative Ophthalmology and Visual Science*, 45(5), pp. 1523–1530. doi:10.1167/iovs.03-1315.

Zetterling, M., Hillered, L., Samuelsson, C., Karlsson, T., Enblad, P. and Ronne-Engström, E. (2009) 'Temporal patterns of interstitial pyruvate and amino acids after subarachnoid haemorrhage are related to the level of consciousness-a clinical microdialysis study', *Acta Neurochirurgica*, 151(7), pp. 771–780. doi:10.1007/s00701-009-0384-4.

Zetterström, T., Sharp, T., Collin, A.K. and Ungerstedt, U. (1988) 'In vivo measurement of extracellular dopamine and DOPAC in rat striatum after various dopamine-releasing drugs implications for the origin of extracellular DOPAC', *European Journal of Pharmacology*, 148(3), pp. 327–334. doi:10.1016/0014-2999(88)90110-0.

Chapter 2:

Theory

2.1 Introduction

The goal of this research project was to develop and characterise a pyruvate biosensor *in-vitro* that is suitable for *in-vivo* use. To achieve this constant potential amperometry (CPA) was utilised throughout the project; this technique is described in further detail in Section 2.4. Since pyruvate is not electrochemically active direct electrochemical detection is not viable. Therefore, this research focused on the exploration of a first-generation biosensor design in which pyruvate oxidase (POx) was incorporated resulting in the production of the electrochemically active hydrogen peroxide (H_2O_2). However, for enzymatic activity POx requires the co-factors flavin adenine dinucleotide (FAD), thiamine pyrophosphate (TPP) and a divalent metal such as magnesium (Mg^{2+}) (Tittmann *et al.*, 2000).

The effectiveness and suitability of the various pyruvate biosensor designs developed (Section 2.6.4) are described and compared by their response to the target substrate and interference species using both linear and non-linear regression and other statistical analyses as described in Section 2.9. Non-linear regression involves fitting the experimental data to Michaelis-Menten kinetics to determine the important parameters V_{max}, K_m and α, which are used to describe the immobilised enzyme's activity towards the substrate of interest (see Section 2.5). The theories of mass transport and electron transfer govern the electrochemical analysis used in this research project. Electron transfer deals with the oxidation or reduction of a species at the active surface of the electrode depending on the applied potential and is detailed in Section 2.2. Mass transport describes the motion of reactants and products to and from the active surface and can be described by three main processes; convection, diffusion and migration, these are discussed in more detail in Section 2.3.

2.2 Oxidation and Reduction

Electrochemical analysis is based on the reactions that take place at the electrode surface. This involves the application of a fixed potential between the working and reference electrode in order for the desired oxidation or reduction of the target analyte to occur at the active surface of the working electrode (Brett and Brett, 1993; Guy and Walker, 2016). First generation biosensors monitor the production of hydrogen peroxide (H_2O_2) at a fixed anodic potential (+700 mV *vs.* Ag/AgCl) or oxygen (O_2) consumption at a fixed cathodic potential (−700 mV *vs.* Ag/AgCl) (Clark and Lyons, 1962; Rocchitta *et al.*, 2016). Equation 2.1 symbolises the oxidation and reduction of a species at the active surface of an electrode, O and R represent the oxidised and reduced species, while n represents the number of electrons transferred.

$$O + ne^- \leftrightharpoons R \qquad \textbf{Equation 2.1}$$

At equilibrium (E_{eq}) the reaction apparently ceases on a macroscopic level as seen with chemical equilibrium. However, from a kinetic standpoint the rate of reaction in the forward direction does not become zero at the equilibrium potential but is instead compensated by an identical rate of reaction in the reverse direction. This constant exchange of charge, in both directions, from a molecular point of view occurs even though the reaction has come to a standstill macroscopically (Vetter, 1967). As a result, an overpotential (η) must be applied. The overpotential is defined as the potential beyond a reversible potential that produces an increased thermodynamic driving force for the process (Newman , Thomas-Alyea, Karen E., 2004). The extent of this is determined by the Fermi level (E_F) of the working electrode. The Fermi level is defined as an energy level that it is exactly half filled with electrons. Levels of lower energy than the Fermi level tend to be entirely filled with electrons, whereas energy levels higher than the Fermi tend to be empty (Janzen, 1979). In a non-spontaneous reaction, the E_F of the working electrode is equal to that of the highest occupied molecular orbital (HOMO) of the species in the solution. The applied overpotential either increases or decreases the Fermi level of the working electrode which results in an energetically favourable transfer of electrons. For an oxidation reaction, the applied potential is positive and greater than E_{eq} resulting in a decrease

in energy of E_F and as a result it is now more energetically favourable for electrons to move from the HOMO of the solution species to the lower E_F of the working electrode. When a negative potential is applied with respect to E_{eq} there is an increase in E_F and it becomes more energetically favourable for electrons to move to the lowest unoccupied molecular orbital (LUMO) of the solution species, this is a reduction reaction (Bard and Faulkner, 2000; Ciobanu *et al.*, 2007; Elgrishi *et al.*, 2018). A schematic of both reactions is shown below in Figure 2.1.

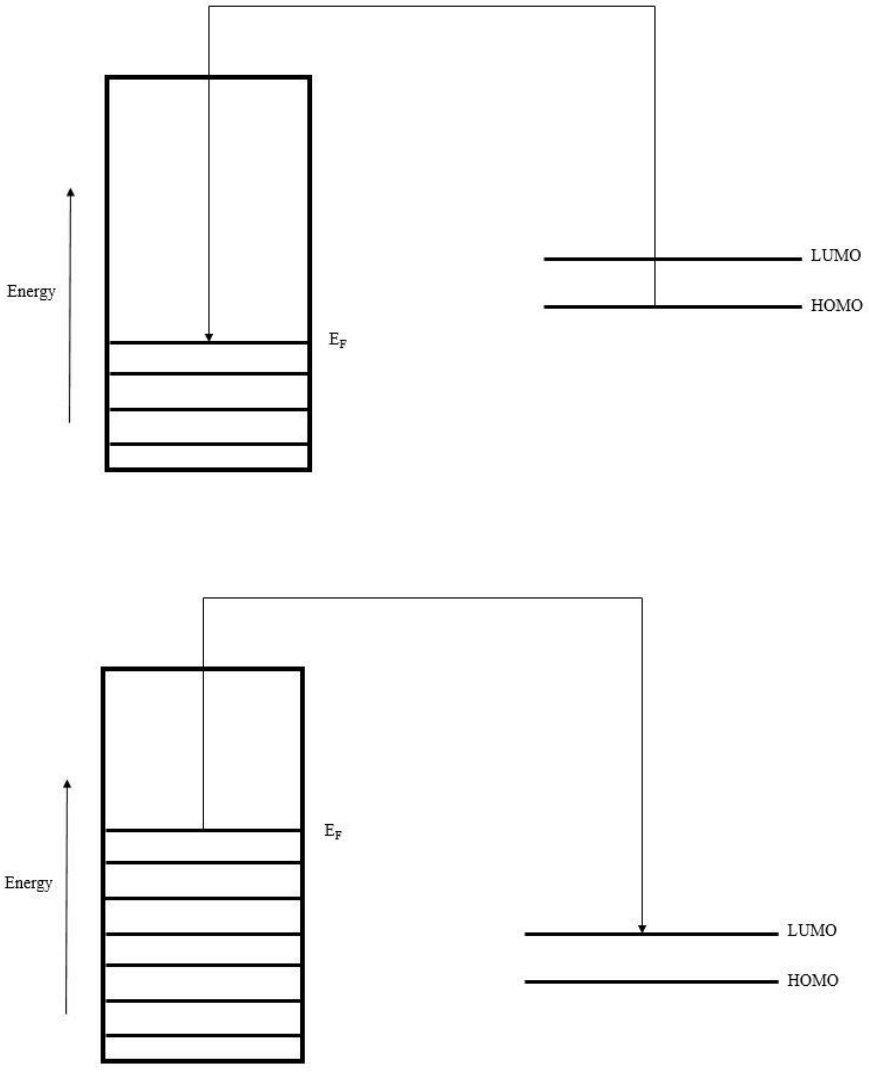

Figure 2.1: Schematic of an oxidation reaction (top) and a reduction reaction (bottom).

Two different processes occur at the electrode surface. The first kind was discussed above where a charge is transferred between the electrode and the solution species which causes either oxidation or reduction. This reaction is known as a faradaic process and is governed by Faraday's law which states that the amount of chemical reaction caused by the flow of current is proportional to the amount of electricity passed. The second kind of process is a non-faradaic process in which adsorption and desorption occur causing the electrode-solution species interface to change when potential is applied (Bard and Faulkner, 2000). As well as this the electrode also acts as a capacitor. Using the concept of an ideal polarisable electrode (IPE), which is an electrode where no charge is passed across the electrode solution species interface when the potential is changed and therefore, behaves like a capacitor in an electric circuit except that the capacitance of the IPE is dependent on the potential applied across it where as a normal capacitor is not (Ciobanu *et al.*, 2007). As a result of this a capacitance (background) current arises even when no target analyte is present and must be subtracted.

2.3 Mass Transport

As an oxidation or reduction reaction occurs at the electrode surface a concentration gradient is created and mass transport becomes an important factor affecting the rate of the reaction. The use of reactants to form products results in a concentration difference with the bulk solution species and the solution acts to address this concentration difference with three different transport mechanisms; migration, convection and diffusion (Brett and Brett, 1993).

2.3.1 Migration

Migration is the movement of charged particles in an electric field (Ciobanu *et al.*, 2007). The external electric field at the electrode solution interface is able to exert an electrostatic force on charged species which induces movement of ions to or from the electrode. However the use of a large quantity of an inert/supporting electrolyte (PBS) which can transport almost all of the current in the cell removes the problem of solution resistance (Brett and Brett, 1993). As a result, the effects of migration were negligible in the work carried out in this research project.

2.3.2 Convection

There are two forms of convection, the first is natural convection such as that caused by thermal gradients, but generally conditions where this movement is negligible are more commonly used. The second form of convection is forced convection which is caused by external forces such as stirring or bubbling (Brett and Brett, 1993; Fisher, 1996). *In-vitro* experiments carried out in this research project utilised forced convection by the use of a magnetic stirrer to ensure a homogenous solution after the addition of an aliquot of the substrate. However, this contribution can be ignored as analysis of the calibration data comes from the steady-state currents of quiescent solutions.

2.3.3 Diffusion

Diffusion is caused by uneven concentration distribution and is the movement of molecules from an area of high concentration to an area of low concentration. This phenomenon is governed by Fick's first law, given in Equation 2.2, which states that the diffusional flux (J), is proportional to the concentration (c), with respect to the direction (x), which is known as the concentration gradient, $\frac{\partial c}{\partial x}$ where D is the diffusional coefficient. The negative sign indicates movement from a higher concentration down to a lower concentration.

$$J = -D\frac{\partial c}{\partial x} \qquad \textbf{Equation 2.2}$$

From Fick's first law it is possible to derive Fick's second law, shown in Equation 2.3, which deals with the change in concentration at a point in time (t):

$$\frac{\partial c}{\partial t} = D\frac{\partial^2 c}{\partial x^2} \qquad \textbf{Equation 2.3}$$

As a reaction proceeds over time the concentration of the reactants decreases as it is consumed resulting in a concentration gradient. However, in the case of microelectrodes which have quite small diameters in the range of 5 – 300 µm, minimal substrate is consumed and only small currents are observed resulting in a steady-state response in which there is no change in concentration with respect to time (Oldham, 1991; O'Neill, Lowry and Mas, 1998).

The disc microelectrodes utilised in this research project were 127-µm in diameter and for the purposes of calculating the variation of current with time, they may be considered to be planar and uniformly accessible to the bulk solution. The Cottrell equation (Equation 2.4), which is calculated from Fick's second law of diffusion, is used to define the current-time dependence for linear diffusion control at a planar electrode:

$$i = nFAJ = \frac{nFAD^{\frac{1}{2}}c_{\infty}}{(\pi t)^{\frac{1}{2}}} \qquad \textbf{Equation 2.4}$$

Where i is the current measured at time t at the electrode surface (area A) which is directly proportional to the concentration of the substrate in the bulk solution (c_{∞}), n is the number of electrons, F is the Faraday constant, J is the flux and D is the diffusion coefficient. For a cylindrical electrode a coordinate system is required as the simple one-dimensional system previously used for planar electrode surfaces is not sufficient. Therefore, Fick's first law (Equation 2.2) is altered to include a Laplacian Operator:

$$J = -D\nabla^2 c \qquad \textbf{Equation 2.5}$$

It is now possible to change coordinate systems freely and as a result Fick's second law is also altered to give Equation 2.6:

$$\frac{\partial c}{\partial t} = D\nabla^2 c \qquad \textbf{Equation 2.6}$$

Since a cylindrical electrode was utilised in this research project a specific Laplacian operator must be used (Brett and Brett, 1993) and is given in Equation 2.7:

$$\frac{\partial^2}{\partial^2 r} + \left(\frac{1}{r}\right)\left(\frac{\partial}{\partial \varphi}\right) + \frac{\partial}{\partial x} \qquad \textbf{Equation 2.7}$$

To solve the above equations, it is necessary to define the conditions of the system. These conditions specify the concentration and/or spatial characteristics in relation to time, at t = 0.

Fick's first law for a species, R at the surface of an electrode determines that the flux, $J_R(0,t)$, is proportional to the current density $\left(\frac{i}{A}\right)$, as the total number of electrons transferred per unit of time must be proportional to the concentration of R reaching the electrode surface in that specific time period.

$$-J_R(0,t) = \frac{i}{nFA} = D_R\left[\frac{\partial c_R(x,t)}{\partial x}\right]_{x=0} \qquad \textbf{Equation 2.8}$$

where A is the surface area of the electrode, F is the Faraday constant, n is the number of electrons transferred and i is the current. The solutions to Equation 2.6 and Equation 2.8 determine the current flowing across the electrode solution species interface as a function of concentration, time or other parameters for any given electrode geometry.

2.4 Constant Potential Amperometry

For this research project CPA was the utilised electrochemical technique. This technique allows for the constant recording of the current produced by the oxidation or reduction of the substrate of interest under the conditions of a fixed applied potential (Hanson, Pappas and Holland, 2005). The use of a fixed potential during amperometric detection results in a negligible charging current which minimises the background signal which can adversely affect the limit

of detection (LOD) (Ronkainen, Halsall and Heineman, 2010). Along with low LODs, CPA is also highly quantitative and easily reproducible (Hanson, Pappas and Holland, 2005). These characteristics make CPA an ideal technique for the *in-vitro/in-vivo* research presented in this thesis.

As per Section 2.3, diffusion is considered to be the only form of mass transport occurring within the system. After the initial application of a fixed voltage the capacitance currents (Section 2.2) decay to almost zero which results in a steady-state current. The potentials used in this research project were chosen to ensure that all the substrate that reached the active surface was oxidised. Therefore, the current measured is directly proportional to the target analytes concentration at all times. This current is the sum of the Cottrell current and steady-state current, given in Equation 2.9.

$$I_{amp} = i_{cot} + i_{ss} \qquad \textbf{Equation 2.9}$$

For large values of time the Cottrell component disappears and the steady-state current dominates. These diffusion limited steady-state currents are given in Equation 2.10 (Forster, 1994).

$$i_{ss} = \frac{nFADc}{r} \qquad \textbf{Equation 2.10}$$

Where i_{ss} is the steady-state current, n is the number of electrons, F is the Faraday constant, A is the area of the electrode, D is the diffusion coefficient, c is the concentration and r is the radius. Various subtleties influence the system such as geometry or the insulation thickness of the electrode (Dayton *et al.*, 1980). As a result, a geometric correction factor, G, is introduced to account for these influences:

$$i_{ss} = G\frac{nFADc}{r}$$ **Equation 2.11**

The resulting current is directly proportional to the diffusion coefficient and substrate concentration.

2.5 Enzymes

Enzymes are highly selective and efficient biological catalysts, they increase the rate of the reaction without being used up and in some cases can accelerate reactions by a factor of as much as a million (Berg, Tymoczko and Stryer, 2012). Nearly all enzymes are proteins and can be classified into six groups based on the general class of organic chemical reaction that the enzyme catalyses. The six groups are oxidoreductases, transferases, hydrolases, lyases, isomerases and ligases (Kennedy and Lloyd, 1994). Enzymes exhibit high specificity in both the reactions they catalyse and in their choice of reactants and usually only catalyses a single chemical reaction (Berg, Tymoczko and Stryer, 2012). As a result of this they are a highly sought after and useful tools in biosensor fabrication. In this research project the use of POx was essential for the development of the pyruvate biosensor.

Enzymes are constructed from long chains of amino acids which are folded into complex structures which in turn produces the active site of the enzyme where the substrate reaction of interest takes place. These active sites have a three-dimensional cleft or indentation on the enzyme surface, which is complementary in shape to the substrate, this is known as geometric complementarity. The amino acid residues that form the binding site are arranged in such a way as to attract the substrate, this is known as electronic complementarity (Voet, Voet and Pratt, 2003). POx is an oxidoreductase enzyme, it is a tetramer of identical subunits each of which contains a tightly non-covalently bound FAD, TPP and Mg^{2+} which anchors the diphosphate moiety of the TPP (Tittmann *et al.*, 2000). A general oxidase enzyme reaction process for a first-generation biosensor is shown below in Figure 2.2.

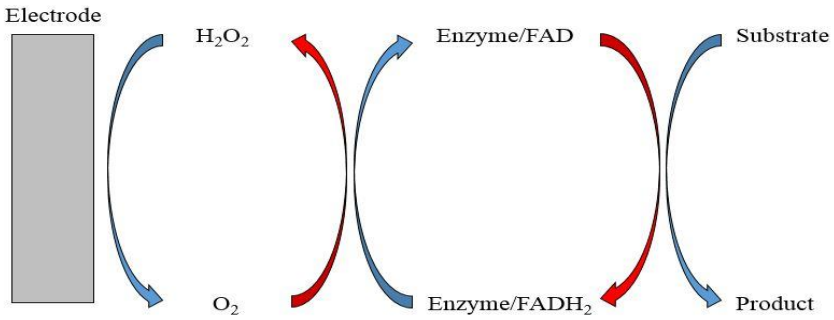

Figure 2.2: Generalised reaction schematic for an oxidase enzyme on a first generation biosensor. The red arrows indicate reduction and the blue arrows indicate oxidation. The oxidation of H_2O_2 is a $2e^-$ transfer which results in a current directly proportional to the substrate concentration.

2.5.1 Enzyme Kinetics

Enzymes have a highly complex nature which in turn leads to complex reaction mechanisms with many variables. These reactions can however be generalised in order to determine the overall kinetic parameters of a specific reaction, shown below in Equation 2.12:

$$E + S \underset{k_{-1}}{\overset{k_1}{\rightleftharpoons}} ES \underset{k_{-2}}{\overset{k_2}{\rightleftharpoons}} E + P \qquad \textbf{Equation 2.12}$$

Where E is the enzyme molecule, S is the substrate, ES is the enzyme-substrate complex, P is the product and k_x is the rate constant where x = 1, -1, 2 or -2. Initially it is found in a reaction that the concentration of the product, P, is low and thus the reverse reaction of product to enzyme-substrate complex, indicated by k_{-2}, is negligible. This results in Equation 2.13, shown below.

$$E + S \underset{k_{-1}}{\overset{k_1}{\rightleftharpoons}} ES \xrightarrow{k_2} E + P \qquad \textbf{Equation 2.13}$$

In 1913 Leonar Michaelis and his student Maud Menten formulated a simple method to account for the kinetic characteristics, they applied the steady-state approximation to the formation and destruction of ES and subsequently derived a rate equation for an enzymatic catalysed reaction (Johnson and Goody, 2011). As a result, the rate of change of ES with time is given by:

$$\frac{d[ES]}{dt} = k_1\,[E][S] - k_{-1}[ES] - k_2[ES] \qquad \textbf{Equation 2.14}$$

Where [E] is the concentration of the unbound enzyme and [ES] is the concentration of the bound enzyme. Hence the total enzyme concentration, $[E]_0$ can be substituted to give Equation 2.15.

$$[E] = [E]_0 - [ES] \qquad \textbf{Equation 2.15}$$

Therefore,

$$\frac{d[ES]}{dt} = k_1\,[E]_0[S] - k_{-1}[ES][S] - k_{-1}[ES] - k_2[ES] \qquad \textbf{Equation 2.16}$$

As stated above the steady-state approximation was applied which indicates the concentration of [ES] remains constant and as a result $\frac{\mathrm{d[ES]}}{\mathrm{dt}} = 0$, which gives:

$$k_1\,[E]_0[S] - k_{-1}[ES][S] - k_{-1}[ES] - k_2[ES] = 0 \qquad \textbf{Equation 2.17}$$

It is possible to isolate the enzyme-substrate [ES] concentration from the above equation to give Equation 2.18:

$$[ES] = \frac{[E]_0[S]}{[S] + \frac{k_{-1} + k_2}{k_1}} \qquad \textbf{Equation 2.18}$$

Michaelis and Menten introduced the Michaelis constant, K_m to replace $\frac{k_{-1} + k_2}{k_1}$ which reduced Equation 2.18 to:

$$[ES] = \frac{[E]_0[S]}{[S] + K_m} \qquad \textbf{Equation 2.19}$$

However, the overall rate of reaction, *v*, is dependent on the concentration of [ES] and the rate of formation of the products, k_2, and is given by:

$$v = k_2[ES] \qquad \textbf{Equation 2.20}$$

Substituting Equation 2.20 into Equation 2.19 gives:

$$v = \frac{k_2[E]_0[S]}{[S] + K_m} \qquad \textbf{Equation 2.21}$$

If the concentration of the substrate is very high in comparison to the enzyme, then the enzyme will only exist as the complex ES and as a result the rate of reaction can reach its maximal initial velocity, V_{max}. Thus, since [S] >> K_m:

$$V_{max} = k_2[E]_0 \qquad \textbf{Equation 2.22}$$

Then

$$v = \frac{V_{max}\,[S]}{[S] + K_m} \qquad \textbf{Equation 2.23}$$

It can be further assumed that the substrate is actually present in a much higher concentration than the enzyme. Therefore, the initial substrate concentration, $[S]_0$, is much higher than the initial enzyme concentration, $[E]_0$, and so $[S] = [S]_0$ which results in Equation 2.23 becoming:

$$v = \frac{V_{max}\,[S]_0}{[S]_0 + K_m} \qquad \textbf{Equation 2.24}$$

Equation 2.24 is the Michaelis-Menten equation where v is the rate of reaction, V_{max} is the maximal initial velocity, $[S]_0$ is the initial substrate concentration and K_m is the Michaelis constant. When experimental values of *v* are plotted against $[S]_0$, shown below in Figure 2.3, a rectangular hyperbola is observed. From the graph the maximal initial velocity, V_{max}, is observed at a particular enzyme concentration $[E]_0$. The K_m can also be determined from the graph as it is the substrate concentration at $v = \frac{V_{max}}{2}$.

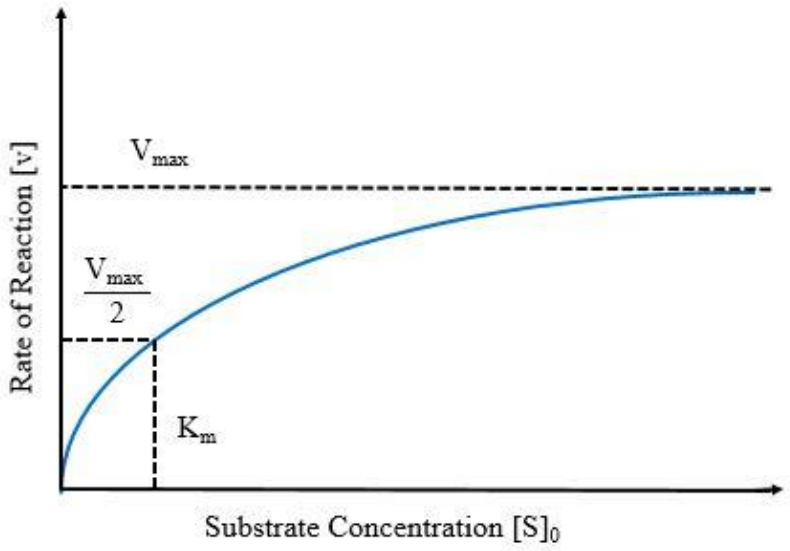

Figure 2.3: Michaelis-Menten kinetics graph which shows the plot of reaction rate (v) against substrate concentration ($[S]_0$) for an enzyme concentration ($[E]_0$) for a single substrate enzyme catalysed reaction.

Michaelis-Menten kinetics is a very useful analytical tool due to its simplicity in making approximations, however, it fails to take into account certain specific circumstances which can occur. One such circumstance is when more than one molecule of substrate binds to a single molecule of enzyme which results in a sigmoidal binding curve as opposed to the hyperbolic one seen in Figure 2.3. In circumstances where this co-operative effect is observed the binding of a substrate to one active site on the enzyme increases the affinity of other active sites on the enzyme to bind more molecules of the substrate (Ricard and Cornish-Bowden, 1987). As a result of this altercations were made to the Michaelis-Menten equation to account for the sigmoidal behaviour and involved the introduction of the constant α (Hill, 1921). The new form of the equation, given in Equation 2.25, is known as the Michaelis-Menten Hill-type equation (Hill, 1913, 1921; Lowry *et al.*, 1994):

$$i = \frac{V_{max}}{1 + \left(\frac{K_m}{[S]}\right)^{\alpha}} \qquad \textbf{Equation 2.25}$$

where i is the observed current for the oxidation of H_2O_2 at the electrode surface. The α value characterises the deviation from ideal Michaelis-Menten kinetics. An α value of 1 indicates ideal Michaelis-Menten behaviour. Values for α that are less than 1 indicate negative cooperativity and conversely α values greater than 1 suggest positive cooperativity, and thus sigmoidal behaviour.

2.6 Structures and Reactions

This section provides an overview of the various other chemicals of importance utilised throughout this research project such as the substrate of interest, co-factors and interferants among others. Details of their relevant structures and reactions of interest are also given.

2.6.1 Pyruvate

Pyruvate is a non-essential nutrient that can be naturally synthesised in the cells of the body. It is the simplest of the alpha-keto acids with a carboxylic acid and ketone functional group (see Figure 2.5). As outlined above, it is a key intermediate product in the glycolytic pathway which is responsible for biological energy production (Akyilmaz and Yorganci, 2007). The normal concentration of pyruvate in the human body is accepted to be in the range of 40-120 µM in blood (Arai *et al.*, 1999) and between 120-300 µM for basal brain levels (Reinstrup *et al.*, 2000; Zetterling *et al.*, 2009; Cordeiro *et al.*, 2015). However, it has also been reported to be as low as 5 – 10 µM in traumatic brain injury (TBI) patients (Gowers *et al.*, 2019).

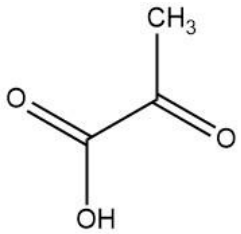

Figure 2.5: Structure of Pyruvate.

Pyruvate is a chemical of great interest and importance in biochemistry. Examples of this include Pyruvate dehydrogenase complex deficiency (PDCD) which is a neurological disorder caused by the build-up of lactic acid. The effects of this disorder range from fatal in the new born period (lactic acidosis), to severe in the form of a chronic neurodegenerative condition with gross structural abnormalities in the central nervous system (Brown *et al.*, 1994). Pyruvate kinase deficiency (PKD), a red blood cell enzyme defect, is another common pyruvate related disease of great interest. It is the most common among glycolytic defects causing chronic non-spherocytic haemolytic anemia (Zanella *et al.*, 2005). It has also been found that due to the brains high reliance on glucose and pyruvate metabolism to generate cellular energy that abnormalities in these have severe consequences and altered pyruvate metabolism has been found in major neurodegenerative disorders such as Leigh's syndrome, Parkinson's disease and Alzheimer's disease (Gray, Tompkins and Taylor, 2014). POx uses oxygen and phosphate for the catalytic oxidative decarboxylation of pyruvate to acetyl phosphate and H_2O_2 in the presence of co-factors FAD, TPP and Mg^{2+} shown below:

$$\text{Pyruvate} + \text{Phosphate} + O_2 + H_2O \xrightarrow[\text{FAD, TPP, } Mg^{2+}]{\text{POx}} \text{Acetyl phosphate} + CO_2 + H_2O_2$$

2.6.2 Flavin Adenine Dinucleotide

FAD is a large molecule, shown below in Figure 2.6, and is one of two flavoprotein coenzymes derived from riboflavin (vitamin B_2). FAD is the rate limiting factor in most enzymatic processes (Kennedy, 2016). FAD is reduced as the pyruvate molecule is oxidised and it is then re-oxidised by molecular oxygen to produce H_2O_2, the reactive components are shown in Figure 2.7, (Berg, Tymoczko and Stryer, 2012).

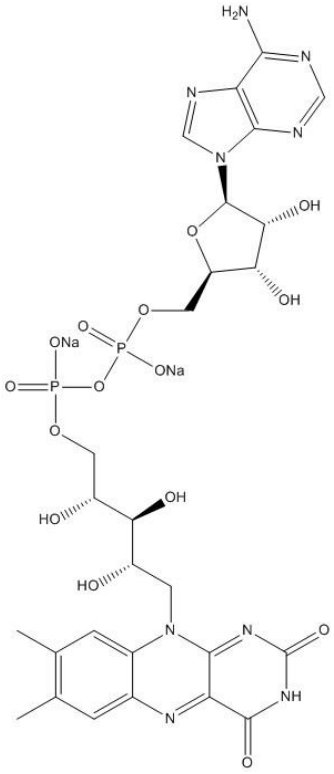

Figure 2.6: Structure of FAD.

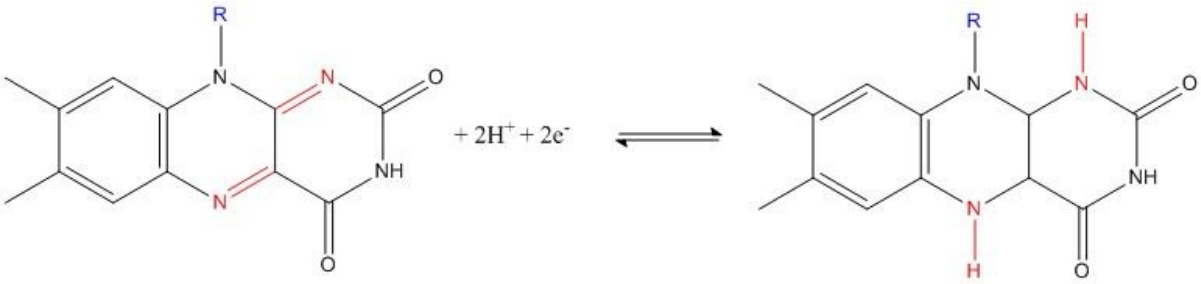

Figure 2.7: Oxidised and reduced forms of FAD.

2.6.3 Thiamine Pyrophosphate

TPP is one of multiple derivatives of thiamine (vitamin B_1), shown in Figure 2.8, and serves as a cofactor for a range of enzymes that are involved in energy metabolism (Fattal-Valevski, 2011). The role of TPP is nucleophilic attack of the carbonyl group of the substrate, pyruvate (Figure 2.9) (Tittmann *et al.*, 2000). TPP also binds to a divalent metal cation, such as Mg^{2+},

forming a metal-cofactor complex which is the actual co-factor and indicates quite a passive role for the Mg^{2+} (Blake *et al.*, 1982).

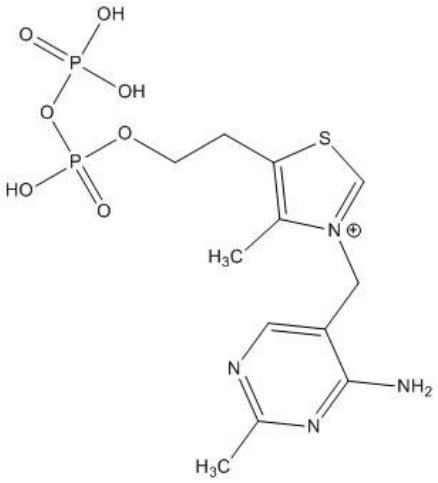

Figure 2.8: Structure of TPP.

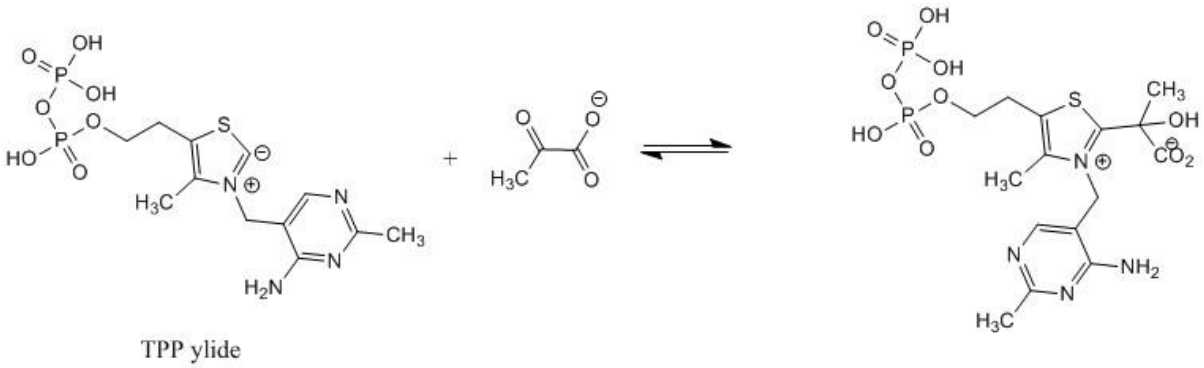

Figure 2.9: Structures of the nucleophilic addition of pyruvate to the TPP ylide.

2.6.4 Hydrogen Peroxide

Pt has been extensively used by various research groups as an electrochemical catalyst for the oxidation of H_2O_2 in amperometric biosensors which incorporate an enzyme (Clark and Lyons, 1962; Lowry *et al.*, 1994; Rocchitta *et al.*, 2013; Baker *et al.*, 2019). These are known as first generation biosensors and are based on the utilisation of an enzyme reaction to generate H_2O_2, the rate of oxidation of which is directly proportional to the analyte concentration (Hall,

Khudaish and Hart, 1998). The oxidation process is a well-known and characterised two electron transfer, it was first proposed by Hickling and Wilson and was further investigated by Lingane and Lingane (Hickling and Wilson, 1951; Lingane and Lingane, 1963). It is based on the formation of a thin oxide film on the Pt surface which is reduced by H_2O_2. The generated current is attributed to the re-oxidation of the Pt, and the mechanism for the oxidation is outlined below in Equations 2.26, 2.27 and 2.28. (Hall, Khudaish and Hart, 1998).

$$H_2O_2 + Pt(OH)_2 \rightleftharpoons Pt(OH)_2.H_2O_2 \qquad \textbf{Equation 2.26}$$

$$Pt(OH)_2.H_2O_2 \rightleftharpoons Pt + 2H_2O + O_2 \qquad \textbf{Equation 2.27}$$

$$Pt + 2H_2O \rightleftharpoons Pt(OH)_2 + 2H^+ + 2e^- \qquad \textbf{Equation 2.28}$$

Equation 2.26 details the complex formation between the oxide film and the H_2O_2 which then breaks down in Equation 2.27 to release water, oxygen and leave behind an un-oxidised metal surface. Finally, in Equation 2.28 water recombines with the Pt surface and releases two protons and two electrons and it is these two electrons that generate the current that is measured at the electrode surface.

2.6.5 Electropolymerisation of *o*-Phenylenediamine

The inclusion of a poly-*o*-phenylenediamine (PPD) interference rejection layer in enzyme-based amperometric biosensor design has been utilised on multiple occasions in the past (Lowry *et al.*, 1994; McMahon *et al.*, 2007; Turkmen *et al.*, 2014; Baker *et al.*, 2019; Ganesana *et al.*, 2019). PPD is deposited electrochemically from *o*-phenylenediamine (*o*-PD) onto the electrode surface which produces a thin self-sealing insulated polymer on the electrode surface (Killoran and O'Neill, 2008). The film thickness of the PPD layer is in the region of 10 – 35 nm (Malitesta *et al.*, 1990; Myler, Eaton and Higson, 1997), and it is this ultra-thin nature that

enables it to efficiently immobilise while not compromising enzyme activity (Rothwell, McMahon and O'Neill, 2010). Another highly significant advantage of PPD is its high permeability to small molecules, such as enzyme generated H_2O_2 while rejecting larger electroactive substances, such as ascorbic acid (AA) (Craig and O'Neill, 2003; Rothwell, McMahon and O'Neill, 2010).

While the structure of the PPD layer and the mechanism by which it occurs, as shown in this work, is still not yet fully understood extensive work has been carried out and two structures have been hypothesised (Prună and Brânzoi, 2012). The two proposed structures appear to be dependent on the conditions in which the polymerisation is carried out. It is believed that under conditions of low pH (<1) the structure observed is a phenazine-like "ladder" structure, as shown in Figure 2.10 (A), whereas when the pH is increased conjugation decreases and more free amino groups are detected on the surface which suggests the PPD film formed in an "open" structure, shown in Figure 2.10 (B), (Losito, Palmisano and Zambonin, 2003; Samanta, Roy and Kar, 2015).

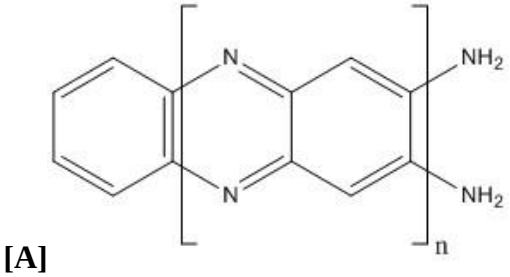

[A]

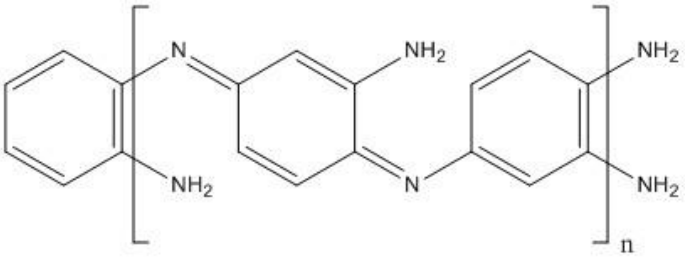

[B]

Figure 2.10: Proposed structures of the polymeric forms of *o*-PD where [A] is the "ladder" structure and [B] is the "open" structure.

2.6.6 Ascorbic Acid

AA is one of the principal electroactive species in the extracellular fluid (ECF) with a concentration of 500 µM (Grünewald, 1993). It has a half-wave potential of a redox couple ($E_{1/2}$) of between -100 to +400 mV (*vs.* SCE) (O'Neill, Lowry and Mas, 1998). The mechanism for the oxidation of AA at the metal electrode surface (Figure 2.11) is a $2H^+$, $2e^-$ process which results in the formation of L-dehydroascorbic acid which is then rapidly hydrolysed in an irreversible reaction to give the electro-inactive open chain product L-2,3-diketogluonic acid.

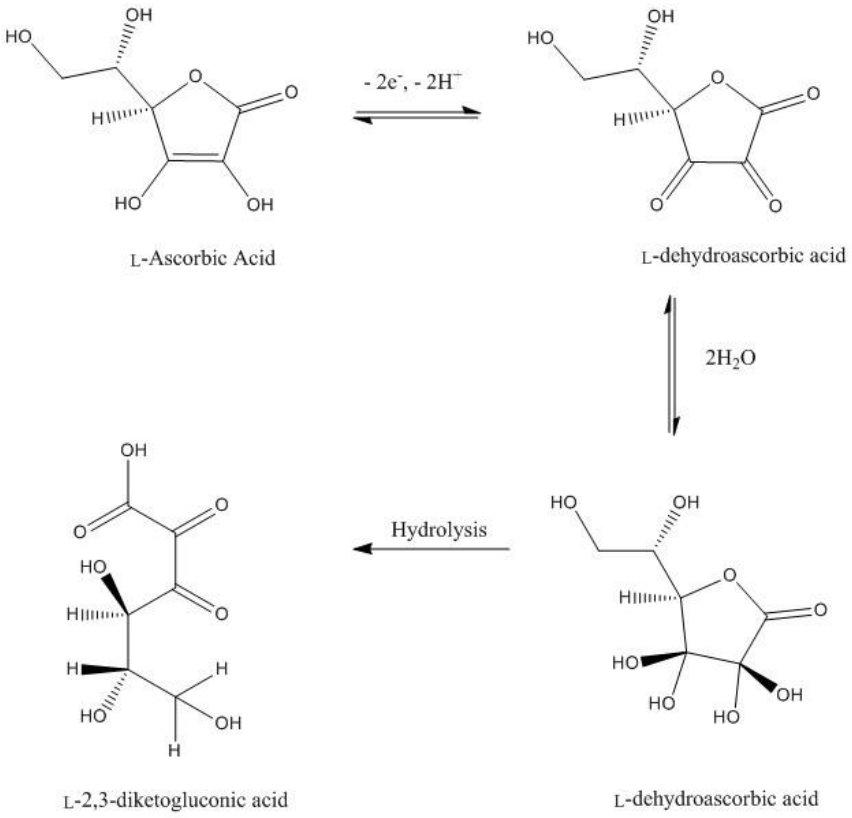

Figure 2.11: Reaction scheme for the oxidation of AA.

2.7 Data Analysis

All calibration data was analysed after the cessation of the experiments using linear and/or non-linear regression. A time averaged response was extracted using eDAQ® Chart. This sample

was taken from a steady-state response period. These extracted data samples were then transferred to GraphPad Prism 8 where the regression analysis was applied and the values plotted on a graph of current response against substrate concentration.

2.7.1 Linear and Non-Linear Regression

Regression fitting involves finding a line or a curve which minimises the sum of the squares of the perpendicular distances of the points to the fitted line or curve, while linear regression is also known as the line of best fit. Linear regression fits were applied to calibrations for responses to, e.g., AA, while non-linear regression fits, taking the form of the Michaelis-Menten equation and the Michaelis-Menten Hill-Type equation (see Section 2.5.1), were applied to enzymatic calibrations for responses to pyruvate. Upon completing linear and non-linear regression various other statistical analyses (see below) were performed on each data set in order to gain additional information and allow comparisons to be made.

2.7.2 Statistical Analysis

Statistical analysis is carried out to determine if there is a significant difference between various sets of data. Various different types of statistical analysis were utilised throughout this research project depending on the type of experimental data obtained. A t-test was used to compare results from two data sets. There are two forms of t-test that can be carried out, paired t-tests and un-paired t-tests. Paired t-tests were used to examine data from the same electrodes which differed only by post-production intervention, e.g., repeated calibrations. While un-paired t-tests were used to examine different electrodes which did differ in their production method, for example different layering processes or the incorporation of different biosensor components. The t-tests were performed using GraphPad Prism 8 and yielded a resulting p-value and t-value.

The assigned p-value is a probability, thus its value lies between $0 \leq p \leq 1$. It describes the statistical difference between two values and allows one to decide whether or not it is significantly different. The smaller the p-value is the more likely it is to be significantly different. A confidence interval of 95 % was used throughout this project, which means a p-

value of < 0.05 is required to indicate a significant difference between two data sets. A p-value greater than 0.05 indicates there is a significant difference between the data sets. The t-value measures the size of the difference relative to the variation in your sample data The greater the magnitude of t, the greater the evidence against the null hypothesis.

The R^2 value, also known as the coefficient of correlation, is the measure of the goodness of fit of a data set to a regression (non-linear and linear). Similar to the p-value it is a unit-less value with a range of $0 \leq R^2 \leq 1$. A value of 0 indicates there is no relationship between the X and Y values in the data set. While a value of 1 indicates a perfect fit where all points lie directly on the line or curve which is proposed as the fit. One-way Analysis of Variance (ANOVA) with a standard Tukey Multiple comparison test was used to compare results from three or more data sets. This method was used to examine electrodes which differed only by postproduction intervention, for example investigating the effect of changing temperature or pH on the electrode performance. The degrees of freedom (F) is the ratio of two mean square values given as $F_{(DFn,\ DFd)}$. DFn is the degree of freedom for the numerator of the F ratio, and DFd is the degree of freedom for the denominator. A large F ratio is seen both when the null hypothesis is wrong (the data are not sampled from populations with the same mean) and when random sampling happened to end up with large values in some groups and small values in others. If the null hypothesis is true, $F \approx 1$ (Feinleib and Zar, 1975). The ANOVA was performed using GraphPad Prism 8 and yielded p-values for the overall comparison as well as multiple comparisons.

Current density was also used as a comparative method due to the use of varying sizes and geometries of electrodes and to facilitate comparisons with the literature. This process requires normalising the currents to the surface area of the electrode from which the currents are obtained.

$$J = \frac{I}{A} \qquad \textbf{Equation 2.28.}$$

Where J is the current density, I is the current flowing and A is the active surface area of the electrode. Thus, the current per unit area is given as J ($\mu A.cm^{-2}$).

2.8 References

Akyilmaz, E. and Yorganci, E. (2007) 'Construction of an amperometric pyruvate oxidase enzyme electrode for determination of pyruvate and phosphate', *Electrochimica Acta*, 52(28), pp. 7972–7977. doi:10.1016/j.electacta.2007.06.058.

Arai, G., Noma, T., Habu, H. and Yasumori, I. (1999) 'Pyruvate sensor based on pyruvate oxidase immobilized in a poly(mercapto-p-benzoquinone) film', *Journal of Electroanalytical Chemistry*, 464(2), pp. 143–148. doi:10.1016/S0022-0728(99)00011-X.

Baker, K.L., Bolger, F.B., Doran, M.M. and Lowry, J.P. (2019) 'Characterisation of a Platinum-based Electrochemical Biosensor for Real-time Neurochemical Analysis of Choline', *Electroanalysis*, 31(1), pp. 129–136. doi:10.1002/elan.201800642.

Bard, A.J. and Faulkner, L.R. (2000) *Electrochemical Methods: Fundamentals and Applications*. Wiley. Available at: https://books.google.ie/books?id=kv56QgAACAAJ.

Berg, J.M., Tymoczko, J.L. and Stryer, L. (2012) *Biochemistry*. Basingstoke: W.H. Freeman.

Blake, R., O'Brien, T.A., Gennis, R.B. and Hager, L.P. (1982) 'Role of the divalent metal cation in the pyruvate oxidase reaction.', *Journal of Biological Chemistry*, 257(16), pp. 9605–9611.

Brett, C.M.A. and Brett, A.M.O. (1993) *Electrochemistry: Principles, Methods, and Applications*. Oxford University Press (Oxford science publications). Available at: https://books.google.ie/books?id=NmmeQgAACAAJ.

Brown, G.K., Otero, L.J., LeGris, M. and Brown, R.M. (1994) 'Pyruvate dehydrogenase deficiency', *Journal of Medical Genetics*, 31(11), pp. 875–879. doi:10.1136/jmg.31.11.875.

Ciobanu, M., Wilburn, J.P., Krim, M.L. and Cliffel, D.E. (2007) 'Fundamentals', in Zoski, C.G. (ed.) *Handbook of Electrochemistry*. Amsterdam: Elsevier, pp. 3–29. doi:10.1016/B978-044451958-0.50002-1.

Clark, L.C. and Lyons, C. (1962) 'Electrode Systems for Continuous Monitoring in Cardiovascular Surgery', *Annals of the New York Academy of Sciences*, 102(1), pp. 29–45. doi:10.1111/j.1749-6632.1962.tb13623.x.

Cordeiro, C.A., de Vries, M.G., Ngabi, W., Oomen, P.E., Cremers, T.I.F.H. and Westerink, B.H.C. (2015) 'In vivo continuous and simultaneous monitoring of brain energy substrates with a multiplex amperometric enzyme-based biosensor device', *Biosensors and Bioelectronics*, 67, pp. 677–686. doi:10.1016/j.bios.2014.09.101.

Craig, J.D. and O'Neill, R.D. (2003) 'Comparison of simple aromatic amines for electrosynthesis of permselective polymers in biosensor fabrication', *Analyst*, 128(7), pp. 905–911. doi:10.1039/b302833j.

Dayton, M.A., Brown, J.C., Stutts, K.J. and Wightman, R.M. (1980) 'Faradaic Electrochemistry at Microvoltammetric Electrodes', *Analytical Chemistry*, 52(6), pp. 946–950. doi:10.1021/ac50056a040.

Elgrishi, N., Rountree, K.J., McCarthy, B.D., Rountree, E.S., Eisenhart, T.T. and Dempsey, J.L. (2018) 'A Practical Beginner's Guide to Cyclic Voltammetry', *Journal of Chemical Education*, 95(2), pp. 197–206. doi:10.1021/acs.jchemed.7b00361.

Fattal-Valevski, A. (2011) 'Thiamine (vitamin B 1)', *Complementary Health Practice Review*, 16(1), pp. 12–20. doi:10.1177/1533210110392941.

Feinleib, M. and Zar, J.H. (1975) *Biostatistical Analysis.*, *Journal of the American Statistical Association*. Prentice Hall. doi:10.2307/2285423.

Fisher, A.C. (1996) *Electrode Dynamics*. Oxford University Press (Oxford chemistry primers). Available at: https://books.google.com/books?id=KVCWQgAACAAJ&pgis=1.

Forster, R.J. (1994) 'Microelectrodes: New dimensions in electrochemistry', *Chemical Society Reviews*, 23(4), pp. 289–297. doi:10.1039/CS9942300289.

Ganesana, M., Trikantzopoulos, E., Maniar, Y., Lee, S.T. and Venton, B.J. (2019) 'Development of a novel micro biosensor for in vivo monitoring of glutamate release in the brain', *Biosensors and Bioelectronics*, 130, pp. 103–109. doi:https://doi.org/10.1016/j.bios.2019.01.049.

Gowers, S.A.N., Rogers, M.L., Booth, M.A., Leong, C.L., Samper, I.C., Phairatana, T., Jewell, S.L., Pahl, C., Strong, A.J. and Boutelle, M.G. (2019) 'Clinical translation of microfluidic sensor devices: focus on calibration and analytical robustness', *Lab Chip*, 19(15), pp. 2537–

2548. doi:10.1039/C9LC00400A.

Gray, L.R., Tompkins, S.C. and Taylor, E.B. (2014) 'Regulation of pyruvate metabolism and human disease', *Cellular and Molecular Life Sciences*, 71(14), pp. 2577–2604. doi:10.1007/s00018-013-1539-2.

Grünewald, R.A. (1993) 'Ascorbic acid in the brain', *Brain Research Reviews*. Elsevier, pp. 123–133. doi:10.1016/0165-0173(93)90010-W.

Guy, O.J. and Walker, K.A.D. (2016) 'Graphene Functionalization for Biosensor Applications', in Saddow, S.E. (ed.) *Silicon Carbide Biotechnology: A Biocompatible Semiconductor for Advanced Biomedical Devices and Applications: Second Edition*. Second Edi. Elsevier, pp. 85–141. doi:10.1016/B978-0-12-802993-0.00004-6.

Hall, S.B., Khudaish, E.A. and Hart, A.L. (1998) 'Electrochemical oxidation of hydrogen peroxide at platinum electrodes. Part II: Effect of potential', *Electrochimica Acta*, 43(14–15), pp. 2015–2024. doi:10.1016/S0013-4686(97)10116-5.

Hanson, K.M., Pappas, T.J. and Holland, L.A. (2005) 'Electrochemical detection in capillary electrophoresis', in Marina, M.L., Ros, A., and Valcrcel, M. (eds) *Comprehensive Analytical Chemistry*. Elsevier (Comprehensive Analytical Chemistry), pp. 413–440. doi:10.1016/S0166-526X(05)45008-4.

Hickling, A. and Wilson, W.H. (1951) 'The Anodic Decomposition of Hydrogen Peroxide', *Journal of The Electrochemical Society*, 98(11), p. 425. doi:10.1149/1.2778020.

Hill, A.V. (1913) 'The Combinations of Haemoglobin with Oxygen and with Carbon Monoxide. I', *Biochemical Journal*, 7(5), pp. 471–480. doi:10.1042/bj0070471.

Hill, A.V. (1921) 'The Combinations of Haemoglobin with Oxygen and Carbon Monoxide, and the effects of Acid and Carbon Dioxide', *Biochemical Journal*, 15(5), pp. 577–586. doi:10.1042/bj0150577.

Janzen, A.F. (1979) 'Photoelectrochemistry I — Photoelectrolysis', in DIXON, A.E. and LESLIE, J.D. (eds) *Solar Energy Conversion*. Pergamon, pp. 905–921. doi:10.1016/b978-0-08-024744-1.50035-8.

Johnson, K.A. and Goody, R.S. (2011) 'The original Michaelis constant: Translation of the 1913 Michaelis-Menten Paper', *Biochemistry*, 50(39), pp. 8264–8269. doi:10.1021/bi201284u.

Kennedy, D.O. (2016) 'B vitamins and the brain: Mechanisms, dose and efficacy—A review', *Nutrients*, 8(2), p. 68. doi:10.3390/nu8020068.

Kennedy, J.F. and Lloyd, L.L. (1994) *Enzyme nomenclature — Recommendations of the Nomenclature Committee of the International Union of Biochemistry and Molecular Biology*, *Carbohydrate Polymers*. San Diego, California, USA: Academic Press. doi:10.1016/0144-8617(94)90194-5.

Killoran, S.J. and O'Neill, R.D. (2008) 'Characterization of permselective coatings electrosynthesized on Pt-Ir from the three phenylenediamine isomers for biosensor applications', *Electrochimica Acta*, 53(24), pp. 7303–7312. doi:10.1016/j.electacta.2008.03.076.

Lingane, J.J. and Lingane, P.J. (1963) 'Chronopotentiometry of hydrogen peroxide with a platinum wire electrode', *Journal of Electroanalytical Chemistry*, 5(6), pp. 411–419. doi:10.1016/0022-0728(63)80050-9.

Losito, I., Palmisano, F. and Zambonin, P.G. (2003) 'O-Phenylenediamine Electropolymerization By Cyclic Voltammetry Combined With Electrospray Ionization-Ion Trap Mass Spectrometry', *Analytical Chemistry*, 75(19), pp. 4988–4995. doi:10.1021/ac0342424.

Lowry, J.P., McAteer, K., El Atrash, S.S., Duff, A. and O'Neill, R.D. (1994) 'Characterization of Glucose Oxidase-Modified Poly(phenylenediamine)-Coated Electrodes in Vitro and in Vivo: Homogeneous Interference by Ascorbic Acid in Hydrogen Peroxide Detection', *Analytical Chemistry*, 66(10), pp. 1754–1761. doi:10.1021/ac00082a025.

Malitesta, C., Palmisano, F., Torsi, L. and Zambonin, P.G. (1990) 'Glucose fast-response amperometric sensor based on glucose oxidase immobilized in an electropolymerized poly(o-phenylenediamine) film', *Analytical Chemistry*, 62(24), pp. 2735–2740. doi:10.1021/ac00223a016.

McMahon, C.P., Rocchitta, G., Kirwan, S.M., Killoran, S.J., Serra, P.A., Lowry, J.P. and

O'Neill, R.D. (2007) 'Oxygen tolerance of an implantable polymer/enzyme composite glutamate biosensor displaying polycation-enhanced substrate sensitivity', *Biosensors and Bioelectronics*, 22(7), pp. 1466–1473. doi:https://doi.org/10.1016/j.bios.2006.06.027.

Myler, S., Eaton, S. and Higson, S.P.J. (1997) 'Poly(o-phenylenediamine) ultra-thin polymer-film composite membranes for enzyme electrodes', *Analytica Chimica Acta*, 357(1–2), pp. 55–61. doi:10.1016/S0003-2670(97)00558-8.

Newman , Thomas-Alyea, Karen E., J.S. (2004) *Electrochemical systems*. Hoboken, N.J.: J. Wiley.

O'Neill, R.D., Lowry, J.P. and Mas, M. (1998) 'Monitoring brain chemistry in vivo: Voltammetric techniques, sensors, and behavioral applications', *Critical Reviews in Neurobiology*, 12(1–2), pp. 69–127. doi:10.1615/CritRevNeurobiol.v12.i1-2.40.

Oldham, K.B. (1991) 'Steady-State Voltammetry', in Montenegro, M.I., Queirós, M.A., and Daschbach, J.L. (eds) *Microelectrodes: Theory and Applications*. Dordrecht: Springer Netherlands, pp. 35–50. doi:10.1007/978-94-011-3210-7_3.

Prună, A. and Brânzoi, F. (2012) 'Electrochemical activity and microscopy of electrosynthesised poly(o-phenylenediamine) nanotubes', *Journal of Polymer Research*, 19(6), p. 9879. doi:10.1007/s10965-012-9879-4.

Reinstrup, P., Ståhl, N., Mellergård, P., Uski, T., Ungerstedt, U. and Nordström, C.H. (2000) 'Intracerebral microdialysis in clinical practice: Baseline values for chemical markers during wakefulness, anesthesia, and neurosurgery', *Neurosurgery*, 47(3), pp. 701–710. doi:10.1227/00006123-200009000-00035.

Ricard, J. and Cornish-Bowden, A. (1987) 'Co-operative and allosteric enzymes: 20 years on', *European Journal of Biochemistry*, 166(2), pp. 255–272. doi:10.1111/j.1432-1033.1987.tb13510.x.

Rocchitta, G., Secchi, O., Alvau, M.D., Farina, D., Bazzu, G., Calia, G., Migheli, R., Desole, M.S., O'Neill, R.D. and Serra, P.A. (2013) 'Simultaneous telemetric monitoring of brain glucose and lactate and motion in freely moving rats', *Analytical Chemistry*, 85(21), pp. 10282–10288. doi:10.1021/ac402071w.

Rocchitta, G., Spanu, A., Babudieri, S., Latte, G., Madeddu, G., Galleri, G., Nuvoli, S., Bagella, P., Demartis, M.I., Fiore, V., Manetti, R. and Serra, P.A. (2016) 'Enzyme biosensors for biomedical applications: Strategies for safeguarding analytical performances in biological fluids', *Sensors (Switzerland)*. Multidisciplinary Digital Publishing Institute, p. 780. doi:10.3390/s16060780.

Ronkainen, N.J., Halsall, H.B. and Heineman, W.R. (2010) 'Electrochemical biosensors', *Chemical Society Reviews*, 39(5), pp. 1747–1763. doi:10.1039/b714449k.

Rothwell, S.A., McMahon, C.P. and O'Neill, R.D. (2010) 'Effects of polymerization potential on the permselectivity of poly(o-phenylenediamine) coatings deposited on Pt-Ir electrodes for biosensor applications', *Electrochimica Acta*, 55(3), pp. 1051–1060. doi:10.1016/j.electacta.2009.09.069.

Samanta, S., Roy, P. and Kar, P. (2015) 'Influence of pH of the Reaction Medium on the Structure and Property of Conducting Poly(o-Phenylenediamine)', *Materials Today: Proceedings*, 2(4), pp. 1301–1308. doi:https://doi.org/10.1016/j.matpr.2015.07.046.

Tittmann, K., Golbik, R., Ghisla, S. and Hubner, G. (2000) 'Mechanism of elementary catalytic steps of pyruvate oxidase from Lactobacillus plantarum.', *Biochemistry*, 39(35), pp. 10747–10754. doi:10.1021/bi0004089.

Turkmen, E., Bas, S.Z., Gulce, H. and Yildiz, S. (2014) 'Glucose biosensor based on immobilization of glucose oxidase in electropolymerized poly(o-phenylenediamine) film on platinum nanoparticles-polyvinylferrocenium modified electrode', *Electrochimica Acta*, 123, pp. 93–102. doi:https://doi.org/10.1016/j.electacta.2013.12.189.

Vetter, K.J. (1967) 'Electrochemical Thermodynamics', in VETTER, K.J. (ed.) *Electrochemical Kinetics*. Academic Press, pp. 1–103. doi:10.1016/b978-1-4832-2936-2.50005-6.

Voet, J.G., Voet, D. and Pratt, C.W. (2003) *Fundamentals of Biochemistry: Life at the Molecular Level, 2nd Edition*. Hoboken, NJ: Wiley.

Zanella, A., Fermo, E., Bianchi, P. and Valentini, G. (2005) 'Red cell pyruvate kinase deficiency: Molecular and clinical aspects', *British Journal of Haematology*, 130(1), pp. 11–

25. doi:10.1111/j.1365-2141.2005.05527.x.

Zetterling, M., Hillered, L., Samuelsson, C., Karlsson, T., Enblad, P. and Ronne-Engström, E. (2009) 'Temporal patterns of interstitial pyruvate and amino acids after subarachnoid haemorrhage are related to the level of consciousness-a clinical microdialysis study', *Acta Neurochirurgica*, 151(7), pp. 771–780. doi:10.1007/s00701-009-0384-4.

Chapter 3:

Experimental

3.1 Introduction

In this chapter the materials and methods used to develop and characterise a pyruvate biosensor *in-vitro* and *in-vivo* are outlined. The biosensor design builds on previous work by members of the research group who have used a Platinum (Pt) based biosensor (Finnerty *et al.*, 2012; Baker *et al.*, 2019) These biosensors utilise an immobiliser such as styrene (Sty) or methyl methacrylate (MMA) and use the dip adsorption method to place the enzyme onto the Pt surface (Doran, Finnerty and Lowry, 2017; Baker *et al.*, 2019). The electropolymerisation of *o*-phenylenediamine (*o*-PD) has also been a regularly utilised method for interference rejection of endogenous electroactive species (O'Neill *et al.*, 2008; Doran, Finnerty and Lowry, 2017; Knyzhnykova *et al.*, 2018).

Section 3.2 details all the computer-based instrumentation and equipment, while in Section 3.3 all the chemicals and solutions used throughout the project are given. Section 3.4 outlines the manufacturing process for the various sensors while Section 3.5 details any modifications carried out. Section 3.6 describes the electrochemical set-up for *in-vitro* development and characterisation experiments, and finally Section 3.7 describes the use of the biosensor in the *in-vivo* environment.

3.2 Computer-Based Instrumentation and Equipment

Experimental data was collected on computer-based instrumentation throughout this research project. The computer-based instrumentation consisted of three main components shown below in Figure 3.1: the potentiostat, the eDAQ e-corder® interface system and the computer. Each of these components and their function are detailed in the next section.

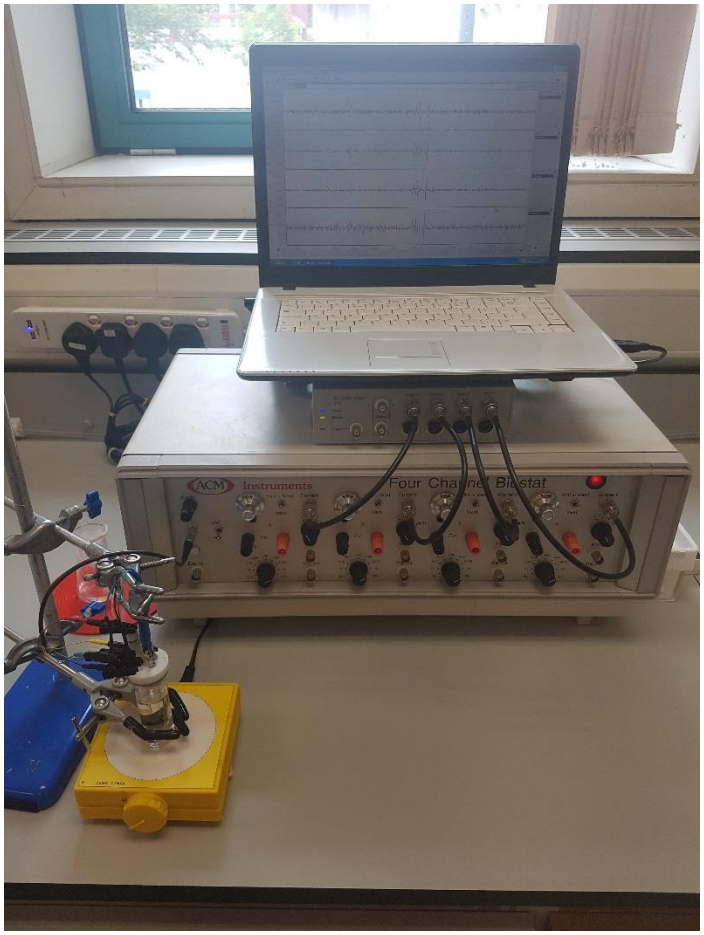

Figure 3.1: The *in-vitro* experimental set-up consisting of the laptop (top), eDAQ e-Corder® (middle) and potentiostat (bottom). The electrochemical cell and magnetic stirrer are in the left foreground.

3.2.1 The Potentiostat

The potentiostat used throughout the research project was a low-noise potentiostat; Biostat IV, ACM Instruments, Cumbria, UK, (Figure 3.2.). The role of the potentiostat was to apply a known potential to the working electrodes and monitor the resulting current.

Figure 3.2: The ACM potentiostat used in the research project.

3.2.2 The eDAQ e-corder®

The eDAQ e-corder® interface system (Greenleaf Scientific, Dublin, Ireland) was used to record and display experimental data. It has digital-to-analogue (DAC) and analogue-to-digital (ADC) converters which allow the potentiostat (analogue) to communicate with the computer (digital). Shown in Figure 3.3 is the eDAQ e-corder 410 (ED410)® that was used throughout this research project.

Figure 3.3: The eDAQ e-corder® interface system (https://www.edaq.com/ED410).

3.2.3 The Computer

A Clevo LogiQ M76T notebook (Intel® Celeron® dual core 1.8 GHz processor) was used throughout the *in-vitro* development and characterisation to store the data and display it in real time. It is shown in Figure 3.1 as part of the *in-vitro* set up.

3.2.4 Computer Programs

Constant potential amperometry (CPA) was carried out and analysed using eDAQ Chart® 5 for windows software. GraphPad Prism (version 8.2.0; GraphPad Software Inc., CA, USA) was used for all data analysis and graphical presentations. The generated signals were baseline subtracted and the calibration curves were fitted with either Michaelis-Menten or Michaelis-Menten Hill-type equations which are explained in more detail in Chapter 2, Section 2.5.1. GraphPad Prism was used to determine which form of enzyme kinetics was most appropriate for each calibration. Results were also fitted using linear regression analysis to determine the sensitivity from the linear region slope (LRS) (Chapter 2, Section 2.7.1). Statistical analysis was also carried out using GraphPad Prism, t-tests (two-tailed paired or unpaired where appropriate) or one-way ANOVA (with Tukey's multiple comparisons test analysis) where values of $P < 0.05$ were considered to indicate statistical significance which is detailed in Chapter 2, Section 2.7.2.

3.2.5 Supplementary Equipment

The following details all other equipment used both *in-vitro* and *in-vivo* throughout the research project.

3.2.5.1 *In-Vitro* Equipment

The electronic balance used was a Sartorius CP225D electronic balance, accurate to ± 0.01 mg, from Sartorius AG, Göttingen, Germany. The pH meter used was the Cyber Scan pH 510 from Eutech Instruments Pte Ltd, Singapore and the magnetic stirrer used was the Yellowline MST mini, all of which were supplied by Lennox, Ireland. The thermal bath used was the Julabo Corio CD-BC4 heating circulator from Julabo GmbH, Germany. The sonicator used was the Fisherbrand FB11002 and the vortex used was the REAX top Vortex, from Heidolph, Germany, all of which were supplied by Fischer Scientific, Dublin, Ireland. The soldering iron used was the WE 1010 Soldering Station, 230V, from Weller, USA. Supplied by Radionics, Ireland. The water purification system utilised was the Milli-Q® Advantage A10 Water Purification System from Merck, Ireland. Finally, the microscope used for electrode fabrication was a stereo microscope (SZ51) from Olympus America Inc. Supplied by Mason Technology Limited, Dublin, Ireland.

3.2.5.2 *In-Vivo* Equipment

The Anaesthetic set-up consisted of a vaporiser for induction (Univentor 400 anaesthesia unit) used in conjunction with a Stellar S30 air pump and a 1.4 L capacity Perspex induction chamber, all of which was supplied by AgnThos, Sweden. The pre-operative anaesthetic set-up was contained within the fume hood while the anaesthetic supplied during surgery came from the same vaporising system and a stereotaxic inhalation mask, this was also supplied by AgnThos, contained within a laminar flow unit from AirScience™. Core body temperature was measured throughout the surgery using a rectal probe and maintained with a heating pad. Both of which were part of the Temperature Control Unit HB 101/2 by Letica Scientific Instruments, Barcelona, Spain. Supplied by World Precision Instruments, Europe. The pulse oximeter utilised throughout the surgical procedure was a VE-H100B Veterinary Pulse Oximeter by Edan, CA, USA. Supplied by MedRay, Ireland. The digital stereotaxic frame was sourced from Kopf, CA, USA. The surgical drill used was a Microspeed 317 IN by Silfradent, Forli, Italy and the microdialysis pump used was the Univentor U-801 Syringe Pump, all of which were

supplied by AgnThos, Sweden. Post-surgery the animals were placed in a 27 ºC pre-heated Thermacage MKII heated incubator supplied by Datesand Ltd, UK.

3.3 Chemicals and Solutions

This section lists all chemical and solutions used and their respective suppliers. All chemicals were used as supplied unless otherwise stated, and all solutions were prepared using Milli-Q® Type 1 water unless otherwise stated.

3.3.1 *In-Vitro* Chemicals

All *in-vitro* chemicals utilised throughout this research project are listed below along with the relevant supplier. Pyruvate oxidase from microorganisms (POx) was supplied by Sorachim, Switzerland. Co-factors Flavin adenine dinucleotide (FAD), Thiamine pyrophosphate (TPP) and Magnesium chloride (Mg^{2+}) were supplied by Sigma-Aldrich Ireland Ltd (Dublin). The 5-Hydroxyindolacetic acid (5-HIAA), 5-hydroxytryptomine (5-HT), acetone, ascorbic acid (AA), bovine serum albumin (BSA), glutaraldehyde (GA), dehydroascorbic acid (DHAA), dihydroxyphenylacetic acid (DOPAC), dopamine (DA), homovanillic acid (HVA), hydrogen peroxide (30 % w/w ACS reagent), L-Cystine, L-Glutathione, L-Tyrosine, L-Tryptophan, methyl methacrylate (MMA), magnesium chloride ($MgCl_2$), *o*-Phenylenediamine (*o*-PD), polyethyleneimine (PEI), potassium phosphate dibasic (K_2HPO_4), potassium phosphate monobasic (KH_2PO_4), sodium chloride (NaCl), sodium pyruvate, styrene and uric acid (UA) were obtained from Sigma-Aldrich Ireland Ltd (Dublin). Nitrogen gas (N_2) and Oxygen gas (O_2) were supplied by BOC gases, Dublin.

3.3.2 *In-Vivo* Chemicals

All *in-vivo* chemicals utilised throughout this research project are listed below along with the relevant supplier. Buprenorphine hydrochloride, isoflurane, lidocaine, EMLA cream (5 %), Vidisic® (0.2 % w/w eye gel) and pentobarbital (Euthanimal) were obtained from the

Bioresource Unit (BRU), Maynooth University. Sodium chloride (NaCl), Calcium Chloride ($CaCl_2$), Magnesium Chloride ($MgCl_2$), Potassium Chloride (KCl) and ascorbic acid (AA) were obtained from Sigma-Aldrich Ireland Ltd (Dublin). Dentalon® was obtained from AgnThos, Sweden and chloral hydrate was obtained from BDH Laboratory Supplies UK.

3.3.3 Solutions

All solutions were prepared on the day the experiment was carried out, unless otherwise stated. As stated above, all solutions were prepared using Milli-Q® Type 1 water, unless otherwise stated.

3.3.3.1 *In-Vitro* Solutions

Co-Factors

A 2 mM stock solution of FAD was made by dissolving 8.29 mg FAD in 5 mL H_2O. A 20 mM stock solution of TPP was prepared by dissolving 46 mg TPP in 5 mL H_2O. A 1 M stock solution of $MgCl_2$ was made by dissolving 2.38 g of $MgCl_2$ in 25 mL H_2O.

Enzyme solutions

Pyruvate Oxidase

A 400 U/mL pyruvate oxidase solution was prepared by dissolving 4.8 mg of POx in 100 µL of PBS (pH 5.7).

Pyruvate Oxidase + FAD

For a 400 U/mL POx with varying FAD concentration solution 4.8 mg of POx was dissolved in PBS (pH 5.7) along with the FAD stock solution as per Table. 3.1.

POx (Conc.)	PBS (Vol.)	FAD (conc.)
400 U/mL (4.8 mg)	98.5 µL	30 µM (1.5 µL)
	97.5 µL	50 µM (2.5 µL)
	96 µL	80 µM (4 µL)
	95 µL	100 µM (5 µL)

Table 3.1: Pyruvate with varying FAD concentrations.

For varying POx concentrations with a fixed 80 µM FAD concentration POx was dissolved in 96 µL PBS (pH 5.7) with 4 µL of FAD stock solution as per Table 3.2.

FAD (conc.)	PBS (Vol.)	POx (Conc.)
80 µM (4 µL)	96 µL	400 U/mL (4.8 mg)
		600 U/mL (7.2 mg)
		800 U/mL (9.6 mg)
		1000 U/mL (12 mg)

Table 3.2: FAD with varying POx concentrations.

Trehalose Stock Solution

A 1 M trehalose stock solution was prepared by dissolving 1.892 g trehalose in 5 mL H_2O.

Sucrose Stock Solution

A 1 M sucrose stock solution was prepared by dissolving 1.712 g of sucrose in 5 mL H_2O.

Pyruvate Oxidase + FAD + Trehalose

This solution was prepared by dissolving 9.6 mg POx in 86 µL PBS (pH 5.7) with 4 µL of the FAD stock solution along with 10 µL of the trehalose stock solution to give an enzyme solution containing 800 U/mL POx + 80 µM FAD + 100 mM trehalose.

Pyruvate Oxidase + FAD + Sucrose

POx + FAD + sucrose solutions were made by dissolving 9.6 mg POx in 86, 76 or 66 µL PBS (pH 5.7) with 4 µL of FAD stock solution and either 10, 20 or 30 µL of 1 M sucrose to give 100 µL enzyme solutions containing 800 U/mL POx + 80 µM FAD and either 100, 200 or 300 mM sucrose.

Enzyme substrate

Three different pyruvate stock solutions were used during sensor development 5 mM, 50 mM and 100 mM. These solutions were prepared by dissolving 13.75 mg, 0.1375 mg and 0.2751 mg in 25 mL PBS respectively.

General solutions

A 0.1 M stock solution of AA was prepared by dissolving 0.176 g in 10 mL H_2O. Three different BSA concentrations were used during sensor development 0.1 %, 1 % and 2 %. These solutions were prepared by dissolving 0.001 g, 0.01 g and 0.02 g in 1 mL H_2O respectively. Four different GA concentrations were investigated during the development process; 0.1 %, 0.25 %, 0.5 % and 1 %. These were prepared by dissolving 4 µL, 10 µL, 20 µL and 40 µL respectively of 25 % stock GA solution in 1 mL of H_2O. 0.324 g of *o*-PD was dissolved in 10 mL of N_2 saturated PBS to give a 300 mM solution. The solution was placed in a sonic bath and agitated with N_2 for at least 10 minutes to ensure complete dissolution. Three different PEI concentrations were used during sensor development; 1 %, 2 % and 3 %. They were prepared by dissolving 0.03125 g, 0.0625 g and 0.09375 g respectively of PEI (80 % ethoxylated 35-40 % solution in water) in 1 mL H_2O. PBS was prepared by dissolving 8.76 g of NaCl (0.15 M), 0.23 g of KH_2PO_4 (1.7 mM) and 1.39 g of K_2HPO_4 (7.98 mM) in 1 L of H_2O. The pH was adjusted to 5.7 or 7.4 as required using KH_2PO_4 and K_2HPO_4.

3.3.3.2 *In-Vivo* Solutions

aCSF was prepared by dissolving 8.766 g of NaCl (0.15 M), 0.178 g of $CaCl_2$ (0.0016 M), 0.204 g of $MgCl_2$ (0.0021 M) and 0.298 g of KCl (0.004 M) in 1L of H_2O. A 0.9 % saline solution was prepared by dissolving 0.9 g of NaCl in 100 mL H_2O. A 0.05 mg/kg solution was prepared based on the animal's weight from a stock solution of 0.3 mg/mL and made up to 1 mL with saline. An 800 mg/kg solution was prepared based on the animal's weight from a stock solution of 200 mg/ml. A 350 mg/kg solution was prepared based on the animal's weight. The chloral hydrate was weighed out and dissolved in 1 mL of saline. A 0.5 g/kg solution was prepared by dissolving 0.5 g of AA in 1 mL of saline. A 500 mM pyruvate stock solution was made by dissolving 0.5502 g sodium pyruvate in 10 mL aCSF.

3.4 Electrode Fabrication

The Pt/Ir working electrodes were constructed using approximately 5 cm of Teflon® insulated Pt/Ir (90 %/10 %) wire (175 µm diameter coated, 127 µm diameter uncoated (5T), Science Products GmbH, Hofheimer Str. 63, 65719 Hofheim am Taunus, Germany). A small section of Teflon® was removed from one end of the wire, which was then soldered into a gold clip to provide rigidity and an electrical contact. The active surface was created on the other end of the wire. For a 0.5 mm cylinder active surface a fresh disc active surface was cut using a scalpel blade and then 0.5 mm of Teflon® was carefully removed to expose the 0.5 mm active surface. For a disc electrode a fresh active surface disc was cut, no Teflon® was removed. Both designs are shown below in Figure 3.5 and Figure 3.6.

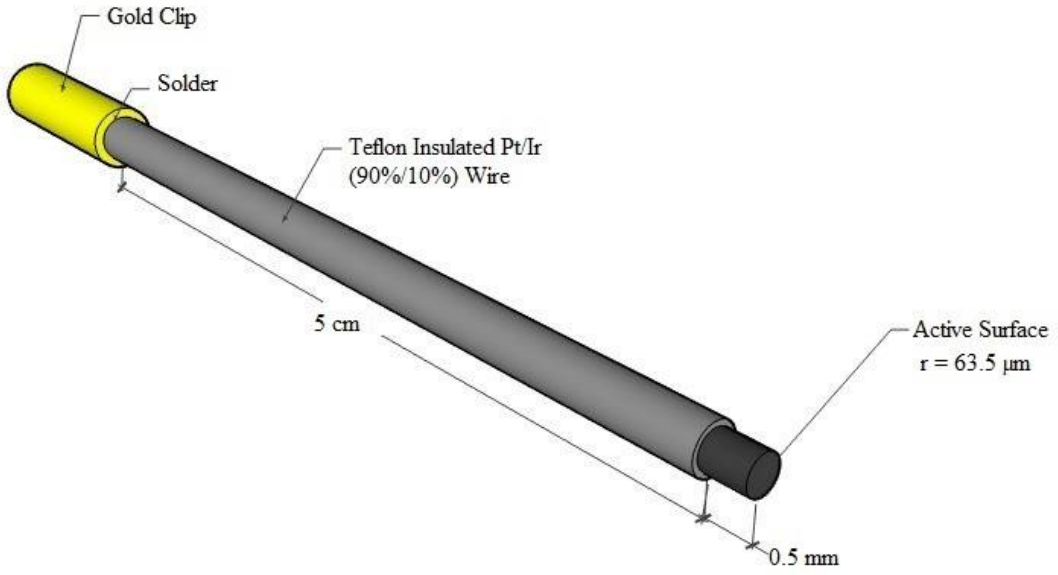

Figure 3.5: A schematic of a 0.5 mm Pt/Ir cylinder working electrode (created using Sketchup.com).

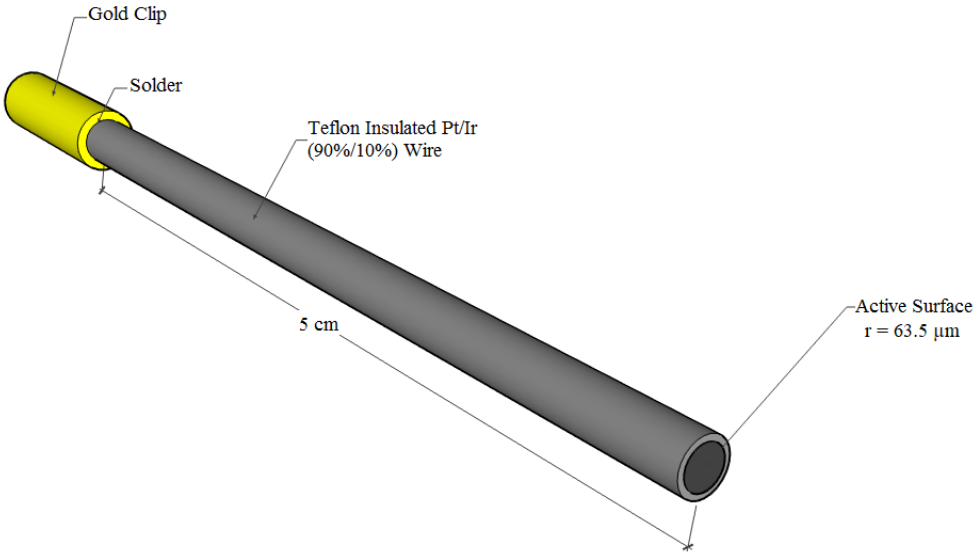

Figure 3.6: A schematic of a Pt/Ir disc working electrode (created using Sketchup.com).

3.5 Electrode Modifications

3.5.1 Interference Rejection Layer

Prior to performing the dipping procedure for determining the best design biosensor the active surface was modified with an interference rejection layer. Poly-*o*-phenylenediamine was electropolymerised onto the electrode surface in a standard three-electrode cell using a fixed potential of +700 mV (*vs.* SCE) for 30 minutes. The cell contained 300 mM *o*-PD which was prepared as per Section 3.3.2.1. The electrochemical cell was N_2 saturated and an N_2 atmosphere was maintained throughout the experiment as *o*-PD is easily oxidised in air. After electropolymerisation the electrodes were allowed to dry for at least 3 hours before any further modifications could take place.

3.5.2 Pyruvate Biosensor

This section details the various different biosensor designs utilised during the development and characterisation process. The optimisation of the enzyme solution and the design modifications are detailed in Table 3.3 and Table 3.4 respectively. A detailed description of the manufacturing process of the finalised design is detailed below with a schematic representation of the layering process shown in Figure 3.7. All modifications were dipped at room temperature and stored overnight at 4 ^{o}C.

Enzyme solution			
POx (U/mL)	**FAD (µM)**	**Sucrose (mM)**	**Trehalose (mM)**
400	30	100	100
600	50	200	
800	80	300	
1000	100		

Table 3.3: Concentrations for the various components of the enzyme solution, the concentrations of the components in the finalised design are highlighted in red.

Geometry	Interference	Immobiliser	BSA (%)	GA (%)	PEI (%)	Layers
0.5 mm Cylinder	PPD	Sty	0.1	0.1	1	5
			1	0.25	2	10
Disc		MMA	2	0.5	3	15
				1		20

Table 3.4: The various components and modifications made to the biosensor design during the development and characterisation process. The concentrations of the components in the finalised design are highlighted in red.

***Pt/Ir (disc) – PPD – {Sty – ([POx (800 U/ml) + FAD (80 µM) + Sucrose (200 mM)] + BSA (1 %) + GA (0.25 %) + PEI (2 %))$_{15}$}*:** A PPD interference rejection layer was electropolymerised onto the active surface of the electrode as per Section 3.5.1 and allowed to dry for a minimum of 3 hours. It was then dipped into a pure solution of styrene followed by a dip into an enzyme solution containing 800 U/mL POx, 80 µM FAD and 200 mM sucrose, after this it was immediately dipped into a 1 % BSA solution followed by a 0.25 % GA solution and finally a 2 % PEI solution it was then allowed to dry for 5 minutes. After this it was re-dipped a further 14 times into the enzyme solution, BSA solution, GA solution and PEI solution with a 5 minute drying time between each dip. Directly after the fifteenth dip it was placed in storage overnight at 4 ^{o}C.

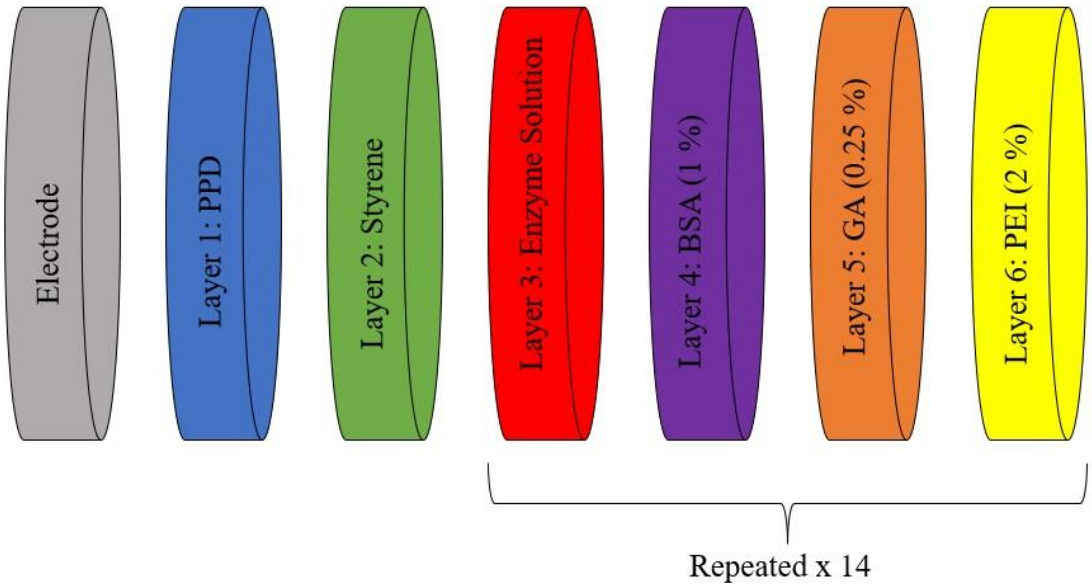

Figure 3.7: A schematic of the various dip coat layers applied to the electrode surface for the finalised design.

3.6 *In-Vitro* Electrochemical Experiments

This section details the equipment and experimental procedures used throughout the *in-vitro* development and characterisation process.

3.6.1 The Electrochemical Cell

The electrochemical cell (Figure 3.8) used throughout this research project consisted of a 25 mL glass vial. A 10 mL beaker was used for PPD polymerisation due to the small volume required for N_2-saturated conditions. Both were fitted with a custom made Teflon® cap which had openings for the auxiliary electrode, reference electrode, working electrodes, and a gas tube inlet. The auxiliary electrode used was a platinum rod which acted as a source or sink of electrons. The reference electrode was a saturated calomel electrode (SCE) which held a fixed potential that the working electrodes could be compared against. The working electrodes, as

detailed above, are where the electrochemical reaction takes place. Unless otherwise stated there was 20 mL PBS (pH 7.4) in the vial at room temperature (23 – 25 ^{o}C). Calibrations carried out at elevated temperatures utilised a jacketed 15 mL cell with an inlet and outlet for connection to a thermal circulating water bath.

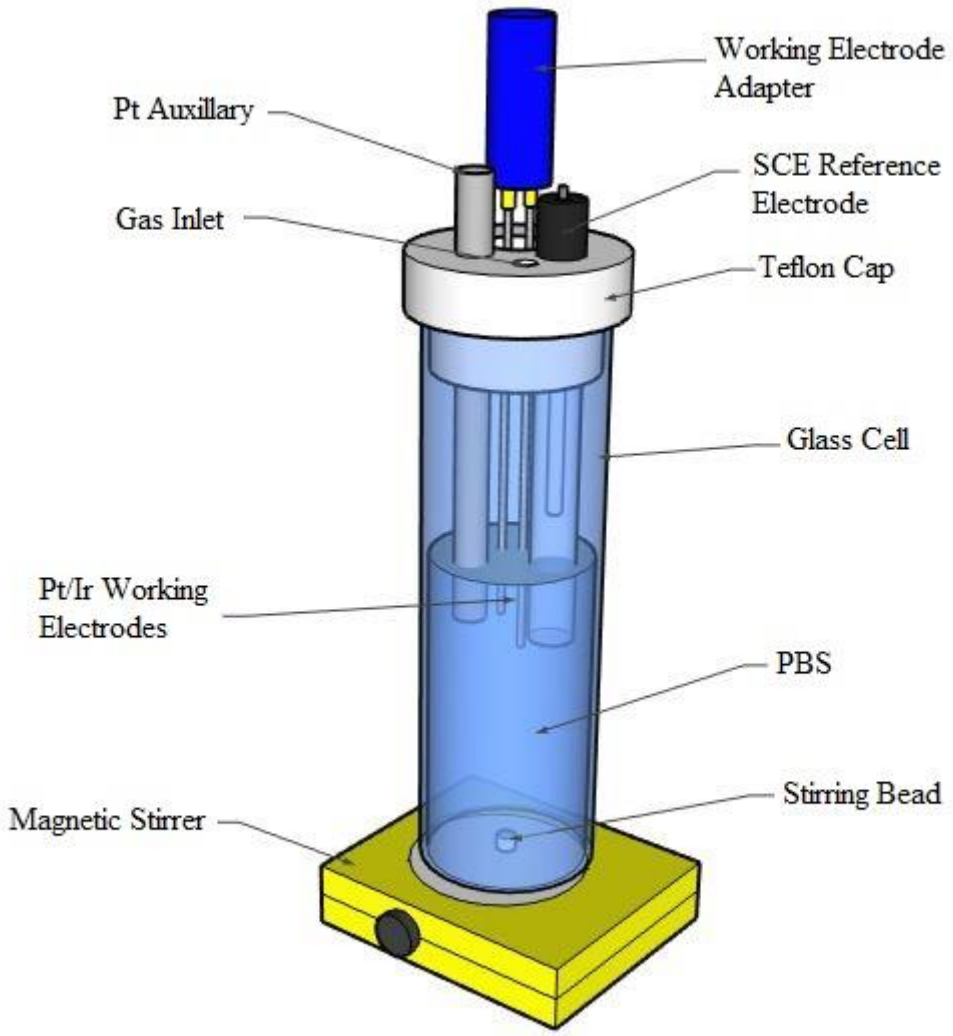

Figure 3.8: A schematic of the *in-vitro* electrochemical cell set-up (created using Sketchup.com).

3.6.2 Constant Potential Amperometry

CPA is a highly quantitative and reproducible technique which utilises the application of a fixed potential at which the redox reaction of interest takes place (Hanson, Pappas and Holland, 2005). All calibrations were carried out at +700 mV *vs.* SCE. An overpotential of at least +500 mV is required for H_2O_2 oxidation (Gerlache *et al.*, 1997) but +700 mV is typically used (O'Neill and Lowry, 2000). This fixed potential was applied to the working electrodes and they were given time, usually 1-2 hrs, to settle to a stable baseline current in the PBS solution. When a stable baseline was reached the calibration was carried out which consisted of injecting a fixed volume of the target analyte into the cell and stirring for approximately 10 s using the magnetic-stirring bead to help mix the solution. The solution was then allowed 3 minutes to reach steady-state before the next aliquot of analyte was injected.

3.6.3 Pyruvate Calibration

Pyruvate calibrations were carried out by placing the four working electrodes into a 20 mL PBS solution containing 10 mM Mg^{2+} before being polarised at +700 mV *vs.* SCE and allowed to settle to a stable baseline current. A fresh solution of pyruvate was made as per Section 3.3.2.1 and depending on the electrode design a calibration was carried out as per Table 3.5, (see below). The first aliquot was injected and the solution was stirred for approximately 10 s and then left for 3 minutes to reach a steady-state before the injection of the next aliquot. All volumes were halved for temperature studies carried out in 10 mL PBS in the jacketed cell.

	5 mM		50 mM		100 mM	
Injection	**Conc. (µM)**	**Vol. (µL)**	**Conc. (mM)**	**Vol. (µL)**	**Conc. (mM)**	**Vol. (µL)**
1	5	15	0.005	2	0.005	1
2	10	15	0.03	10	0.03	5
3	20	30	0.05	8	0.05	4
4	30	30	0.1	20	0.1	10
5	50	60	0.2	40	0.2	20
6	100	150	0.4	80	0.4	40
7	150	150	0.7	120	0.7	60
8	200	150	1	120	1	60
9	300	310	1.6	240	1.6	120
10	400	320	2.8	480	2.8	240
11	500	320	4	480	4	240
12	700	640	6.4	960	6.4	480
13	1000	960	8.8	960	11.2	960
14	1300	960	11.2	960	16	960
15	1600	960	-	-	20.8	960

Table 3.5: Concentration ranges for the various pyruvate calibrations.

3.6.4 Oxygen Calibration

Oxygen calibrations were performed at +700 mV *vs.* SCE to determine the oxygen sensitivity of the pyruvate biosensor from low physiological concentrations of oxygen (0 – 100 µM) to air saturation (200 µM) (Baker, Bolger and Lowry, 2017). 20 mL of PBS was N_2 saturated in a 25 mL glass cell for at least 2 hours. The electrodes were placed in this solution and allowed to settle to a stable baseline. In a separate 15 mL glass cell, 10 mL of PBS was O_2 saturated for at least the same amount of time to ensure complete saturation. Prior to beginning the calibration, the N_2 gas tube was removed from the N_2-saturated PBS and placed just above the liquid to form a nitrogen cloud. As per Table 3.6, standard aliquots of O_2-saturated PBS were injected into the cell which was then stirred for approximately 10 s to ensure thorough mixing and was then allowed to return to a steady-state. After 3 minutes the next aliquot was injected. This process was repeated until the calibration was complete.

	O_2 Calibration	
Injection	**Conc. (µM)**	**Vol. (µL)**
1	12.5	208
2	25	208
3	50	425
4	75	434
5	100	443
6	125	452
7	150	461
8	175	470
9	200	479

Table 3.6: Concentration range for the oxygen calibrations.

3.6.5 Ascorbic Acid Calibration

AA calibrations were carried out at +700 mV *vs.* SCE in 20 mL PBS to determine the biosensors response to AA either when PPD was or wasn't incorporated into the design. The electrodes were placed in the cell and allowed to reach a stable baseline. A fresh 0.1 M solution of AA was made as per Section 3.3.2.1. Aliquots of the stock solution were injected into the cell as per Table 3.7. The solution was stirred for approximately 10 minutes to ensure sufficient mixing and was then allowed to return to a steady-state. The next aliquot was injected after 10 minutes and the process was repeated until the calibration was completed.

	AA Calibration	
Injection	**Conc. (µM)**	**Vol. (µL)**
1	200	40
2	400	40
3	600	40
4	800	40
5	1000	40

Table 3.7: Concentration range for the AA calibrations.

3.6.6 Full Interference Calibration

A full interference study was conducted at +700 mV *vs.* SCE in 20 mL PBS to determine the biosensors response to an array of interferants. The compounds selected for testing were the most common species present in the ECF (O'Neill and Lowry, 2000). They were the neurotransmitters 5-hydroxytryptomine (5-HT) and dopamine (DA), their metabolites homovanillic acid (HVA), dihydroxyphenylacetic acid (DOPAC) and 5-Hydroxyindolacetic acid (5-HIAA), the amino acids L-cystine, L-tyrosine and L-tryptophan, AA and its oxidised form dehydroascorbic acid (DHAA), the anti-oxidant L-glutathione and finally the purine metabolite uric acid (UA) (Baker *et al.*, 2019).

The various substances were added as per Table 3.8. The electrodes were allowed settle for 1 – 2 hours with 500 µM AA added at the beginning of the settling process to ensure mimicking of the brain environment and adequate self-sealing and to establish a stable baseline (Rothwell, McMahon and O'Neill, 2010). This was followed by a second physiological concentration of AA which was then left for 1 hour to allow for accurate measurement of the AA response. This was followed by L-cystine, which was allowed settle for 30 minutes as larger concentrations of L-cystine can cause interference (Kulagina, Shankar and Michael, 1999). All subsequent injections were left for 10 minutes after injection to ensure a steady-state was reached.

Substance injected	Concentration (µM)	Volume (µL)
AA	500	100
L-cystine	50	50
L-tyrosine	100	50
UA	50	50
DOPAC	20	50
L-glutathione	50	50
DHAA	100	50
5-HIAA	50	50
L-tryptophan	100	50
HVA	10	50
DA	0.05	50
5-HT	0.01	50
Pyruvate	200	20

Table 3.8: The list of common interferants injected, their volume and relevant ECF concentrations. A pyruvate injection is listed at the end with the volume injected and the relevant concentration also, this injection was to ensure the sensor still reliably detected pyruvate after all interferants were added.

3.7 *In-Vivo* Experiments

This section details the equipment and materials, as well as the experimental procedures utilised in the implantation of the pyruvate biosensors for *in-vivo* characterisation.

3.7.1 Subjects

The animals utilised in the *in-vivo* experiments were male Wistar rats. They were acquired from Charles River UK Ltd. (Manston Rd., Margate, Kent, CT9 4LT UK), and weighed between 50 and 250 g at the time of delivery. Animals were housed in a temperature (17 - 23 ºC), humidity (40 – 70 %) and light (07:00 on and 19:00 off cycle) controlled environment.

Access to water and food was *ad libitum*. All animals were subjected to regular handling prior to surgery.

3.7.2 Surgical Protocol

All surgical procedures were carried out under aseptic conditions. Prior to each surgery all equipment and the surgical area were sterilised and all necessary instruments were autoclaved. The animal was anesthetised in a Perspex induction chamber for *ca.* 5 minutes using isoflurane (4 % in air; IsoFlo). Once anesthetised the subject was weighed and the top of its head was shaved. The subject was then placed back into the induction chamber for a further 4 minutes. The subject was then transferred to the stereotaxic frame (Figure 3.9) in a laminar flow hood and anaesthesia was maintained (between 1.5-3 % in air) using a nosepiece. Ear bars, coated with EMLA cream, were positioned and adjusted to ensure the subjects head did not move during surgery. A rectal temperature probe was inserted and physiological temperature (*ca.* 37 ^{o}C) was maintained using a heating pad under the animal. Vidisic (0.2 % w/w) eye gel was applied to both eyes and a gauze moistened with saline was placed over the eyes to prevent irritation and dryness throughout the surgery. The animal was also connected to the VetOx pulse oximeter. Iodine was applied to the shaved area of the head to sterilize the skin and prevent contamination of the wound. Lidocaine (2 %, *ca.* 50µL) was administered subcutaneously to the subject prior to incision and allowed to take effect (*ca.* 5 minutes) while the surgeon gowned up.

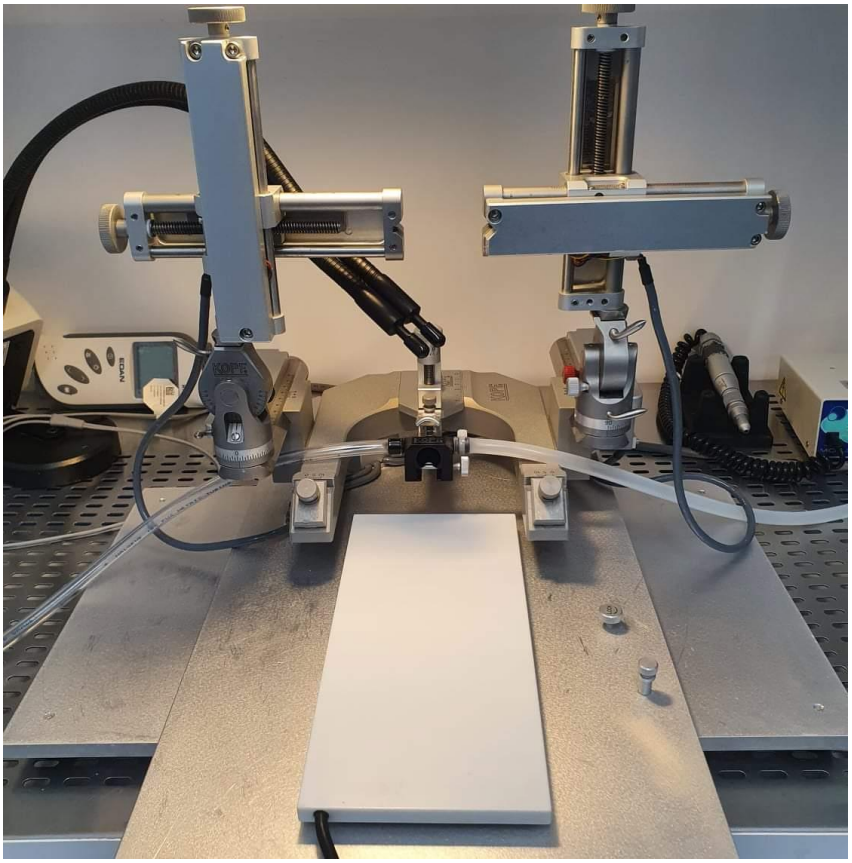

Figure 3.9: The stereotaxic frame.

The pedal reflex was used to confirm the level of anaesthesia and an incision was then made along the anterior-posterior plane. The skull was exposed using sterile cotton swabs to push aside any tissue remaining and six clamps were used to keep the incision open. A stereotaxic arm was placed on the stereotaxic frame and positioned at bregma which was then considered the zero mark. The relevant coordinates were identified from this based on the rat atlas by Paxinos and Watson (Paxinos and Watson, 1982):

	Striatum Coordinates		
Electrodes	**A-P**	**M-L**	**D-V**
1 pyruvate biosensor and 1 composite blank	+ 1.0 mm	-2.5 mm	-5.0 mm
1 pyruvate biosensor and 1 composite blank	+ 1.0 mm	+2.5 mm	-5.0 mm

Table 3.9: Stereotaxic coordinates for bi-lateral implantation of two pyruvate and two composite blank electrodes in the brain.

The coordinates for the working electrodes were marked on the skull using a permanent marker. Two bore holes were drilled for the working electrodes as well as 3 support screw holes, a hole for the reference electrode and a hole for the auxiliary screw at all the relevant co-ordinates, shown below in Figure 3.10, using a handheld drill. After all the holes were drilled the support screws were placed in position. The working electrodes were then lowered into position at – 5 mm as per Table 3.9. The working electrodes were implanted either uni-laterally (pyruvate biosensor/pyruvate biosensor – composite blank/composite blank) or bi-laterally (pyruvate biosensor/composite blank – pyruvate biosensor/composite blank).

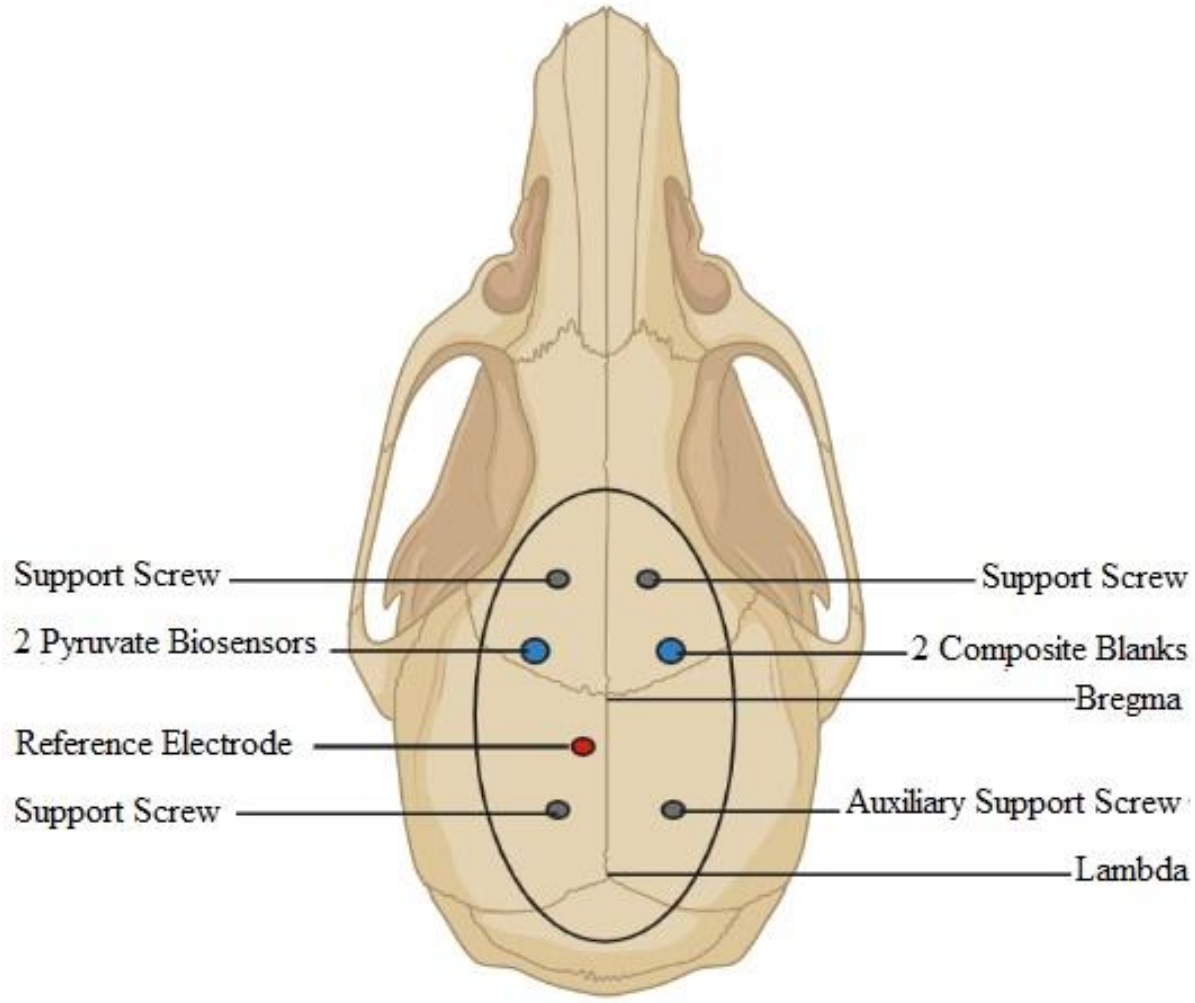

Figure 3.10: Schematic of the typical orientation of drill holes for the placement of support screws, auxiliary screw, reference electrode and uni-lateral working electrodes (created using BioRender.com).

A thin layer of dental cement (Dentalon Plus) was applied over the skull to hold the electrodes and/or the guide cannula in place and once dry the arms of the stereotaxic holding the electrodes were removed. The gold clips of the various electrodes were inserted into their relevant holes in the pedestal as per Figure 3.11 below and then cemented in place.

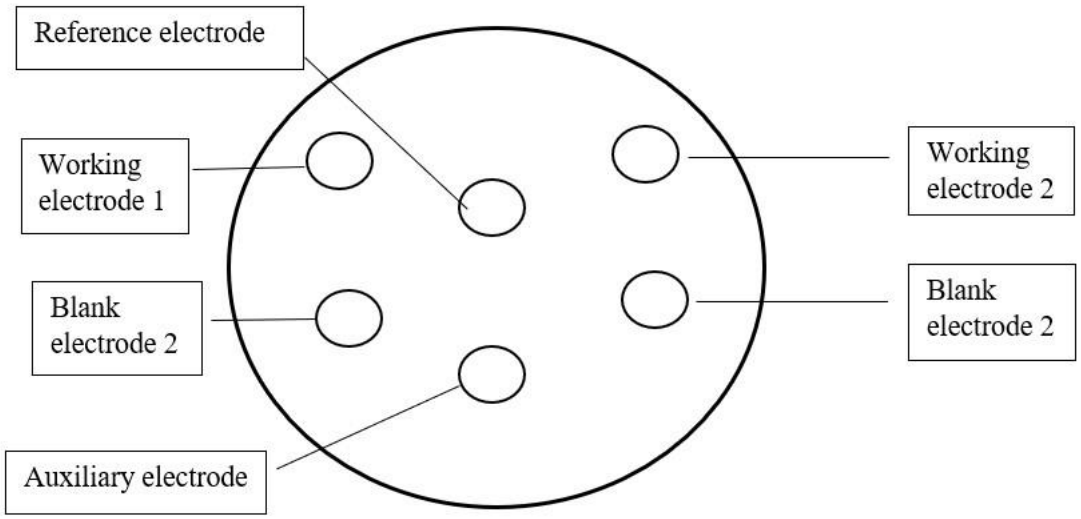

Figure 3.11: Schematic of the pedestal with relevant electrode slots.

The wires were then tidied into the centre of the head piece and coved with more dental cement until there was no longer any visible wire (Figure 3.12). The animal was then given an injection of Bupacare (0.05 mg/kg) and saline (0.95 mL) followed by a further 1 mL saline injection for postoperative analgesia and sedation. Finally, the animal was removed from the stereotaxic frame and placed into a heated incubator chamber at 28 ^{o}C and continuously monitored for 1-2 hrs until it was deemed to have sufficiently recovered and was in good health. It was then transferred back to the home bowl. The animal was then connected no sooner than 72 hrs post-surgery (Figure 3.12).

Figure 3.12: An implanted animal connected to the BASi Raturn system (black arm)and the potentiostat (silver cable) for continuous recording.

3.7.3 *In-Vivo* Reference Electrode

The Pt/Ir reference electrodes were constructed using approximately 5 cm of Teflon® insulated Pt/Ir (90 %/10 %) wire (200-µm diameter coated, 127-µm diameter uncoated (5T), Science Products GmbH, Hofheimer Str. 63, 65719 Hofheim am Taunus, Germany). A small section of Teflon® was removed from one end of the wire, which was then soldered into a gold clip to provide rigidity and an electrical contact. 5 mm of Teflon® was removed from the opposite end of the wire and looped, as shown below in Figure 3.13, to ensure contact with the brain tissue but also to prevent it from moving or changing depth.

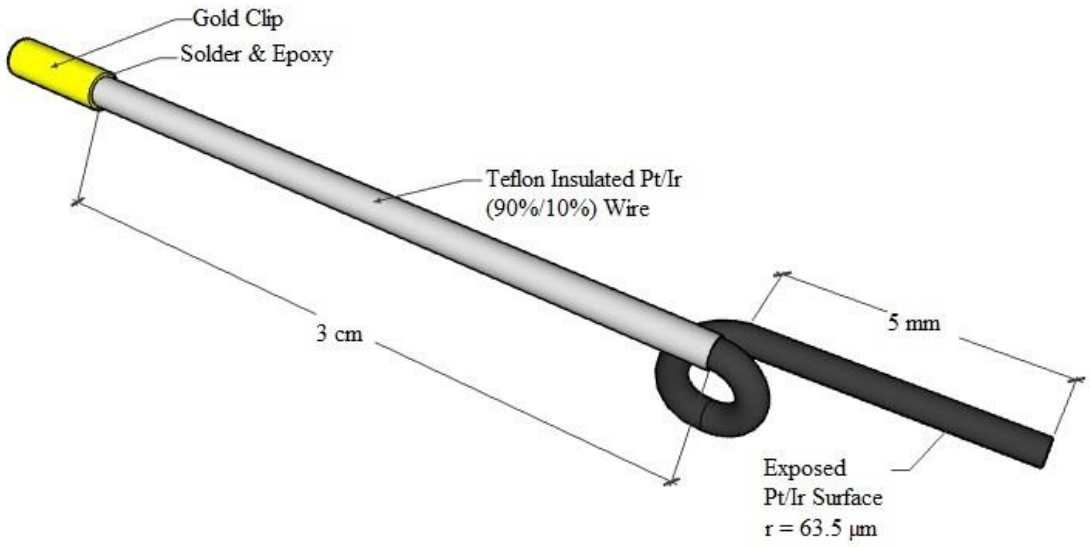

Figure 3.13: A schematic of a Pt/Ir reference electrode (created using Sketchup.com).

3.7.4 *In-Vivo* Auxiliary Electrode

The auxiliary electrode was prepared in a similar fashion to the reference electrode. However, the exposed Pt/Ir wire was tightly wrapped around a stainless steel surgical screw (Fine Science Tools, USA), shown below in Figure 3.14. This ensured the electrode would not move during surgery and provided electrical contact with the brain tissue.

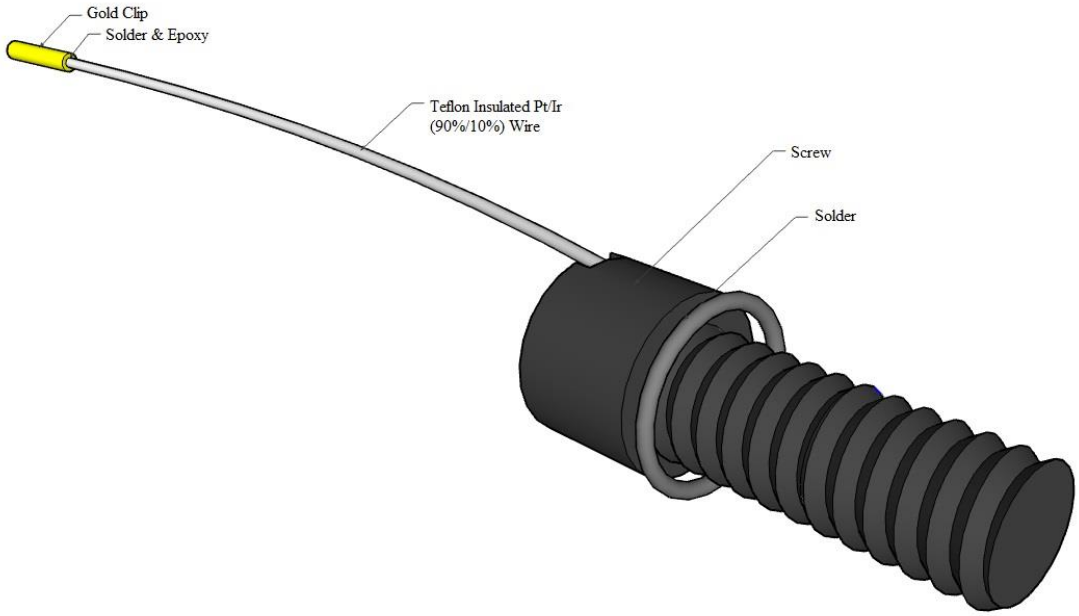

Figure 3.14: A schematic of a Pt/Ir auxiliary electrode wrapped around a support screw (created using Sketchup.com).

3.7.5 Composite Blank Electrode

This section details the fabrication of the composite blank sensor for *in-vivo* experiments. The blank was constructed in the exact same way as the finalised biosensor design only no enzyme solution was incorporated. The sensor was dipped at room temperature and stored overnight at 4 ^{o}C.

***Pt/Ir (disc) – PPD – {Sty – (BSA (1 %) + GA (0.25 %) + PEI (2 %))$_{15}$}*:** A PPD interference rejection layer was electropolymerised onto the active surface of the electrode as per Section 3.5.1 and allowed to dry for a minimum of 3 hours. It was then dipped into a pure solution of styrene followed by a dip into a 1 % BSA, solution followed by a 0.25 % GA solution, and finally a 2 % PEI solution and it was then allowed to dry for 5 minutes. After this it was re-dipped a further 14 times into the BSA solution, GA solution and PEI solution with a 5 minute

drying time between each dip. Directly after the fifteenth dip it was placed in storage overnight at 4 ^{o}C.

3.7.6 Guide Cannula

The surgical protocol, detailed in section 3.7.2, can be adapted for the implantation of an intracerebral guide cannula (BASi Research Products, 2701 Kent Avenue, West Lafayette, IN 47906 USA), shown in Figure 3.15. Two working electrodes were glued to the guide cannula (Figure 3.16) with the active surface of the electrode roughly 1 mm beyond the end of the cannula using a non-conductive 2-part-epoxy (Sigma Aldrich Co.). The guide cannula and working electrodes were implanted and cemented in place in the same manner as the working electrodes detailed in section 3.7.2. However, they were only lowered – 4 mm to allow for the protrusion of the 2 mm microdialysis probe beyond the end of the cannula.

Figure 3.15: A schematic of a Brain "BR" Intracerebral Guide Cannula supplied by BASi Research Products (https://www.basinc.com/microdialysis-cannula/intracerebral-br).

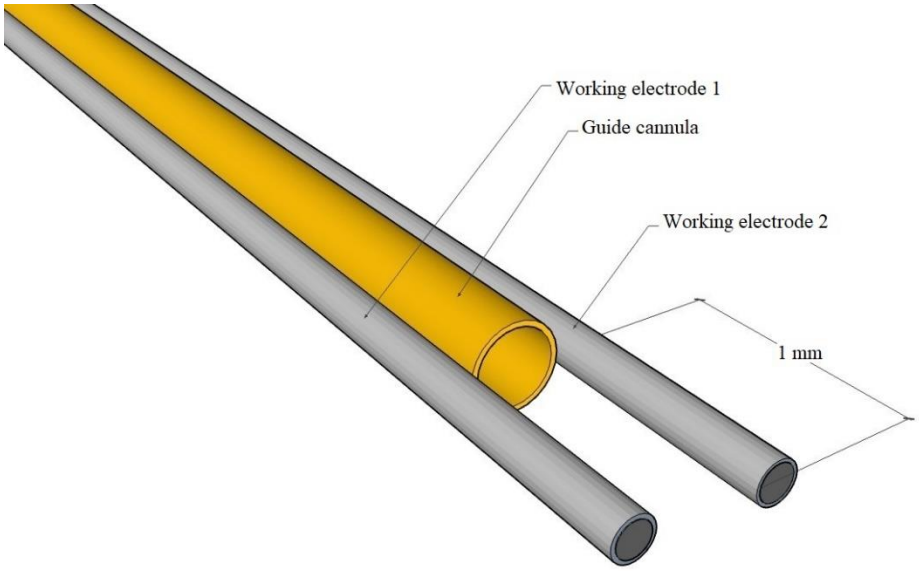

Figure 3.16: A schematic of two working electrode glued to a guide cannula (created using Sketchup.com).

3.7.7 Microdialysis Probe

For local perfusion experiments a 2 mm microdialysis probe, shown below in Figure 3.17, (BASi Research Products, 2701 Kent Avenue, West Lafayette, IN 47906 USA) was used as supplied. The perfusion experiments were carried out from a stable baseline and utilised a microdialysis pump, a 1 mL gastight syringe, tubing and connectors.

Figure 3.17: A schematic of a 2 mm Brain "BR" Style Microdialysis Probe supplied by BASi Research Products (https://www.basinc.com/products/MD-2200).

3.7.8 Continuous Monitoring

CPA was used to measure the response of the implanted biosensors during *in-vivo* experiments. The initial connection to the potentiostat involved connecting the Teflon® pedestal to an insulated 6-pin cable which was in turn connected to the potentiostat (Figure 3.18). The appropriate potential was then applied to each electrode with a short interval between each application to ensure there was no cross-talk. Once the potential was applied the electrodes were allowed to stabilise to a steady baseline, approximately 24 hrs, prior to carrying out any procedures.

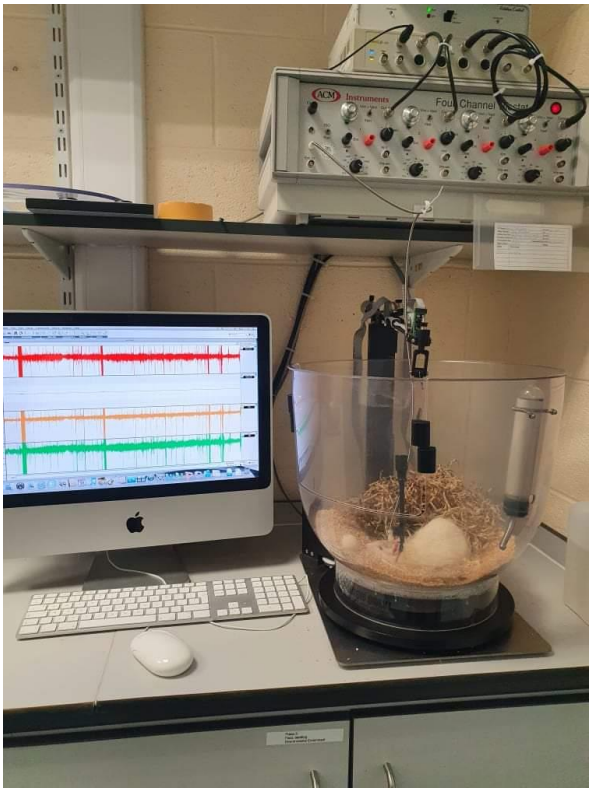

Figure 3.18: The *in-vivo* recording set-up which consisted of the computer (front left), the BASi Raturn System (front right) and the potentiostat, eDAQ e-Corder® and BASi Movement Monitor (top).

3.7.9 *In-Vivo* Procedures

This section details the experimental procedures used throughout the *in-vivo* characterisation process.

3.7.9.1 Intraperitoneal Injection

Intraperitoneal (i.p) injections were performed at a 45^{o} angle into the peritoneal cavity in the lower quarter of the abdomen. The animal was restrained, positioned on its back and tilted downward to avoid any vital organs being present in the area the injection was administered.

3.7.9.2 Termination

When *in-vivo* experimentation has concluded, euthanasia was carried out by the administration of Euthatal (800 mg/kg, i.p). Expiration took approximately 10-20 minutes after administration of the drug and was confirmed by the onset of rigor mortis. The brain was removed following decapitation and stored in a 10 % formaldehyde solution for histology.

3.7.9.3 Local Perfusions

Local perfusion experiments consisted of perfusions of aCSF and 500 mM pyruvate solutions prepared in aCSF. All solutions were freshly prepared before use. Before each perfusion experiment, all tubing and syringes were purged with aCSF and the pyruvate solution when required. The syringe and tubing were then filled with the appropriate solution while taking care to avoid any air bubbles. The syringe was then placed into the Univentor pump and the tubing was connected to the implanted microdialysis probe. A flow rate of 2 $\mu L.min^{-1}$ was set/used for all experiments. The dialysate was not required for further analysis and therefore was not collected. All perfusions were preformed from a steady baseline.

3.8 References

Baker, K.L., Bolger, F.B., Doran, M.M. and Lowry, J.P. (2019) 'Characterisation of a Platinum-based Electrochemical Biosensor for Real-time Neurochemical Analysis of Choline', *Electroanalysis*, 31(1), pp. 129–136. doi:10.1002/elan.201800642.

Baker, K.L., Bolger, F.B. and Lowry, J.P. (2017) 'Development of a microelectrochemical biosensor for the real-time detection of choline', *Sensors and Actuators, B: Chemical*, 243, pp. 412–420. doi:10.1016/j.snb.2016.11.110.

Doran, M.M., Finnerty, N.J. and Lowry, J.P. (2017) 'In–Vitro Development and Characterisation of a Superoxide Dismutase-Based Biosensor.', *ChemistrySelect*, 2(14), pp. 4157–4164. doi:10.1002/slct.201700793.

Finnerty, N.J., O'Riordan, S.L., Brown, F.O., Serra, P.A., O'Neill, R.D. and Lowry, J.P. (2012) 'In vivo characterisation of a Nafion ®-modified Pt electrode for real-time nitric oxide monitoring in brain extracellular fluid', *Analytical Methods*, 4(2), pp. 550–557. doi:10.1039/c2ay05924j.

Gerlache, M., Senturk, Z., Quarin, G. and Kauffmann, J.M. (1997) 'Electrochemical Behavior of H2O2 on Gold', *Electroanalysis*, 9(14), pp. 1088–1092. doi:10.1002/elan.1140091411.

Hanson, K.M., Pappas, T.J. and Holland, L.A. (2005) 'Electrochemical detection in capillary electrophoresis', in Marina, M.L., Ros, A., and Valcrcel, M. (eds) *Comprehensive Analytical Chemistry*. Elsevier (Comprehensive Analytical Chemistry), pp. 413–440. doi:10.1016/S0166-526X(05)45008-4.

Knyzhnykova, D. V., Topolnikova, Y. V., Kucherenko, I.S. and Soldatkin, O.O. (2018) 'Development of pyruvate oxidase-based amperometric biosensor for pyruvate determination', *Biopolymers and Cell*, 34(1), pp. 14–23. doi:10.7124/bc.00096C.

Kulagina, N. V., Shankar, L. and Michael, A.C. (1999) 'Monitoring glutamate and ascorbate in the extracellular space of brain tissue with electrochemical microsensors', *Analytical Chemistry*, 71(22), pp. 5093–5100. doi:10.1021/ac990636c.

O'Neill, R.D. and Lowry, J.P. (2000) 'Voltammetry In Vivo for Chemical Analysis of the

Living Brain', in *Encyclopedia of Analytical Chemistry*. American Cancer Society. doi:10.1002/9780470027318.a0216.

O'Neill, R.D., Rocchitta, G., McMahon, C.P., Serra, P.A. and Lowry, J.P. (2008) 'Designing sensitive and selective polymer/enzyme composite biosensors for brain monitoring in vivo', *TrAC - Trends in Analytical Chemistry*, 27(1), pp. 78–88. doi:10.1016/j.trac.2007.11.008.

Paxinos, G. and Watson, C. (1982) *The Rat Brain in Stereotaxic Coordinates: Hard Cover Edition (Google eBook)*. Elsevier.

Rothwell, S.A., McMahon, C.P. and O'Neill, R.D. (2010) 'Effects of polymerization potential on the permselectivity of poly(o-phenylenediamine) coatings deposited on Pt-Ir electrodes for biosensor applications', *Electrochimica Acta*, 55(3), pp. 1051–1060. doi:10.1016/j.electacta.2009.09.069.

Chapter 4:

Development

4.1 Introduction

Pyruvate is a non-essential nutrient that can be naturally synthesised in the cells of the body. It is the simplest of the alpha-keto acids with a carboxylic acid and ketone functional group, and it is a key intermediate product in the glycolytic pathway which is responsible for biological energy production (Akyilmaz and Yorganci, 2007). Pyruvate is a chemical of significant interest and importance in biochemistry. For example, pyruvate dehydrogenase complex deficiency (PDCD) is a neurological disorder caused by the build-up of lactic acid. The effects of this disorder range from fatal, in the new born period in the form of lactic acidosis, to severe in old age in the form of a chronic neurodegenerative condition with gross structural abnormalities in the central nervous system (Brown *et al.*, 1994). Pyruvate kinase deficiency (PKD), a red blood cell enzyme defect, is another common pyruvate related disease of great interest. It is the most common among glycolytic defects causing chronic non-spherocytic haemolytic anemia (Zanella *et al.*, 2005). The normal concentration of pyruvate in the human body is accepted to be in the range of 40-120 µM in blood (Arai *et al.*, 1999) and between 120-213µM for basal levels in the brain (Reinstrup *et al.*, 2000; Schulz *et al.*, 2000; Zetterling *et al.*, 2009). However, as recently as 2015 Cordeiro *et al.* determined that the basal brain level of pyruvate was higher at *ca.* 300 µM (Cordeiro *et al.*, 2015). Thus, precise detection methods with appropriate selectivity and specificity are clearly required.

An array of different pyruvate biosensors has been developed, for different applications, by various research groups over the years. However, these have generally suffered from a lack of sensitivity (Bergmann, Rudolph and Spohn, 1999) and selectivity (Mizutani *et al.*, 2000) or both (Tu, Long and Deng, 2008) and as a result have not been suitable for *in-vivo* use. There have been various reports of *in-vivo* recordings of pyruvate but these have typically been recorded using microdialysis (MD) (Reinstrup *et al.*, 2000; Zetterling *et al.*, 2009; Gowers *et al.*, 2019). Cordeiro *et al.* developed a multiplex system for pyruvate, lactate and glucose and have reported preliminary basal levels for pyruvate in the rat brain (Cordeiro *et al.*, 2015).

This chapter outlines the developmental steps taken to design a highly sensitive pyruvate oxidase (POx)-based biosensor for *in-vivo* neurochemical applications. The influence of the various co-factors was investigated as well as the different immobilisation strategies used to immobilise the POx on the electrode surface. The effects of stabilisers and cross-linkers were

also examined with respect to how they interact with the enzyme and affect the sensitivity and the kinetic parameters, with the goal of determining the best design for optimal pyruvate detection.

4.2 Experimental

All the instrumentation and experimental software used in this chapter are described in Chapter 3, Section 2. All chemicals and solutions used are presented in Section 3.3. The designs investigated were constructed from either 0.5 mm Pt/Ir cylinder electrodes or Pt/Ir disc electrodes as detailed in Section 3.4. The various biosensor designs utilised in this chapter along with the manufacturing process of each design is explained in detail in Section 3.5.

The cell setup described in Section 3.6.1 was used to collect all experimental data. Experiments were performed in phosphate buffer saline (PBS), initially this PBS also contained 10 µM flavin adenine dinucleotide (FAD), 300 µM thiamine pyrophosphate (TPP) and 10 mM Magnesium chloride (Mg^{2+}) until the FAD and TPP were eliminated as outlined in Sections 4.3.1.2.2 & 4.3.1.3 respectively. After this all PBS solutions contained 10 mM Mg^{2+}. Constant potential amperometry (CPA) was utilised where the biosensor was held at +700 mV (*vs.* SCE). This potential has been previously determined to be the optimal potential for the oxidation of H_2O_2 (Lowry *et al.*, 1994). As per Section 3.6.3, different aliquots of 100 mM sodium pyruvate were injected into the electrochemical cell. POx uses oxygen and phosphate with co-factors FAD, TPP and magnesium for catalysed oxidative decarboxylation of pyruvate to acetyl phosphate and H_2O_2 (Bayram and Akyilmaz, 2014). The ratio of pyruvate to H_2O_2 is 1:1, therefore the current produced from the oxidation of the H_2O_2 is directly related to the concentration of pyruvate injected into the electrochemical cell.

All data reported are provided as mean ± S.E.M. where n denoted the number of electrodes used. The significance of differences was determined using two-tailed t-tests or one-way ANOVAs where appropriate. Paired t-tests were used for comparisons between the same set of electrodes whereas, unpaired t-tests were used for different sets of electrodes. All calibrations obeyed either Michaelis-Menten or Michaelis-Menten Hill-type kinetics. The kinetic parameters V_{max}, K_m and sensitivity, given as the linear region slope (LRS), were used to

compare the various biosensor designs. The sensitivity was defined as the LRS up to 1000 µM or the nearest concentration within the K_m unless otherwise stated. The Hill coefficient, α, was used to determine the deviation from ideal enzyme kinetics and thus determine if the calibration plot obeyed either Michaelis-Menten or Michaelis-Menten Hill-type kinetics. All these parameters are described in more detail in Chapter 2, Section 2.5.1

4.3 Results and Discussion

This section details the different steps involved in the design and development of the POx-based biosensor. The aim of this was to find an optimal design which maximised the sensor's sensitivity.

4.3.1 Co-Factors

As previously stated POx is a homotetramer which binds one TPP and one FAD in the presence of either Mn^{2+} or Mg^{2+} (Bergmann, Rudolph and Spohn, 1999). It is widely known that these three co-factors are essential for enzymatic activity (Bayram and Akyilmaz, 2014). As a consequence, the first step in development was to eliminate the dependence of the biosensor on these co-factors being present in either the bulk solution *in-vitro* or in the ECF of the *in-vivo* environment.

4.3.1.1 FAD Concentration in Enzyme Solution

To begin the study, a biosensor design was chosen based on previous designs developed by the Lowry research group, as well as other research groups (Lyne and O'Neill, 1990). The design chosen was:

$$Pt/Ir\ (0.5\ mm\ cylinder) - \{Sty - [POx\ (400\ U/mL) + FAD\ (X\ \mu M)]_{10}\}$$

Pt/Ir wire was used as the transducer (Lowry *et al.*, 1994; Baker, Bolger and Lowry, 2017), with styrene (Sty) being used as the principle immobilisation technique (O'Brien *et al.*, 2007; Doran, Finnerty and Lowry, 2017). The number of units of POx was set to 400 as the literature review indicated a wide variance in the number of units used; 6.78 U/mL (Gajovic *et al.*, 1999), 150 U/mL (Arai *et al.*, 1999), 356 U/mL (Bayram and Akyilmaz, 2014) and 750 U/mL (Gowers *et al.*, 2019). FAD is one of three co-factors, along with TPP and Mg^{2+} ions, widely reported to be essential for enzymatic activity of POx (Sedewitz, Schleifer and Gotz, 1984) and as a result was chosen as the starting point for the co-factor study. Finally the number of layers of enzyme was set to 10 based on data from previous research (Baker, Bolger and Lowry, 2017).

Figure 4.1 below, shows the effect of increasing the FAD concentration in the enzyme solution. Sensitivity increased significantly ($F_{(2, 17)} = 158.6$, $p < 0.0001$, ANOVA) up to 50 µM FAD (33.4 ± 0.61 nA/µM, n = 7) before sequentially decreasing for both 80 µM (31.3 ± 0.8 nA/µM (n = 6) and 100 µM (27.4 ± 0.6 nA/µM, n = 6). There was no significant difference ($t_{(1.76)}$, p = 0.1066) between 50 µM FAD and 80 µM FAD. The kinetic parameters V_{max}, K_m, sensitivity and α are summarised in Table 4.1. At concentrations of 50 and 80 µM FAD in the enzyme solution produced the highest V_{max} and sensitivity and was therefore carried forward to the next part of the study. Lower concentrations of FAD in the enzyme solution resulted in insufficient FAD present for high levels of enzymatic activity and thus a lower sensitivity was observed. However, a response was still noted even at 0 µM FAD (12.35 ± 0.3 nA/µM, n = 8) which is due to the presence of FAD in the enzyme. While 100 µM FAD in the enzyme solution may have resulted in an excessive FAD presence which may have hindered access to the active sites and thus lowered sensitivity as well. Therefore, both 50 and 80 µM FAD designs were carried forward to the next part of the study.

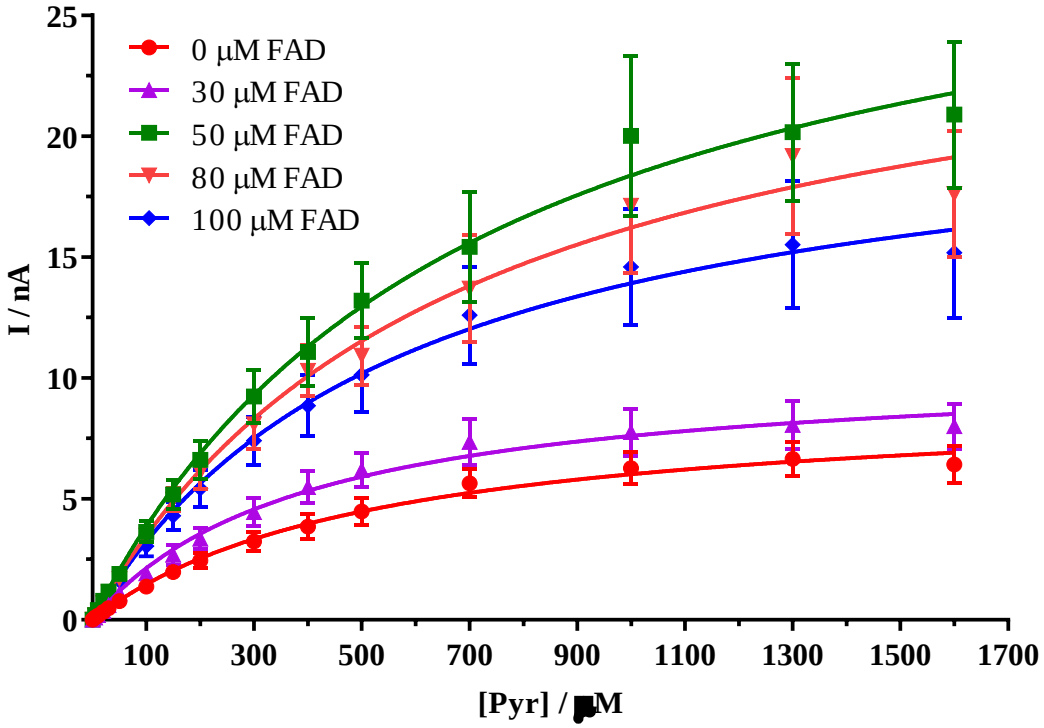

Figure 4.1: The mean current-concentration profiles for Pyr calibrations carried out in PBS (pH 7.4) buffer solution containing 10 µM FAD, 300 µM TPP and 10 mM Mg^{2+} at 21 ºC using the design *Pt/Ir (0.5 mm cylinder) – {Sty – [POx (400 U/mL) + FAD (X µM)]$_{10}$}*, where X is the varied concentration of FAD. CPA was carried out at +700 mV *vs.* SCE.

	0 µM FAD			30 µM FAD			50 µM FAD			80 µM FAD			100 µM FAD		
Kinetic Parameters	**Mean**	**S.E.M.**	**n**	**Mean**	**S.E.M.**	**n**	**Mean**	**S.E.M.**	**n**	**Mean**	**S.E.M.**	**n**	**Mean**	**S.E.M.**	**n**
V_{max} (nA)	9.2	0.7	8	10.6	0.7	5	31.6	3.5	7	27.3	3	6	21.9	2.4	6
K_m (µM)	524	91	8	398	72	5	718	167	7	685	163	6	580	144	6
α	1.15	0.19	8	1.27	0.22	5	1.14	0.25	7	1.08	0.25	6	1.15	0.28	6
Sensitivity (pA/µM)	12.4	0.3	8	17.1	0.5	5	33.4	0.6	7	31.3	0.8	6	27.4	0.6	6
R^2	0.99	-	8	0.99	-	5	0.99	-	7	0.99	-	6	0.99	-	6

Table 4.1: Comparison table of the kinetic parameters for the various concentrations of FAD in the bulk solution.

4.3.1.2 FAD Concentration in Bulk Solution

This section investigates the removal of the FAD from the bulk solution. The two best designs from the previous section were both used to examine what effect, if any, removing the FAD would have on the kinetic parameters. For both of these designs there was 10 µM FAD in the bulk solution (Kwan *et al.*, 2005). This 10 µM FAD may be influencing the kinetic parameters and thus must be eliminated to investigate this. Calibrations were carried out both in the presence and absence of 10 µM FAD in the bulk solution for both designs.

Figure 4.2 (A) shows that while 50 µM FAD in the enzyme solution yielded the best kinetic parameters when there was 10 µM FAD in the bulk solution. There was a significant decrease ($t_{(11.70)}$, $p < 0.0001$) in these same parameters once the 10 µM FAD was removed from the bulk and as a result it was decided to not carry this design forward for future experiments. In comparison, Figure 4.2 (B) shows the removal of the FAD from the bulk solution does not affect the kinetic parameters for designs incorporating 80 µM FAD in the enzyme solution. It can be seen that there was no significant difference ($t_{(0.22)}$, $p = 0.8265$) between any of the kinetic parameters (Table 4.2) as there is sufficient FAD available to facilitate the reaction. In

conclusion, 80 µM FAD was incorporated into all future designs and FAD was also eliminated from the bulk solution in all future calibrations.

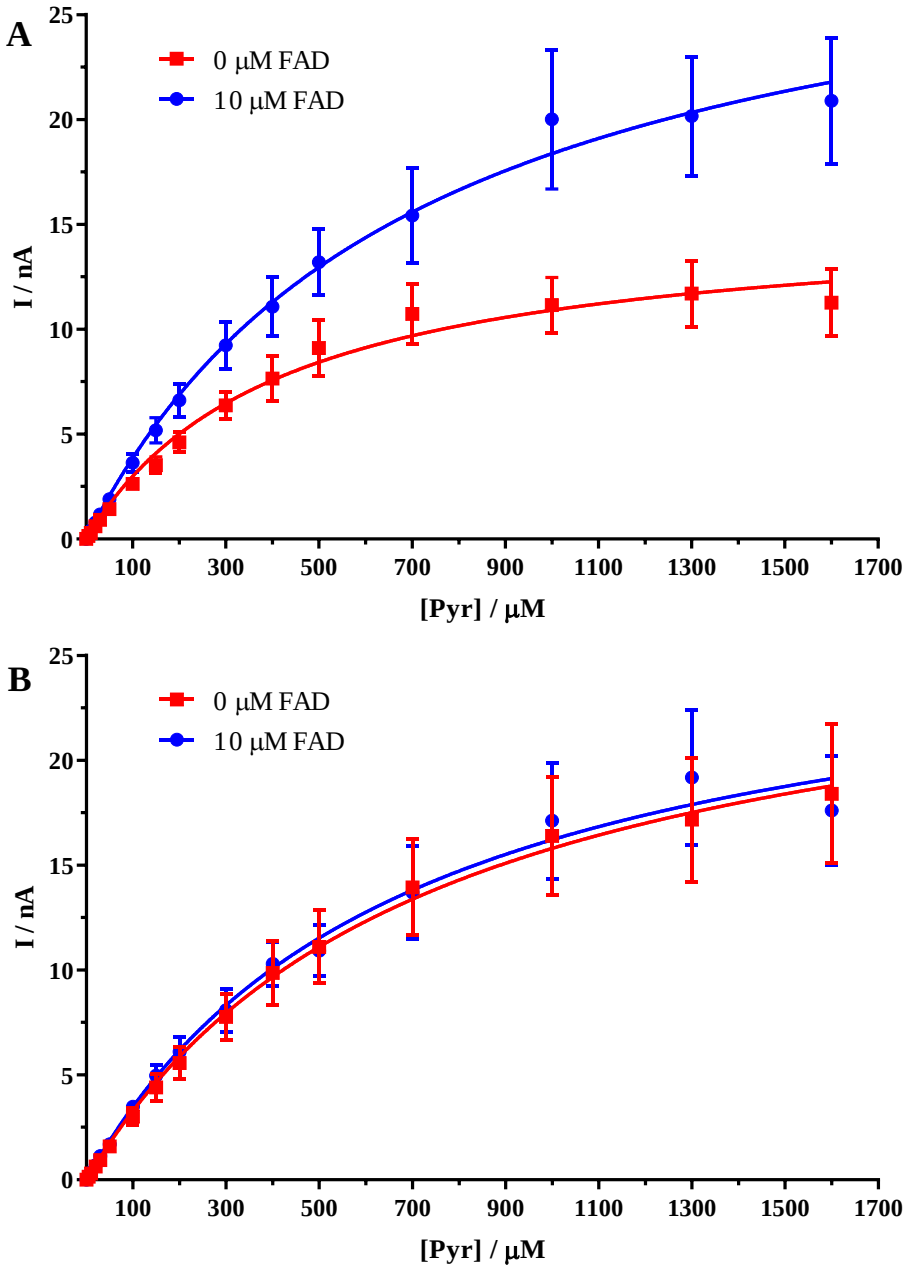

Figure 4.2:(A) The mean current-concentration profiles for Pyr calibrations carried out with either 0 µM or 10 µM FAD in the bulk solution using the 50 µM FAD design. (B) The mean current-concentration profiles for Pyr calibrations carried out with either 0 µM or 10 µM FAD in the bulk solution using the 80 µM FAD in the enzyme solution. Both calibrations were performed at 21 ºC in PBS (pH 7.4) buffer solution containing 300 µM TPP and 10 mM Mg^{2+}. CPA was carried out at +700 mV *vs.* SCE.

	50 µM FAD						80 µM FAD					
	0 µM FAD			10 µM FAD			0 µM FAD			10 µM FAD		
Kinetic Parameters	**Mean**	**S.E.M.**	**n**	**Mean**	**S.E.M.**	**n**	**Mean**	**S.E.M.**	**n**	**Mean**	**S.E.M.**	**n**
V_{max} (nA)	15.5	1.2	7	31.6	3.5	7	27.4	3.6	10	27.3	3.1	6
K_m (µM)	417	83	7	717	166	7	733	202	10	684	163	6
α	1.36	0.26	7	1.14	0.25	7	1.16	0.3	10	1.8	0.25	6
Sensitivity (pA/µM)	22.9	0.7	7	33.3	0.6	7	28.2	0.5	10	31.3	0.8	6
R^2	0.994	-	7	0.997	-	7	0.998	-	10	0.995	-	6

Table 4.2: Comparison of the kinetic parameters for the two different designs in the presence and absence of FAD in the bulk solution.

4.3.1.3 TPP Concentration in Bulk Solution

This section investigates the removal of the TPP from the bulk solution. Similar to FAD, any reliance on TPP in the bulk solution must be eliminated. For this study 300 µM was the chosen TPP concentration as reports in the literature vary greatly, from 1 µM (Rahman *et al.*, 2006) to 600 µM (Ikebukuro *et al.*, 1996), on what is optimum. Initially TTP was eliminated from the bulk solution to establish what effect, if any, this would have on the kinetic parameters.

It can be seen in Figure 4.3 that the removal of TPP from the bulk solution has no detrimental effect on any of the kinetic parameters. There was no significant difference seen in any of the kinetic parameters, given in Table 4.3. While it has been well noted in the literature that TPP is a required co-factor for enzymatic activity (Sedewitz, Schleifer and Gotz, 1984) it has also been noted that certain POx sources are independent of additional TPP (Risse *et al.*, 1992). This enzyme source has been used in this biosensor design and as a result the removal of the TPP from the bulk solution has no effect on any of the kinetic parameters. Similarly, there is no need to add additional TPP to the enzyme solution as it will have no effect. Therefore, since there is no reliance or benefit from additional TPP it can be eliminated from the bulk solution

for all future calibrations. There was no need to remove the Mg^{2+} from the bulk solution as this is readily available in the ECF (Coury, 2013).

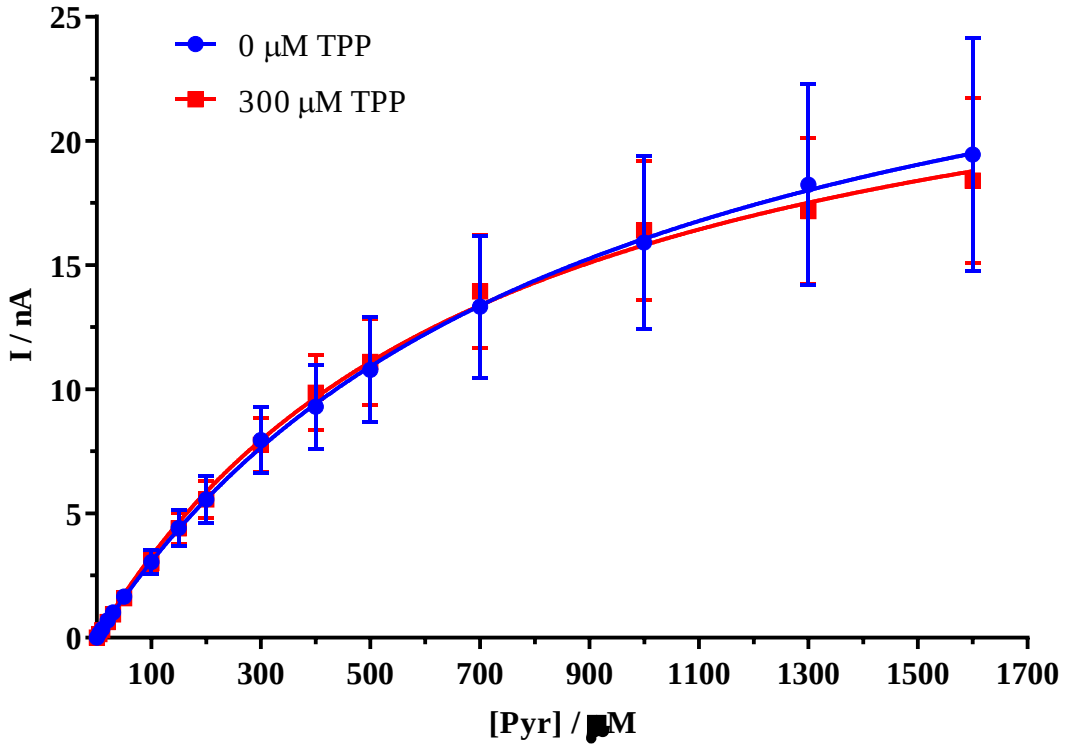

Figure 4.3: The mean current-concentration profiles for Pyr calibrations carried out in PBS (pH 7.4) buffer solution containing 0 µM or 300 µM TPP and 10 mM Mg^{2+} at 21 °C using the design; *Pt/Ir (0.5 mm cylinder) – {Sty – [POx (400 U/mL) + FAD (80 µM)]$_{10}$}*. CPA was carried out at +700 mV *vs*. SCE.

	300 µM TPP			0 µM TPP		
Kinetic Parameters	**Mean**	**S.E.M.**	**n**	**Mean**	**S.E.M.**	**n**
V_{max} (nA)	27.4	3.6	10	30.3	5.7	7
K_m (µM)	733	202	10	888	325	7
α	1.16	0.3	10	0.98	0.34	7
Sensitivity (pA/µM)	28.2	0.5	10	28.1	0.6	7
R^2	0.998	-	10	0.997	-	7

Table 4.3 Comparison of the kinetic parameters for the removal of TPP from the bulk solution.

4.3.2 Number of Layers

As stated in Section 4.3.1.1 a biosensor design was chosen based on previous designs in the literature. While this design was a sufficient starting point none of the parameters were optimised for pyruvate detection. Therefore, parameters such as enzyme concentration, immobiliser and number of layers must be optimised before the introduction of various cross-linkers and stabilisers. This process began with the number of layers of enzyme solution. The design can be represented as:

$$Pt/Ir\ (disc) - \{Sty - [POx\ (400\ U/mL) + FAD\ (80\ \mu M)]_X\}$$

where X is the number of layers. Experiments were performed using 5, 10, 15 and 20 layers of enzyme solution. Figure 4.4 shows the effect of increasing the number of layers of enzyme in the biosensor design. There was a significant increase ($F_{(2, 30)} = 404.3$, $p < 0.0001$, ANOVA) in sensitivity up to 15 layers (0.76 ± 0.02 pA/µM, n = 10) before a decrease for 20 layers (0.66 ± 0.01 pA/µM, n = 15). The kinetic parameters for each design are summarised in Table 4.4. It can be seen that 15 layers of enzyme solution immobilised on the electrode surface resulted in the highest V_{max} and sensitivity. 5 and 10 layers suffered from a lack of enzyme loading which resulted in a lower V_{max} and sensitivity as there wasn't sufficient enzyme present on the

electrode surface. While 20 layers may have suffered from enzyme overloading where a decrease in response is seen with high loading due to restricted access to the support surface (Turner, Karube and Wilson, 1989; Chaubey and Malhotra, 2002). This led to a reduced V_{max} and sensitivity however, the K_m values remained quite similar which suggests that the increase in the number of layers does not affect the diffusional properties. As a result, 15 layers was incorporated into all future designs.

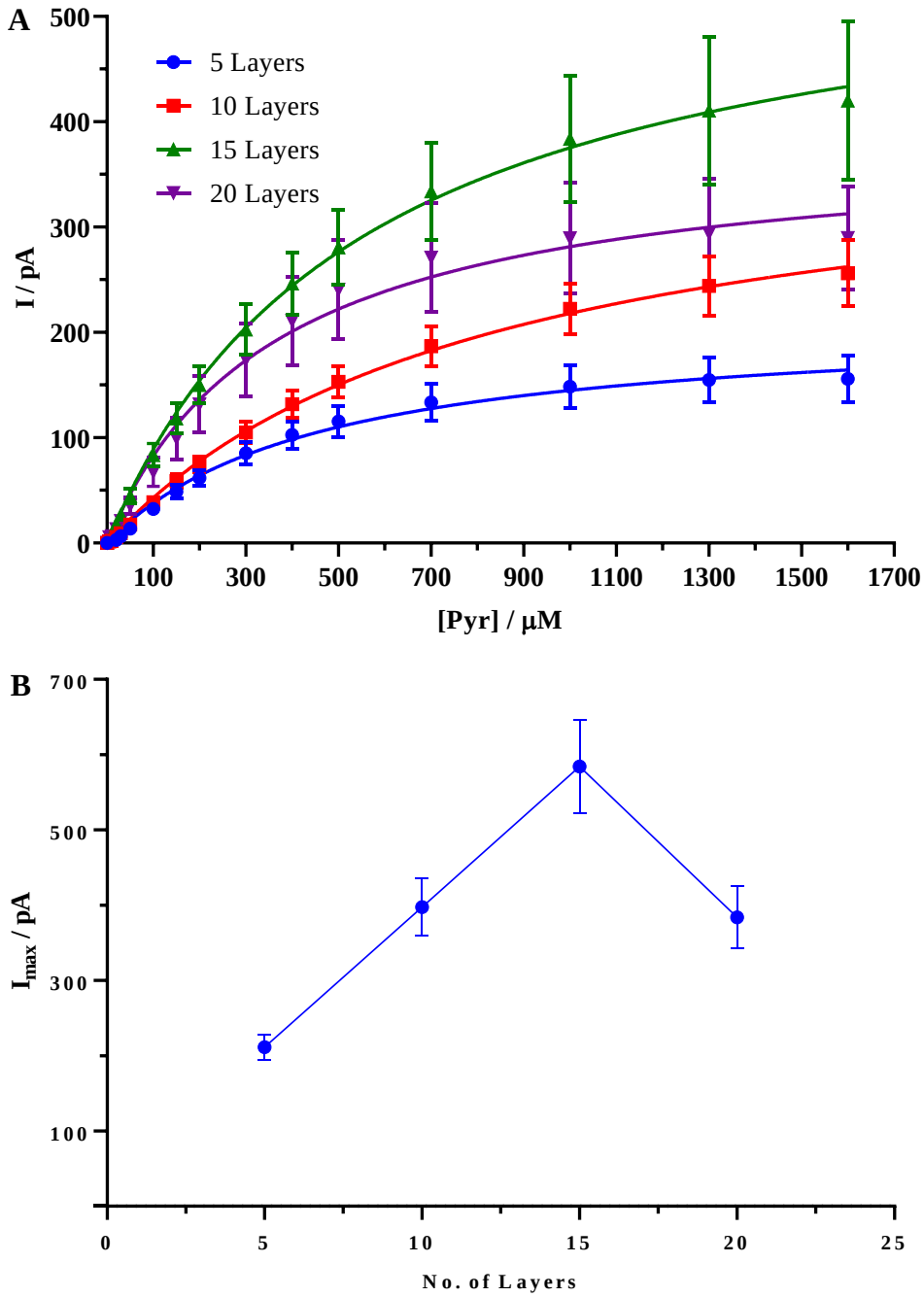

Figure 4.4:(A) The mean current-concentration profiles for Pyr calibrations carried out in PBS (pH 7.4) buffer solution containing 10 mM Mg^{2+} at 21 °C using the design; *Pt/Ir (disc) – {Sty – [POx (400 U/mL) + FAD (80 µM)]$_X$}*. CPA was carried out at +700 mV *vs.* SCE. (B) Maximum current as a function of the number of layers of enzyme.

	5 Layers			10 Layers			15 Layers			20 Layers		
Kinetic Parameters	**Mean**	**S.E.M.**	**n**	**Mean**	**S.E.M.**	**n**	**Mean**	**S.E.M.**	**n**	**Mean**	**S.E.M.**	**n**
V_{max} (pA)	212	17	7	397	38	16	584	62	10	384	41	15
K_m (µM)	460	94	7	823	158	16	557	135	10	364	105	15
α	1.38	0.27	7	1.18	0.21	16	1.13	0.27	10	1.44	0.40	15
Sensitivity (pA/µM)	0.33	0.01	7	0.39	0.01	16	0.76	0.02	10	0.66	0.01	15
R^2	0.996	-	7	0.998	-	16	0.996	-	10	0.999	-	15

Table 4.4: Comparison of the kinetic parameters for the different number of layers for the four designs utilised in this section.

4.3.3 Enzyme Unit Activity

This section examines the effect of changing the concentration of the enzyme in the enzyme solution. As stated in Section 4.3.1.1 a wide range of unit activities have been reported from as low as 6.78 U/mL (Gajovic *et al.*, 1999) to as high as 750 U/mL (Gowers *et al.*, 2019). It was thus decided to use a unit activity of 400 U/mL for initial experiments. However, this concentration was not optimised. Therefore, a unit activity study was performed testing different concentrations, 400 U/mL, 600 U/mL, 800 U/mL and 1000 U/mL. The FAD concentration was held at 80 µM for each of the different enzyme concentrations as per Section 4.3.1.2 this concentration demonstrated the highest sensitivity when mixed with the enzyme solution.

The data presented in Figure 4.5 and Table 4.5 shows the kinetic parameters and mean current-concentration profile associated with varying the unit activity of the enzyme. It can be seen that sensitivity significantly increased ($F_{(2, 25)} = 114.7$, $p < 0.0001$, ANOVA) with increased enzyme concentration up to 800 U/mL (1.09 ± 0.02 pA/µM, n = 8). There is then a significant drop ($t_{(22.45)}$, $p < 0.0001$) in sensitivity for 1000 U/mL (0.60 ± 0.02 pA/µM, n = 7), which is most likely due to enzyme overload blocking the active sites or restricting access to the electrode

surface. This concentration of 800 U/mL corresponds well to literature values of 750 U/mL (Gowers *et al.*, 2019). Concentrations as low as 6.78 U/mL (Gajovic *et al.*, 1999) have been reported in the literature however, these low concentrations are generally used when drop casting on a macro-electrode and thus the entire enzyme solution is deposited on the electrode surface which is not the case for the dip-coating method employed in this design. As a result, 800 U/mL was determined to be the optimal concentration and was incorporated into all future designs.

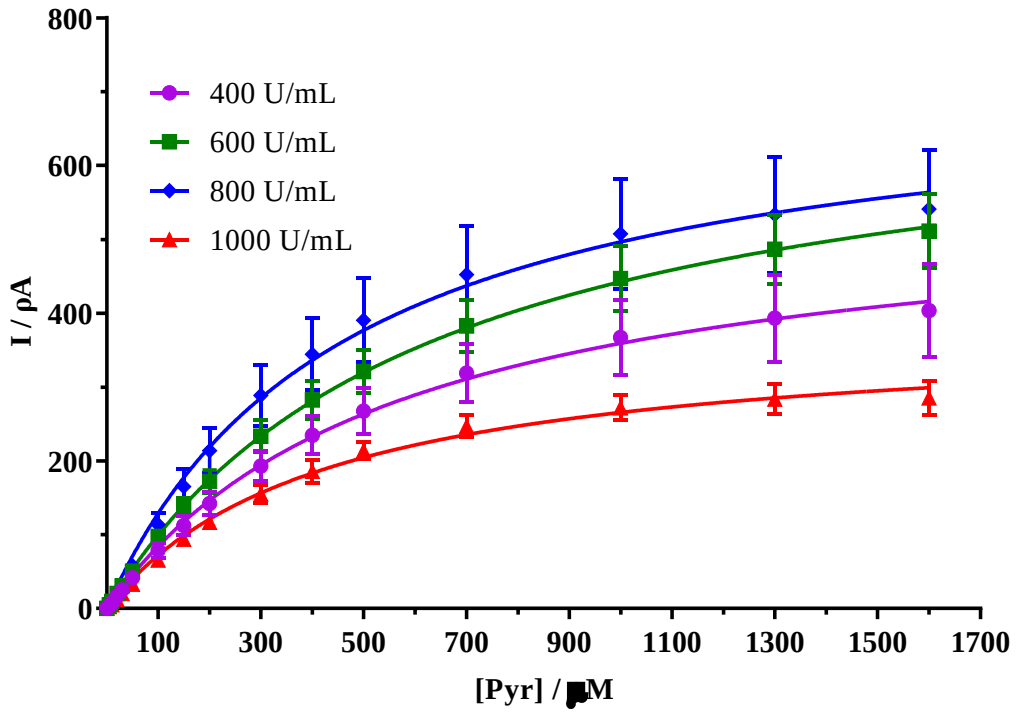

Figure 4.5: The mean current-concentration profiles for Pyr calibrations carried out in PBS (pH 7.4) buffer solution containing 10 mM Mg^{2+} at 21 ºC using the design; *Pt/Ir (disc) – {Sty – [POx (X U/mL) + FAD (80 µM)]$_{15}$}*. CPA was carried out at +700 mV *vs*. SCE.

	400 U/mL			600 U/mL			800 U/mL			1000 U/mL		
Kinetic Parameters	**Mean**	**S.E.M.**	**n**	**Mean**	**S.E.M.**	**n**	**Mean**	**S.E.M.**	**n**	**Mean**	**S.E.M.**	**n**
V_{max} (pA)	564	54	12	718	49	8	728	66	8	379	16	7
K_m (µM)	571	124	12	624	94	8	466	103	8	426	47	7
α	1.13	0.24	12	1.05	0.16	8	1.25	0.27	8	1.23	0.13	7
Sensitivity (pA/µM)	0.72	0.02	12	0.88	0.02	8	1.09	0.02	8	0.60	0.02	7
R^2	0.997	-	12	0.996	-	8	0.999	-	8	0.996	-	7

Table 4.5: Comparison of the kinetic parameters for varying enzyme concentrations in the biosensor design.

4.3.4 Immobilisation

The immobilisation of the enzyme on the electrode surface is a vital step in the design process. Various methods of immobilisation have been utilised in the development of biosensors including cross-linking, entrapment within a membrane, physical adsorption & covalent bonding. The following 5 techniques are the most commonly used for the immobilisation of a biological recognition element at the transducers surface (Thvenot *et al.*, 1999; Mateo *et al.*, 2007; Sassolas, Blum and Leca-Bouvier, 2012):

1. Entrapment behind a membrane: an enzyme solution, a slice of tissue or a suspension of cells is trapped, as a thin film over the surface of the transducer, by an analyte permeable membrane.
2. Entrapment of biological receptors within a polymeric matrix such as polyurethane (PU), polyacrylonitrile, poly (vinyl-alcohol) (PVAL) membranes, agar gel, sol gels or redox hydrogels with redox centres.
3. Entrapment of biological receptors within a bilayer lipid membrane (BLM) or a self-assembled monolayer (SAM).

4. Receptors covalently bonded onto surfaces or membranes activated by means of bifunctional groups or spacers, such as carbodiimide, glutaraldehyde, avidin-biotin silanisation or SAM's,
5. Bulk modification of entire electrode material, e.g., enzyme-modified carbon paste or graphite epoxy resin.

Previous work published by the research group have utilised the enzyme entrapment method using synthetic polymers such as styrene or methyl methacrylate (MMA) (Baker, Bolger and Lowry, 2017; Doran, Finnerty and Lowry, 2017). Both of these are liquids at room temperature and therefore ideal of the entrapment of POx using the dip-coating method for enzyme loading.

The design that incorporated styrene as the immobiliser produced significantly higher ($t_{(1.41)}$, $p < 0.0001$) V_{max} and sensitivity compared to designs that incorporated MMA as the immobilising agent. This is shown below in Figure 4.6 and in the kinetic parameters given in Table 4.6. This decrease in sensitivity when utilising MMA could be attributed to the differences in structure between the polystyrene and MMA polymers. Polystyrene, which contains benzene rings, will form a denser and less porous polymer which may be advantageous in retaining more enzyme. While the polymeric form of MMA contains flexible side chains, instead of benzene rings, which could be less successful at retaining the enzyme solution. Therefore, all future designs utilised styrene for immobilisation.

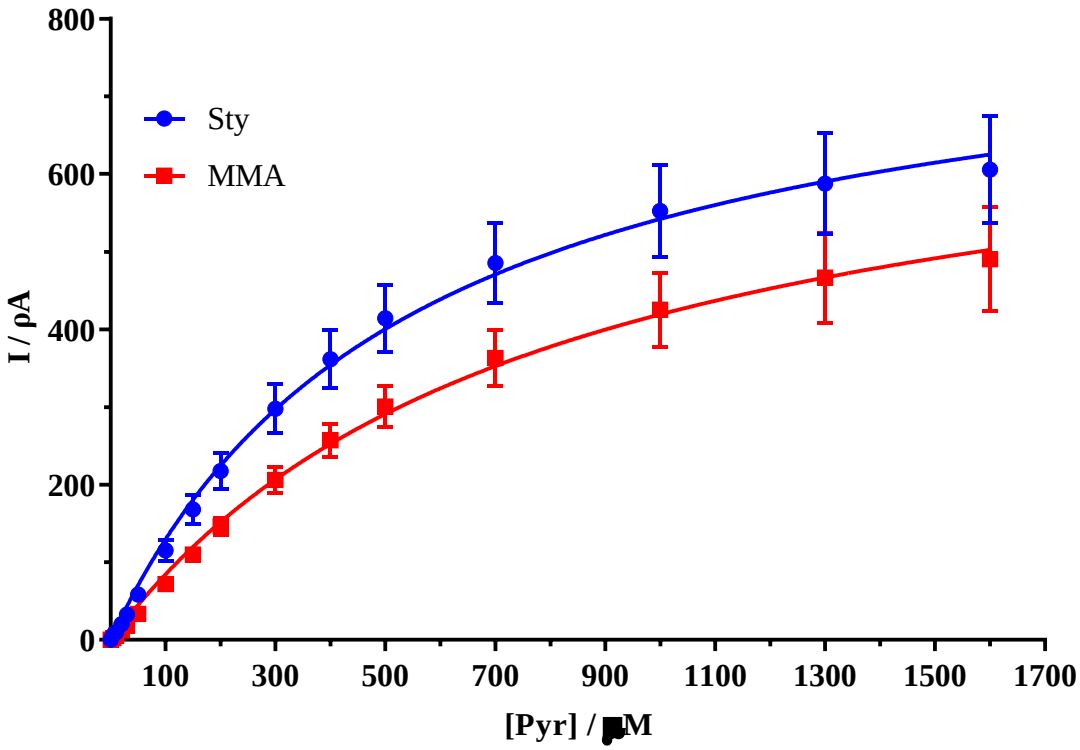

Figure 4.6: The mean current-concentration profiles for Pyr calibrations carried out in PBS (pH 7.4) buffer solution containing 10 mM Mg^{2+} at 21 °C using the design; *Pt/Ir (disc) – {X – [POx (800 U/mL) + FAD (80 μM)]$_{15}$}*. CPA was carried out at +700 mV *vs*. SCE.

	Sty			MMA		
Kinetic Parameters	**Mean**	**S.E.M.**	**n**	**Mean**	**S.E.M.**	**n**
V_{max} (pA)	839	63	16	750	70	8
K_m (µM)	548	96	16	790	149	8
α	1.22	0.2	16	1.22	0.21	8
Sensitivity (pA/µM)	1.10	0.01	16	0.74	0.01	8
R^2	0.999	-	16	0.999	-	8

Table 4.6: Comparison of the kinetic parameters for both immobilisers investigated in this study.

4.3.5 Introduction of Glutaraldehyde

Glutaraldehyde (GA) is a linear 5-carbon dialdehyde which reacts with various functional groups on proteins such as thiols, amines, imidazoles & phenols. It is low cost, commercially available and it is highly reactive thus, is used extensively for the immobilisation of enzymes in biosensor construction (Migneault *et al.*, 2004). GA usually cross-links to the ε-amino groups of the lysine residues of an enzyme which increases its stability as the intra and intermolecular cross-links lead to a more rigid molecule which has a higher resistance to conformational change (Migneault *et al.*, 2004). These lysine residues are normally located on the surface of the protein away from the catalytic site of the enzyme therefore, the biological conformation and structure are generally preserved (Migneault *et al.*, 2004). It has been noted in the literature that the concentration of GA used will affect the amount of cross-linking that takes place with concentrations that are too high resulting in extensive cross-linking which in turn distorts the active site of the enzyme leading to a decrease in activity (Chui and Wan, 1997).

Initial experiments were conducted to determine the position of GA in the dipping procedure. A 0.5 % GA solution was used as this concentration had previously been utilised by the

research group in the development of a choline biosensor (Baker, Bolger and Lowry, 2017). GA was introduced into 2 designs, the first incorporated a layer of GA after every layer of enzyme and the second incorporated a single layer of GA after the 15 dips in the enzyme solution:

$$Pt/Ir\ (disc) – \{Sty – ([POx\ (800\ U/mL) + FAD\ (80\ \mu M)] + GA\ (0.5\ \%))_{15}\}$$

or

$$Pt/Ir\ (disc) – \{Sty – [POx\ (800\ U/mL) + FAD\ (80\ \mu M)]_{15} + GA\ (0.5\ \%)\}$$

Figure 4.7 and Table 4.7. show that the introduction of GA with every layer does not significantly change the V_{max} ($t_{(0.9326)}$, $p = 0.3621$) or the K_m ($t_{(0.9665)}$, $p = 0.3454$) but has a detrimental effect on the sensitivity. The large K_m (9.17 ± 15.21 mM, n = 6, GA every layer) suggests there is an increase in the diffusional constraints for the substrate to reach the active site of the enzyme. In comparison, GA as a final layer greatly increases the V_{max} and K_m but unlike GA with every layer there is also a significant increase ($t_{(42.59)}$, $p < 0.0001$) in sensitivity (2.05 ± 0.02 pA/µM, n = 8). This increase is due to the GA cross-linking to the enzyme and keeping a greater amount of it bound to the electrode surface while also not excessively cross-linking to the point that the active sites on the enzyme are restricted, as a result this was carried forward for future designs. Due to the large increases in both V_{max} and K_m the calibration range and defined LRS were adjusted accordingly for all future experiments.

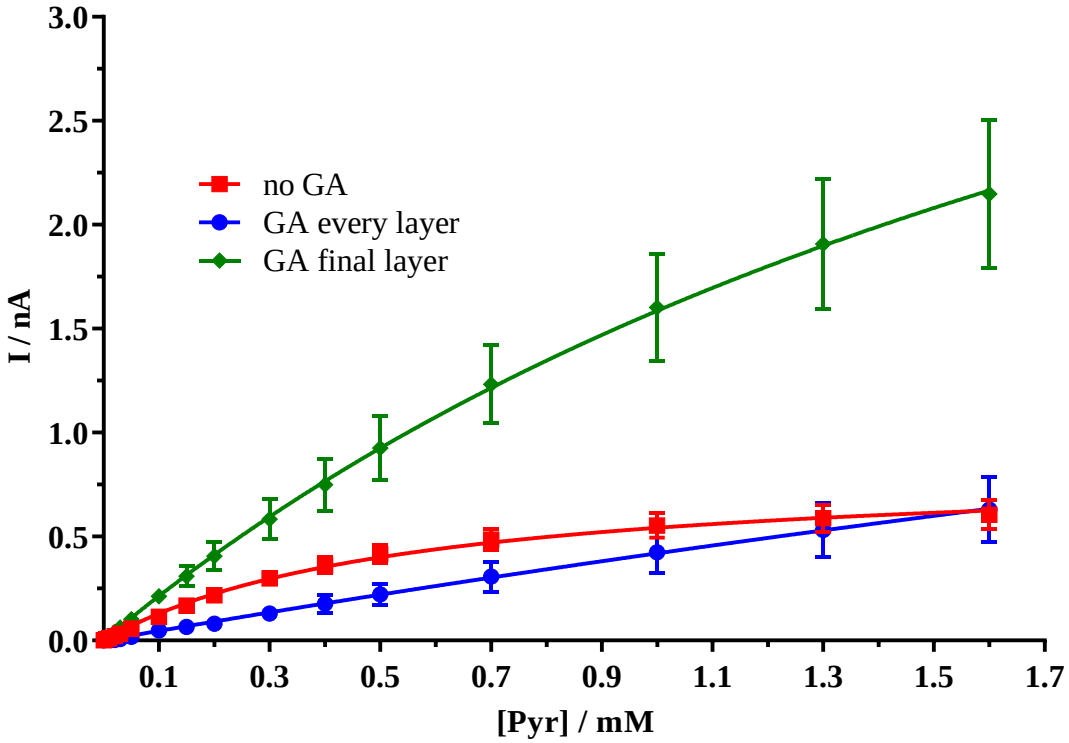

Figure 4.7: The mean current-concentration profiles for Pyr calibrations carried out in PBS (pH 7.4) buffer solution containing 10 mM Mg^{2+} at 21 ºC using the design; *Pt/Ir (disc) – {Sty – ([POx (800 U/mL) + FAD (80 µM)] + GA (0.5 %))$_{15}$}* or *Pt/Ir (disc) – {Sty – [POx (800 U/mL) + FAD (80 µM)]$_{15}$ + GA (0.5 %)}*. CPA was carried out at +700 mV *vs.* SCE.

	No GA			GA Every layer			GA Final layer		
Kinetic Parameters	**Mean**	**S.E.M.**	**n**	**Mean**	**S.E.M.**	**n**	**Mean**	**S.E.M.**	**n**
V_{max} (nA)	0.84	0.06	16	4.27	6.26	6	5.53	1.65	8
K_m (mM)	0.55	0.10	16	9.17	15.22	6	2.49	1.06	8
α	1.22	0.20	16	1.12	0.48	6	1.05	0.28	8
Sensitivity (pA/μM)	1.10	0.01	16	0.44	0.02	6	2.05	0.02	8
R^2	0.999	-	16	0.986	-	6	0.999	-	8

Table 4.7: Comparison of the kinetic parameters for the incorporation of 0.5 % GA in the biosensor design.

4.3.6 Glutaraldehyde Concentration

The concentration of GA (0.5 %) used in Section 4.3.4 to determine its position in the design was based on a previously published design (Baker, Bolger and Lowry, 2017), however, this is not to say that this concentration would be optimal for this particular biosensor design. As previously stated in the literature, high concentrations of GA result in extensive crosslinking and thus blocking of the active site of the enzyme. This results in a lower concentration being required, as seen by the work reported by Chui & Wan who used a 0.05 % GA solution (Chui and Wan, 1997). However, it is also reported in the literature that low concentrations of GA don't provide sufficient cross-linkage to effect the precipitation of the enzyme (Broun, 1976) so it was considered possible that higher concentration might be more beneficial. Thus, four different concentrations of GA were examined, 0.1 %, 0.25 %, 0.5 % and 1 % in an effort to determine the optimal concentration of GA for this particular biosensor design. As stated in Section 4.3.4 the addition of GA greatly increased the K_m values for the designs where it was incorporated and therefore the calibration range was extended to 11.2 mM.

The results given below in Figure 4.7 and Table 4.7 show that the incorporation of a 0.25 % GA final layer results in significant increases ($F_{(3, 28)}$ = 10.04, p < 0.0001, ANOVA) in sensitivity (4.38 ± 0.09 pA/µM, n = 12) compared to all other concentrations. There is no significant difference in V_{max} with exception of 0.1 % GA which suggests that the concentration of GA is too low to provide sufficient cross-linkage as expected from the literature (Broun, 1976) . The increased V_{max} for the higher GA concentrations indicates that there is a similar amount of enzyme immobilised on the electrode surface but concentrations above 0.25 % result in a higher degree of cross-linking which may hinder access to the active site by decreasing enzyme conformity, thus lowering sensitivity. Therefore, 0.25 % GA was incorporated into all future designs.

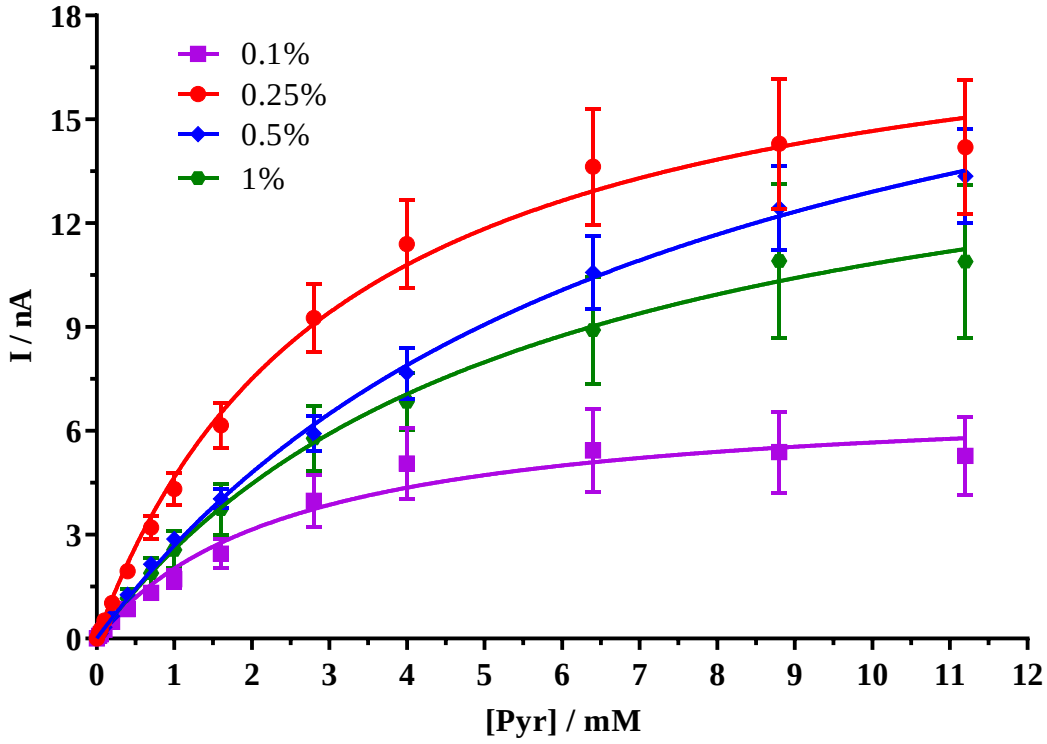

Figure 4.8: The mean current-concentration profiles for Pyr calibrations carried out in PBS (pH 7.4) buffer solution containing 10 mM Mg^{2+} at 21 ºC using the design; *Pt/Ir (disc) – {Sty – [POx (800 U/mL) + FAD (80 µM)]$_{15}$ + GA (X %)}*. CPA was carried out at +700 mV *vs*. SCE.

	0.1 %			0.25 %			0.5 %			1 %		
Kinetic Parameters	**Mean**	**S.E.M.**	**n**	**Mean**	**S.E.M.**	**n**	**Mean**	**S.E.M.**	**n**	**Mean**	**S.E.M.**	**n**
V_{max} (nA)	7.1	0.80	6	19.3	1.48	12	22.4	2.18	7	16.8	2.60	7
K_m (mM)	2.50	0.78	6	3.14	0.62	12	7.34	1.36	7	5.51	1.80	7
α	1.49	0.44	6	1.24	0.23	12	0.94	0.15	7	1.01	0.30	7
Sensitivity (pA/µM)	1.74	0.07	6	4.38	0.09	12	2.94	0.06	7	2.60	0.05	7
R^2	0.99	-	6	0.997	-	12	0.998	-	7	0.997	-	7

Table 4.8: Comparison of the kinetic parameters for various concentrations of GA.

4.3.7 Introduction of Bovine Serum Albumin

It has been reported in the literature that the addition of bovine serum albumin (BSA) drastically increases stability, protein recovery, activity recovery and thermal stability (Dong *et al.*, 2010). BSA is commonly used in conjunction with GA in most biosensor designs (Ogabiela *et al.*, 2015; Chan *et al.*, 2017). It is an inert lysine rich globular protein and is known as a "soft" protein which means it has great conformational adaptability (Kopac, Bozgeyik and Yener, 2008). GA cross-links to the lysine residues on both the BSA and the enzyme and as a result limits the amount of direct enzyme cross-linking which in turn results in a higher enzyme activity and a higher stability. The concentration of BSA also has to be taken into consideration. At low concentrations of BSA, there are not enough lysine residues from the BSA to stop excessive cross-linking to the lysine residues on the enzyme. While at high concentrations of BSA the lysine residues of the BSA compete with the lysine residues of the enzyme which in turn prevents necessary cross-linking between the GA and the enzyme (Shah, Sharma and Gupta, 2006). BSA has been previously used in other biosensor designs in the range of 0.1 % - 1 % (Baker, Bolger and Lowry, 2017). As a result, it was decided to examine the use of 0.1 %, 1 % and 2 % BSA. The BSA was positioned directly after the final layer of enzyme solution

and before the 0.25 % GA. The calibration range was also extended further (0 – 20.8 mM) to incorporate the plateau region.

The data presented below in Figure 4.9 and Table 4.9 shows that the introduction of BSA significantly increases ($F_{(2, 16)} = 603.2$, $p < 0.0001$, ANOVA) the sensitivity up to 1 % (6.75 ± 0.09 pA/µM, n = 7) before a significant decrease ($t_{(25.27)}$, $p < 0.0001$) to 4.72 ± 0.05 pA/µM (n = 7, 2 % BSA) which may be due to the excessive lysine residues of the BSA competing with the lysine residues of the enzyme and thus there is insufficient cross-linking of the enzyme resulting in a less stable confirmation or possibly lower enzyme retention. This in turn leads to a decrease in sensitivity. There was no significant change ($F_{(3, 22)} = 0.5589$, $p = 0.6477$, ANOVA) in K_m which indicates that BSA does not affect the diffusional constraint on the substrate reaching the enzyme active site. Thus, it was determined that the addition of 1 % BSA improved the sensitivity without any negative impact on any of the other kinetic parameters when compared to the same sensor design incorporating just GA and as a result was used in experiments going forward.

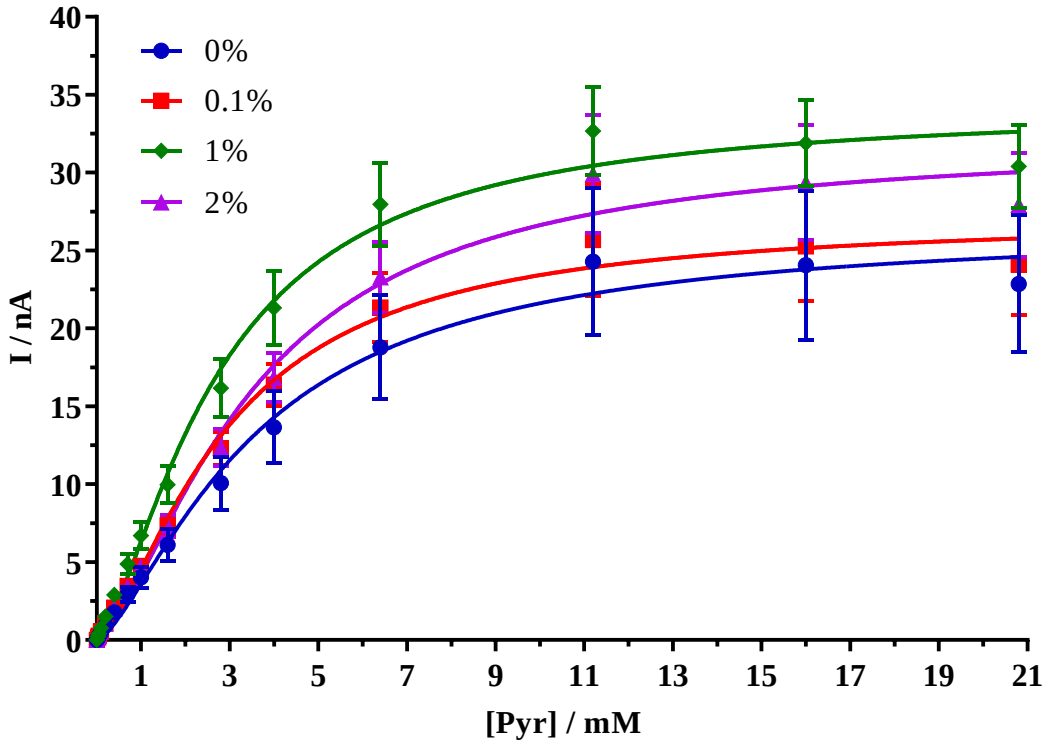

Figure 4.9: The mean current-concentration profiles for Pyr calibrations carried out in PBS (pH 7.4) buffer solution containing 10 mM Mg^{2+} at 21 ºC using the design; *Pt/Ir (disc) – {Sty – [POx (800 U/mL) + FAD (80 µM)]$_{15}$ + BSA (X %) + GA (0.25 %)}*. CPA was carried out at +700 mV *vs*. SCE.

	0 %			0.1 %			1 %			2 %		
Kinetic Parameters	**Mean**	**S.E.M.**	**n**	**Mean**	**S.E.M.**	**n**	**Mean**	**S.E.M.**	**n**	**Mean**	**S.E.M.**	**n**
V_{max} (nA)	32.1	3.38	6	32.3	2.19	6	40.2	1.96	7	39.4	2.68	7
K_m (mM)	5.47	1.49	6	4.31	0.78	6	3.90	0.54	7	5.49	0.97	7
α	1.45	0.36	6	1.50	0.25	6	1.47	0.19	7	1.52	0.24	7
Sensitivity (pA/μM)	4.05	0.06	6	4.79	0.07	6	6.75	0.09	7	4.72	0.05	7
R^2	0.998	-	6	0.999	-	6	0.998	-	7	0.999	-	7

Table 4.9: Comparison of the kinetic parameters for various concentrations of BSA incorporated into the biosensor design.

4.3.8 Introduction of Polyethyleneimine

Polyethyleneimine (PEI) is a polybasic positively charged polyelectrolyte (pKa 9.7) aliphatic amine (Gupta, Nath and Chand, 2000). It produces large porous particles with uniform distribution of pores. This is due to the osmotic pressure gradient produced between the PEI particle core and the external aqueous phase (Gupta and Ahsan, 2011). PEI has been used in biosensor design for both stabilisation (Patel *et al.*, 2000) and immobilisation (Trivedi *et al.*, 2009). PEI has also been used to increase sensitivity in certain biosensor designs (McMahon *et al.*, 2007). This beneficial effect is thought to arise from the formation of polyanionic/polycationic complexes between the PEI (polycationic) and the enzyme (polyanionic) (Jezkova *et al.*, 1997). The positive charges of the PEI electrostatically interact with the negative charges on the enzyme resulting in a stable configuration which increases the biosensor's stability. PEI was introduced as a final layer directly after the GA to examine what effect it would have on the stability of the electrode. Baker *et al.* incorporated a 2 % PEI solution into their design (Baker, Bolger and Lowry, 2017) and this was chosen as a starting point for this biosensor. The concentration was also decreased to 1 % and increased to 3 % to determine the optimum concentration for this specific design.

Figure 4.10 and Table 4.10 below, show the effect of the introduction of a varying concentration of PEI. There is a significant decrease in K_m following the introduction of PEI, it has been reported in the literature that PEI is an effective addition to biosensor design to reduce K_m (McMahon *et al.*, 2007). PEI reduces the electrostatic barrier between the enzyme and the anionic substrate. However, diffusion of the substrate is not affected and therefore increasing PEI concentrations result in an increase in the K_m as the diffusional barrier increases. A significant decrease ($F_{(3, 21)} = 36.06$, $p < 0.0001$, ANOVA) was observed in the V_{max} for all concentrations of PEI. However, the V_{max} occurs at high substrate concentrations and as a result is not critical for *in-vivo* applications. No significant change ($t_{(1.09)}$, $p = 0.2962$) in sensitivity was observed for the incorporation of 2 % PEI (6.61 ± 0.09 pA/µM, n = 7) and there is also a marked decrease in the S.E.M. As a consequence of this 2 % PEI was incorporated into all future designs as it improved the reproducibility of the design. The three designs that incorporated PEI all displayed α values greater than 1.5 which suggests sigmoidal behaviour. This kinetic behaviour is observed when more than one molecule of substrate binds to a single molecule of enzyme and is known as Michaelis-Menten Hill-Type. See Chapter 2, Section 2.5.1.

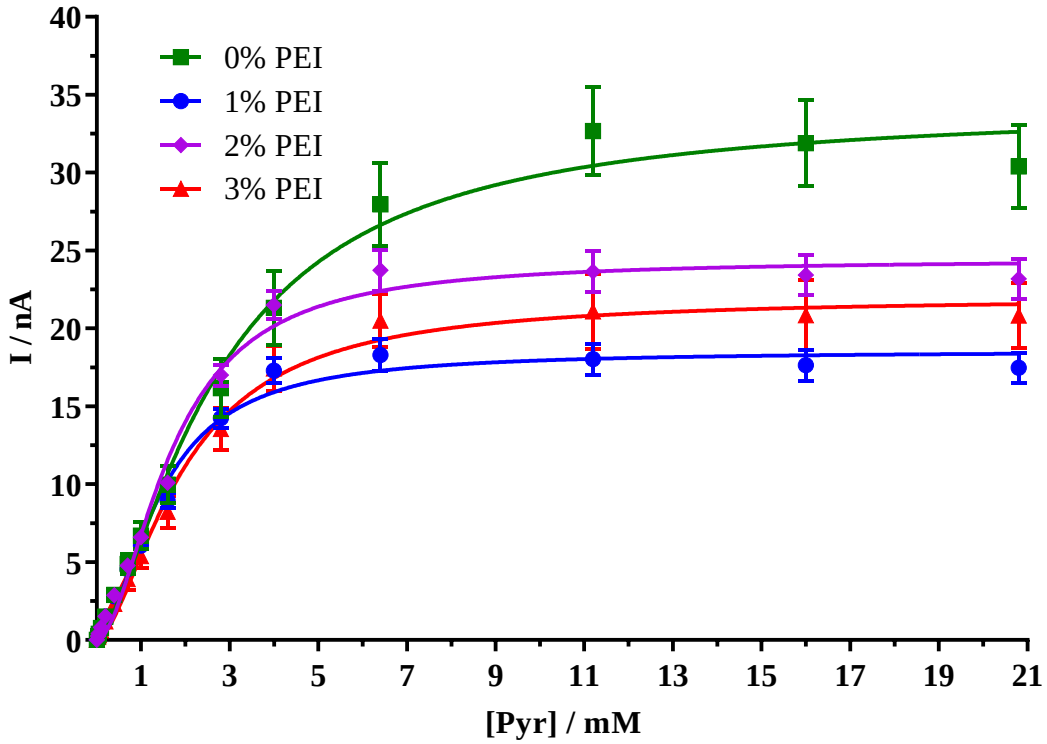

Figure 4.11: The mean current-concentration profiles for Pyr calibrations carried out in PBS (pH 7.4) buffer solution containing 10 mM Mg^{2+} at 21 ºC using the design; *Pt/Ir (disc) – {Sty – [POx (800 U/mL) + FAD (80 µM)]$_{15}$ + BSA (1 %) + GA (0.25 %) + PEI (X %)}*. CPA was carried out at +700 mV *vs.* SCE.

	0 %			1 %			2 %			3 %		
Kinetic Parameters	**Mean**	**S.E.M.**	**n**	**Mean**	**S.E.M.**	**n**	**Mean**	**S.E.M.**	**n**	**Mean**	**S.E.M.**	**n**
V_{max} (nA)	34.3	1.74	7	18.6	0.42	5	24.4	0.51	7	22.0	0.93	6
K_m (mM)	2.74	0.32	7	1.42	0.08	5	1.7	0.09	7	1.96	0.2	6
α	1.47	0.19	7	1.74	0.15	5	1.81	0.14	7	1.65	0.22	6
Sensitivity (pA/μM)	6.75	0.09	7	6.14	0.15	5	6.61	0.09	7	5.42	0.07	6
R^2	0.999	-	7	0.996	-	5	0.999	-	7	0.999	-	6

Table 4.10: Comparison of the kinetic parameters for varying concentrations of PEI incorporated in the biosensor design.

4.3.9 Verification of Optimal Design

Prior to advancing to the characterisation process, it was decided to verify certain components of the best biosensor design. Until this point each design parameter was examined and optimised sequentially. However, this did not guarantee that these parameters were still optimal following further modifications at a later time. To examine this, previous design parameters; immobiliser, unit activity, number of layers and GA concentration were each changed individually in the final design. Each parameter was changed to the second best performer from each of the respective studies (Section 4.3.2, 4.3.3, 4.3.4 and 4.3.6).

Figure 4.11 and Table 4.11 below, show the effect of varying each of the parameters individually and there is a significant decrease in both V_{max} ($F_{(4, 30)} = 27.97$, $p < 0.0001$, ANOVA) and sensitivity ($F_{(4, 30)} = 216.8$, $p < 0.0001$, ANOVA). This indicated that previous studies on the optimisation of each of these parameters were still valid.

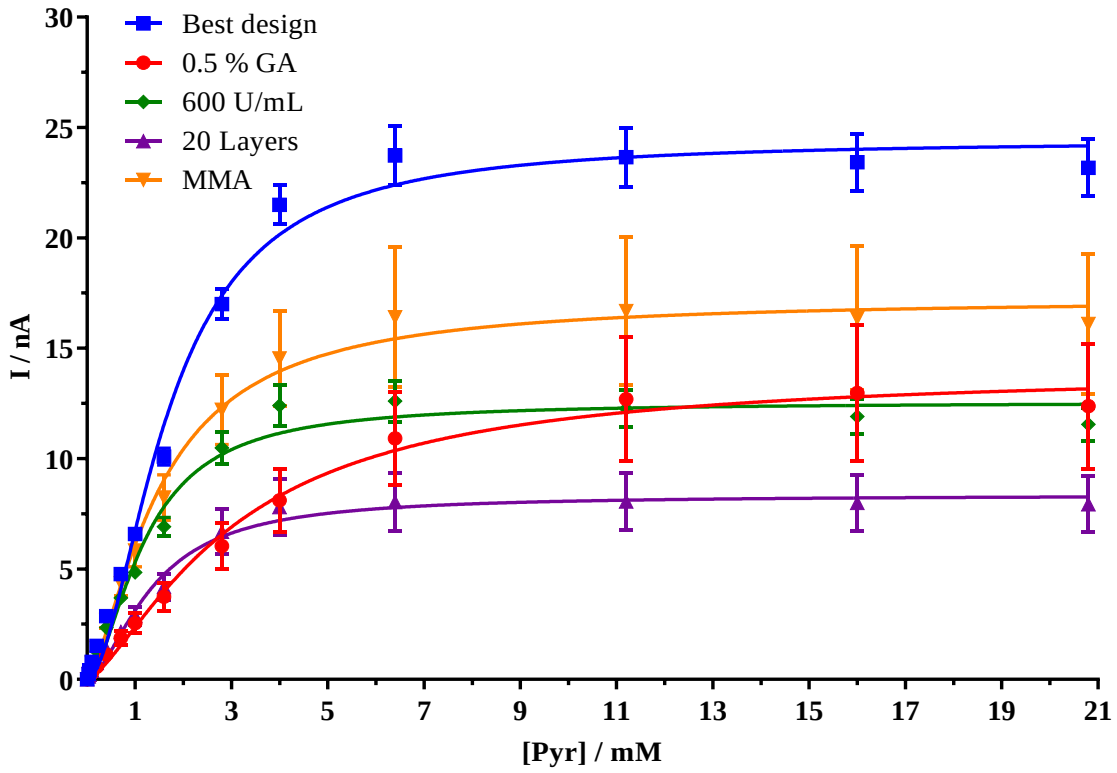

Figure 4.11: The mean current-concentration profiles for Pyr calibrations carried out in PBS (pH 7.4) buffer solution containing 10 mM Mg^{2+} at 21 ºC using the following four designs; *Pt/Ir (disc) – {Sty – [POx (800 U/mL) + FAD (80 µM)]$_{15}$ + BSA (1 %) + GA (0.25 %) + PEI (2 %)}, Pt/Ir (disc) – {Sty – [POx (800 U/mL) + FAD (80 µM)]$_{15}$ + BSA (1 %) + GA (0.5 %) + PEI (2 %)}, Pt/Ir (disc) – {Sty – [POx (600 U/mL) + FAD (80 µM)]$_{15}$ + BSA (1 %) + GA (0.25 %) + PEI (2 %)}, Pt/Ir (disc) – {Sty – [POx (800 U/mL) + FAD (80 µM)]$_{20}$ + BSA (1 %) + GA (0.25 %) + PEI (2 %)}, Pt/Ir (disc) – {MMA – [POx (800 U/mL) + FAD (80 µM)]$_{15}$ + BSA (1 %) + GA (0.25 %) + PEI (2 %)}*. CPA was carried out at +700 mV *vs*. SCE.

	Best Design			0.5 % GA			600 U/mL			20 Layers			MMA		
Kinetic Parameters	**Mean**	**S.E.M.**	**n**	**Mean**	**S.E.M.**	**n**	**Mean**	**S.E.M.**	**n**	**Mean**	**S.E.M.**	**n**	**Mean**	**S.E.M.**	**n**
V_{max} (nA)	24.4	0.51	7	14.1	1.76	8	12.6	0.34	9	8.3	0.48	5	17.3	1.31	6
K_m (mM)	1.7	0.09	7	3.07	0.89	8	1.2	0.09	9	1.36	0.21	5	1.5	0.3	6
α	1.81	0.14	7	1.42	0.4	8	1.72	0.19	9	1.69	0.38	5	1.47	0.36	6
Sensitivity (pA/µM)	6.61	0.09	7	2.58	0.04	8	4.92	0.16	9	2.9	0.08	5	5.91	0.14	6
R^2	0.999	-	7	0.998	-	8	0.993	-	9	0.994	-	5	0.996	-	6

Table 4.11: Comparison of the kinetic parameters for the optimum design with varying components to confirm their validity in the finalised design.

4.4 Conclusion

The main aim of this chapter was to develop a POx-based biosensor that had a high sensitivity and an appropriate K_m concentration. The immobilisation matrix utilised was styrene. 15 layers of an enzyme solution (800 U/mL + 80 µM FAD) immobilised within the styrene matrix was determined to be optimal for this biosensor design. The incorporation of the stabiliser BSA prior to a layer of GA followed by a final layer of PEI resulted in a highly stable, reproducible and sensitive design. Each of these three stabilising components were extensively studied in order to determine optimal concentrations for each. The final design was:

Pt/Ir (disc) – {Sty – [POx (800 U/mL) + FAD (80 µM)]$_{15}$ + BSA (1 %) + GA (0.25 %) + PEI (2 %)}

Figure 4.12 and Table 4.12 summarise the kinetic parameters for the best design biosensor for the detection of pyruvate. This design has a high V_{max} of 24.43 ± 0.51 nA (n = 9), a low K_m of 1.7 ± 0.09 mM (n = 9) and a high sensitivity of 7.16 ± 0.12 pA/µM (n = 9). The current density (J) was calculated to be 58.37 ± 0.97 nA.µM^{-1}.cm^{-2}. This is required for comparison between this design and various reported designs in the literature due to differences in size and shape of

the electrode active surface. This value compares very well with what is currently reported in the literature. This pyruvate biosensor displays a higher current density than the following published biosensors; 6.23 nA.µM^{-1}.cm^{-2} (Bergmann, Rudolph and Spohn, 1999), 51.70 nA.µM^{-1}.cm^{-2} (Mizutani *et al.*, 2000), 0.13 nA.µM^{-1}.cm^{-2} (Revzin *et al.*, 2002), 8.46 nA.µM^{-1}.cm^{-2} (Rahman *et al.*, 2006), 25.92 nA µM^{-1} cm^{-2} (Cordeiro *et al.*, 2015) and 15.83 nA.µM^{-1}.cm^{-2} (Knyzhnykova *et al.*, 2018).

	Best Design		
Kinetic Parameters	**Mean**	**S.E.M.**	**n**
V_{max} (nA)	24.43	0.51	9
K_m (mM)	1.7	0.09	9
α	1.81	0.14	9
Sensitivity (pA/µM)	7.16	0.12	9
R^2	0.999	-	9
J (nA.µM^{-1}.cm^{-2})	58.37	0.97	9

Table 4.12: Kinetic parameters for the best design pyruvate biosensor.

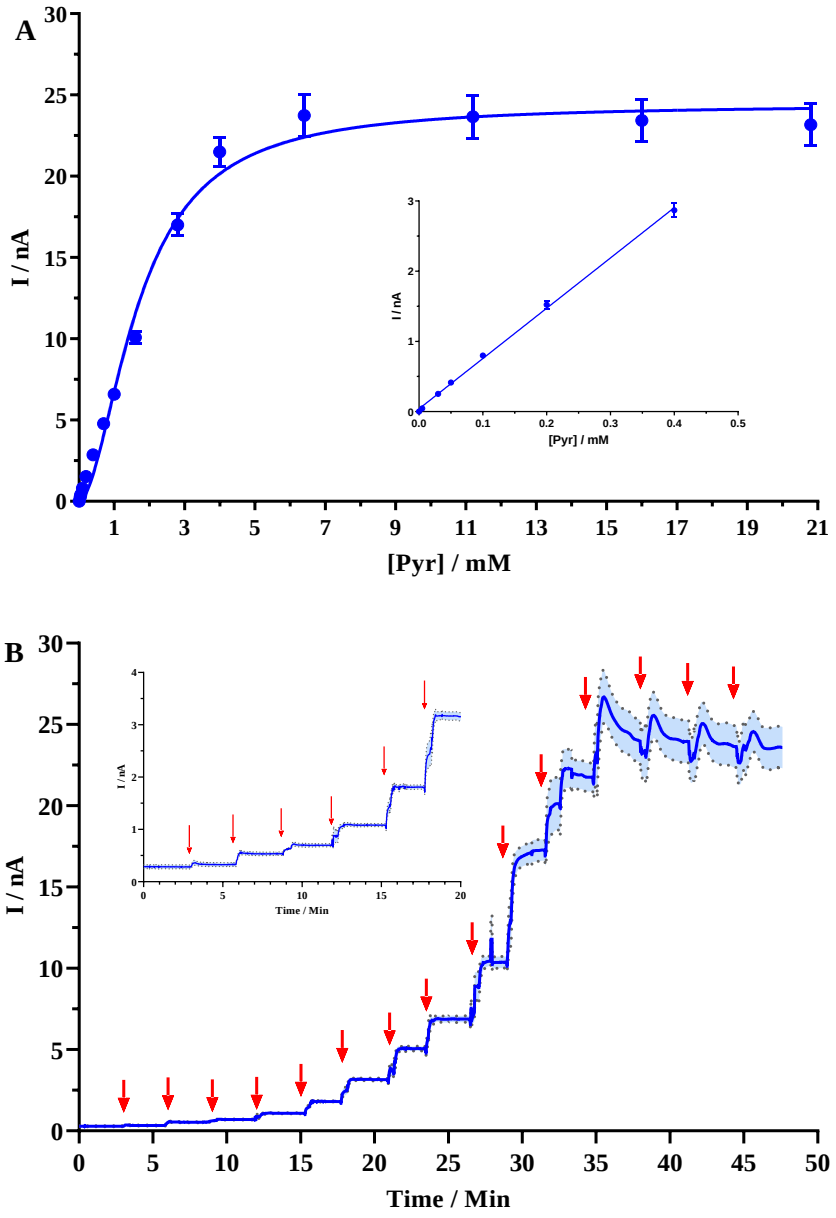

Figure 4.12:(A) The mean current-concentration profiles for Pyr calibrations carried out in PBS (pH 7.4) buffer solution containing 10 mM Mg^{2+} at 21 ºC using the best design; *Pt/Ir (disc) – {Sty – [POx (800 U/mL) + FAD (80 µM)]$_{15}$ + BSA (1 %) + GA (0.25 %) + PEI (2 %)}*. (Inset) The LRS used to determine the sensitivity of the biosensor. (B) Typical raw data trace of the best design. The arrows indicate injections as described in Chapter 3 Section 3.6.3. (Inset) Close-up showing the initial six injections. All calibrations were carried out at +700 mV (vs. SCE).

4.5 References

Akyilmaz, E. and Yorganci, E. (2007) 'Construction of an amperometric pyruvate oxidase enzyme electrode for determination of pyruvate and phosphate', *Electrochimica Acta*, 52(28), pp. 7972–7977. doi:10.1016/j.electacta.2007.06.058.

Arai, G., Noma, T., Habu, H. and Yasumori, I. (1999) 'Pyruvate sensor based on pyruvate oxidase immobilized in a poly(mercapto-p-benzoquinone) film', *Journal of Electroanalytical Chemistry*, 464(2), pp. 143–148. doi:10.1016/S0022-0728(99)00011-X.

Baker, K.L., Bolger, F.B. and Lowry, J.P. (2017) 'Development of a microelectrochemical biosensor for the real-time detection of choline', *Sensors and Actuators, B: Chemical*, 243, pp. 412–420. doi:10.1016/j.snb.2016.11.110.

Bayram, E. and Akyilmaz, E. (2014) 'A new pyruvate oxidase biosensor based on 3-mercaptopropionic acid/6-aminocaproic acid modified gold electrode', *Artificial Cells, Nanomedicine and Biotechnology*, 42(6), pp. 418–422. doi:10.3109/21691401.2013.815626.

Bergmann, W., Rudolph, R. and Spohn, U. (1999) 'A bienzyme modified carbon paste electrode for amperometric detection of pyruvate', *Analytica Chimica Acta*, 394(2–3), pp. 233–241. doi:10.1016/S0003-2670(99)00296-2.

Broun, G.B. (1976) '[20] Chemically aggregated enzymes', in *Immobilized Enzymes*. Academic Press (Methods in Enzymology), pp. 263–280. doi:https://doi.org/10.1016/S0076-6879(76)44022-3.

Brown, G.K., Otero, L.J., LeGris, M. and Brown, R.M. (1994) 'Pyruvate dehydrogenase deficiency', *Journal of Medical Genetics*, 31(11), pp. 875–879. doi:10.1136/jmg.31.11.875.

Chan, D., Barsan, M.M., Korpan, Y. and Brett, C.M.A. (2017) 'L-lactate selective impedimetric bienzymatic biosensor based on lactate dehydrogenase and pyruvate oxidase', *Electrochimica Acta*, 231, pp. 209–215. doi:10.1016/j.electacta.2017.02.050.

Chaubey, A. and Malhotra, B.D. (2002) 'Mediated biosensors', *Biosensors and Bioelectronics*, 17(6–7), pp. 441–456. doi:10.1016/S0956-5663(01)00313-X.

Chui, W.K. and Wan, L.S.C. (1997) 'Prolonged retention of cross-linked trypsin in calcium

alginate microspheres', *Journal of Microencapsulation*, 14(1), pp. 51–61. doi:10.3109/02652049709056467.

Cordeiro, C.A., de Vries, M.G., Ngabi, W., Oomen, P.E., Cremers, T.I.F.H. and Westerink, B.H.C. (2015) 'In vivo continuous and simultaneous monitoring of brain energy substrates with a multiplex amperometric enzyme-based biosensor device', *Biosensors and Bioelectronics*, 67, pp. 677–686. doi:10.1016/j.bios.2014.09.101.

Coury, A.J. (2013) 'Chemical and Biochemical Degradation of Polymers Intended to be Biostable', in Ratner, B.D., Hoffman, A.S., Schoen, F.J., and Lemons, J.E.B.T.-B.S. (Third E. (eds) *Biomaterials Science: An Introduction to Materials: Third Edition*. Academic Press, pp. 696–715. doi:10.1016/B978-0-08-087780-8.00060-7.

Dong, T., Zhao, L., Huang, Y. and Tan, X. (2010) 'Preparation of cross-linked aggregates of aminoacylase from Aspergillus melleus by using bovine serum albumin as an inert additive', *Bioresource Technology*, 101(16), pp. 6569–6571. doi:10.1016/j.biortech.2010.03.061.

Doran, M.M., Finnerty, N.J. and Lowry, J.P. (2017) 'In–Vitro Development and Characterisation of a Superoxide Dismutase-Based Biosensor.', *ChemistrySelect*, 2(14), pp. 4157–4164. doi:10.1002/slct.201700793.

Gajovic, N., Habermüller, K., Warsinke, A., Schuhmann, W. and Scheller, F.W. (1999) *A pyruvate oxidase electrode based on an electrochemically deposited redox polymer*, *Electroanalysis*. doi:10.1002/(SICI)1521-4109(199912)11:18<1377::AID-ELAN1377>3.0.CO;2-B.

Gowers, S.A.N., Rogers, M.L., Booth, M.A., Leong, C.L., Samper, I.C., Phairatana, T., Jewell, S.L., Pahl, C., Strong, A.J. and Boutelle, M.G. (2019) 'Clinical translation of microfluidic sensor devices: focus on calibration and analytical robustness', *Lab Chip*, 19(15), pp. 2537–2548. doi:10.1039/C9LC00400A.

Gupta, V. and Ahsan, F. (2011) 'Influence of PEI as a core modifying agent on PLGA microspheres of PGE_1, a pulmonary selective vasodilator', *International journal of pharmaceutics*. 2011/04/16, 413(1–2), pp. 51–62. doi:10.1016/j.ijpharm.2011.04.017.

Gupta, V., Nath, S. and Chand, S. (2000) 'Estimation of proteins in the presence of

polyethylenimine', *Biotechnology Letters*, 22(11), pp. 927–929. doi:10.1023/A:1005676531595.

Ikebukuro, K., Nishida, R., Yamamoto, H., Arikawa, Y., Nakamura, H., Suzuki, M., Kubo, I., Takeuchi, T. and Karube, I. (1996) 'A novel biosensory system for the determination of phosphate', *Journal of Biotechnology*, 48(1–2), pp. 67–72. doi:10.1016/0168-1656(96)01398-3.

Jezkova, J., Iwuoha, E.I., Smyth, M.R. and Vytras, K. (1997) 'Stabilization of an osmium bis-bipyridyl polymer-modified carbon paste amperometric glucose biosensor using polyethyleneimine', *Electroanalysis*, 9(13), pp. 978–984. doi:10.1002/elan.1140091303.

Knyzhnykova, D. V., Topolnikova, Y. V., Kucherenko, I.S. and Soldatkin, O.O. (2018) 'Development of pyruvate oxidase-based amperometric biosensor for pyruvate determination', *Biopolymers and Cell*, 34(1), pp. 14–23. doi:10.7124/bc.00096C.

Kopac, T., Bozgeyik, K. and Yener, J. (2008) 'Effect of pH and temperature on the adsorption of bovine serum albumin onto titanium dioxide', *Colloids and Surfaces A: Physicochemical and Engineering Aspects*, 322(1–3), pp. 19–28. doi:10.1016/j.colsurfa.2008.02.010.

Kwan, R.C.H., Leung, H.F., Hon, P.Y.T., Cheung, H.C.F., Hirota, K. and Renneberg, R. (2005) 'Amperometric biosensor for determining human salivary phosphate', *Analytical Biochemistry*, 343(2), pp. 263–267. doi:10.1016/j.ab.2005.05.021.

Lowry, J.P., McAteer, K., El Atrash, S.S., Duff, A. and O'Neill, R.D. (1994) 'Characterization of Glucose Oxidase-Modified Poly(phenylenediamine)-Coated Electrodes in Vitro and in Vivo: Homogeneous Interference by Ascorbic Acid in Hydrogen Peroxide Detection', *Analytical Chemistry*, 66(10), pp. 1754–1761. doi:10.1021/ac00082a025.

Lyne, P.D. and O'Neill, R.D. (1990) 'Stearate-Modified Carbon Paste Electrodes for Detecting Dopamine in Vivo: Decrease in Selectivity Caused by Lipids and Other Surface-Active Agents', *Analytical Chemistry*, 62(21), pp. 2347–2351. doi:10.1021/ac00220a016.

Mateo, C., Palomo, J.M., Fernandez-Lorente, G., Guisan, J.M. and Fernandez-Lafuente, R. (2007) 'Improvement of enzyme activity, stability and selectivity via immobilization techniques', *Enzyme and Microbial Technology* [Preprint].

doi:10.1016/j.enzmictec.2007.01.018.

McMahon, C.P., Rocchitta, G., Kirwan, S.M., Killoran, S.J., Serra, P.A., Lowry, J.P. and O'Neill, R.D. (2007) 'Oxygen tolerance of an implantable polymer/enzyme composite glutamate biosensor displaying polycation-enhanced substrate sensitivity', *Biosensors and Bioelectronics*, 22(7), pp. 1466–1473. doi:https://doi.org/10.1016/j.bios.2006.06.027.

Migneault, I., Dartiguenave, C., Bertrand, M.J. and Waldron, K.C. (2004) 'Glutaraldehyde: Behavior in aqueous solution, reaction with proteins, and application to enzyme crosslinking', *BioTechniques*, 37(5), pp. 790–802. doi:10.2144/04375rv01.

Mizutani, F., Yabuki, S., Sato, Y., Sawaguchi, T. and Iijima, S. (2000) 'Amperometric determination of pyruvate, phosphate and urea using enzyme electrodes based on pyruvate oxidase-containing poly(vinyl alcohol)/polyion complex-bilayer membrane', *Electrochimica Acta*, 45(18), pp. 2945–2952. doi:10.1016/S0013-4686(00)00373-X.

O'Brien, K.B., Killoran, S.J., O'Neill, R.D. and Lowry, J.P. (2007) 'Development and characterization in vitro of a catalase-based biosensor for hydrogen peroxide monitoring', *Biosensors and Bioelectronics*, 22(12), pp. 2994–3000. doi:10.1016/j.bios.2006.12.020.

Ogabiela, E., Adeloju, S.B., Cui, J., Wu, Y. and Chen, W. (2015) 'A novel ultrasensitive phosphate amperometric nanobiosensor based on the integration of pyruvate oxidase with highly ordered gold nanowires array', *Biosensors and Bioelectronics*, 71, pp. 278–285. doi:10.1016/j.bios.2015.04.026.

Patel, N.G., Erlenkötter, A., Cammann, K. and Chemnitius, G.C. (2000) 'Fabrication and characterization of disposable type lactate oxidase sensors for dairy products and clinical analysis', *Sensors and Actuators, B: Chemical*, 67(1), pp. 134–141. doi:10.1016/S0925-4005(00)00410-X.

Rahman, M.A., Park, D.S., Chang, S.C., McNeil, C.J. and Shim, Y.B. (2006) 'The biosensor based on the pyruvate oxidase modified conducting polymer for phosphate ions determinations', *Biosensors and Bioelectronics*. 2005/05/17, 21(7), pp. 1116–1124. doi:10.1016/j.bios.2005.04.008.

Reinstrup, P., Ståhl, N., Mellergård, P., Uski, T., Ungerstedt, U. and Nordström, C.H. (2000)

'Intracerebral microdialysis in clinical practice: Baseline values for chemical markers during wakefulness, anesthesia, and neurosurgery', *Neurosurgery*, 47(3), pp. 701–710. doi:10.1227/00006123-200009000-00035.

Revzin, A.F., Sirkar, K., Simonian, A. and Pishko, M. V. (2002) 'Glucose, lactate, and pyruvate biosensor arrays based on redox polymer/oxidoreductase nanocomposite thin-films deposited on photolithographically patterned gold microelectrodes', *Sensors and Actuators, B: Chemical*, 81(2–3), pp. 359–368. doi:10.1016/S0925-4005(01)00982-0.

Risse, B., Stempfer, G., Rudolph, R., Möllering, H. and Jaenicke, R. (1992) 'Stability and reconstitution of pyruvate oxidase from lactobacillus plantarum: Dissection of the stabilizing effects of coenzyme binding and subunit interaction', *Protein Science*, 1(12), pp. 1699–1709. doi:10.1002/pro.5560011218.

Sassolas, A., Blum, L.J. and Leca-Bouvier, B.D. (2012) 'Immobilization strategies to develop enzymatic biosensors', *Biotechnology Advances*, pp. 489–511. doi:10.1016/j.biotechadv.2011.09.003.

Schulz, M.K., Wang, L.P., Tange, M. and Bjerre, P. (2000) 'Cerebral microdialysis monitoring: Determination of normal and ischemic cerebral metabolisms in patients with aneurysmal subarachnoid hemorrhage', *Journal of Neurosurgery*, 93(5), pp. 808–814. doi:10.3171/jns.2000.93.5.0808.

Sedewitz, B., Schleifer, K.H. and Gotz, F. (1984) 'Purification and biochemical characterization of pyruvate oxidase from Lactobacillus plantarum', *Journal of Bacteriology*, 160(1), pp. 273–278. doi:10.1128/jb.160.1.273-278.1984.

Shah, S., Sharma, A. and Gupta, M.N. (2006) 'Preparation of cross-linked enzyme aggregates by using bovine serum albumin as a proteic feeder', *Analytical Biochemistry*, 351(2), pp. 207–213. doi:10.1016/j.ab.2006.01.028.

Thvenot, D.R., Toth, K., Durst, R.A. and Wilson, G.S. (1999) 'Electrochemical biosensors: Recommended definitions and classification (Technical Report)', *Pure and Applied Chemistry*, 71(12), pp. 2333–2348. doi:10.1351/pac199971122333.

Trivedi, U.B., Lakshminarayana, D., Kothari, I.L., Patel, N.G., Kapse, H.N., Makhija, K.K.,

Patel, P.B. and Panchal, C.J. (2009) 'Potentiometric biosensor for urea determination in milk', *Sensors and Actuators, B: Chemical*, 140(1), pp. 260–266. doi:10.1016/j.snb.2009.04.022.

Tu, Y., Long, Y. and Deng, K. (2008) 'Study on a pyruvate oxidase biosensor based on (β-cyclodextrin included ferrocene as electron-transfer mediator', *Proceedings of the 3rd International Conference on Sensing Technology, ICST 2008*, 42(2), pp. 403–408. doi:10.1109/ICSENST.2008.4757136.

Turner, A., Karube, I. and Wilson, G.S. (1989) 'Biosensors: Fundamentals and Applications'. Oxford, New York: Oxford University Press, p. 770. Available at: http://urn.kb.se/resolve?urn=urn:nbn:se:liu:diva-92008.

Zanella, A., Fermo, E., Bianchi, P. and Valentini, G. (2005) 'Red cell pyruvate kinase deficiency: Molecular and clinical aspects', *British Journal of Haematology*, 130(1), pp. 11–25. doi:10.1111/j.1365-2141.2005.05527.x.

Zetterling, M., Hillered, L., Samuelsson, C., Karlsson, T., Enblad, P. and Ronne-Engström, E. (2009) 'Temporal patterns of interstitial pyruvate and amino acids after subarachnoid haemorrhage are related to the level of consciousness-a clinical microdialysis study', *Acta Neurochirurgica*, 151(7), pp. 771–780. doi:10.1007/s00701-009-0384-4.

Chapter 5:

Characterisation

5.1 Introduction

The measurement of real time chemical events in the living brain presents an immensely difficult challenge. There are numerous criteria that need to be met in order for a biosensor to be deemed viable for *in-vivo* use. While the two main issues pyruvate biosensors have generally suffered from have been a lack of sensitivity and/or selectivity (Bergmann, Rudolph and Spohn, 1999; Mizutani *et al.*, 2000; Akyilmaz and Yorganci, 2007; Tu, Long and Deng, 2008) there are other criteria which must also be met. O'Neill *et al.* outlined the criteria a biosensor must meet if it is to be considered for *in-vivo* use; as well as being highly sensitive and selective to the target analyte it must also be an appropriate size and independent of oxygen (O_2) (O'Neill *et al.*, 2008). It is also important to consider the storage life and stability of the biosensor and the effects, if any, of physiologically relevant pH and temperature changes, as well as determining the limit of detection (LOD) and response time (Baker *et al.*, 2019).

In the previous chapter the sensitivity of the biosensor was optimised. This chapter focuses on examining how this biosensor performs with respect to the above criteria. Issues are expected with temperature as both Rahman *et al.* and Pundir *et al.* noted the poor preformance of POx at temperatures elevated above 30 ^{o}C (Rahman *et al.*, 2006; Malik, Chaudhary and Pundir, 2019). It is also expected that increasing pH may have a negative impact on sensitivity as the optimum pH of the enzyme indicated by the manufacturer is 5.7.

5.2 Experimental

All the instrumentation and experimental software used in this chapter are described in Chapter 3, Section 2. All chemicals and solutions used are presented in Chapter 3, Section 3. The electrodes used were constructed from Pt/Ir disc electrodes as detailed in Chapter 3, Section 4. The manufacturing process of the optimised biosensor design from Chapter 4 is explained in detail in Chapter 3, Section 5.2.

All experimental data was collected using the cell set-ups described in Chapter 3, Section 6.1. Experiments were performed in phosphate buffer saline (PBS). The pH of the PBS was altered between 7.2 - 7.6. as the experiments required and this is explained in Chapter 3, Section 5.3.2.

Constant potential amperometry (CPA) was utilised where the biosensor was held at +700 mV (*vs.* SCE). Different aliquots of 100 mM sodium pyruvate were injected into the electrochemical cell as described in Chapter 3, Section 6.3.

The data reported is given as mean ± S.E.M. where n denoted the number of electrodes used. The significance of difference was determined using two-tailed t-tests or one-way ANOVA. Paired t-tests were used for comparisons between the same set of electrodes whereas, unpaired t-tests were used for different sets of electrodes. The best design biosensor from the previous chapter is given as:

$$Pt/Ir\ (disc) - \{Sty - [POx\ (800\ U/mL) + FAD\ (80\ \mu M)]_{15} + BSA\ (1\ \%) + GA\ (0.25\ \%) + PEI\ (2\ \%)\}$$

Hereafter, this polymer composite (PC) electrode is referred to as Pt/Ir-PC/POx/PC. It has well defined kinetic parameters and obeys Michaelis-Menten Hill-type kinetics as outlined in Chapter 4 Section 4.3.9. Generally, biosensors are designed to operate in the *in-vivo* environment within their linear region response to analyte (O'Neill *et al.*, 2008). Therefore, the main kinetic parameter of interest is the sensitivity, linear region slope (LRS). The LRS was determined from the concentration range of 0 – 400 µM. This is used to analyse the performance of the biosensor in determining its viability for *in-vivo* use. For modifications to the Pt/Ir-PC/POx/PC biosensor the kinetic parameters V_{max}, K_m, sensitivity and the Hill coefficient, α, are determined as in Chapter 4.

5.3 Results and Discussion

This chapter details the various experiments carried out to determine the viability of using this sensor in the *in-vivo* environment. The biosensor was examined under the following criteria: temperature, pH, O_2 dependence, shelf life, stability, interference rejection, LOD and response time.

5.3.1 Temperature Study 1

While elevated temperatures can be advantageous and increase enzymatic activity for certain enzymes, this is not the case for pyruvate oxidase (POx). Multiple reports in the literature have highlighted the issue of elevated temperatures on enzyme activity, with anything over 30 ^{o}C, having a detrimental effect (Rahman *et al.*, 2006; Malik, Chaudhary and Pundir, 2019). However, this seems to be enzyme source dependant as an increase in activity was seen with increasing temperature for pyruvate oxidase from *Aerococcus viridans* (*Av*POx) (Gowers *et al.*, 2019). Unfortunately, this source is not a viable option due to its dependence on TPP in the bulk solution.

In this section calibrations were carried out at 25 ^{o}C and 37 ^{o}C to determine what effect temperature would have on the kinetic parameters. Calibrations were carried out in 10 mL PBS in a jacketed cell using a thermal bath to control the temperature which is described in more detail in Section 3.6.3. From the results presented in Figure 5.1 below, it can be seen that there is a significant decrease ($t_{(50.42)}$, $p < 0.0001$) in sensitivity from 7.16 ± 0.12 pA/µM (n = 9, 25 ^{o}C) to 1.72 ± 0.03 pA/µM (n = 10, 37 ^{o}C). This decrease is most likely due to denaturation of the enzyme at elevated temperatures which was to be expected based on publications in the literature. Due to the poor performance of the biosensor at 37 ^{o}C, this design was rendered unsuitable for any further temperature studies until the substantial decrease in activity was addressed.

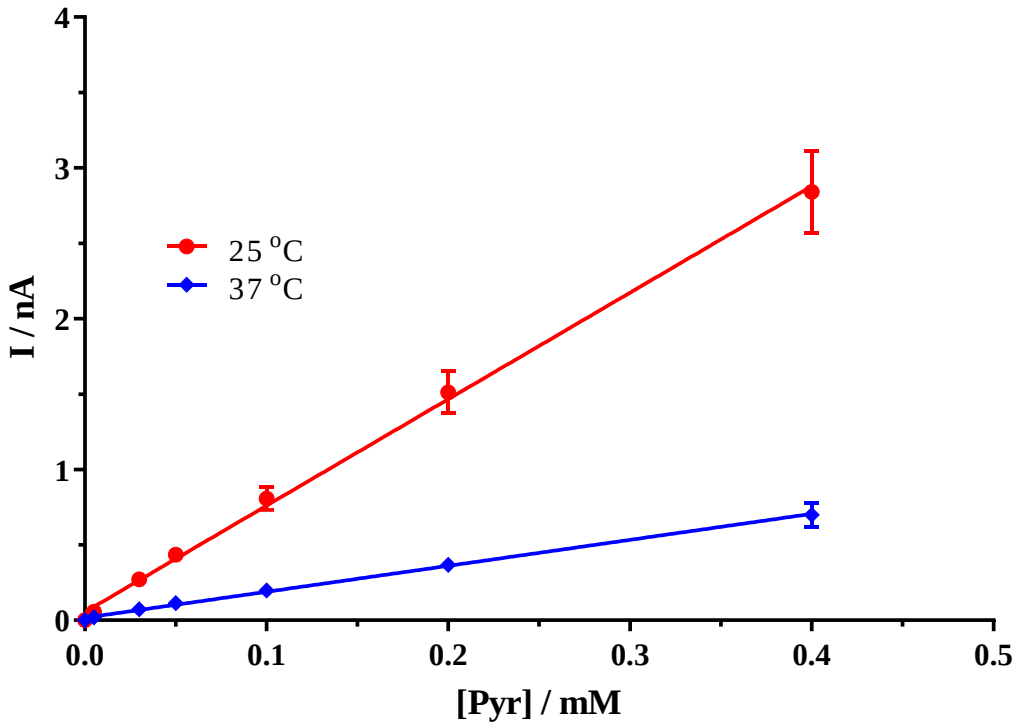

Figure 5.1: The mean LRS profiles for Pyr calibrations using the *Pt/Ir-PC/POx/PC* electrode, carried out in PBS (pH 7.4) buffer solution containing 10 mM Mg^{2+} at 25 °C (R^2 = 0.998) and 37 °C (R^2 = 0.998). CPA was carried out at +700 mV *vs.* SCE.

5.3.1.1 Introduction of Sugars

Sugars have a wide range of uses, one of which is protein stabilisation. (Arakawa and Timasheff, 1982; Kaushik and Bhat, 2003; James and McManus, 2012). During lyophilisation, it is thought to occur due to the sugar acting as a water substitute which stabilises the protein against unfolding by forming hydrogen bonds to specific sites on the proteins surface (Allison *et al.*, 1999). However, in aqueous solution, it is hypothesised that the stabilisation is due to the repulsive forces between the protein chain and the sugar. This is known as preferential hydration of the protein or preferential exclusion of the sugar (Lin and Timasheff, 2008; Kim, Thapa and Jeong, 2018). This is supported by the hypothesis that protein-sugar interactions are less favourable than protein-water interactions (Xie and Timasheff, 1997; Wang, 1999). As a

result, the protein is preferentially hydrated and the sugar, in this case, is preferentially excluded from the protein surface which gives rise to an increase in chemical potential. This positive change in chemical potential is concentration dependent and therefore increases at higher concentrations. The chemical potential increase is also directly proportional to the proteins surface area that is exposed to the solvent. Since a denatured protein has a much greater surface area than that of a folded protein, the preferential exclusion of the sugar from the surface of the unfolded protein is more unfavourable than exclusion of the sugar from the folded protein and thus increases protein stabilisation (Wang, 1999; Shimizu and Smith, 2004).

Following the work of James and McManus, it was decided to introduce sucrose and trehalose into the enzyme solution as both have been shown to increase the thermal stability of enzymes. Glucose, however, was not introduced as it is not stable over time, it is a reducing sugar which reacts with lysine and arginine residues of the enzyme (James and McManus, 2012). Two separate enzyme solutions were made, each containing the usual enzyme mix of 800 U/mL POx + 80 µM FAD and then either 100 mM sucrose or 100 mM trehalose. The rest of the design did not change. Figure 5.2 and Table 5.1 show that the introduction of 100 mM sucrose into the biosensor design significantly increases both the V_{max} (32.51 ± 1.00 nA, n = 7, $t_{(4.178)}$, p = 0.0015) and sensitivity (8.20 ± 0.10 pA/µM, n = 7, $t_{(7.059)}$, p < 0.0001), while the introduction of 100 mM trehalose has no effect ($t_{(1.102)}$, p = 0.2876) on the V_{max} and decreases sensitivity. Trehalose occupies 2.5 times more space than sucrose for the same concentration, this increase in occupied space is thought to increase the thermal stability (Sola-Penna and Meyer-Fernandes, 1998). However, this increase in occupied space may be having a negative impact on the efficiency and stability of the biosensor by limiting access to the enzyme active site. As a result, sucrose was incorporated into the PC biosensor design for all further experiments.

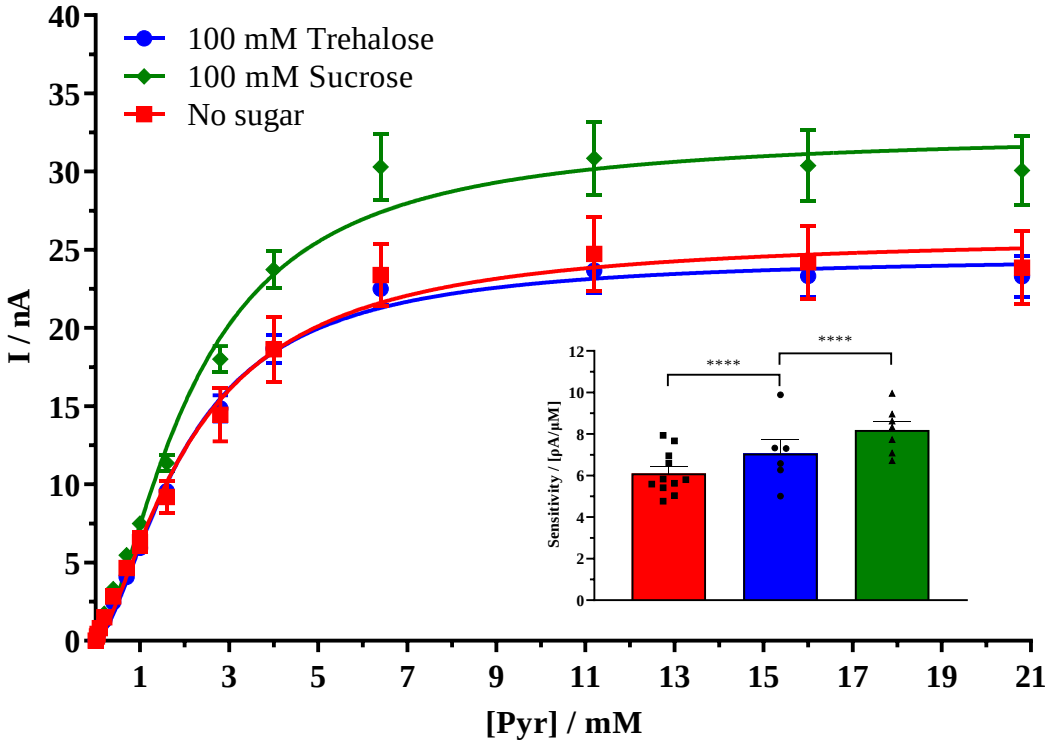

Figure 5.2: The mean current-concentration profiles for Pyr calibrations carried out in PBS (pH 7.4) buffer solution containing 10 mM Mg^{2+} at 25 ºC using the designs *Pt/Ir-PC/POx/PC, Pt/Ir-PC/[POx (800 U/mL) + FAD (80 µM) + Sucrose (100 mM)]/PC* and *Pt/Ir-PC/[POx (800 U/mL) + FAD (80 µM) + Trehalose (100 mM)]/PC.* (Inset) Comparison of LRS; ****p < 0.0001, t-test. CPA was carried out at +700 mV *vs*. SCE.

	No sugar			100 mM Trehalose			100 mM Sucrose		
Kinetic Parameters	**Mean**	**S.E.M.**	**n**	**Mean**	**S.E.M.**	**n**	**Mean**	**S.E.M.**	**n**
V_{max} (nA)	25.98	1.23	6	24.64	0.61	11	32.51	1	7
K_m (mM)	2.17	0.25	6	2.02	0.12	11	2.18	0.16	7
α	1.48	0.19	6	1.6	0.12	11	1.56	0.14	7
Sensitivity (pA/µM)	7.06	0.13	6	6.11	0.08	11	8.20	0.10	7
R^2	0.997	-	6	0.999	-	11	0.998	-	7

Table 5.1: Comparison of the kinetic parameters for the introduction of sucrose and trehalose into the enzyme solution.

5.3.1.2 Sucrose Concentration

In the previous section, it was demonstrated that the introduction of sucrose increased the sensitivity of the biosensor due to preferential hydration of the enzyme. This is due to an increase in chemical potential which is concentration dependant (Wang, 1999). Therefore, the optimum sucrose concentration was investigated.

Three different sucrose concentrations were examined 100, 200 and 300 mM. Each enzyme solution was made up fresh with the corresponding sucrose concentration and 800 U/mL POx and 80 µM FAD. Figure 5.3 shows that the introduction of 200 mM sucrose results in a significant increase ($t_{(3.85)}$, $p = 0.0014$) in sensitivity from 8.20 ± 0.10 pA/µM ($n = 7$, 100 mM) to 8.95 ± 0.14 pA/µM ($n = 11$, 200 mM). The kinetic parameters V_{max}, K_m and α are summarised in Table 5.2. The increase in sensitivity is due to the increased concentration of sucrose increasing stability by preferential hydration. In comparison, the introduction of 300 mM sucrose significantly decreases V_{max} ($t_{(13.37)}$, $p < 0.0001$) and sensitivity ($t_{(6.674)}$, $p < 0.0001$). This indicates that the excessive concentration of sucrose possibly restricts access to

the active sites or hinders optimal enzyme immobilisation. Therefore, 200 mM sucrose was incorporated into the biosensor design.

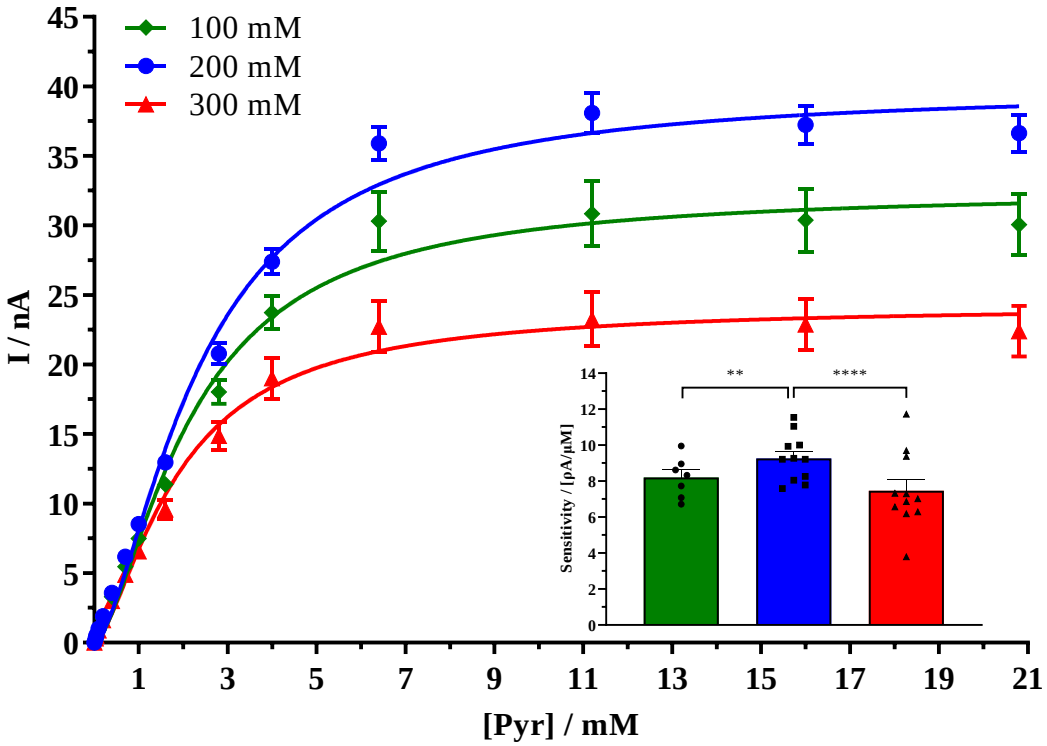

Figure 5.3: The mean current-concentration profiles for Pyr calibrations, carried out in PBS (pH 7.4) buffer solution containing 10 mM Mg^{2+} at 25 ºC using the design *Pt/Ir-PC/[POx (800 U/mL) + FAD (80 µM) + Sucrose (X mM)]/PC.* (Inset) Comparison of LRS; **p = 0.0014; ****p < 0.0001, t-tests. CPA was carried out at +700 mV *vs.* SCE.

	100 mM			200 mM			300 mM		
Kinetic Parameters	**Mean**	**S.E.M.**	**n**	**Mean**	**S.E.M.**	**n**	**Mean**	**S.E.M.**	**n**
V_{max} (nA)	32.51	1	7	39.82	0.76	11	24.24	0.88	11
K_m (mM)	2.18	0.16	7	2.37	0.11	11	1.88	0.17	11
α	1.56	0.14	7	1.58	0.09	11	1.52	0.17	11
Sensitivity (pA/µM)	8.20	0.10	7	8.95	0.14	11	7.46	0.17	11
R^2	0.998	-	7	0.999	-	11	0.996	-	11

Table 5.2: Comparison of the kinetic parameters for varying concentrations of sucrose in the enzyme solution.

5.3.1.3 Temperature Study 2

With the optimum sucrose concentration determined in the previous section, a second temperature study was conducted to determine what improvements, if any, the sucrose makes. As further modifications were possibly required calibrations were only conducted at 25 ^{o}C and 37 ^{o}C.

Similar to Section 5.3.1, calibrations were performed in 10 mL PBS in a jacketed cell at either 25 ^{o}C or 37 ^{o}C using a thermal bath to control the temperature. This is described in more detail in Section 3.6.3. The results presented in Figure 5.4 show a significant decrease ($t_{(21.1)}$, $p < 0.0001$) in sensitivity from 8.95 ± 0.14 pA/µM (n = 11) at 25 ^{o}C to 4.68 ± 0.12 pA/µM (n = 7) at 37 ^{o}C. This large decrease is similar to the decrease in sensitivity seen in Section 5.3.1 and as previously reported in the literature (Malik, Chaudhary and Pundir, 2019). The sensitivity of the biosensor at 37 ^{o}C is roughly half that of the sensitivity at 25 ^{o}C. However, the introduction of the 200 mM sucrose has induced partial thermal stability, but unfortunately there is still a considerable decrease in sensitivity at 37 ^{o}C. If the sensitivities of the biosensor design including 200 mM sucrose is compared to the biosensor design from Section 5.3.1 an increase in sensitivity from 1.72 ± 0.03 pA/µM (n = 10, 37 ^{o}C no sucrose) to 4.68 ± 0.12

pA/µM (n = 7, 37 ºC 200 mM sucrose) is observed. However, this is still significantly lower ($t_{(14.38)}$, $p < 0.0001$) than 7.16 ± 0.12 pA/µM (n = 9, 25 ºC no sucrose). It is evident that this biosensor is still quite temperature dependant and further measures need to be introduced to offset the sensitivity decrease with increasing temperature and therefore this design was rendered unsuitable for any further temperature studies.

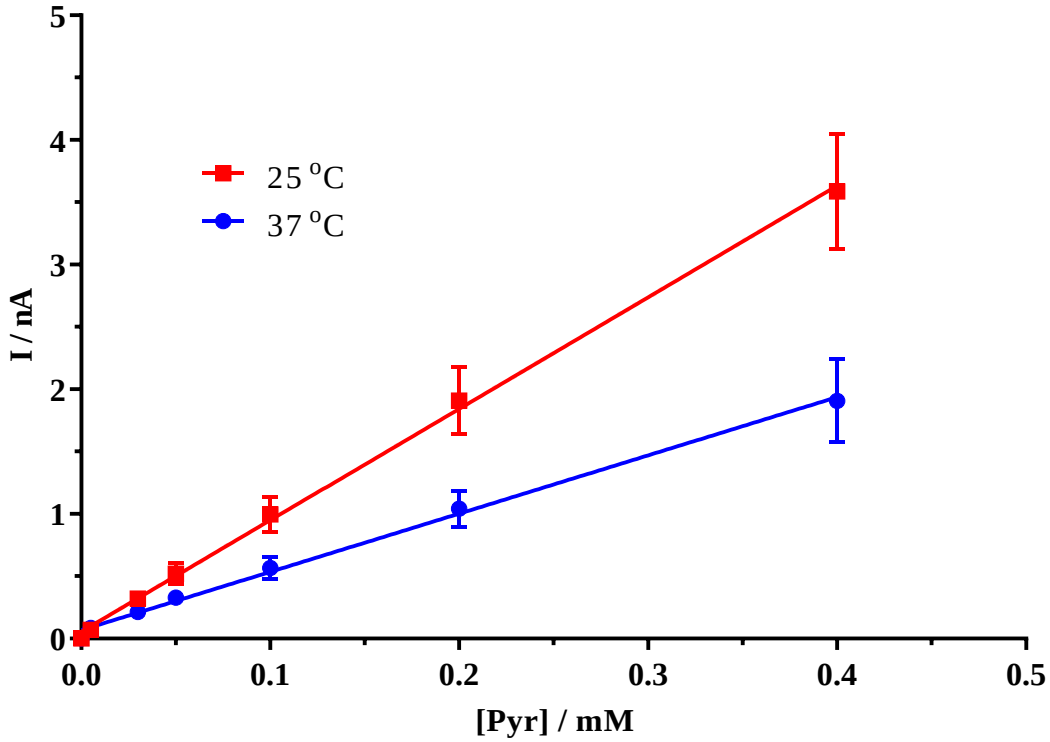

Figure 5.4: The mean LRS profiles for Pyr calibrations carried out in PBS (pH 7.4) buffer solution containing 10 mM Mg^{2+} at 25 ºC (R^2 = 0.999) and 37 ºC (R^2 = 0.997) using the design *Pt/Ir-PC/POx/PC*. CPA was carried out at +700 mV *vs.* SCE.

5.3.1.4 Increased Layers

As stated previously in Chapter 4 Section 4.3.7, BSA is widely used in biosensor development as it increases the stability of the enzyme, but it is also known for increasing thermal stability (Dong *et al.*, 2010). Therefore, it was decided to increase the layers of BSA in the biosensor design to investigate what thermal stability, if any, it provided. However, the increase in BSA

concentration in the biosensor design must be taken into consideration as, at high concentrations, the lysine residues of the BSA compete with the lysine residues of the enzyme preventing necessary cross-linking between the GA and the enzyme (Shah, Sharma and Gupta, 2006). To overcome this issue, it was decided to not only increase the layers of BSA in the design but all three of the cross-linkers and stabilisers, and to add them after every layer of enzyme.

The concentration of BSA, GA and PEI remained the same as in previous designs, 1 %, 0.25 % and 2 % respectively. As in Section 5.3.1.1, since there is a change in the overall design, a full calibration was carried out to determine what changes, if any, occur to all of the kinetic parameters. Figure 5.5 and Table 5.3 show there is a significant increase in all kinetic parameters. Most importantly, there is a significant increase ($t_{(4.279)}$, $p = 0.0004$) in sensitivity from 8.95 ± 0.14 pA/µM (n = 11, Final Layer) to 9.66 ± 0.08 pA/µM (n = 10, Every Layer). This increase can be attributed to the increased concentration of GA and BSA. The function of each component and the method by which this is achieved has been previously discussed in Chapter 4 Section 4.3.5 and Section 4.3.7. It is hoped that this increase in sensitivity coupled with the increased thermal stability provided by the extra BSA layers will offset the thermal denaturation of the enzyme at physiological relevant temperatures. The biosensor design was then given as:

$$Pt/Ir\ (disc) - \{Sty - ([POx\ (800\ U/mL) + FAD\ (80\ \mu M) + Sucrose\ (200\ mM)] + BSA\ (1\ \%) + GA\ (0.25\ \%) + PEI\ (2\ \%))_{15}\}$$

This was then considered the best design and referred to as Pt/Ir-PC/POx/PC_{15} for all further characterisation unless changed again.

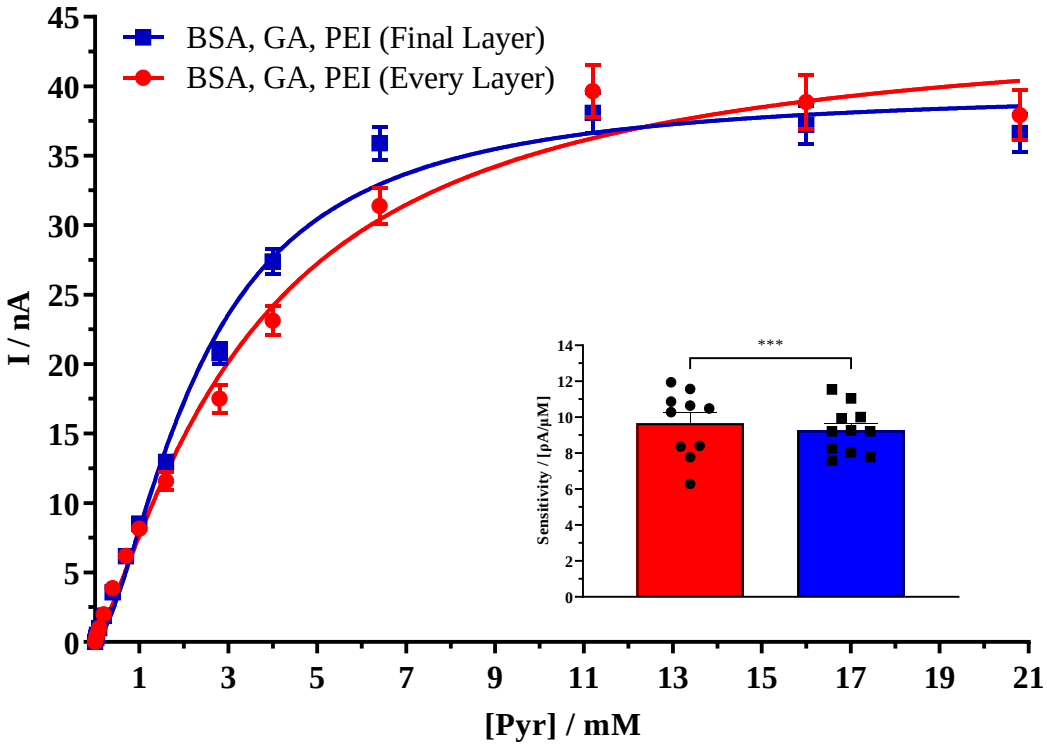

Figure 5.5: The mean current-concentration profiles for Pyr calibrations carried out in PBS (pH 7.4) buffer solution containing 10 mM Mg^{2+} at 25 °C using the design *Pt/Ir (disc) – {Sty – [POx (800 U/mL) + FAD (80 µM) + Sucrose (200 mM)]* $_{15}$ *+ BSA (1 %) + GA (0.25 %) + PEI (2 %)}* and *Pt/Ir (disc) – {Sty – ([POx (800 U/mL) + FAD (80 µM) + Sucrose (200 mM)] + BSA (1 %) + GA (0.25 %) + PEI (2 %))*$_{15}$*}*. (Inset) Comparison of LRS; ***p = 0.0004, t-test. CPA was carried out at +700 mV *vs*. SCE.

	BSA, GA, PEI (Final Layer)			BSA, GA, PEI (Every Layer)		
Kinetic Parameters	**Mean**	**S.E.M.**	**n**	**Mean**	**S.E.M.**	**n**
V_{max} (nA)	39.82	0.76	11	44.74	1.73	10
K_m (mM)	2.37	0.11	11	3.52	0.32	10
α	1.58	0.09	11	1.25	0.09	10
Sensitivity (pA/μM)	8.95	0.14	11	9.66	0.08	10
R^2	0.999	-	11	0.999	-	10

Table 5.3: Comparison of the kinetic parameters for varying layers of cross-linkers and stabilisers.

5.3.1.5 Temperature Study 3

To evaluate what improvements, if any, the increase in BSA, GA and PEI layers have on the thermal stability of the biosensor a third temperature study was carried out. Brain temperature fluctuates by 3.5 - 4.0 ^{o}C with the accepted temperature range between 35.5 ^{o}C and 38.8 ^{o}C (Kiyatkin, Wakabayashi and Lenoir, 2013). Therefore, to determine the temperature dependence of this biosensor, calibrations were carried out at 34 ^{o}C and 40 ^{o}C, which represent physiological extremes, compared to the standard physiological temperature of 37 ^{o}C. 25 ^{o}C was included as a reference for performance of the biosensor as all design testing (Chapter 4) was carried out at room temperature. Changes in temperature can drastically affect the performance of a biosensor, either positively or negatively and in the case of this biosensor, negatively. However, once this is accounted for the biosensor can still be accurate even outside its optimum range (Rocchitta *et al.*, 2016).

Similarly, to Section 5.3.1 and 5.3.1.3, calibrations were performed in 10 mL PBS in a jacketed cell at either 25 ^{o}C, 34 ^{o}C, 37 ^{o}C or 40 ^{o}C using a thermal bath to control the temperature. Similarly, to the previous temperature studies a general downward trend in sensitivity with increasing temperature was observed (Figure 5.6). While a decrease in sensitivity is still

observed at physiologically relevant temperatures in comparison to room temperature for Pt/Ir-PC/POx/PC_{15}, when compared against physiological temperatures from the previous temperature study, Section 5.3.1.3, an increase is seen. For 37 ^{o}C, a significant increase ($t_{(17.81)}$, $p < 0.0001$) can be seen from 4.68 ± 0.12 pA/µM (n = 7) to 8.24 ± 0.15 (n = 8). When compared to the initial temperature study carried out in Section 5.3.1, it can be seen that the sensitivity of the original best design (Pt/Ir-PC/POx/PC) at 25 ^{o}C was 7.16 ± 0.12 pA/µM (n = 9) which is significantly lower ($t_{(5.583)}$, $p < 0.0001$) than the sensitivity of this latest design (Pt/Ir-PC/POx/PC_{15}) at a physiological temperature of 37 ^{o}C, given as 8.24 ± 0.15 (n = 8). As a result, the modifications applied in Section 5.3.1.2 and 5.3.1.4 have added sufficient thermal stability to the biosensor design. There is, however, still a large degree of denaturation occurring at 40 ^{o}C (Figure 5.6). While this is viewed as physiologically extreme and it is not ideal, these excessively high physiological temperatures are only seen in specific situations such as induced psychomotor stimulation via methamphetamine or 3,4-methylenedioxymethamphetamine (MDMA) (Brown, Wise and Kiyatkin, 2003; Brown and Kiyatkin, 2004). Cordeiro *et al.* published preliminary data on recorded basal pyruvate levels *in-vivo* with a multiplex biosensor which utilised the same enzyme employed in this design (Cordeiro *et al.*, 2015). This indicated that, despite the decrease in sensitivity at physiological temperatures, the sensor may be viable for *in-vivo* use. Therefore, the Pt/Ir-PC/POx/PC_{15} biosensor will be further characterised to determine its suitability for neurochemical monitoring.

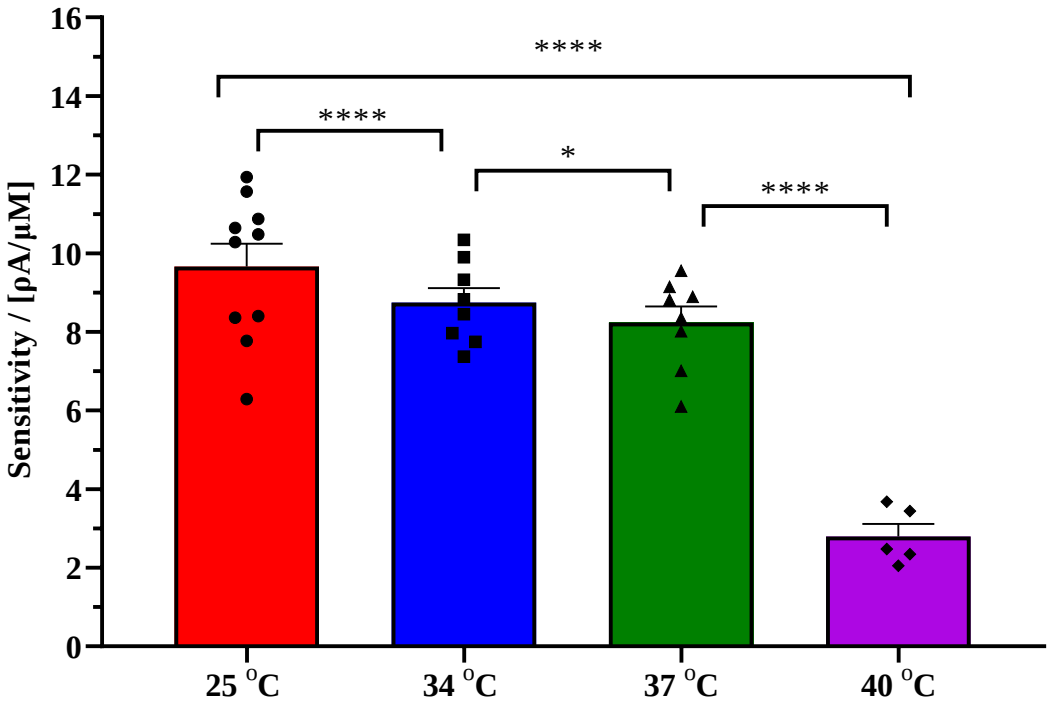

Figure 5.6: The mean LRS for Pyr calibrations carried out in PBS (pH 7.4) buffer solution containing 10 mM Mg^{2+} at 25 °C (R^2 = 0.999), 34 °C (R^2 = 0.999), 37 °C (R^2 = 0.998) and 40 °C (R^2 = 0.990) using design *Pt/Ir-PC/POx/PC*$_{15}$. $F_{(3, 27)}$ = 521.2, *p = 0.0234, ****p < 0.0001, ANOVA, multiple comparisons. CPA was carried out at +700 mV *vs.* SCE.

5.3.2 pH Study

pH is another common characterisation parameter that must be investigated for a biosensor to determine the viability for *in-vivo* application. pH in the brain is approximately 7.3 – 7.4 (Casey, Grinstein and Orlowski, 2010). Ion pump transport (active and passive) mechanisms tightly regulate this parameter (Orlowski *et al.*, 2011). Therefore, pH is generally tested over a relatively small physiological range of 7.2 – 7.6 (Baker *et al.*, 2019). The optimum pH of POx is 5.5 – 6.5 depending on the enzyme source (Rahman *et al.*, 2006; Malik, Chaudhary and Pundir, 2019). The POx used in the developed biosensor has an optimum pH of 5.7 as per the manufacturer and was prepared in PBS solution (pH 5.7) as described in Chapter 3 Section

3.3.2.1. In this section the pH of the bulk solution was altered to investigate what effect changing the pH has on the LRS. pH 7.2, pH 7.4 and pH 7.6 were examined.

Figure 5.7 show the effect of increasing pH on the sensitivity of the biosensor. A clear downward trend in sensitivity is seen with increasing pH. The significant decrease ($F_{(2, 20)}$ = 461.2, $p < 0.0001$, ANOVA, multiple comparisons) from 11.57 ± 0.09 pA/µM (n = 7) at pH 7.2 to 9.66 ± 0.08 pA/µM (n = 10) at pH 7.4 and subsequently to 7.42 ± 0.11 pA/µM (n = 6) at pH 7.6 corresponds with what is seen in the literature. Multiple publications state that with the low optimum pH of the enzyme source, pH 5.7, increases in pH above 6 or 7 generally result in drastic decrease in sensitivity (Rahman *et al.*, 2006; Bayram and Akyilmaz, 2014; Malik, Chaudhary and Pundir, 2019). Despite the enzyme solution being buffered to pH 5.7 in accordance with the manufacturer's recommendations, it is not sufficient to stop significant decreases ($F_{(2, 20)}$ = 461.2, $p < 0.0001$, ANOVA, multiple comparisons) with increases in pH across the entire experimental range. While this is not ideal, pH in the brain is tightly regulated between 7.3 - 7.4 (Casey, Grinstein and Orlowski, 2010) and pH imbalances, such as brain alkalosis, are only seen in specific situations where there is damage to the blood brain barrier (Pannier *et al.*, 1978). Due to this tightly regulated nature of pH in the brain coupled with extreme physiological levels only seen in very specific situations, it is hoped that minimal fluctuations in pH will be seen and therefore not affect the capability of the biosensor to be deployed in the *in-vivo* environment.

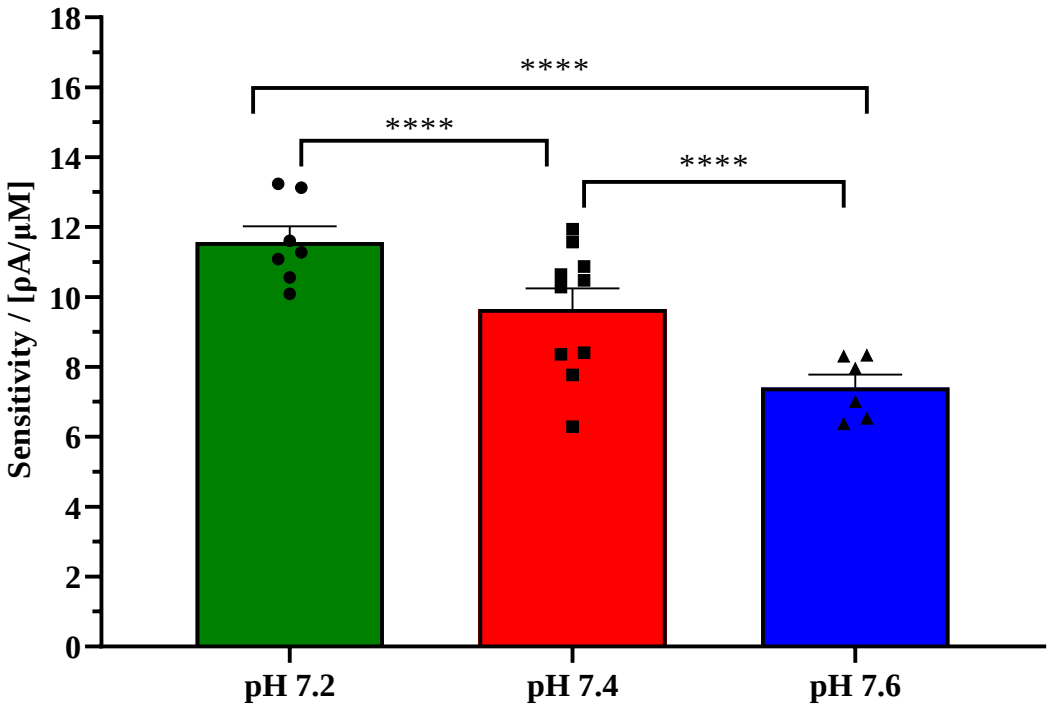

Figure 5.7: The mean LRS for Pyr calibrations carried out in PBS buffer solution at pH 7.2 (R^2 = 0.999), 7.4 (R^2 = 0.999) and 7.6 (R^2 = 0.999) containing 10 mM Mg^{2+} at 25 ºC using the design *Pt/Ir-PC/POx/PC*$_{15}$. ****p < 0.0001, ANOVA, multiple comparisons. CPA was carried out at +700 mV *vs*. SCE.

5.3.3 Oxygen Dependence

The next step of the characterisation process was to examine the O_2 dependence of the biosensor. Most enzyme based biosensors utilise the bio-catalytic oxidation of an analyte by using an oxidase enzyme (O'Neill *et al.*, 2008). Scheme 5.1 shows how this design utilises pyruvate oxidase to catalytically convert the substrate (pyruvate) and co-substrates (O_2, H_2O and phosphate) into the products (acetyl phosphate, CO_2 and H_2O_2) in the presence of the co-factors flavin adenine dinucleotide (FAD), thiamine pyrophosphate (TPP) and a divalent metal cation such as Magnesium (Mg^{2+}) (Bayram and Akyilmaz, 2014). It can be seen from this that O_2 is required by the reaction to generate the H_2O_2 which is detected at the electrode surface. Basal O_2 levels in the brain range from 40 – 80 µM (Kayama *et al.*, 1991; Murr *et al.*, 1994; Bolger and Lowry, 2005) therefore, it is important that fluctuations in brain O_2 levels don't affect the response of the pyruvate sensor. An oxygen dependence study was performed to determine what effect, if any, changing O_2 levels have on the pyruvate response. In the standard cell setup, a 100 µM concentration of pyruvate was injected into 20 mL N_2 saturated PBS which was then followed by a full O_2 calibration (0 – 200 µM). This is described in more detail in Chapter 3 Section 3.6.4.

$$\text{Pyruvate} + \text{Phosphate} + O_2 + H_2O \xrightarrow[\text{POx}]{\text{FAD,TPP,Mg}^{2+}} \text{Acetyl phosphate} + CO_2 + H_2O_2 \qquad [1]$$

$$H_2O_2 \rightarrow O_2 + 2H^+ + 2e^- \ (+700\ \text{mV}\ vs.\ \text{SCE}) \qquad [2]$$

Scheme 5.1:[1] The conversion of pyruvate, phosphate, O_2 and H_2O into acetyl phosphate, CO_2 and H_2O_2 by pyruvate oxidase in the presence of the co-factors FAD, TPP and Mg^{2+}. [2] The oxidation of H_2O_2 at the electrode surface at +700 mV *vs.* SCE.

The data presented in Figure 5.8 and Table 5.4 shows the Michaelis-Menten curve for the O_2 calibration. The K_m of 6.18 ± 1.43 µM (n = 7) is quite low and compares well with choline ($K_m(O_2)$ = 16.5 µM, n = 7) and glucose ($K_m(O_2)$ = 15 ± 1 µM, n = 7) biosensors previously published by the research group (Dixon, Lowry and O'Neill, 2002; Baker, Bolger and Lowry, 2017). While a larger K_m is preferred for the target substrate a small K_m is preferred for co-substrates as then the current generated for the substrate is independent of the co-substrate

unless at very low concentrations of the co-substrate (Dixon, Lowry and O'Neill, 2002; Berg, Tymoczko and Stryer, 2012). When O_2 concentrations are below 25 µM, there is a decrease in the pyruvate response. However, the O_2 calibration is well into the plateau region of the curve for the relevant basal O_2 concentration range of 40 – 80 µM. This indicates that changes in O_2 levels in the brain will have no effect on the pyruvate signal. Therefore, the biosensor is sufficiently independent of changes in O_2 levels within the relevant physiological range indicating that it may be reliably used in the *in-vivo* environment to monitor pyruvate.

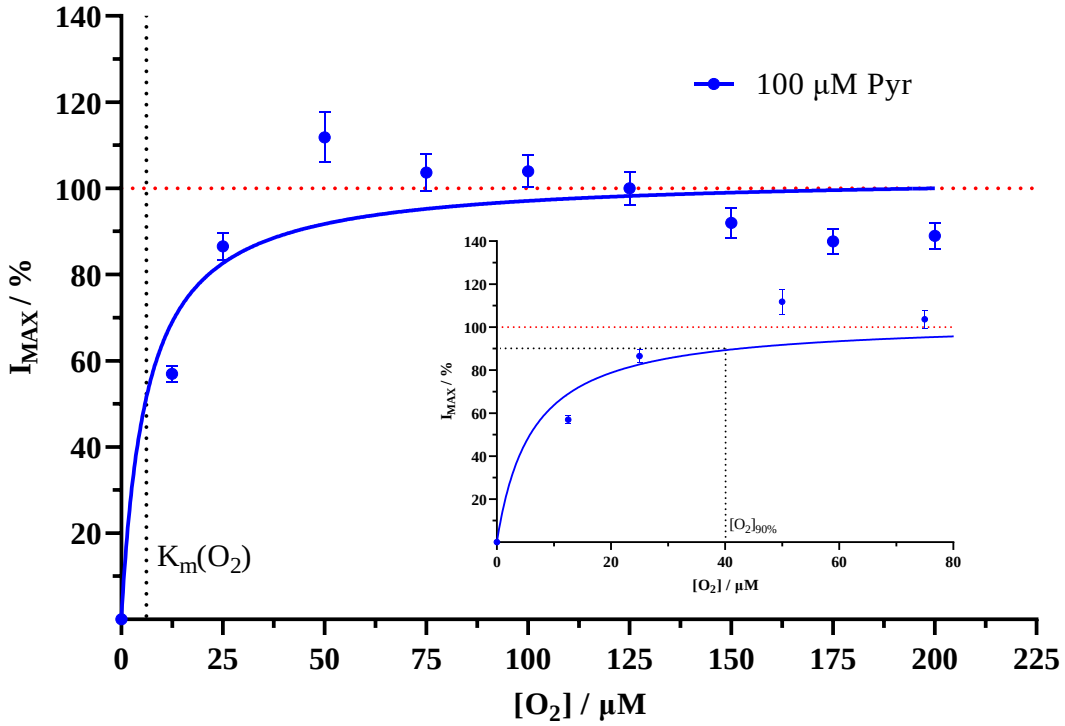

Figure 5.8: The effect of changing oxygen levels (0 to 200 µM) on the averaged normalised *Pt/Ir-PC/POx/PC15* biosensor signal for 100 µM pyruvate (n = 8). Non-linear regression analysis yielded $K_m(O_2)$ = 6.18 ± 1.43 µM (R^2 = 0.8341). (Inset) Pooled data for 100 µM pyruvate over physiological O_2 range used to determine $[O_2]_{90\ \%}$ (ca. 40 µM).

O_2 (µM)	Mean	S.E.M.	n
0	0.00	0.00	7
12.5	0.43	0.01	7
25	0.66	0.02	7
50	0.85	0.04	7
75	0.79	0.03	7
100	0.79	0.03	7
125	0.76	0.03	7
150	0.70	0.03	7
175	0.67	0.02	7
200	0.68	0.02	7

Table 5.4: Mean 100 µM pyruvate current responses associated with changing O_2 concentration.

5.3.4 Shelf-Life

The performance of the biosensor, up to this point, has shown a high degree of sensitivity. However, all experiments have been conducted 24 hrs after fabrication. This section investigates the effect storage time has on the biosensor response. It has been noted in the literature that the response of a biosensor can be affected by exposure to certain stresses such as oxygen, humidity and elevated temperatures (Chaniotakis, 2004; Snyder *et al.*, 2011). The shelf-life of a biosensor is one of two biosensor stability elements which involves the fabrication of a biosensor and then storing it for a period of time to investigate its stability when not in use. The second element of biosensor stability is operational stability where the stability over repeated measurements is investigated (Chaniotakis, 2004), see Section 5.3.5. The shelf-life of a biosensor plays an important role in the transfer of a biosensor to a commercial market (Gibson *et al.*, 1992). This is especially evident in biosensors such as blood glucose sensors for diabetes where sensors have a prolonged shelf-life before use where they remain stable for several months (Hoss and Budiman, 2017).

In this section sensors were fabricated on day 0 and stored at -20 ^{o}C for either 7 or 14 days and then calibrated. The LRS from the day 7 and day 14 electrodes were then compared to a

reference set of day 1 best design electrodes to determine what effect, if any, storage time has on the biosensor response. Figure 5.9 shows the effect of shelf life on the LRS of the biosensor design and it can be seen that there is a slight decrease in sensitivity across the time period from day 1 to day 14. While this is significant ($F_{(2, 20)} = 5.88$, $p = 0.0098$, ANOVA, multiple comparisons), there is only a 0.48 nA difference across the two week period. However, over 7 day periods this change is not significant ($p = 0.8043$, ANOVA, multiple comparisons). This indicates the biosensor is stable over time, up to at least 14 days. This storage stability is possibly due to the sucrose (Section 5.3.1.2) and PEI (Chapter 4) It may also be due to the storage at –20 ^{o}C, as per the manufacturer's recommendations, as it has been reported in the literature that low temperature storage increases stability over time (Puggioni *et al.,* 2019). Prior to implantation all electrodes are pre-calibrated for pyruvate over the linear range (0 – 400 µM) to determine the exact sensitivity of each biosensor to be implanted and this accounts for any decrease in sensitivity caused by prolonged storage.

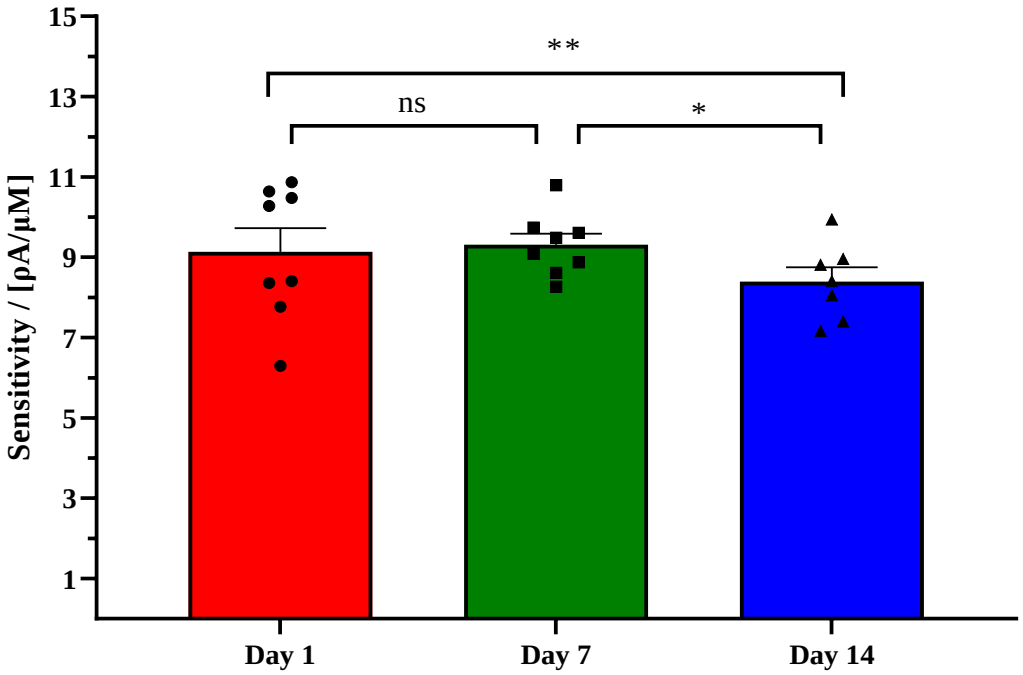

Figure 5.9: The mean LRS for Pyr calibrations carried out on days 1 (R^2 = 0.999), 7 (R^2 = 0.999) and 14 (R^2 = 0.999) in PBS (pH 7.4) buffer solution containing 10 mM Mg^{2+} at 25 ºC using the design *Pt/Ir-PC/POx/PC*$_{15}$. ns = 0.8043, *p = 0.0105, **p = 0.0098, ANOVA, multiple comparisons. A different set of electrodes was used on each day. CPA was carried out at +700 mV *vs.* SCE.

5.3.5 Stability

As highlighted in the previous section shelf-life and stability are similar characterisation parameters. While the previous section focused on shelf-life stability this section focuses on operational stability. This refers to the precision of the same biosensor over a specific time period under continuous or intermittent monitoring with the most important factor being the enzyme activity (Chaniotakis, 2004). Operational stability is often the more quoted stability parameter in biosensor publications as it is related to both the devices reusability and to its operating lifetime (Gibson, 1999). This is important in the context of this biosensor as it can provide an estimated *in-vivo* operational life-span. However, operational stability can be

irrelevant in certain cases while shelf-life stability is of critical importance, such as for single use disposable glucose biosensors (Gibson, 1999).

For this study sensors were fabricated on day 0 and calibrated on day 1, they were then stored at -20 ^{o}C for 7 days and then re-calibrated. Following this calibration, they were again placed in dry storage at – 20 ^{o}C for a further 7 days and then re-calibrated for a third time on day 14. The LRS value from day 1, day 7 and day 14 were compared for each electrode to determine what effect, if any, repeated calibrations have on the sensitivity of the biosensor. It can be seen from the data shown below in Figure 5.10 that there is a significant decrease ($F_{(2, 24)} = 363.7$, $p < 0.0001$, ANOVA) in sensitivity from 8.12 ± 0.04 pA/µM (n = 8) on Day 1 to 7.49 ± 0.08 pA/µM (n = 8) on day 7 and subsequently to 5.25 ± 0.11 pA/µM (n = 8) on Day 14. This indicates that repeated calibrations and storage cycles have a diminishing effect on the biosensor's response. This is possibly due to loss of enzyme activity and has been reported in the literature previously (Saurina *et al.*, 1998; Baker *et al.*, 2019). Despite this decrease being quite significant there is still a relatively large sensitivity retained on Day 14 of 5.25 ± 0.11 pA/µM (n = 8). This decrease in sensitivity over time indicates that the biosensor may not be stable for sustained periods of recording *in-vivo*. However, while operational stability indicates the performance of the biosensor over a period of time it is not comparable with continuous recording *in-vivo* and therefore operational stability in the *in-vivo* environment also had to be examined (Chapter 6, Section 6.5.3.3).

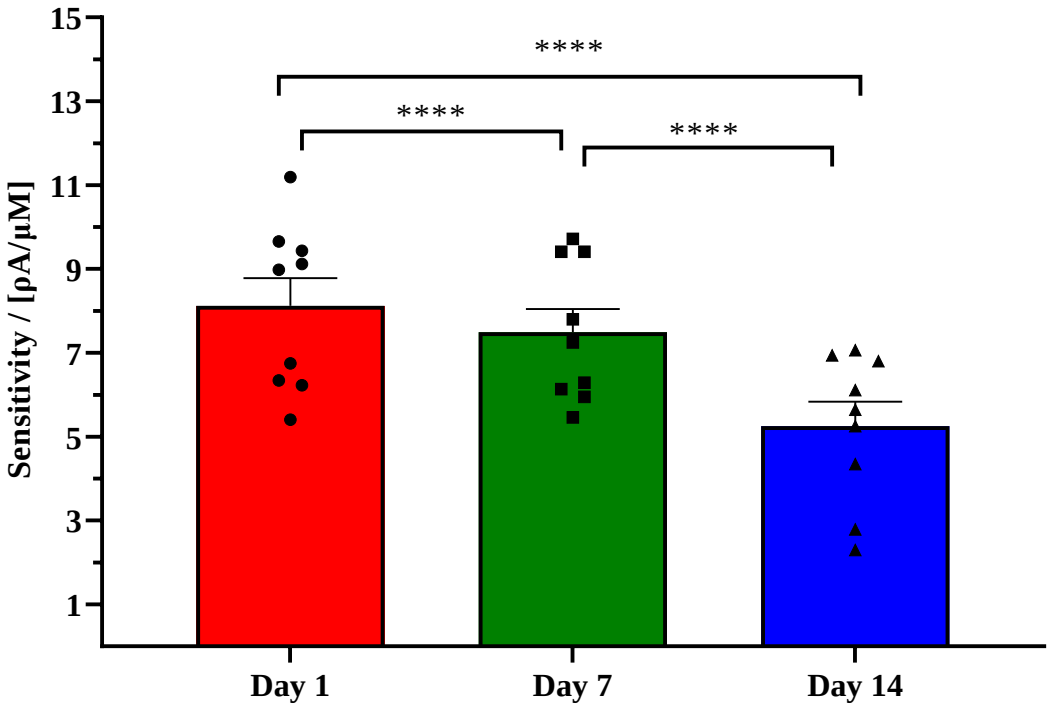

Figure 5.10: The mean LRS for Pyr calibrations carried out on day 1 (R^2 = 0.999), 7 (R^2 = 0.997) and 14 (R^2 = 0.998) in PBS (pH 7.4) buffer solution containing 10 mM Mg^{2+} at 25 ºC using the design *Pt/Ir-PC/POx/PC*$_{15}$. ****p < 0.0001, ANOVA. The same set of electrodes were used on each day. CPA was carried out at +700 mV *vs.* SCE.

5.3.6 Interference Rejection Layer

Pyruvate biosensors have generally suffered from selectivity issues as previously stated. To deal with this issue an interference rejection layer was used. The incorporation of an *o*-phenylenediamine (*o*-PD) (see Chapter 3 Section 3.5.1) layer onto the electrode surface can provide sufficient interference rejection. The electropolymerisation of *o*-PD has been a regularly utilised method for interference rejection (O'Neill *et al.*, 2008; Doran, Finnerty and Lowry, 2017; Knyzhnykova *et al.*, 2018; Baker *et al.*, 2019). This poly-phenylenediamine (PPD) layer is permeable to H_2O_2 but isn't permeable to larger molecules such as AA (Killoran and O'Neill, 2008) which is the main interferant in brain extracellular fluid (ECF) with a concentration of 500 µM (Grünewald, 1993). AA and other larger molecules are eliminated by

a process known as ‘self-blocking’ where at high concentrations the interferant blocks access to the electrode surface which decreases its response without hindering the response of the target analyte (Lowry and O’Neill, 1992; Craig and O’Neill, 2003).

5.3.6.1 Pyruvate calibration

As stated above PPD is permeable to H_2O_2 and therefore, should not affect the biosensors response to pyruvate (Lowry and O’Neill, 1994). Pyruvate calibrations were carried out in the presence and absence of PPD to ensure the PPD layer does not affect the LRS of the biosensor. A pyruvate LRS calibration was performed in 20 mL PBS at +700 mV (*vs.* SCE) using the best design pyruvate biosensor, one set of these electrodes also incorporated a PPD interference rejection layer to investigate what effect, if any, the PPD layer has on the pyruvate response. From the data presented in Figure 5.11 it is clear that the introduction of PPD does not hinder the response to pyruvate. There is no significant difference ($t_{(0.3571)}$, p = 0.7254) between the LRS of biosensors incorporating PPD, given as 10.01 ± 0.23 pA/µM (n = 9), and the LRS of the biosensor design without PPD at 10.1 ± 0.05 pA/µM (n = 10). PPD was thus incorporated into the best design (Pt/Ir-PPD-PC/POx/PC_{15}).

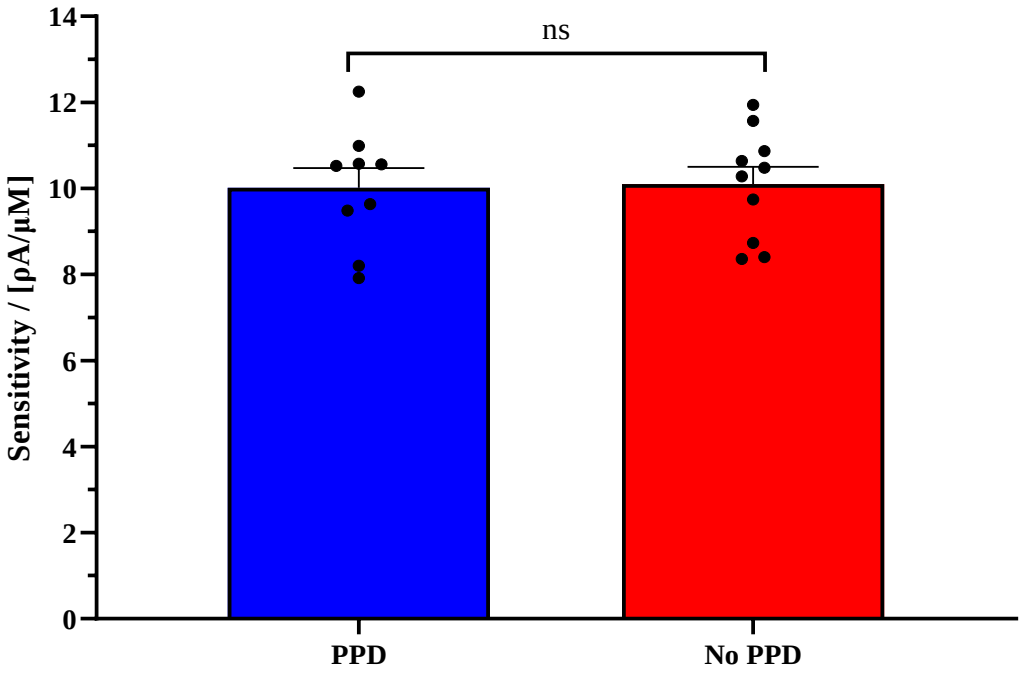

Figure 5.11: The mean LRS for Pyr calibrations carried out in PBS (pH 7.4) buffer solution containing 10 mM Mg^{2+} at 25 °C using the designs; *Pt/Ir-PC/POx/PC$_{15}$* (R^2 =0.999) and *Pt/Ir – PPD – PC/POx/PC$_{15}$* (R^2 = 0.997). ns = 0.7254, t-test. CPA was carried out at +700 mV *vs.* SCE.

5.3.6.2 AA calibration

As the PPD layer has no effect on the response to the target analyte. The next step was to investigate how effective this layer was at eliminating the response of AA, the main interferant in the brain (Grünewald, 1993).

A full AA calibration (0 – 1000 µM) was performed in 20 mL PBS at +700 mV (*vs.* SCE) on the best design pyruvate biosensor (Chapter 3 section 3.6.5) both in the presence and absence of the PPD interference rejection layer to ensure the biosensor sufficiently removed AA interference when PPD was incorporated. Figure 5.12 shows that PPD significantly decreases ($t_{(16.24)}$, $p < 0.0001$) the AA response from 24.99 ± 1.54 pA/µM (n = 8, no PPD) to -0.01 ± 0.1 pA/µM (n = 8, PPD). Basal pyruvate levels in the brain are in the region of 120 – 300 µM

(Schulz *et al.*, 2000; Zetterling *et al.*, 2009; Cordeiro *et al.*, 2015) and the current produced by this biosensor for this concentration range is between 0.99 ± 0.04 nA (n = 11, 100 µM) and 3.59 ± 0.15 nA (n = 9, 400 µM). In comparison the current response to a physiological concentration of AA is between 7.75 ± 0.77 nA (n = 7, 200 µM) and 13.78 ± 0.87 nA (n = 7, 400 µM). This would completely mask the pyruvate response, however, the current response to physiological concentration of AA on a pyruvate biosensor incorporating the PPD interference rejection layer is negligible illustrating the effectiveness of the self-blocking effect (Lowry and O'Neill, 1994; Craig and O'Neill, 2003).

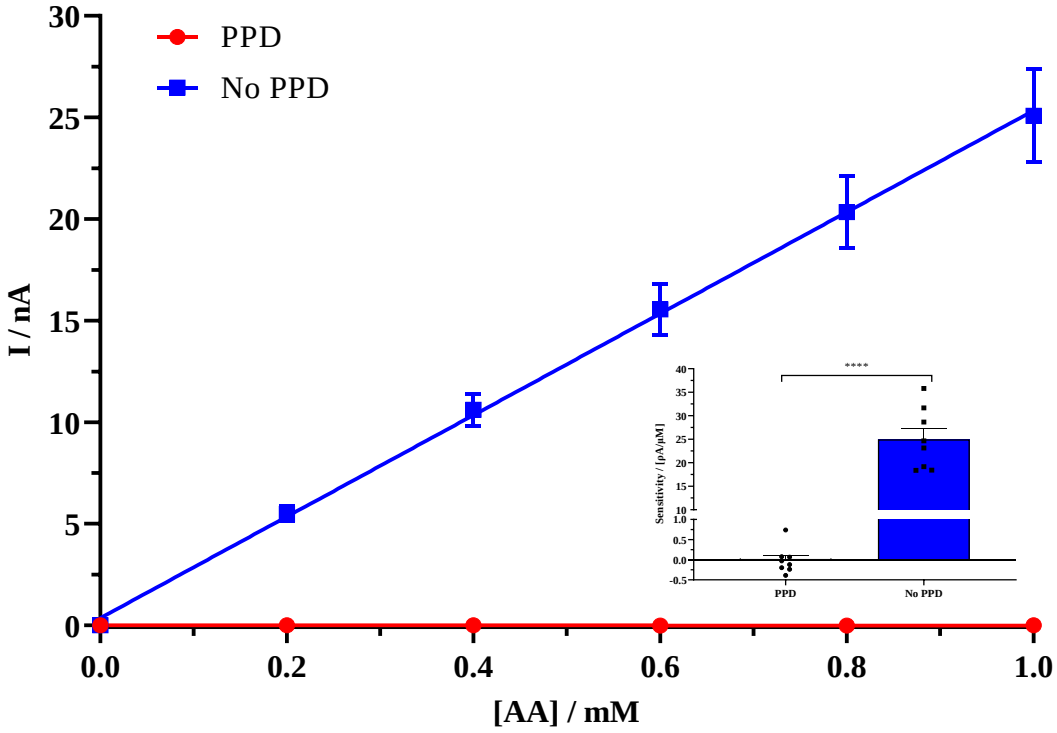

Figure 5.12: The mean current-concentration profiles for AA calibrations carried out in PBS (pH 7.4) buffer solution containing 10 mM Mg^{2+} at 25 ºC using the designs; *Pt/Ir-PC/POx/PC*$_{15}$ (R^2 = 0.852) and *Pt/Ir – PPD – PC/POx/PC*$_{15}$ (R^2 = 0). (Inset) Comparison of sensitivity; ****p < 0.0001, t-test. CPA was carried out at +700 mV *vs*. SCE.

5.3.6.3 Extensive Interference Study

It has been established that the PPD interference rejection layer does not affect the pyruvate response while effectively eliminating the AA response. However, the brain is a highly complex structure with a wide range of electroactive substances. It also contains electro-catalysts and a tissue matrix that not only restricts mass transport to the biosensor but also reacts physiologically to the electrodes presence in the tissue (O'Neill and Lowry, 2000). Therefore, the selectivity of the biosensor must be examined against a range of potential interferants and surface modifying agents found in the ECF. The compounds selected for testing were the most common species present in the ECF (O'Neill and Lowry, 2000). They were the neurotransmitters 5-hydroxytryptomine (5-HT) and dopamine (DA), their metabolites homovanillic acid (HVA), dihydroxyphenylacetic acid (DOPAC) and 5-Hydroxyindolacetic acid (5-HIAA), the amino acids L-cystine, L-tyrosine and L-tryptophan, AA and its oxidised form dehydroascorbic acid (DHAA), the anti-oxidant L-glutathione and finally the purine metabolite uric acid (UA) (Baker *et al.*, 2019). A full interference study was performed in 20 mL PBS at +700 mV (*vs.* SCE) on the best design pyruvate biosensor (Chapter 3 section 3.6.6).

Figure 5.13 shows the relative current change with respect to a physiological pyruvate concentration of 200 µM. A slight increase in current of 0.10 ± 0.03 nA (n = 7) was observed, indicating there is an initial small response to AA as expected, but this response represents only a 5.16 ± 1.32 % portion of the total pyruvate response. After AA all the remaining interferants were added as described in Chapter 3 Section 3.6.6 and little to no response was observed indicating no detection of the specific interferant. In some cases where there was no detection of the interferent negative values attributable to baseline drift/random noise were observed (Bolger, Bennett and Lowry, 2011). These results show that the pyruvate biosensor is highly selective towards pyruvate. The small initial response to AA is negligible, and as stated above the self-sealing effect will diminish this response over time. This high level of selectivity was therefore indicative of suitability for pyruvate detection in the *in-vivo* environment.

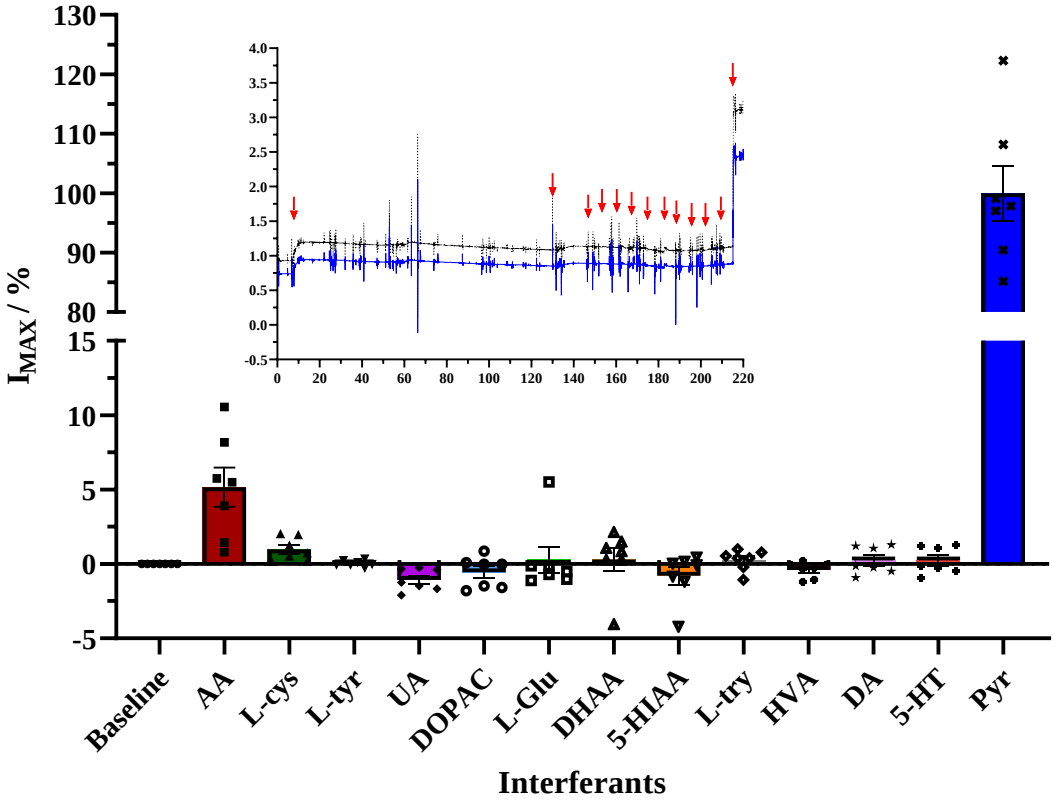

Figure 5.13: The mean current-change from the previous response is shown for a full interferant calibrations, carried out in PBS (pH 7.4) buffer solution containing 10 mM Mg^{2+} and 500 µM AA at 25 ºC using the *Pt/Ir-PC/POx/PC*. (Inset) Average raw data trace (blue) with error (grey) for a full interference calibration. Arrows indicate injections of each interferant and pyruvate in the same order as presented in the histogram. CPA was carried out at +700 mV *vs.* SCE.

	Response from interferant (nA)			Relative Change (%)		
Interferant	**Mean**	**S.E.M.**	**n**	**Mean**	**S.E.M.**	**n**
Baseline	0	0	7	0	0	7
500 µM AA	0.10	0.03	7	5.16	1.32	7
50 µM L-Cys	0.02	0.01	7	0.97	0.30	7
100 µM L-Tyr	0	0	7	0	0	7
50 µM UA	-0.02	0.01	7	0	0	7
20 µM DOPAC	-0.01	0.01	7	0	0	7
50 µM L-Glu	0.01	0.02	7	0.27	0.88	7
100 µM DHAA	0.01	0.01	7	0.28	0.77	7
50 µM 5-HIAA	-0.02	0.01	7	0	0	7
100 µM L-Try	0	0	7	0	0	7
10 µM HVA	-0.01	0	7	0	0	7
0.05 µM DA	0	0	7	0	0	7
0.01 µM 5-HT	0	0	7	0	0	7
200 µM Pyr	1.90	0.09	7	100	4.61	7

Table 5.5: The mean current response, in nA, and the relative change to the baseline current as a percentage of the pyruvate response for all interferants.

5.3.7 Limit of Detection

The next performance parameter that was investigated was the LOD. The LOD is particularly important when fabricating a biosensor to monitor fast transients in brain neurotransmitters which have quite low ECF concentrations (O'Neill *et al.*, 2008). The LOD is described as three times the standard deviation of the baseline (Baker *et al.*, 2019). This value is the minimum concentration of a substrate, in this case pyruvate, that the sensor can reliably detect. Anything below this calculated value is said to be compromised by the background noise from the electrochemical setup and as a result is unreliable and cannot be attributed to changes in pyruvate levels.

The combined baseline current of eight pyruvate biosensors was 2.9 ± 0.46 pA (n = 8), with a sensitivity of 8.71 ± 0.12 pA/µM (n = 10). Therefore, the LOD was determined to be 0.33 ± 0.17 µM. As already stated, the physiological range for brain ECF pyruvate is between 120 – 300 µM (Schulz *et al.*, 2000; Cordeiro *et al.*, 2015) therefore, the LOD is sufficiently lower than the physiological range thus indicating suitability for *in-vivo* applications.

5.3.8 Response Time

Another important performance parameter that must be taken into consideration is the response time. Response time is defined as the time taken for the substrate response to rise from 10 % to 90 % ($t_{10\text{-}90\ \%}$) of the steady-state signal for a fixed increase in concentration (Kulagina, Shankar and Michael, 1999; Baker *et al.*, 2019). However, during *in-vitro* calibrations a stock concentration aliquot of the substrate is injected into the cell and reaches equilibrium (steady-state) in a certain time. This is dependent on mass transfer, which is dictated by diffusion and thermodynamic constraints, i.e., the amount of material being removed from the bulk along with the rate at which this transfer happens. Convection is introduced after the injection to ensure a quick and even distribution of the analyte. As a result, it is quite difficult to separate the response time from the stirring time for *in-vitro* calibrations such as the ones used here.

From the data shown in Figure 5.14 it can be seen that the $t_{10\text{-}90\ \%}$ response is instantaneous and within the mixing time at *ca.* 10 s (n = 4). While this generally indicates a sub-second *in-vivo* response (Lowry *et al.*, 1994; Baker *et al.*, 2019) it is only an indication/estimation of response time as it is difficult to directly translate from the *in-vitro* to *in-vivo* environment (Versmold *et al.*, 1978). However, previous biosensor designs published by the research group, which are similar in design to this one, have shown that $t_{10\text{-}90\ \%}$ values less than the mixing time *in-vitro* have yielded millisecond response times *in-vivo* (Bolger *et al.*, 2011; Teles-Grilo Ruivo *et al.*, 2017; Baker *et al.*, 2019). This suggests the pyruvate biosensor will have a sub-second response *in-vivo*.

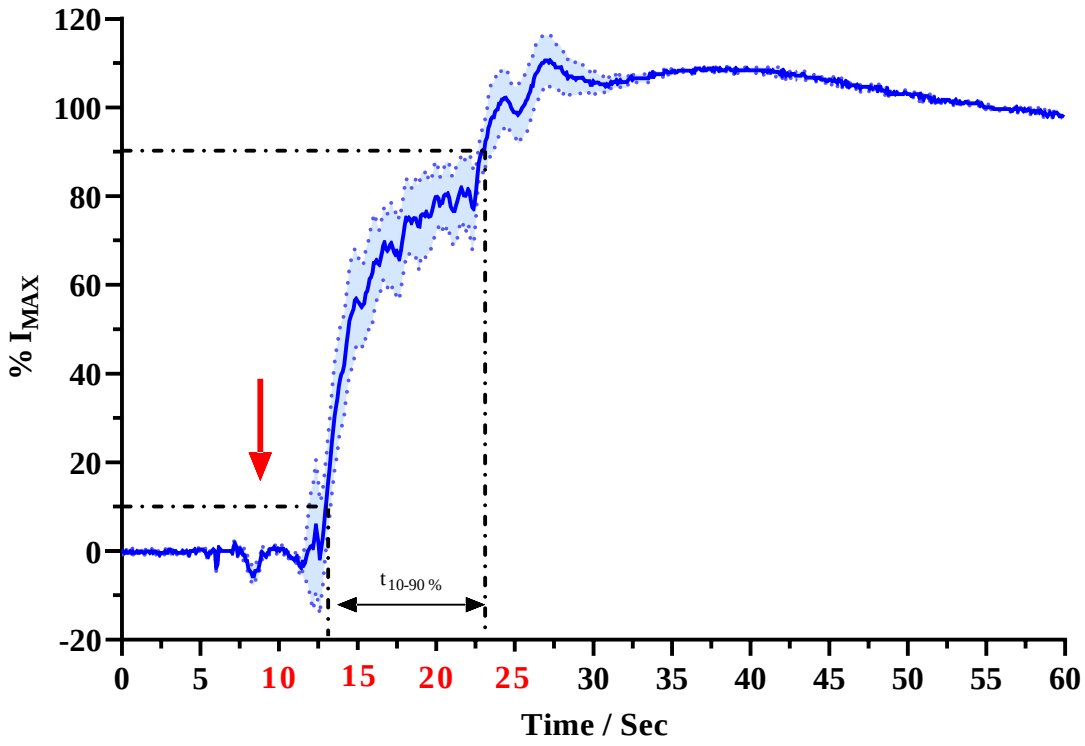

Figure 5.14: Average normalised current change (response time, $t_{10\text{-}90\ \%}$) for the *Pt/Ir-PC/POx/PC* biosensor in response to 100 µM pyruvate injection in PBS (pH 7.4) buffer solution containing 10 mM Mg^{2+} at 25 ºC. The red arrow indicates the point of injection and the red numerals indicate stirring time.

5.3.9 Conclusion

The aim of this chapter was to fully characterise the pyruvate biosensor *in-vitro* to determine if the sensor is viable for use in the *in-vivo* environment. The performance of the sensor was examined under certain conditions beginning with temperature dependence. As stated previously there is a significant decrease in sensitivity for pyruvate biosensors at elevated temperatures seen in the literature. To combat this 200 mM sucrose was introduced to the enzyme solution along with an increase in cross-linking and stabilising layers in the design. These measures ensured a sufficient degree of thermal stabilisation was achieved at physiologically relevant temperatures. The effect of pH was also evaluated and there was a

minor downward trend in sensitivity seen with increasing pH. The biosensor was then shown to be sufficiently oxygen independent across the physiological range typically seen in the brain. The shelf-life of the biosensor showed no significant change over a 14 day period indicating good storage capabilities while there was a 35 % decrease in sensitivity over the same time period for stability studies, however this may be attributed to the repeated calibration effect (Baker *et al.*, 2019). The incorporation of a PPD interference rejection layer resulted in the effective removal of interference from endogenous electroactive species without hampering the pyruvate response. Finally, the limit of detection was determined to be 0.33 ± 0.17 µM with a response time of approximately 10 s. Therefore, it can be concluded that the biosensor sufficiently met the required criteria to be deemed viable for *in-vivo* recording.

5.4 References

Akyilmaz, E. and Yorganci, E. (2007) 'Construction of an amperometric pyruvate oxidase enzyme electrode for determination of pyruvate and phosphate', *Electrochimica Acta*, 52(28), pp. 7972–7977. doi:10.1016/j.electacta.2007.06.058.

Allison, S.D., Chang, B., Randolph, T.W. and Carpenter, J.F. (1999) 'Hydrogen bonding between sugar and protein is responsible for inhibition of dehydration-induced protein unfolding', *Archives of Biochemistry and Biophysics*, 365(2), pp. 289–298. doi:10.1006/abbi.1999.1175.

Arakawa, T. and Timasheff, S.N. (1982) 'Stabilization of Protein Structure by Sugars', *Biochemistry*, 21(25), pp. 6536–6544. doi:10.1021/bi00268a033.

Baker, K.L., Bolger, F.B., Doran, M.M. and Lowry, J.P. (2019) 'Characterisation of a Platinum-based Electrochemical Biosensor for Real-time Neurochemical Analysis of Choline', *Electroanalysis*, 31(1), pp. 129–136. doi:10.1002/elan.201800642.

Baker, K.L., Bolger, F.B. and Lowry, J.P. (2017) 'Development of a microelectrochemical biosensor for the real-time detection of choline', *Sensors and Actuators, B: Chemical*, 243, pp. 412–420. doi:10.1016/j.snb.2016.11.110.

Bayram, E. and Akyilmaz, E. (2014) 'A new pyruvate oxidase biosensor based on 3-mercaptopropionic acid/6-aminocaproic acid modified gold electrode', *Artificial Cells, Nanomedicine and Biotechnology*, 42(6), pp. 418–422. doi:10.3109/21691401.2013.815626.

Berg, J.M., Tymoczko, J.L. and Stryer, L. (2012) *Biochemistry*. Basingstoke: W.H. Freeman.

Bergmann, W., Rudolph, R. and Spohn, U. (1999) 'A bienzyme modified carbon paste electrode for amperometric detection of pyruvate', *Analytica Chimica Acta*, 394(2–3), pp. 233–241. doi:10.1016/S0003-2670(99)00296-2.

Bolger, F. and Lowry, J. (2005) 'Brain Tissue Oxygen: In Vivo Monitoring with Carbon Paste Electrodes', *Sensors*, 5(11), pp. 473–487. doi:10.3390/s5110473.

Bolger, F.B., Bennett, R. and Lowry, J.P. (2011) 'An in vitro characterisation comparing carbon paste and Pt microelectrodes for real-time detection of brain tissue oxygen', *Analyst*,

136(19), pp. 4028–4035. doi:10.1039/c1an15324b.

Bolger, F.B., McHugh, S.B., Bennett, R., Li, J., Ishiwari, K., Francois, J., Conway, M.W., Gilmour, G., Bannerman, D.M., Fillenz, M., Tricklebank, M. and Lowry, J.P. (2011) 'Characterisation of carbon paste electrodes for real-time amperometric monitoring of brain tissue oxygen', *Journal of Neuroscience Methods*, 195(2), pp. 135–142. doi:https://doi.org/10.1016/j.jneumeth.2010.11.013.

Brown, P.L. and Kiyatkin, E.A. (2004) 'Brain hyperthermia induced by MDMA (ecstasy): modulation by environmental conditions.', *The European journal of neuroscience*, 20(1), pp. 51–58. doi:10.1111/j.0953-816X.2004.03453.x.

Brown, P.L., Wise, R.A. and Kiyatkin, E.A. (2003) 'Brain Hyperthermia Is Induced by Methamphetamine and Exacerbated by Social Interaction', *Journal of Neuroscience*, 23(9), pp. 3924–3929. doi:10.1523/JNEUROSCI.23-09-03924.2003.

Casey, J.R., Grinstein, S. and Orlowski, J. (2010) 'Sensors and regulators of intracellular pH', *Nature Reviews Molecular Cell Biology*, 11(1), pp. 50–61. doi:10.1038/nrm2820.

Chaniotakis, N.A. (2004) 'Enzyme stabilization strategies based on electrolytes and polyelectrolytes for biosensor applications', *Analytical and Bioanalytical Chemistry*, 378(1), pp. 89–95. doi:10.1007/s00216-003-2188-3.

Cordeiro, C.A., de Vries, M.G., Ngabi, W., Oomen, P.E., Cremers, T.I.F.H. and Westerink, B.H.C. (2015) 'In vivo continuous and simultaneous monitoring of brain energy substrates with a multiplex amperometric enzyme-based biosensor device', *Biosensors and Bioelectronics*, 67, pp. 677–686. doi:10.1016/j.bios.2014.09.101.

Craig, J.D. and O'Neill, R.D. (2003) 'Comparison of simple aromatic amines for electrosynthesis of permselective polymers in biosensor fabrication', *Analyst*, 128(7), pp. 905–911. doi:10.1039/b302833j.

Dixon, B.M., Lowry, J.P. and O'Neill, R.D. (2002) 'Characterization in vitro and in vivo of the oxygen dependence of an enzyme/polymer biosensor for monitoring brain glucose', *Journal of Neuroscience Methods*, 119(2), pp. 135–142. doi:10.1016/S0165-0270(02)00170-X.

Dong, T., Zhao, L., Huang, Y. and Tan, X. (2010) 'Preparation of cross-linked aggregates of aminoacylase from Aspergillus melleus by using bovine serum albumin as an inert additive', *Bioresource Technology*, 101(16), pp. 6569–6571. doi:10.1016/j.biortech.2010.03.061.

Doran, M.M., Finnerty, N.J. and Lowry, J.P. (2017) 'In–Vitro Development and Characterisation of a Superoxide Dismutase-Based Biosensor.', *ChemistrySelect*, 2(14), pp. 4157–4164. doi:10.1002/slct.201700793.

Gibson, T.D. (1999) 'Biosensors: The stability problem', *Analusis*, 27(7), pp. 630–638. doi:10.1051/analusis:1999270630.

Gibson, T.D., Hulbert, J.N., Parker, S.M., Woodward, J.R. and Higgins, I.J. (1992) 'Extended shelf life of enzyme-based biosensors using a novel stabilization system', *Biosensors and Bioelectronics*, 7(10), pp. 701–708. doi:10.1016/0956-5663(92)85052-C.

Gowers, S.A.N., Rogers, M.L., Booth, M.A., Leong, C.L., Samper, I.C., Phairatana, T., Jewell, S.L., Pahl, C., Strong, A.J. and Boutelle, M.G. (2019) 'Clinical translation of microfluidic sensor devices: focus on calibration and analytical robustness', *Lab Chip*, 19(15), pp. 2537–2548. doi:10.1039/C9LC00400A.

Grünewald, R.A. (1993) 'Ascorbic acid in the brain', *Brain Research Reviews*. Elsevier, pp. 123–133. doi:10.1016/0165-0173(93)90010-W.

Hoss, U. and Budiman, E.S. (2017) 'Factory-calibrated continuous glucose sensors: The science behind the technology', *Diabetes Technology and Therapeutics*, 19(S2), pp. S44–S50. doi:10.1089/dia.2017.0025.

James, S. and McManus, J.J. (2012) 'Thermal and solution stability of lysozyme in the presence of sucrose, glucose, and trehalose', *Journal of Physical Chemistry B*, 116(34), pp. 10182–10188. doi:10.1021/jp303898g.

Kaushik, J.K. and Bhat, R. (2003) 'Why is trehalose an exceptional protein stabilizer? An analysis of the thermal stability of proteins in the presence of the compatible osmolyte trehalose', *Journal of Biological Chemistry*, 278(29), pp. 26458–26465. doi:10.1074/jbc.M300815200.

Kayama, T., Yoshimoto, T., Fujimoto, S. and Sakurai, Y. (1991) 'Intratumoral oxygen pressure

in malignant brain tumor', *Journal of Neurosurgery*, 74(1), pp. 55–59. doi:10.3171/jns.1991.74.1.0055.

Killoran, S.J. and O'Neill, R.D. (2008) 'Characterization of permselective coatings electrosynthesized on Pt-Ir from the three phenylenediamine isomers for biosensor applications', *Electrochimica Acta*, 53(24), pp. 7303–7312. doi:10.1016/j.electacta.2008.03.076.

Kim, N.A., Thapa, R. and Jeong, S.H. (2018) 'Preferential exclusion mechanism by carbohydrates on protein stabilization using thermodynamic evaluation', *International Journal of Biological Macromolecules*, 109, pp. 311–322. doi:10.1016/j.ijbiomac.2017.12.089.

Kiyatkin, E.A., Wakabayashi, K.T. and Lenoir, M. (2013) 'Physiological fluctuations in brain temperature as a factor affecting electrochemical evaluations of extracellular glutamate and glucose in behavioral experiments', *ACS Chemical Neuroscience*, 4(5), pp. 652–665. doi:10.1021/cn300232m.

Knyzhnykova, D. V., Topolnikova, Y. V., Kucherenko, I.S. and Soldatkin, O.O. (2018) 'Development of pyruvate oxidase-based amperometric biosensor for pyruvate determination', *Biopolymers and Cell*, 34(1), pp. 14–23. doi:10.7124/bc.00096C.

Kulagina, N. V., Shankar, L. and Michael, A.C. (1999) 'Monitoring glutamate and ascorbate in the extracellular space of brain tissue with electrochemical microsensors', *Analytical Chemistry*, 71(22), pp. 5093–5100. doi:10.1021/ac990636c.

Lin, T.-Y. and Timasheff, S.N. (2008) 'On the role of surface tension in the stabilization of globular proteins', *Protein Science*, 5(2), pp. 372–381. doi:10.1002/pro.5560050222.

Lowry, J.P., McAteer, K., El Atrash, S.S., Duff, A. and O'Neill, R.D. (1994) 'Characterization of Glucose Oxidase-Modified Poly(phenylenediamine)-Coated Electrodes in Vitro and in Vivo: Homogeneous Interference by Ascorbic Acid in Hydrogen Peroxide Detection', *Analytical Chemistry*, 66(10), pp. 1754–1761. doi:10.1021/ac00082a025.

Lowry, J.P. and O'Neill, R.D. (1992) 'Homogeneous Mechanism of Ascorbic Acid Interference in Hydrogen Peroxide Detection at Enzyme-Modified Electrodes', *Analytical Chemistry*, 64(4), pp. 453–456. doi:10.1021/ac00028a022.

Lowry, J.P. and O'Neill, R.D. (1994) 'Partial characterization in vitro of glucose oxidase-modified poly(phenylenediamine)-coated electrodes for neurochemical analysis in vivo', *Electroanalysis*, 6(5–6), pp. 369–379. doi:10.1002/elan.1140060504.

Malik, M., Chaudhary, R. and Pundir, C.S. (2019) 'An improved enzyme nanoparticles based amperometric pyruvate biosensor for detection of pyruvate in serum', *Enzyme and Microbial Technology*, 123, pp. 30–38. doi:10.1016/j.enzmictec.2019.01.006.

Mizutani, F., Yabuki, S., Sato, Y., Sawaguchi, T. and Iijima, S. (2000) 'Amperometric determination of pyruvate, phosphate and urea using enzyme electrodes based on pyruvate oxidase-containing poly(vinyl alcohol)/polyion complex-bilayer membrane', *Electrochimica Acta*, 45(18), pp. 2945–2952. doi:10.1016/S0013-4686(00)00373-X.

Murr, R., Berger, S., Schürer, L., Peter, K. and Baethmann, A. (1994) 'A novel, remote-controlled suspension device for brain tissue PO2 measurements with multiwire surface electrodes', *Pflügers Archiv European Journal of Physiology*, 426(3–4), pp. 348–350. doi:10.1007/BF00374792.

O'Neill, R.D. and Lowry, J.P. (2000) 'Voltammetry In Vivo for Chemical Analysis of the Living Brain', in *Encyclopedia of Analytical Chemistry*. American Cancer Society. doi:10.1002/9780470027318.a0216.

O'Neill, R.D., Rocchitta, G., McMahon, C.P., Serra, P.A. and Lowry, J.P. (2008) 'Designing sensitive and selective polymer/enzyme composite biosensors for brain monitoring in vivo', *TrAC - Trends in Analytical Chemistry*, 27(1), pp. 78–88. doi:10.1016/j.trac.2007.11.008.

Orlowski, P., Chappell, M., Park, C.S., Grau, V. and Payne, S. (2011) 'Modelling of pH dynamics in brain cells after stroke', *Interface Focus*, 1(3), pp. 408–416. doi:10.1098/rsfs.2010.0025.

Pannier, J.L., Weyne, J., Demeester, G. and Leusen, I. (1978) 'Effect of non-respiratory alkalosis on brain tissue and cerebral blood flow in rats with damaged blood-brain barrier.', *Stroke*, 9(4), pp. 354–359. doi:10.1161/01.str.9.4.354.

Puggioni, G., Calia, G., Arrigo, P., Bacciu, A., Bazzu, G., Migheli, R., Fancello, S., Serra, P.A. and Rocchitta, G. (2019) 'Low-temperature storage improves the over-time stability of

implantable glucose and lactate biosensors', *Sensors (Switzerland)*, 19(2), p. 422. doi:10.3390/s19020422.

Rahman, M.A., Park, D.S., Chang, S.C., McNeil, C.J. and Shim, Y.B. (2006) 'The biosensor based on the pyruvate oxidase modified conducting polymer for phosphate ions determinations', *Biosensors and Bioelectronics*. 2005/05/17, 21(7), pp. 1116–1124. doi:10.1016/j.bios.2005.04.008.

Rocchitta, G., Spanu, A., Babudieri, S., Latte, G., Madeddu, G., Galleri, G., Nuvoli, S., Bagella, P., Demartis, M.I., Fiore, V., Manetti, R. and Serra, P.A. (2016) 'Enzyme biosensors for biomedical applications: Strategies for safeguarding analytical performances in biological fluids', *Sensors (Switzerland)*. Multidisciplinary Digital Publishing Institute, p. 780. doi:10.3390/s16060780.

Saurina, J., Hernández-Cassou, S., Fàbregas, E. and Alegret, S. (1998) 'Potentiometric biosensor for lysine analysis based on a chemically immobilized lysine oxidase membrane', *Analytica Chimica Acta*, 371(1), pp. 49–56. doi:10.1016/S0003-2670(98)00310-9.

Schulz, M.K., Wang, L.P., Tange, M. and Bjerre, P. (2000) 'Cerebral microdialysis monitoring: Determination of normal and ischemic cerebral metabolisms in patients with aneurysmal subarachnoid hemorrhage', *Journal of Neurosurgery*, 93(5), pp. 808–814. doi:10.3171/jns.2000.93.5.0808.

Shah, S., Sharma, A. and Gupta, M.N. (2006) 'Preparation of cross-linked enzyme aggregates by using bovine serum albumin as a proteic feeder', *Analytical Biochemistry*, 351(2), pp. 207–213. doi:10.1016/j.ab.2006.01.028.

Shimizu, S. and Smith, D.J. (2004) 'Preferential hydration and the exclusion of cosolvents from protein surfaces', *Journal of Chemical Physics*, 121(2), pp. 1148–1154. doi:10.1063/1.1759615.

Snyder, S.L., McAuley, K.B., McLellan, P.J., Brouwer, E.B. and McCaw, T. (2011) 'Modeling the thermal stability of enzyme-based in vitro diagnostics biosensors', *Sensors and Actuators, B: Chemical*, 156(2), pp. 621–630. doi:10.1016/j.snb.2011.02.008.

Sola-Penna, M. and Meyer-Fernandes, J.R. (1998) 'Stabilization against thermal inactivation

promoted by sugars on enzyme structure and function: Why is trehalose more effective than other sugars?', *Archives of Biochemistry and Biophysics*, 360(1), pp. 10–14. doi:10.1006/abbi.1998.0906.

Teles-Grilo Ruivo, L.M., Baker, K.L., Conway, M.W., Kinsley, P.J., Gilmour, G., Phillips, K.G., Isaac, J.T.R., Lowry, J.P. and Mellor, J.R. (2017) 'Coordinated Acetylcholine Release in Prefrontal Cortex and Hippocampus Is Associated with Arousal and Reward on Distinct Timescales', *Cell Reports*, 18(4), pp. 905–917. doi:https://doi.org/10.1016/j.celrep.2016.12.085.

Tu, Y., Long, Y. and Deng, K. (2008) 'Study on a pyruvate oxidase biosensor based on (β-cyclodextrin included ferrocene as electron-transfer mediator', *Proceedings of the 3rd International Conference on Sensing Technology, ICST 2008*, 42(2), pp. 403–408. doi:10.1109/ICSENST.2008.4757136.

Versmold, H.T., Linderkamp, O., Stuffer, K.H., Holzmann, M. and Riegel, K.P. (1978) 'In Vivo vs. In Vitro Response Time of Trancutaneous Po2 Electrodes A comparison of four devices in newborn infants', *Acta Anaesthesiologica Scandinavica*, 22(s68), pp. 40–48. doi:10.1111/j.1399-6576.1978.tb01391.x.

Wang, W. (1999) 'Instability, stabilization, and formulation of liquid protein pharmaceuticals', *International Journal of Pharmaceutics*, pp. 129–188. doi:10.1016/S0378-5173(99)00152-0.

Xie, G. and Timasheff, S.N. (1997) 'The thermodynamic mechanism of protein stabilization by trehalose', in *Biophysical Chemistry*, pp. 25–43. doi:10.1016/S0301-4622(96)02222-3.

Zetterling, M., Hillered, L., Samuelsson, C., Karlsson, T., Enblad, P. and Ronne-Engström, E. (2009) 'Temporal patterns of interstitial pyruvate and amino acids after subarachnoid haemorrhage are related to the level of consciousness-a clinical microdialysis study', *Acta Neurochirurgica*, 151(7), pp. 771–780. doi:10.1007/s00701-009-0384-4.

Chapter 6:

In-Vivo

Characterisation

6.1 Introduction

The overall aim of this body of research was to produce a pyruvate oxidase (POx)-based biosensor suitable for detecting pyruvate and monitoring relative changes in its concentration in the mammalian brain. The resultant biosensor was developed (Chapter 4) and characterised *in-vitro* (Chapter 5) and having obtained satisfactory results it was then necessary to evaluate its performance in the *in-vivo* environment. Despite a robust characterisation process there are many factors *in-vivo* which cannot be accounted for in an *in-vitro* environment. Mass transport to the sensor surface is restricted by the effect of a tissue matrix which cannot be simulated accurately *in-vitro* (O'Neill, 1993). In addition to this there is also the issue of the foreign body response (FBR) associated with the implantation of a device into brain tissue (Morais, Papadimitrakopoulos and Burgess, 2010). Directly after the biosensor is implanted the acute inflammatory response starts in which inflammatory cells and plasma proteins migrate to the site of the foreign body (Wilson and Gifford, 2005). After this acute response a chronic foreign body reaction may set in which leads to an encapsulation layer forming around the biosensor. This is known as a 'glial scar' and can hinder diffusion (Polikov, Tresco and Reichert, 2005). Although, noteworthy is a previously implanted choline biosensor, similar to the device developed here, indicated no glial response at the site of implantation (Teles-Grilo Ruivo *et al.*, 2017). Considering all of the above, a preliminary *in-vivo* characterisation is required to determine if the biosensor can successfully operate as expected.

In the classical model for brain energy metabolism glucose is the main source of energy with lesser contributions from lactate and pyruvate (Vannucci, Maher and Simpson, 1997). Pyruvate is formed under aerobic conditions while lactate is formed under anaerobic conditions and as a result the ratio between the two, known as the lactate to pyruvate ratio (L/P), has been used as an indicator of cerebral ischemia (Skjøth-Rasmussen *et al.*, 2004). It has also been shown that reductions in the cerebral metabolic rate may precede the onset of substantial deficits in cognition in both early and late onset dementia of Alzheimer's type (DAT) patients (Hoyer, 1992). A clinically significant increase in pyruvate levels has been seen in the cerebrospinal fluid (CSF) of DAT patients, with the CSF pyruvate levels closely correlated with the severity of dementia (Parnetti *et al.*, 1995). There is also reduced pyruvate dehydrogenase (PDH) activity seen in Alzheimer's patients despite no change in PDH protein levels (Rex Sheu *et al.*,

1985). These studies suggest that dysfunctional pyruvate metabolism is a contributing factor to neurodegenerative disease.

As outlined above pyruvate plays an important role in normal metabolic function in the brain and as a result fast reliable detection of any abnormalities is vital. Unfortunately, the majority of currently developed biosensors do not meet the criteria for use in the *in-vivo* environment. These biosensors have suffered from selectivity issues, most notably ascorbic acid (AA) (Bergmann, Rudolph and Spohn, 1999; Gajovic *et al.*, 1999), performance at physiological temperature (Rahman *et al.*, 2006; Malik, Chaudhary and Pundir, 2019) and poor sensitivity (Revzin *et al.*, 2002). As a result the primary technique used to detect pyruvate in the ECF has been microdialysis (Reinstrup *et al.*, 2000; Schulz *et al.*, 2000; Yao and Yano, 2004; Gowers *et al.*, 2019). Unfortunately, this technique suffers from poor temporal resolution as well as a large probe size. The development and characterisation processes (Chapters 4 and 5) have resolved these issues. The *in-vivo* characterisation presented here involves examination of basal changes associated with sleep/wake cycles, injection stress, oxygen dependence, AA interference and stability (Baker, Bolger and Lowry, 2015).

6.2 Experimental

The software and instrumentation used for all experiments carried out in this chapter is detailed in Chapter 3, Section 3.2. All chemicals and solutions are detailed in Chapter3, Section 3.3. Finally, all surgical procedures and treatments are detailed in Chapter 3, Section 3.7. The pyruvate biosensor design deemed suitable for use in the *in-vivo* environment in Chapter 5 Section 5.3 and thus used for all *in-vivo* experiments detailed in this chapter is given as:

$$Pt/Ir\ (disc) - PPD - \{Sty - ([POx\ (800\ U/ml) + FAD\ (80\ \mu M) + Sucrose\ (200\ mM)] + BSA\ (1\ \%) + GA\ (0.25\ \%) + PEI\ (2\ \%))_{15}\}$$

Hereafter, this polymer composite (PC) electrode is referred to as Pt/Ir-PC/POx/PC_{15}. A constant potential of +700 mV *vs.* SCE was used. All experiments were carried out in freely-moving male Wistar rats. Continuous recording was carried out for up to 96 hrs. All drug treatments were administered via intraperitoneal (i.p) injection, at approximately 10:00 – 11:00

am, with a maximum of four injections per animal. Local perfusions were carried out in the morning, *ca.* 10:00 am, and afternoon, *ca.* 14:00 pm, twice a week for two weeks. All data is reported as mean ± S.E.M. where n denotes the number of electrodes, unless otherwise stated. GraphPad Prism was used for graphical presentation and to carry out statistical analysis. Area under the curve (AUC) was preformed to quantify observed changes in the biosensor signal. Net area values were taken and unpaired t-tests were used to determine what significant difference, if any, there was between these results.

6.3 Results and Discussion

This section examines the results of the various procedures carried out to determine the performance in the *in-vivo* environment. All data shown is obtained from pyruvate biosensors and composite blank electrodes that have been implanted bi-laterally or uni-laterally in the striatum of the rat brain as detailed in Chapter 3, Section 3.7.2. There was no observable difference in response between bi-lateral or uni-lateral implants suggesting no cross-talk interference. As a result, both data sets were pooled.

6.3.1 Bi-lateral *vs.* Uni-lateral Implantation

While there are many advantages to first generation biosensors, one of the issues is cross-talk between adjacent sensors. This is caused by the inter-electrode diffusion of the biocatalytically generated H_2O_2 (Petrou, Moser and Jobst, 2003). Cross-talk depends on the combined effects of several factors such as electrode geometry, inter-electrode distance and concentration of generated H_2O_2 (Palmisano *et al.*, 2000). Therefore, the first step in the *in-vivo* characterisation process was to determine that each electrode was independent of the others when the potential was initially applied (Figure 6.1). Following this the next step was to investigate if the composite blank suffered from cross-talk interference from the pyruvate biosensor.

To examine the possibility of cross-talk two biosensors and two composite blanks were implanted bi-laterally in the striatum of freely moving male Wistar rats as per Chapter 3, Section 3.7.2. The baseline data recorded in this section was analysed using 4 biosensors in 2

animal and 4 composite blanks in 2 animals. The data was recorded over a continuous 24 hr period and analysed over 12 hr light/dark cycle. The real-time continuous traces are shown below in Figure 6.2 A and a correlation analysis of the changes in normalised pyruvate currents with respect to the changes in normalised composite blank currents are shown in Figure 6.2 B The correlation coefficient was 0.07389. This indicated that cross-talk interference was negligible on the composite blank electrode. The real-time continuous trace and correlation analysis for uni-lateral implantation (Figure 6.3 A and B) also shows no cross-talk, the correlation coefficient was 0.08601. While this result was to be expected there may be a level of cross-talk between the two pyruvate biosensors. However, this doesn't really affect the pyruvate signal other than possibly enhancing it slightly for both devices.

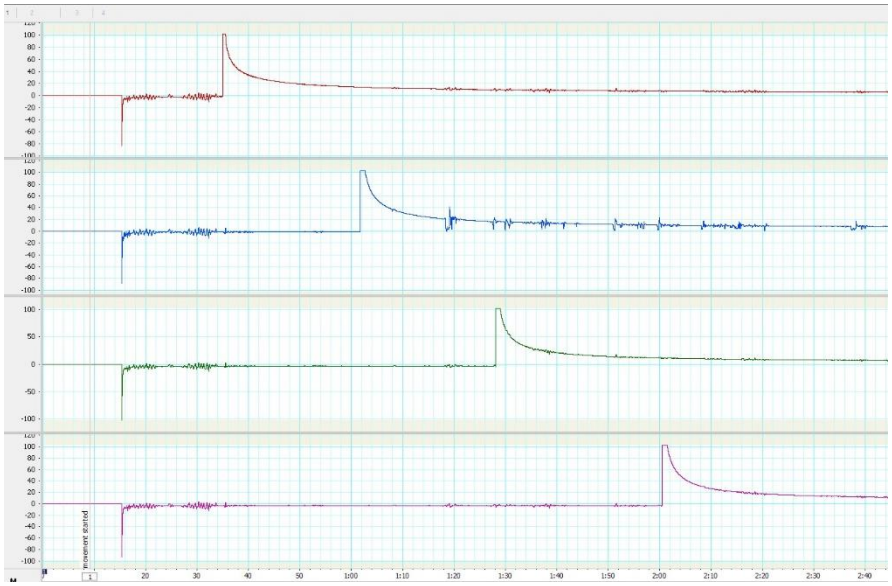

Figure 6.1: Application of appropriate potential to each of the four working electrodes to ensure no cross-talk.

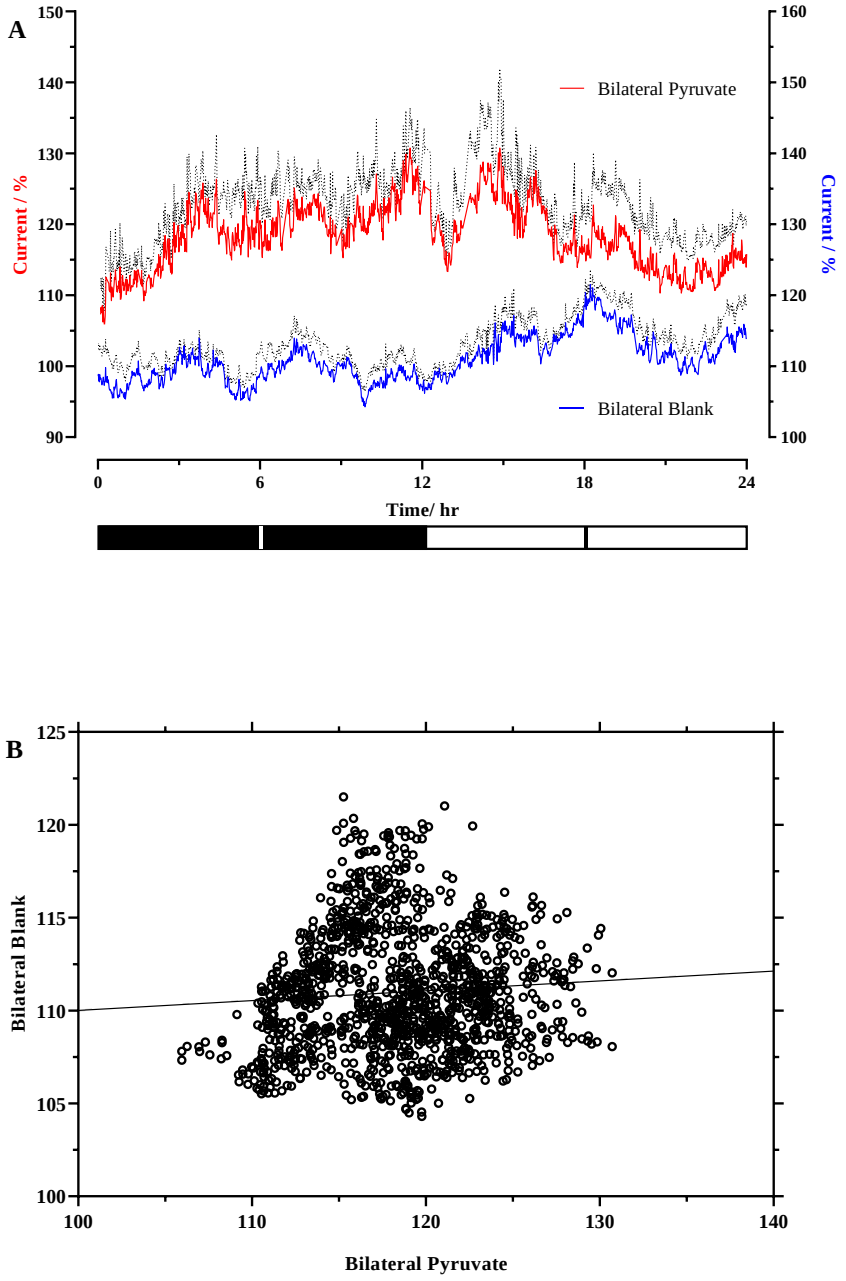

Figure 6.2: (A) The normalised current *vs.* time change for bi-laterally implanted Pt/Ir-PC/POx/PC$_{15}$ biosensor (red, n = 4 in 2 animals) and composite blank (blue, n = 4 in 2 animals) recorded from rat striatum. (B) Bivariate scattergram recorded simultaneously with bi-laterally implanted Pt/Ir-PC/POx/PC$_{15}$ biosensor and composite blank. All recordings used CPA at +700 mV over 24 hrs with 12 hr light (7 am – 7 pm)/dark (7 pm – 7 am) cycles. Error (grey) on data points represents SEM.

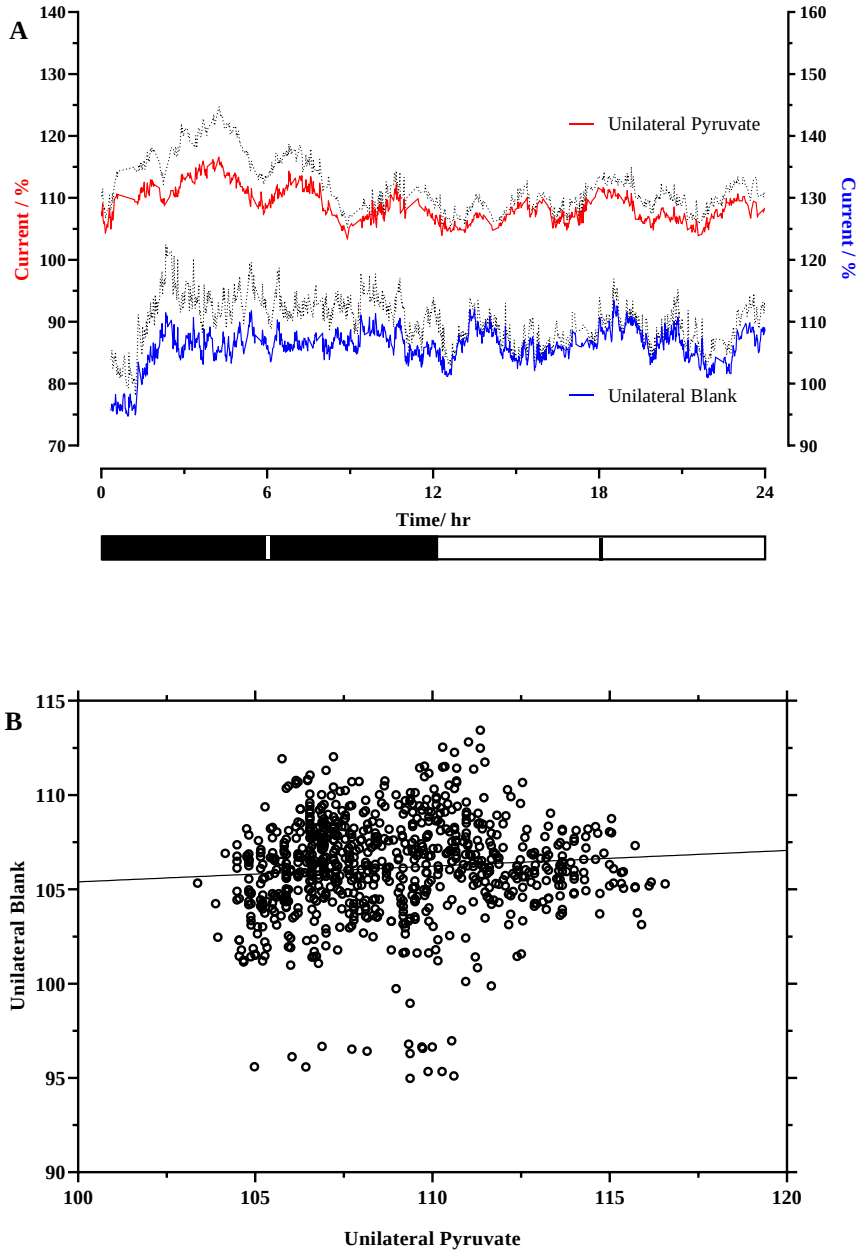

Figure 6.3: (A) The normalised current *vs.* time change for uni-laterally implanted Pt/Ir-PC/POx/PC$_{15}$ biosensor (red, n = 3 in 1 animal) and composite blank (blue, n = 3 in 2 animals) recorded from rat striatum. (B) Bivariate scattergram recorded simultaneously with uni-laterally implanted Pt/Ir-PC/POx/PC$_{15}$ biosensor and composite blank. All recordings used CPA at +700 mV over 24 hrs with 12 hr light (7 am – 7 pm)/dark (7 pm – 7 am) cycles. Error (grey) on data points represents SEM.

6.3.2 Baseline Pyruvate Recording

The next step of the *in-vivo* characterisation process was to establish the normal physiological changes in basal levels of pyruvate. The restoration of energy during sleep has been shown to involve major changes in the central nervous system (CNS). Measurements of brain energy metabolism during non-REM sleep have shown a decrease in brain energy expenditure (Kalinchuk *et al.*, 2003). Cerebral metabolic rate (Braun *et al.*, 1997) and cerebral blood flow both decrease (Kennedy *et al.*, 1982) while glucose and adenosine triphosphate (ATP) concentrations increase (Van den Noort and Brine, 1970; Reich, Geyer and Karnovsky, 1972). Decreases were also seen in extracellular pyruvate and lactate during sleep further indicating a decrease in brain energy expenditure during sleep (Van den Noort and Brine, 1970; Reich, Geyer and Karnovsky, 1972; Bourdon *et al.*, 2018). To examine these diurnal changes in pyruvate two biosensors and two composite blanks were implanted either bi-laterally or uni-laterally in the striatum of freely moving male Wistar rats as per Chapter 3, Section 3.7.2. The baseline data recorded in this section was analysed using 6 biosensors in 3 animals and 7 composite blanks in 4 animals. The data was recorded over a continuous 60 hr period and analysed over 12 hr light/dark cycles.

From the real-time continuous trace (Figure 6.4 A and B) it can be seen that pyruvate levels in the extracellular fluid (ECF) change depending on the time of day while there is little to no change on the blank electrodes. Movement data indicated increased activity during the dark phase (2.7 sensor counts/min^{-1}) in comparison to the light phase (1.1 sensor counts/min^{-1}) when the animals tend to sleep. This decrease in movement during the light phase corresponds to the decrease in pyruvate which, as detailed in the literature, corresponds with a decrease in brain energy expenditure during sleep (Van den Noort and Brine, 1970; Bourdon *et al.*, 2018).This baseline data shows a stable circadian pattern in the pyruvate response over the 60 hr recording period. Establishing the circadian pattern was required to help determine the appropriate time to administer a drug or preform a local perfusion and any deviation from this baseline can be attributed to the treatment. Therefore, all drug treatment were carried out between 10:00 – 11:00 am as this removes any variance caused by the decrease in pyruvate associated with the start of the light phase (7 am) while simultaneously allowing enough time to observe the effects of the treatment before pyruvate began to increase again in the dark phase.

To estimate the pyruvate concentration in the ECF it was expected that the sensitivity of the biosensor would decrease by up to 50 % due to implantation (Baker *et al.*, 2019). From the pyruvate signal, and accounting for the sensitivity decrease, the ECF concentration was estimated to be 197 ± 18 µM. This approach to estimating ECF concentrations has been demonstrated previously by Lowry *et al.* where the estimated sensitivity was validated by the use of zero net flux (Lowry *et al.*, 1998). The estimated pyruvate concentration falls within the reported physiological range for brain ECF pyruvate (120 – 300 µM) (Schulz *et al.*, 2000; Cordeiro *et al.*, 2015).

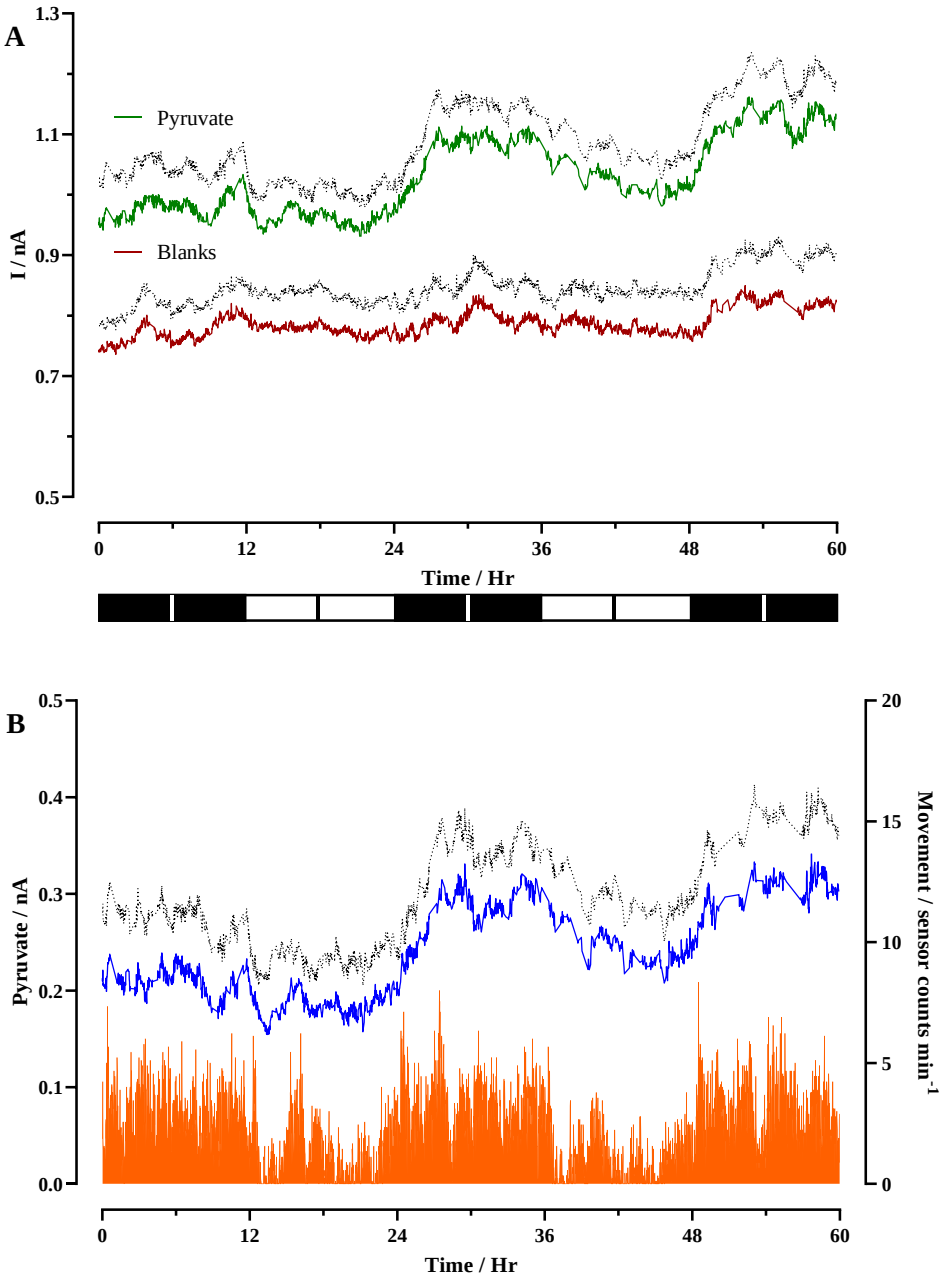

Figure 6.4: (A) The current *vs.* time change for the Pt/Ir-PC/POx/PC$_{15}$ biosensor (green, n = 6 in 3 animals) and composite blank (red, n = 7 in 4 animals) recorded from rat striatum using CPA at +700 mV over 60 hrs with 12 hr light (7 am – 7 pm)/dark (7 pm – 7 am) cycles. (B) The current *vs.* time change for the differential signal (blue, pyruvate – blank). Error (grey) on data points represents SEM. Orange lines represent simultaneously monitored motor activity.

6.3.3 Injection Stress

Injection of the vehicle in which a drug of interest is dissolved is used as a control for the drug treatment. However, this injection may still result in a "treatment stress" which can affect certain stress sensitive indices (Freiman *et al.*, 2016). Saline (NaCl 0.9 %) is used as the vehicle for all drug treatments applied and therefore prior to the administration of any drug treatment the injection stress was examined with a 1 mL saline administration. The effect of saline administration on both the pyruvate and composite blank biosensors is shown below in Figure 6.5 (A) while Figure 6.5 (B) shows the differential signal (pyruvate – blank) response and movement data.

Upon administration there is a small increase observed from 1.35 ± 0.31 nA to a peak response of 1.4 ± 0.3 nA (*ca.* 8 mins, pyruvate, red trace, $t_{(0.1362)}$, p = 0.8961, n = 4) and 1.05 ± 0.26 nA to a peak response of 1.1 ± 0.28 nA, n = 3 (*ca.* 8 mins, composite blank, green trace, $t_{(0.1152)}$, p = 0.9138, n = 3). This represents a 5.2 ± 2.1 % increase in pyruvate and 3.4 ± 1.8 % increase in the blank. This is due to the physical manipulation of the animal to administer the treatment followed by post-injection activity as highlighted by the movement data. The differential signal (Figure 6.5 B) shows a sharp 5.5 ± 2.7 % increase after administration but returns to the pre-injection baseline after *ca*. 3 mins and this compares with previously published work in which the signal for the target analyte (nitric oxide) showed a small increase post-injection but returned to baseline relatively soon after administration (Finnerty *et al.*, 2013). This section demonstrated that the pyruvate response, which is attributed to the injection itself, is minimal with no difference between pre and post-injection baselines. Finally, no lasting effect on the response of the biosensor was seen post-injection with the pyruvate signal returning to the same pre-injection levels after *ca.* 30 minutes.

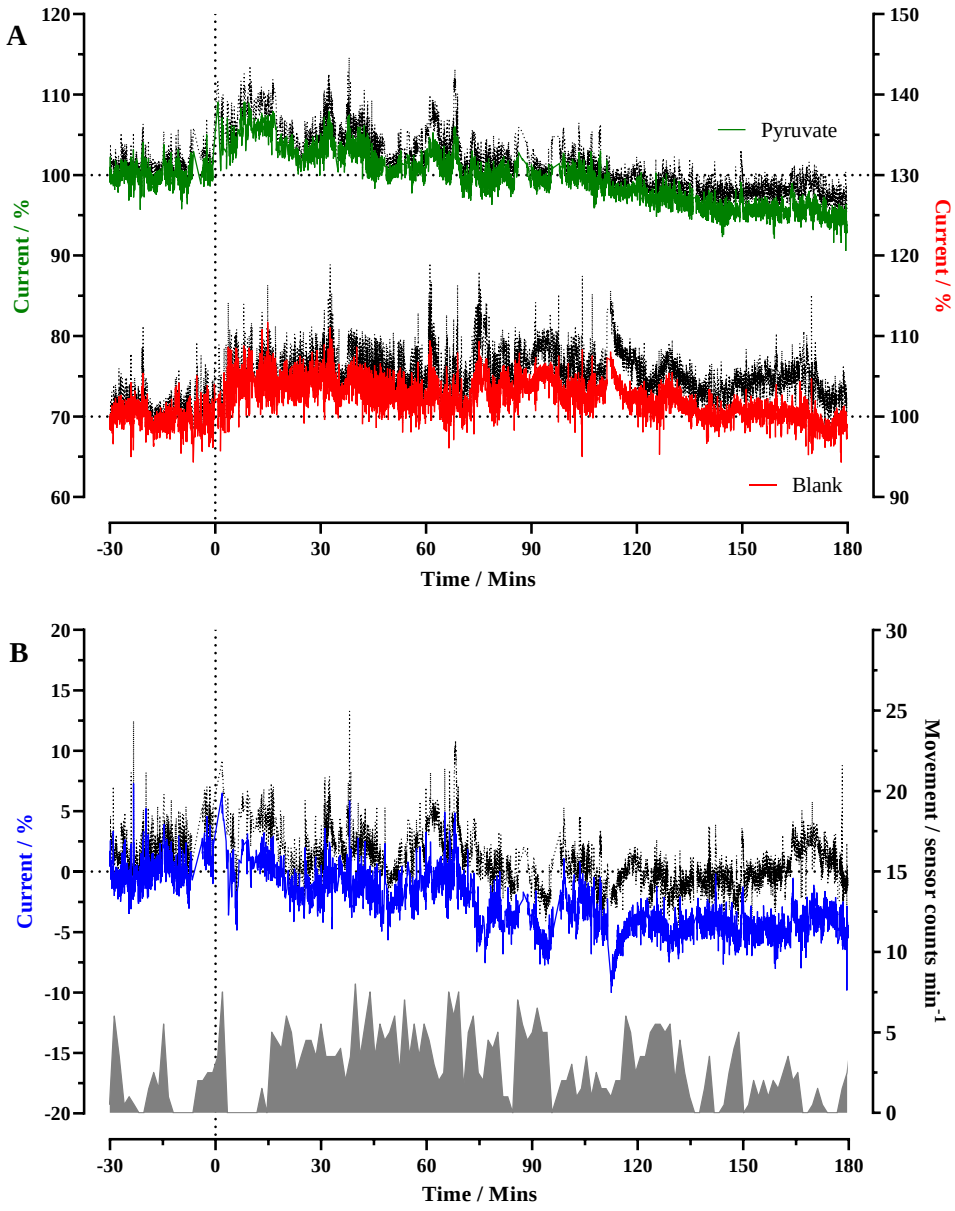

Figure 6.5: (A) Mean current *vs.* time response following the administration of a 1 mL saline injection (NaCl, 0.9 %, i.p.) on pyruvate biosensors (green, n = 6 sensors in 3 animals) and composite blanks (red, n = 7 sensors in 4 animals). The vertical dashed lines indicate the time of injection while the horizontal dashed lines indicate basal levels. (B) The differential signal (blue, pyruvate – blank) response as a percentage of the pre-injection baseline. Error (black) on all data points represents S.E.M. Grey lines represent simultaneously monitored motor activity.

6.3.4 Chloral Hydrate

The next *in-vivo* characterisation parameter examined was the oxygen dependence of the biosensor. The oxygen dependence of the biosensor was examined as part of the *in-vitro* characterisation (Chapter 5, Section 5.3.3) and was shown to be sufficiently oxygen independent over the physiological range of 50 – 80 µM. However, this must be validated in the *in-vivo* environment. To do this a 350 mg/kg dose of Chloral hydrate was administered intraperitoneally. Chloral hydrate has been used previously to increase striatal O_2 levels (Lowry and Fillenz, 2001) and is also commonly used as a non-volatile anaesthetic agent for animal surgery (Erhorn, 2007). It is metabolised into trichloroethanol and trichloroacetic acid which causes general central nervous system (CNS) depression (Kawamoto *et al.*, 1987). It is believed that the trichloroethanol is the active substance for the induced anaesthesia (Tao and Auerbach, 1994). Chloral hydrate also produces a sharp increase in regional cerebral blood flow (rCBF) and O_2 which then declines to pre-injection levels as the animal recovers from the anaesthetic (Lowry and Fillenz, 2001).

Figure 6.6 (A) and Figure 6.6 (B) show the effect of chloral hydrate (350 mg/kg) administration on both the pyruvate and composite blank biosensors and the differential signal (pyruvate – blank) response and motor activity. The inset shows a typical example of the effect of a chloral hydrate (350 mg/kg, i.p) treatment on O_2 levels monitored in the rat striatum. A sharp initial response to the injection with a quick return to baseline was observed, this is most likely due to injection stress as discussed previously. The pyruvate response increased by 0.9 ± 1.4 % from 1.09 ± 0.12 nA to 1.1 ± 0.11 nA and the composite blank decreased by 3.37 ± 2.9 % from 4.67 ± 3.88 nA to 4.43 ± 3.6 nA. Both changes are not significant ($t_{(0.04)}$, p = 0.9643 pyruvate, $t_{(0.05)}$, p = 0.9650 composite blank). The differential signal in Figure 6.6 (B) showed no significant change ($t_{(0.23)}$, p = 0.8261) from the normalised pre-injection baseline (0.06 ± 1.38 %) at the peak O_2 response (-1.01 ± 4.51 %) , which occurs after *ca.* 27 mins. The inset shows a typical O_2 response (provided by Dr. Michelle Doran) recorded at a carbon paste electrode at -650 mV. There is an initial sharp, brief increase in O_2 followed by a slower longer lasting change with a peak current increase of 35 % after *ca.* 27 mins corresponding with the behavioural changes associated with the anaesthesia and illustrated by the lack of movement. The duration of the anaesthesia was measured by pedal withdrawal reflexes and spontaneous

movement of the animal recorded by the movement monitor and lasted *ca*. 90 mins. An increase in the pyruvate response was seen after *ca.* 90 mins and could possibly be due to the animal's recovery from the anaesthetic. This is illustrated by the increase in movement from 0.19 ± 0.08 sensor counts/min^{-1} (n = 4, 0 – 90 mins) to 1.1 ± 0.46 sensor counts/min^{-1} (n = 4, 90 – 180 mins) and as previously discussed (Section 6.3.1) pyruvate increases with increases in activity.

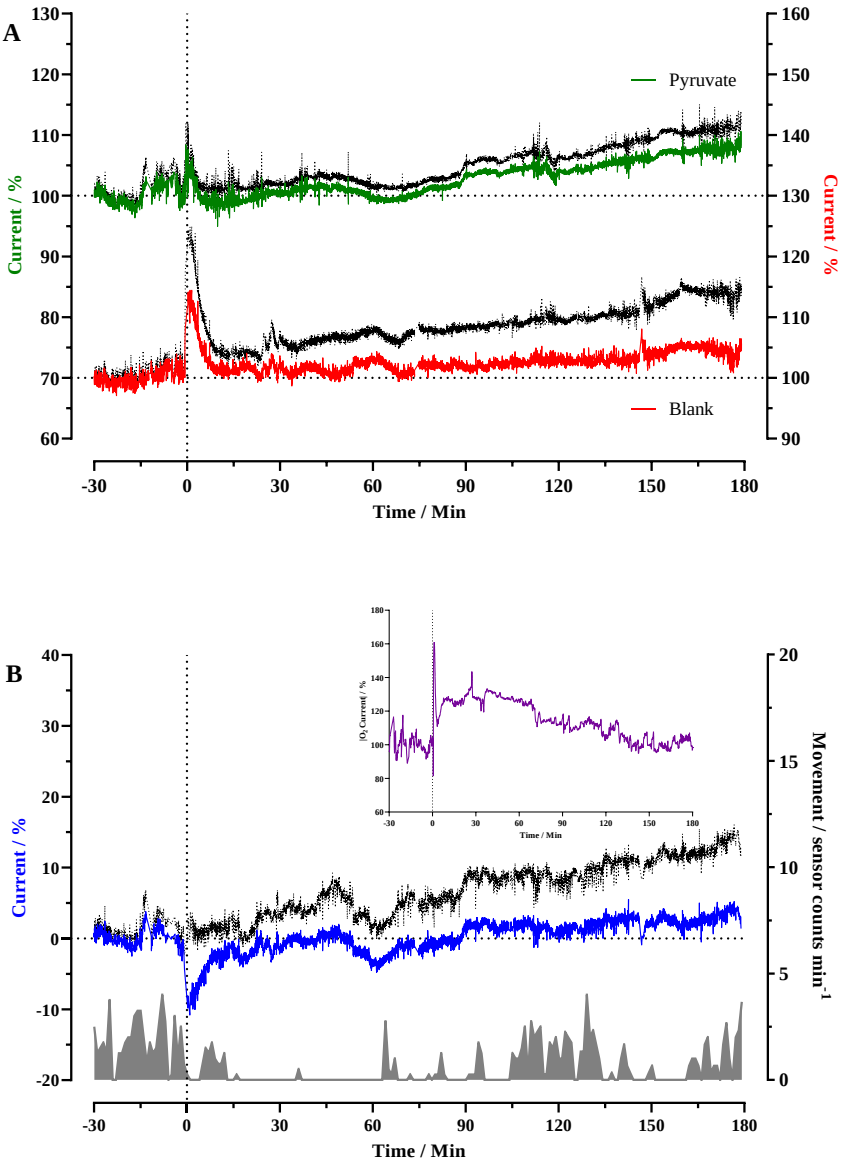

Figure 6.6: (A) Mean current *vs.* time response following the administration of a 1 mL Chloral Hydrate injection (350 mg/kg, i.p) on pyruvate biosensors (green, n = 5 sensors in 3 animals) and composite blanks (red, n = 4 sensors in 3 animals). The vertical dashed lines indicate the time of injection while the horizontal dashed lines indicate basal levels. (B) The differential signal (blue, pyruvate – blank) response as a percentage of the pre-injection baseline. Error (black) on all data points represents S.E.M. Grey lines represent simultaneously monitored motor activity. (Inset) A typical oxygen response to a 1 mL chloral hydrate (350 mg/kg, i.p) injection.

6.3.5 Ascorbic Acid

As previously discussed in Chapter 5, Section 5.3.6 extensive work was carried out *in-vitro* to ensure the biosensor was sufficiently able to reject potential electroactive interferants. This was achieved via the electropolymerisation of a permselective membrane poly-*o*-phenylenediamine (PPD). Ascorbic acid (AA) is the main interferent present in the ECF with a concentration of between 400 – 500 µM (Grünewald, 1993; Miele and Fillenz, 1996). To evaluate the selectivity of both the biosensor and the composite blank a 0.5 g/kg dose of AA was administered i.p. Figure 6.7 (A) illustrates the effect of an i.p injection of ascorbate on both the pyruvate biosensor and the composite blank while Figure 6.7 (B) shows the differential signal (pyruvate – blank) response and movement data. The inset shows a typical example of an AA (0.5 g/kg, i.p) treatment on AA levels monitored in the rat striatum

A small non-significant increase ($t_{(0.27)}$, p = 0.7915, pyruvate and $t_{(0.26)}$, p = 0.7983, composite blank) from the pre-injection baseline (0.92 ± 0.14 nA, n = 6, pyruvate and 0.54 ± 0.06 nA, n = 5, composite blank) was seen for both pyruvate (0.98 ± 0.16 nA, n = 6) and composite blank electrodes (0.57 ± 0.07 nA, n = 5) post-injection (Figure 6.7 A). This represented a 5.9 ± 2.2 % increase for pyruvate and a 3.9 ± 1.7 % increase for the composite blank. This slight increase in pyruvate response may be due to the increase in activity (Section 6.3.1). The increase in activity was seen from 1.4 ± 0.54 sensor counts/min^{-1} (n = 5) pre-injection to 2.8 ± 1.26 sensor counts/min^{-1} (n = 5) post-injection for approximately 45 mins before returning to pre-injection levels (0.98 ± 0.37 sensor counts/min^{-1}, n = 5) shown in Figure 6.7 (B). This may be due to the irritation and discomfort that can arise from the administration of AA. Finally, there is no significant change ($t_{(0.44)}$, p = 0.6717) observed in the normalised differential signal (pyruvate – blank) response pre-injection (-0.14 ± 1.99 %,) compared to post-injection (1.51 ± 3.18 %) (Figure 6.7 B). The inset shows a typical AA response (provided by Dr. Keeley Baker) recorded at a carbon paste electrode at +250 mV. There is an immediate sharp increase in AA which reaches a peak current change of 184 % after *ca.* 11 mins before gradually decreasing back to baseline. There was no significant change ($t_{(0.3250)}$, p = 0.7535) in the differential signal from the pre-injection baseline (-0.14 ± 1.99 %,) compared to the response at the peak AA response 1.52 ± 4.71 % (11 mins); This demonstrates the integrity of the PPD layer in the *in-vivo*

environment and illustrates that both the biosensor and the composite blank do not detect interfering species.

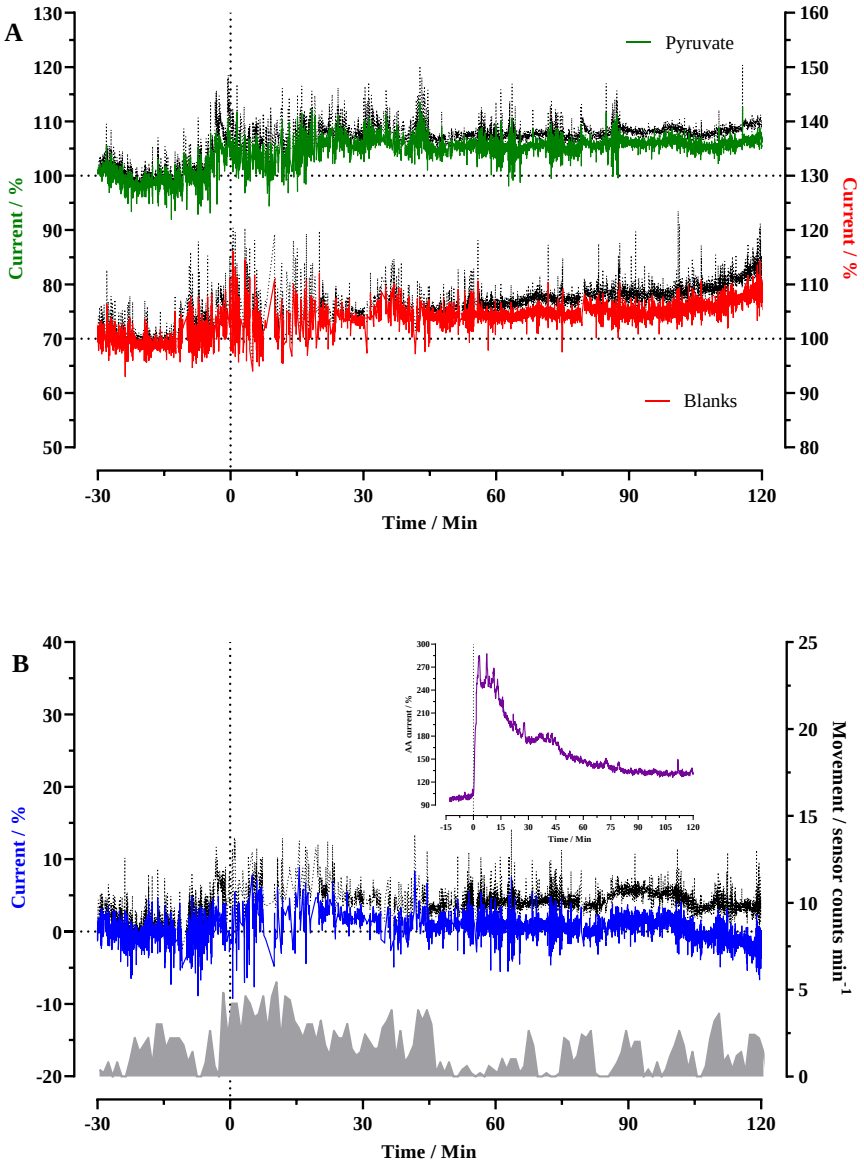

Figure 6.7: (A) Mean current *vs.* time response following the administration of a 1 mL AA injection (0.5 g/kg, i.p.) on pyruvate biosensors (green, n = 6 sensors in 4 animals) and composite blanks (red, n = 5 sensors in 3 animals). The vertical dashed lines indicate the time of injection while the horizontal dashed lines indicate basal levels. (B) The differential signal (blue, pyruvate – blank) response as a percentage of the pre-injection baseline. Error (black) on all data points represents S.E.M. Grey lines represent simultaneously monitored motor activity. (Inset) A typical AA response to a 1 mL AA (0.5 g/kg, i.p.) injection.

6.3.6 Local Perfusions

To determine the pyruvate biosensor's ability to detect changes in pyruvate in the *in-vivo* environment a biosensor was implanted adjacent to a guide cannula which allowed the use of a microdialysis probe (Chapter 3, Section 3.7.6.). This allows for local perfusions of the target analyte through the microdialysis probe to increase the ECF concentration in the local environment of the sensor and provides evidence of the biosensors ability to respond to changes in ECF concentrations of the target analyte. This process is termed retrodialysis (Huynh *et al.*, 2007). This technique has previously been demonstrated for glucose (Lowry *et al.*, 1998), choline (Baker, Bolger and Lowry, 2017) and nitric oxide (Finnerty *et al.*, 2012).

6.3.6.1 aCSF Baseline

Initially perfusions of artificial cerebrospinal fluid (aCSF) were carried out as a control experiment as aCSF is used as the vehicle for all pyruvate perfusions. The perfusion of aCSF results in the removal of pyruvate from the ECF surrounding the biosensor and the probe into the dialysate. The aCSF was perfused through the microdialysis probe at a flow rate of 2 µL/min into the left striatum and changes in the pyruvate current response were recorded at a biosensor in the left striatum and also in the right striatum. The results are shown below in Figure 6.8 (A) with AUC analysis shown in Figure 6.8 (B).

Figure 6.8 (A) illustrates the decrease in pyruvate in the ECF surrounding the biosensor and probe implanted in the left striatum while no change was observed at the probe in the right striatum. The AUC value of the baseline of the left striatum biosensor pre-perfusion was 1.8 ± 1.7 % change/min (n = 3). The perfusion began after 45 minutes of a stable baseline and a minimum current of 0.65 ± 0.1 nA was reached after *ca.* 40 mins. The AUC value of the aCSF perfusion was -286 ± 31 % change/min (n = 3), this was a significant decrease ($t_{(9.18)}$, p = 0.0008) from the pre-perfusion baseline and represented a 10 ± 2.5 % decrease in the pyruvate current response. In comparison, the pyruvate biosensor implanted in the right striatum had an AUC value of 1.7 ± 2 % change/min (n = 3) for the pre-perfusion baseline, which showed no significant difference ($t_{(1.53)}$, p = 0.2007) from the AUC value (-27.8 ± 19.1 % change/min, n =

3) post aCSF perfusion (0.66 ± 0.1 nA, n = 3), given as. Cessation of the perfusion resulted in a gradual return to the pre-perfusion baseline. All pyruvate perfusions were carried out from this aCSF baseline.

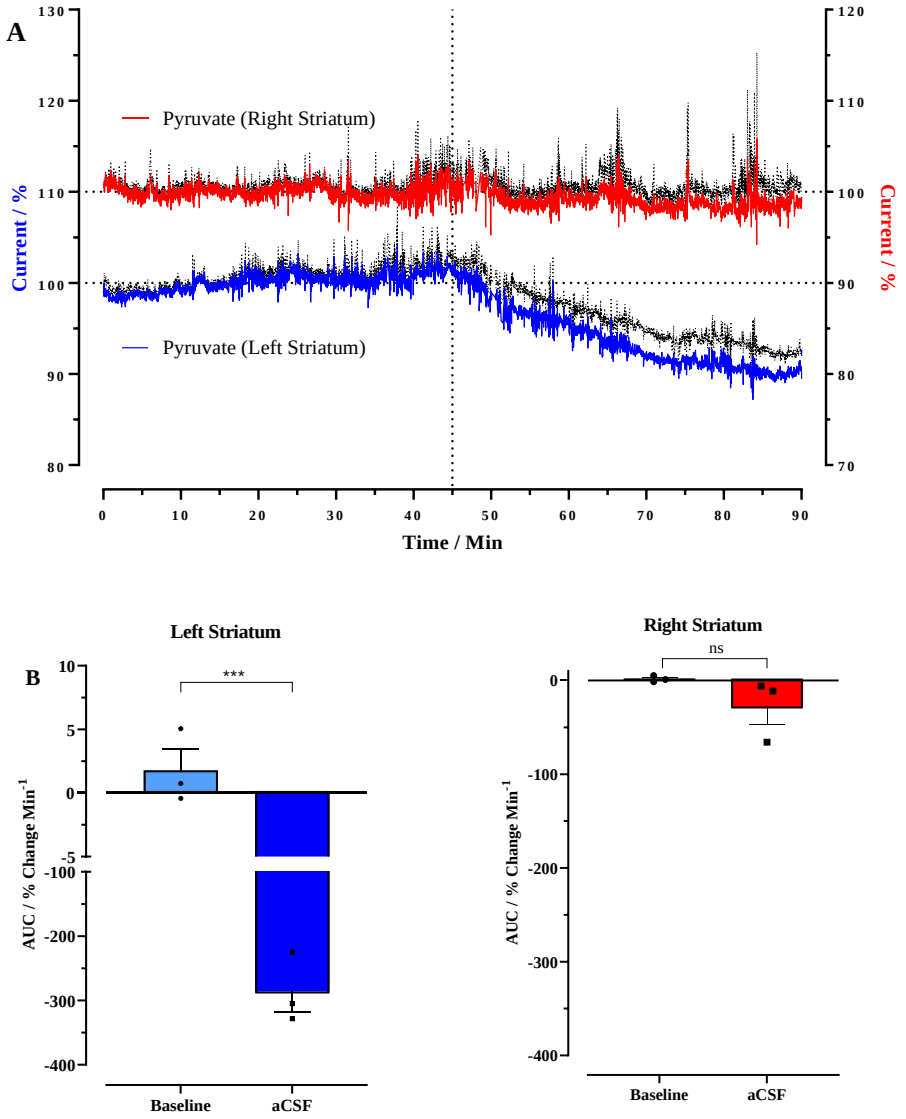

Figure 6.8: (A) The effect of a perfusion of aCSF through a microdialysis probe on the current recorded at the adjacent pyruvate biosensor (blue, n = 3 sensors in 3 animals, pre-perfusion baseline 0.73 ± 0.2 nA) and a pyruvate biosensor in the opposite hemisphere (red, n = 3 sensors in 3 animals, pre-perfusion baseline 0.67 ± 0.11 nA, n = 3). The horizontal dashed lines represent the pre-perfusion baseline while the vertical dashed line represents the start point of the perfusion. Error (black) on all data points represents S.E.M. (B) AUC analysis for baseline pyruvate levels after an aCSF perfusion for bi-laterally implanted pyruvate biosensors. ns = 0.2007, ***p = 0.0008, t-test. CPA was carried out at +700 mV *vs.* SCE.

6.3.6.2 Pyruvate Response

The previous section determined that upon perfusion of aCSF a decrease was observed in pyruvate current recorded at the pyruvate biosensor. This is due to the removal of endogenous species in the ECF, which includes pyruvate, by way of diffusion into the perfusion medium. To determine if the biosensor can detect an increase in pyruvate concentration in the local environment pyruvate was perfused through the microdialysis probe immediately after a stable aCSF baseline was established. The *in-vivo* concentration of pyruvate is reported to be in the range of 120-300 µM for the basal brain level (Zetterling *et al.*, 2009; Cordeiro *et al.*, 2015). However, for this study 500 mM was chosen for perfusion into the microdialysis probe which is substantially higher than the *in-vivo* concentration. Initially lower concentrations were examined but these yielded no change in the current and it has previously been reported that local micro-injections have used high millimolar concentrations to elicit a response (Samson *et al.*, 1997). Furthermore, traumatic injury to surrounding tissue can be caused by the relatively large microdialysis probe resulting in alterations in tissue adjacent to the probe in comparison to undisturbed tissue (Khan and Michael, 2003), which may hinder diffusion of the full concentration of the substrate to the biosensor.

The data presented in Figure 6.9 (A) illustrates the increase in pyruvate current recorded at the pyruvate biosensor. Initially aCSF was perfused at a flow rate of 2 µL/min until a stable baseline was obtained. Once the aCSF baseline was established the syringes and tubing were swapped to 500 mM pyruvate and perfusions began immediately, again at a flow rate of 2µL/min. There was an observed increase in current of approximately 11.3 ± 1.1 % from the aCSF baseline. The peak current (1.2 ± 0.2 nA, n = 15) was reached after *ca.* 20 mins. AUC analysis, shown in Figure 6.9 (B), was also carried out on the aCSF baseline and the 500 mM peak. This analysis showed there was a significant increase ($t_{(9.02)}$, $p < 0.0001$) in AUC from -1.2 ± 6.4 % change/min (n = 4 sensors in 4 animals, aCSF baseline) to 419 ± 48 % change/min (n = 4 sensors in 4 animals, 500 mM pyruvate peak). Upon reaching a stable response to the 500 mM pyruvate perfusion the experiment was stopped and the signal allowed to return to pre-perfusion basal levels before the entire cycle is ran a second time. A typical trace of one full perfusion cycle is shown in Figure 6.9 (A) (inset). It can be seen from this graph that after

the cessation of the 500 mM pyruvate perfusion the observed pyruvate current returns to the pre-perfusion baseline after approximately 1 hour.

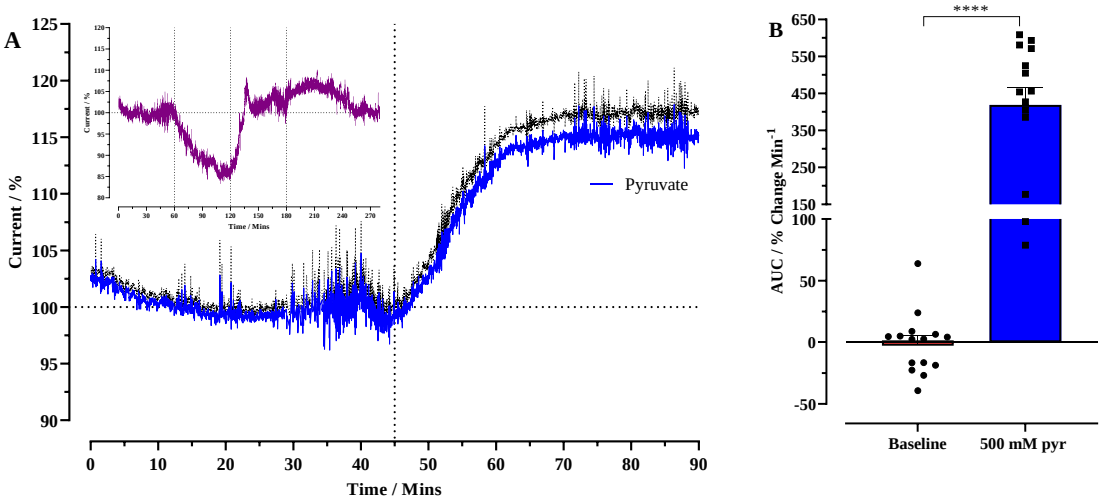

Figure 6.9:(A) The effect of a perfusion of 500 mM pyruvate through a microdialysis probe on the current recorded at the adjacent pyruvate biosensor (blue, n = 4 sensors in 4 animals). The horizontal dashed lines represent the aCSF baseline (1.02 ± 0.1 nA, n = 15) while the vertical dashed line represents the start point of the perfusion. Error (black) on all data points represents S.E.M. (Inset) A typical trace of a full perfusion cycle beginning from a stable baseline (horizontal dashed line) an aCSF perfusion was commenced (first vertical line), followed immediately by a 500 mM pyruvate perfusion (second vertical dashed line) and finally returned to per-perfusion baseline after cessation of treatment (final vertical line). (B) AUC analysis for baseline aCSF and 500 mM pyruvate. ****p < 0.0001, t-test. CPA was carried out at +700 mV *vs.* SCE.

6.3.6.3 Pyruvate Stability

The final step of the characterisation process was to determine the operational stability of the biosensor. The operational stability of the biosensor was examined previously *in-vitro* (Chapter 5, Section 3.5.5) and a significant decrease ($F_{(2, 24)} = 363.7$, $p < 0.0001$, ANOVA) in sensitivity was seen over the 2 week period. However, this must still be examined *in-vivo* as it has been

reported that some biosensors have been stable under laboratory conditions for over a year but their practical lifetime is either limited to days or weeks or not yet known when they are employed in biological tissue or and industrial setting (Hamdan and Mohd Zain, 2014). To examine the operational stability of the biosensor local perfusions of 500 mM pyruvate were again used. Perfusions were carried out twice a day on days 6, 7, 13 and 14. The results were then pooled into weeks 1 and 2 for comparison. All perfusions were carried out from an aCSF baseline and are graphed below in Figure 6.10 (A) with AUC analysis shown in Figure 6.10 (B).

From the data presented below a decrease in pyruvate sensitivity was seen over a 2-week period. For week 1 there was an observed increase in current of 16.1 ± 2 % from the aCSF baseline to the peak pyruvate response (0.92 ± 0.12 nA, n = 11), which occurred after *ca.* 60 mins. The AUC analysis, given in Figure 6.10 (B), showed this was a significant increase ($t_{(22.47)}$, $p < 0.0001$) from -0.35 ± 3.13 % change/min (n = 4 sensors in 4 animals, aCSF baseline) to 554 ± 24 % change/min (n = 4 sensors in 4 animals, 500 mM pyruvate peak). There was also an observed increase in current from the aCSF baseline to the peak pyruvate response (1.6 ± 0.3 nA, n = 7) for week 2. The peak occurred after *ca.* 60 mins and represented an 11.2 ± 2.8 % increase. Again, AUC analysis in Figure 6.10 (B) showed there was a significant increase ($t_{(3.729)}$, $p = 0.0039$) from -17.1 ± 7.9 % change/min (n = 2 sensors in 2 animals, aCSF baseline) to 290 ± 82 % change/min (n = 2 sensors in 2 animals, 500 mM pyruvate peak). There was an approximate 4 % decrease in current change from week 1 (16.1 ± 2 %) to week 2 (11.2 ± 2.8 %). The AUC analysis of this showed a significant decrease ($t_{(3.649)}$, $p = 0.0029$) from 554 ± 24 % change/min (n = 4 sensors in 4 animals, Week 1) to 290 ± 82 % change/min (n = 2 sensors in 2 animals, Week 2). While this significant decrease is not ideal it is not uncommon as biosensors generally suffer from varying degrees of biofouling over time (Wisniewski and Reichert, 2000). Significant decreases (40 – 50 %) have also been observed following implantation for similar biosensors (Finnerty *et al.*, 2012; Baker *et al.*, 2019; Ganesana *et al.*, 2019). This stability study showed that the pyruvate biosensor is capable of detecting relative pyruvate changes for at least 2 weeks, and most likely longer.

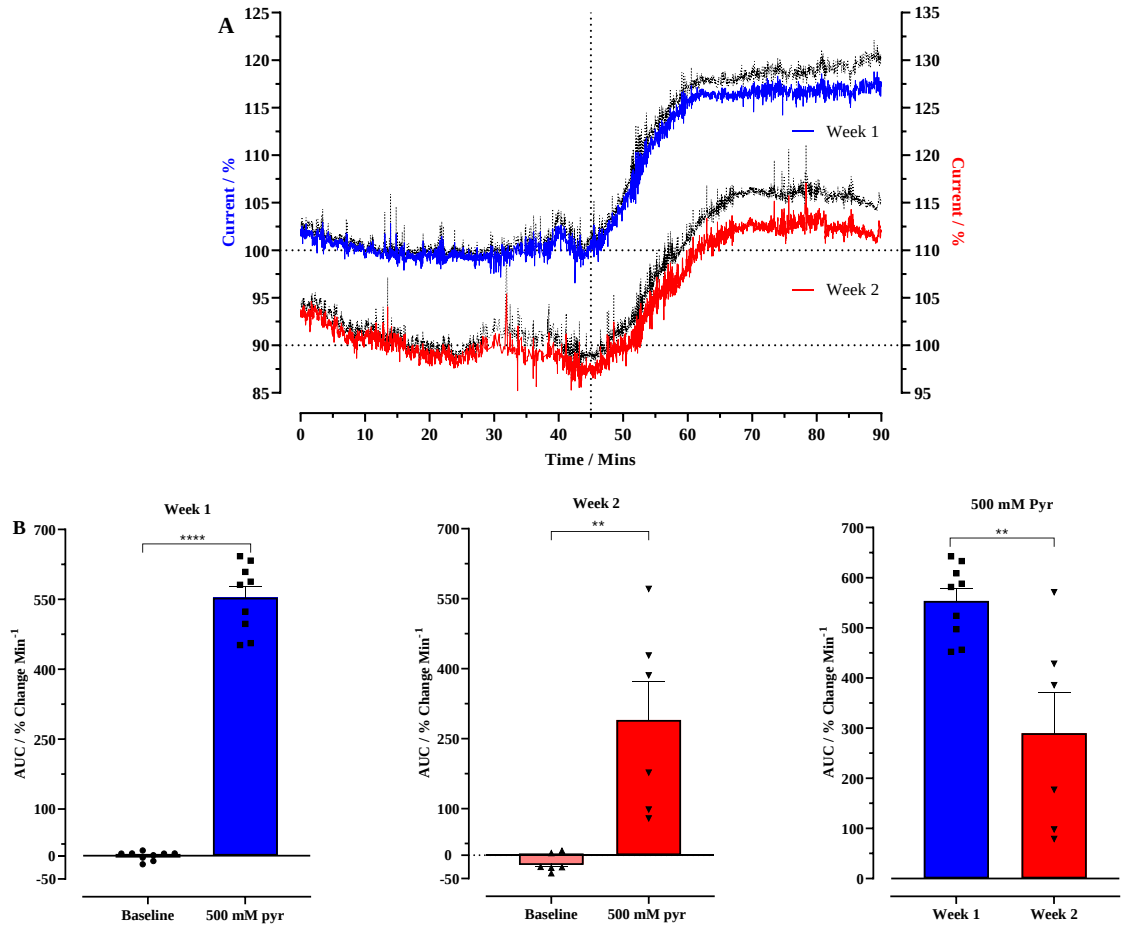

Figure 6.10: (A) The effect of a perfusion of 500 mM pyruvate through a microdialysis probe on the current recorded at the adjacent pyruvate biosensor on week 1 (blue, n = 4 sensors in 4 animals) *vs* week 2 (red, n = 2 sensors in 2 animals). The horizontal dashed lines represent the aCSF baseline (0.76 ± 0.09 nA, n = 11 week 1, 1.4 ± 0.2 nA, n = 7 week 2) while the vertical dashed line represents the start point of the perfusion. Error (black) on all data points represents S.E.M. (B) AUC analysis for baseline aCSF and 500 mM pyruvate for week 1 (left), week 2 (middle) and pyruvate response week 1 *vs.* week 2 (right). ****p < 0.0001, **p = 0.0039, **p = 0.0029, t-test. CPA was carried out at +700 mV *vs.* SCE.

6.4 Conclusion

In conclusion, this chapter has detailed the *in-vivo* characterisation carried out to determine the viability of using the developed pyruvate biosensor to reliably detect pyruvate in the *in-vivo* environment. Initial experiments were performed in order to establish if any cross-talk interference was present. Pyruvate biosensors and composite blanks were implanted both bi-laterally and uni-laterally and stable 24 hr baseline recordings were obtained. Correlation analysis was carried out and it was found that regardless of implantation method cross-talk interference was negligible on the composite blank electrode. Following this, the characteristics of basal pyruvate levels as well as what changes occur with sleep/wake cycles were examined. The data showed that there was a decrease in pyruvate during the sleep phase and an increase during the wake phase where the animal was typically more active and thus had higher energy expenditure which compared favourably with to various reports in the literature. This circadian pattern was stable over a 60 hr period.

Following the determination of basal pyruvate changes control experiments were then carried out. Initially injection stress was examined by the administration of a 1 mL saline injection (NaCl 0.9 %, i.p.). Saline was the vehicle of choice for all i.p injections and as a result the effect of this vehicle on the pyruvate response had to be examined. It was found that there was a negligible change in the pyruvate response. The i.p. administration of chloral hydrate (350 mg/kg) was preformed to determine the oxygen dependence of the biosensor. A non-significant decrease ($t_{(0.23)}$, $p = 0.8261$) was observed in the differential signal (pyruvate – blank) response at the peak oxygen response. This slight decrease could be attributed to the anaesthetic effect and the previously mentioned decrease in pyruvate during sleep cycles. These results determined that the biosensor was sufficiently oxygen independent. The i.p. administration of sodium ascorbate (0.5 g/kg) was then carried out to determine the effect of interferents on the biosensor. No observable change was seen in the differential signal (pyruvate – blank) response. This demonstrated that AA did not affect the pyruvate current observed at the pyruvate biosensor and the integrity of the PPD layer was maintained.

Local perfusions experiments were then carried out using a guide cannula and microdialysis probe to determine if the pyruvate biosensor was capable of detecting exogenously administered pyruvate. These experiments were carried out from an aCSF baseline and showed

an increase in current of approximately 15 % from the aCSF baseline for a 500 mM pyruvate perfusion indicating the biosensor is capable of detecting increases in pyruvate concentration. Finally local perfusion experiments were again utilised to determine the stability of the biosensor over a 2 week period. The results showed that the biosensor was still reliably detecting an increase in pyruvate concentration on week 2, indicating the biosensor is suitable for monitoring relative changes in pyruvate concentration for at least 2 weeks and possibly longer.

This chapter has demonstrated that the pyruvate biosensor is viable for application in the *in-vivo* environment. It has been shown to be capable of detecting basal changes in pyruvate associated with sleep/wake cycles. It is sufficiently independent of changes in oxygen levels. The integrity of the PPD layer has been maintained and the biosensor is not affected by interferants. It is capable of detecting exogenous pyruvate through microdialysis and is stable for at least 2 weeks.

6.5 References

Baker, K.L., Bolger, F.B., Doran, M.M. and Lowry, J.P. (2019) 'Characterisation of a Platinum-based Electrochemical Biosensor for Real-time Neurochemical Analysis of Choline', *Electroanalysis*, 31(1), pp. 129–136. doi:10.1002/elan.201800642.

Baker, K.L., Bolger, F.B. and Lowry, J.P. (2015) 'A microelectrochemical biosensor for real-time in vivo monitoring of brain extracellular choline', *Analyst*, 140(11), pp. 3738–3745. doi:10.1039/c4an02027h.

Baker, K.L., Bolger, F.B. and Lowry, J.P. (2017) 'Development of a microelectrochemical biosensor for the real-time detection of choline', *Sensors and Actuators, B: Chemical*, 243, pp. 412–420. doi:10.1016/j.snb.2016.11.110.

Bergmann, W., Rudolph, R. and Spohn, U. (1999) 'A bienzyme modified carbon paste electrode for amperometric detection of pyruvate', *Analytica Chimica Acta*, 394(2–3), pp. 233–241. doi:10.1016/S0003-2670(99)00296-2.

Bourdon, A.K., Spano, G.M., Marshall, W., Bellesi, M., Tononi, G., Serra, P.A., Baghdoyan, H.A., Lydic, R., Campagna, S.R. and Cirelli, C. (2018) 'Metabolomic analysis of mouse prefrontal cortex reveals upregulated analytes during wakefulness compared to sleep', *Scientific Reports*, 8(1). doi:10.1038/s41598-018-29511-6.

Braun, A.R., Balkin, T.J., Wesensten, N.J., Carson, R.E., Varga, M., Baldwin, P., Selbie, S., Belenky, G. and Herscovitch, P. (1997) 'Regional cerebral blood flow throughout the sleep-wake cycle. An H215O PET study', *Brain*, 120(7), pp. 1173–1197. doi:10.1093/brain/120.7.1173.

Cordeiro, C.A., de Vries, M.G., Ngabi, W., Oomen, P.E., Cremers, T.I.F.H. and Westerink, B.H.C. (2015) 'In vivo continuous and simultaneous monitoring of brain energy substrates with a multiplex amperometric enzyme-based biosensor device', *Biosensors and Bioelectronics*, 67, pp. 677–686. doi:10.1016/j.bios.2014.09.101.

Erhorn, S. (2007) 'Chloral hydrate', in Enna, S.J. and Bylund, D.B.B.T.T.C.P.R. (eds) *xPharm: The Comprehensive Pharmacology Reference*. New York: Elsevier, pp. 1–5. doi:10.1016/B978-008055232-3.61437-0.

Finnerty, N.J., Bolger, F.B., Paišlsson, E. and Lowry, J.P. (2013) 'An investigation of hypofrontality in an animal model of schizophrenia using real-time microelectrochemical sensors for glucose, oxygen, and nitric oxide', *ACS Chemical Neuroscience*, 4(5), pp. 825–831. doi:10.1021/cn4000567.

Finnerty, N.J., O'Riordan, S.L., Brown, F.O., Serra, P.A., O'Neill, R.D. and Lowry, J.P. (2012) 'In vivo characterisation of a Nafion ®-modified Pt electrode for real-time nitric oxide monitoring in brain extracellular fluid', *Analytical Methods*, 4(2), pp. 550–557. doi:10.1039/c2ay05924j.

Freiman, S. V., Onufriev, M. V., Stepanichev, M.Y., Moiseeva, Y. V., Lazareva, N.A. and Gulyaeva, N. V. (2016) 'The stress effects of a single injection of isotonic saline solution: systemic (blood) and central (frontal cortex and dorsal and ventral hippocampus)', *Neurochemical Journal*, 10(2), pp. 115–119. doi:10.1134/S1819712416020033.

Gajovic, N., Habermüller, K., Warsinke, A., Schuhmann, W. and Scheller, F.W. (1999) *A pyruvate oxidase electrode based on an electrochemically deposited redox polymer*, *Electroanalysis*. doi:10.1002/(SICI)1521-4109(199912)11:18<1377::AID-ELAN1377>3.0.CO;2-B.

Ganesana, M., Trikantzopoulos, E., Maniar, Y., Lee, S.T. and Venton, B.J. (2019) 'Development of a novel micro biosensor for in vivo monitoring of glutamate release in the brain', *Biosensors and Bioelectronics*, 130, pp. 103–109. doi:https://doi.org/10.1016/j.bios.2019.01.049.

Gowers, S.A.N., Rogers, M.L., Booth, M.A., Leong, C.L., Samper, I.C., Phairatana, T., Jewell, S.L., Pahl, C., Strong, A.J. and Boutelle, M.G. (2019) 'Clinical translation of microfluidic sensor devices: focus on calibration and analytical robustness', *Lab Chip*, 19(15), pp. 2537–2548. doi:10.1039/C9LC00400A.

Grünewald, R.A. (1993) 'Ascorbic acid in the brain', *Brain Research Reviews*. Elsevier, pp. 123–133. doi:10.1016/0165-0173(93)90010-W.

Hamdan, S.K. and Mohd Zain, A. (2014) 'In vivo Electrochemical Biosensor for Brain Glutamate Detection: A Mini Review', *The Malaysian journal of medical sciences : MJMS*, 21(Spec Issue), pp. 12–26. Available at: https://pubmed.ncbi.nlm.nih.gov/25941459.

Hoyer, S. (1992) 'Oxidative energy metabolism in Alzheimer brain - Studies in early-onset and late-onset cases', *Molecular and Chemical Neuropathology*, 16(3), pp. 207–224. doi:10.1007/BF03159971.

Huynh, G.H., Ozawa, T., Deen, D.F., Tihan, T. and Szoka, F.C. (2007) 'Retro-convection enhanced delivery to increase blood to brain transfer of macromolecules', *Brain Research*, 1128(1), pp. 181–190. doi:10.1016/j.brainres.2006.10.041.

Kalinchuk, A. V., Urrila, A.S., Alanko, L., Heiskanen, S., Wigren, H.K., Suomela, M., Stenberg, D. and Porkka-Heiskanen, T. (2003) 'Local energy depletion in the basal forebrain increases sleep', *European Journal of Neuroscience*, 17(4), pp. 863–869. doi:10.1046/j.1460-9568.2003.02532.x.

Kawamoto, T., Hobara, T., Kobayashi, H., Iwamoto, S., Sakai, T., Takano, T. and Miyazaki, Y. (1987) 'The Metabolite Ratio as a Function of Chloral Hydrate Dose and Intracellular Redox State in the Perfused Rat Liver', *Pharmacology & Toxicology*, 60(5), pp. 325–329. doi:10.1111/j.1600-0773.1987.tb01519.x.

Kennedy, C., Gillin, J.C., Mendelson, W., Suda, S., Miyaoka, M., Ito, M., Nakamura, R.K., Storch, F.I., Peetigrew, K., Mishkin, M. and Sokoloff, L. (1982) 'Local cerebral glucose utilization in non-rapid eye movement sleep', *Nature*, 297(5864), pp. 325–327. doi:10.1038/297325a0.

Khan, A.S. and Michael, A.C. (2003) 'Invasive consequences of using micro-electrodes and microdialysis probes in the brain', *TrAC - Trends in Analytical Chemistry*, 22(8), pp. 503–508. doi:10.1016/S0165-9936(03)00908-7.

Lowry, J.P. and Fillenz, M. (2001) 'Real-time monitoring of brain energy metabolism in vivo using microelectrochemical sensors: The effects of anesthesia', *Bioelectrochemistry*, 54(1), pp. 39–47. doi:10.1016/S1567-5394(01)00109-8.

Lowry, J.P., O'Neill, R.D., Boutelle, M.G. and Fillenz, M. (1998) 'Continuous monitoring of extracellular glucose concentrations in the striatum of freely moving rats with an implanted glucose biosensor', *Journal of Neurochemistry*, 70(1), pp. 391–396. doi:10.1046/j.1471-4159.1998.70010391.x.

Malik, M., Chaudhary, R. and Pundir, C.S. (2019) 'An improved enzyme nanoparticles based amperometric pyruvate biosensor for detection of pyruvate in serum', *Enzyme and Microbial Technology*, 123, pp. 30–38. doi:10.1016/j.enzmictec.2019.01.006.

Miele, M. and Fillenz, M. (1996) 'In vivo determination of extracellular brain ascorbate', *Journal of Neuroscience Methods*, 70(1), pp. 15–19. doi:10.1016/S0165-0270(96)00094-5.

Morais, J.M., Papadimitrakopoulos, F. and Burgess, D.J. (2010) 'Biomaterials/tissue interactions: Possible solutions to overcome foreign body response', *AAPS Journal*, 12(2), pp. 188–196. doi:10.1208/s12248-010-9175-3.

Van den Noort, S. and Brine, K. (1970) 'Effect of sleep on brain labile phosphates and metabolic rate.', *The American journal of physiology*, 218(5), pp. 1434–1439. doi:10.1152/ajplegacy.1970.218.5.1434.

O'Neill, R.D. (1993) 'Sensor-tissue interactions in neurochemical analysis with carbon paste electrodes in vivo', *The Analyst*, 4(118), pp. 433–438. doi:10.1039/AN9931800433.

Palmisano, F., Rizzi, R., Centonze, D. and Zambonin, P.G. (2000) 'Simultaneous monitoring of glucose and lactate by an interference and cross-talk free dual electrode amperometric biosensor based on electropolymerized thin films', *Biosensors and Bioelectronics*, 15(9–10), pp. 531–539. doi:10.1016/S0956-5663(00)00107-X.

Parnetti, L., Gaiti, A., Polidori, M.C., Brunetti, M., Palumbo, B., Chionne, F., Cadini, D., Cecchetti, R. and Senin, U. (1995) 'Increased cerebrospinal fluid pyruvate levels in Alzheimer's disease', *Neuroscience Letters*, 199(3), pp. 231–233. doi:10.1016/0304-3940(95)12058-C.

Petrou, P.S., Moser, I. and Jobst, G. (2003) 'Microdevice with integrated dialysis probe and biosensor array for continuous multi-analyte monitoring', *Biosensors and Bioelectronics*, 18(5), pp. 613–619. doi:https://doi.org/10.1016/S0956-5663(03)00038-1.

Polikov, V.S., Tresco, P.A. and Reichert, W.M. (2005) 'Response of brain tissue to chronically implanted neural electrodes', *Journal of Neuroscience Methods*, 148(1), pp. 1–18. doi:10.1016/j.jneumeth.2005.08.015.

Rahman, M.A., Park, D.S., Chang, S.C., McNeil, C.J. and Shim, Y.B. (2006) 'The biosensor

based on the pyruvate oxidase modified conducting polymer for phosphate ions determinations', *Biosensors and Bioelectronics*. 2005/05/17, 21(7), pp. 1116–1124. doi:10.1016/j.bios.2005.04.008.

Reich, P., Geyer, S.J. and Karnovsky, M.L. (1972) 'Metabolism of Brain During Sleep and Wakefulness', *Journal of Neurochemistry*, 19(2), pp. 487–497. doi:10.1111/j.1471-4159.1972.tb01358.x.

Reinstrup, P., Ståhl, N., Mellergård, P., Uski, T., Ungerstedt, U. and Nordström, C.H. (2000) 'Intracerebral microdialysis in clinical practice: Baseline values for chemical markers during wakefulness, anesthesia, and neurosurgery', *Neurosurgery*, 47(3), pp. 701–710. doi:10.1227/00006123-200009000-00035.

Revzin, A.F., Sirkar, K., Simonian, A. and Pishko, M. V. (2002) 'Glucose, lactate, and pyruvate biosensor arrays based on redox polymer/oxidoreductase nanocomposite thin-films deposited on photolithographically patterned gold microelectrodes', *Sensors and Actuators, B: Chemical*, 81(2–3), pp. 359–368. doi:10.1016/S0925-4005(01)00982-0.

Rex Sheu, K. -F, Kim, Y. -T, Blass, J.P. and Weksler, M.E. (1985) 'An immunochemical study of the pyruvate dehydrogenase deficit in Alzheimer's disease brain', *Annals of Neurology*, 17(5), pp. 444–449. doi:10.1002/ana.410170505.

Samson, H.H., Hodge, C.W., Erickson, H.L., Niehus, J.S., Gerhardt, G.A., Kalivas, P.W. and Floyd, E.A. (1997) 'The effects of local application of ethanol in the n. accumbens on dopamine overflow and clearance', *Alcohol*, 14(5), pp. 485–492. doi:10.1016/S0741-8329(96)00216-9.

Schulz, M.K., Wang, L.P., Tange, M. and Bjerre, P. (2000) 'Cerebral microdialysis monitoring: Determination of normal and ischemic cerebral metabolisms in patients with aneurysmal subarachnoid hemorrhage', *Journal of Neurosurgery*, 93(5), pp. 808–814. doi:10.3171/jns.2000.93.5.0808.

Skjøth-Rasmussen, J., Schulz, M., Kristensen, S.R. and Bjerre, P. (2004) 'Delayed neurological deficits detected by an ischemic pattern in the extracellular cerebral metabolites in patients with aneurysmal subarachnoid hemorrhage', *Journal of Neurosurgery*, 100(1), pp. 8–15. doi:10.3171/jns.2004.100.1.0008.

Tao, R. and Auerbach, S.B. (1994) 'Anesthetics block morphine-induced increases in serotonin release in rat CNS', *Synapse*, 18(4), pp. 307–314. doi:10.1002/syn.890180406.

Teles-Grilo Ruivo, L.M., Baker, K.L., Conway, M.W., Kinsley, P.J., Gilmour, G., Phillips, K.G., Isaac, J.T.R., Lowry, J.P. and Mellor, J.R. (2017) 'Coordinated Acetylcholine Release in Prefrontal Cortex and Hippocampus Is Associated with Arousal and Reward on Distinct Timescales', *Cell Reports*, 18(4), pp. 905–917. doi:https://doi.org/10.1016/j.celrep.2016.12.085.

Vannucci, S.J., Maher, F. and Simpson, I.A. (1997) 'Glucose transporter proteins in brain: Delivery of glucose to neurons and glia', *Glia*, 21(1), pp. 2–21. doi:10.1002/(SICI)1098-1136(199709)21:1<2::AID-GLIA2>3.0.CO;2-C.

Wilson, G.S. and Gifford, R. (2005) 'Biosensors for real-time in vivo measurements', *Biosensors and Bioelectronics*, 20(12), pp. 2388–2403. doi:10.1016/j.bios.2004.12.003.

Wisniewski, N. and Reichert, M. (2000) 'Methods for reducing biosensor membrane biofouling', *Colloids and Surfaces B: Biointerfaces*, 18(3–4), pp. 197–219. doi:10.1016/S0927-7765(99)00148-4.

Yao, T. and Yano, T. (2004) 'On-line microdialysis assay of L-lactate and pyruvate in vitro and in vivo by a flow-injection system with a dual enzyme electrode', *Talanta*, 63(3), pp. 771–775. doi:10.1016/j.talanta.2003.11.033.

Zetterling, M., Hillered, L., Samuelsson, C., Karlsson, T., Enblad, P. and Ronne-Engström, E. (2009) 'Temporal patterns of interstitial pyruvate and amino acids after subarachnoid haemorrhage are related to the level of consciousness-a clinical microdialysis study', *Acta Neurochirurgica*, 151(7), pp. 771–780. doi:10.1007/s00701-009-0384-4.

Chapter 7: Conclusions and Future Work

7.1 General Conclusion

The brain is the most complex organ in the human body, it is responsible for a wide array of functions including sensory input and processing, behavioural response, memory and emotion. Therefore, extensive work has been carried out to determine the structure, metabolism and the role of neurochemical transmitters in the brain. A number of different techniques have been employed to do this. They include non-invasive techniques such as magnetoencephalography (MEG) (Cohen, 1972), functional magnetic resonance imaging (fMRI) (Glover, 2011), electroencephalography (EEG) (İnce, Adanır and Sevmez, 2020), and positron emission tomography (PET) (Wagner, 1998). As well as this there has been surgically invasive techniques such as microdialysis (MD) (Reinstrup *et al.*, 2000) and Long Term *In-vivo* Electrochemistry (LIVE) (O'Neill and Lowry, 2000). LIVE allows for *in-situ* detection of substances in the extracellular fluid (ECF). This technique involves the implantation of electrodes into specific brain regions , application of a suitable potential and recording of the resulting Faradaic current which monitors the changes in the concentration of a variety of substances in the ECF. This is done with high temporal resolution over extended time periods. This allows for precise monitoring of a multitude of analytes involved in neuronal signals, drug actions and behaviours.

Several neurochemicals have been detected using LIVE including oxygen (O_2) (Bolger and Lowry, 2005), nitric oxide (NO) (Brown, Finnerty and Lowry, 2009) and ascorbic acid (AA) (Ormonde and O'Neill, 1990). However, for analytes that are electroactive a biosensor must be used. This is defined as a self-contained integrated device which incorporates a biological recognition element in close proximity to the electrochemical transducer (Wilson and Gifford, 2005). Biosensors have allowed for the detection of a number of electroinactive species that are of great interest such as glucose (Panjan, Virtanen and Sesay, 2017), lactate (Cordeiro *et al.*, 2015), choline (Baker *et al.*, 2019) and glutamate (Chatard, Meiller and Marinesco, 2018). Unfortunately, the electroactive species present in the ECF tend to oxidise at similar potentials to the target analytes which can lead to selectivity problems for biosensors. To prevent this interference permselective membranes, such as polyphenylenediamine (PPD) and overoxidized polypyrrole (PPYox), have been utilised in biosensor development to great effect (Palmisano *et al.*, 2000; Dixon, Lowry and O'Neill, 2002; Baker *et al.*, 2019). Additionally,

the use of this technique in the intact brain poses specific challenges, as brain tissue demonstrates restricted mass transport in comparison with the *in-vitro* environment (O'Neill, 1993) and decrease in biosensor sensitivity as a result of fouling (Garguilo and Michael, 1995). The aim of this thesis was to develop and characterise a pyruvate biosensor. The detection of pyruvate in the *in-vitro* environment, with appropriate sensitivity and selectivity, was verified followed by an *in-vivo* characterisation study.

Electrochemical biosensors for the detection of pyruvate have been previously developed by various research groups. However, these have generally suffered from a variety of issues which rendered them unsuitable for use *in-vivo*. A glucose, lactate and pyruvate sensor array was developed by Revzin *et al.* in 2002. This was done by depositing electrostatically complexed monolayers on lithographically patterned, individually addressable, gold microelectrodes. The biosensors sensitivity towards pyruvate was given as 0.13 nA. μM^{-1}. cm^{-2} and no interference study was conducted (Revzin *et al.*, 2002). Mizutani *et al.* utilised a 1.6 mm gold disc electrode (GDE) and the pyruvate oxidase was immobilised on a polyion complex membrane. The biosensor had a high sensitivity of 51.7 nA. μM^{-1}. cm^{-2} , but unfortunately responded to interferants AA, uric acid (UA), L-cystine and acetaminophen (AAP) (Mizutani *et al.*, 2000). Knyzhnykova *et al*. developed a pyruvate oxidase-based biosensor in 2018 using a 3.5 mm diameter glass capillary electrode with a 0.5 mm diameter platinum active surface. Again, this biosensor displayed a high degree of sensitivity, given as 15.8 nA. μM^{-1}. cm^{-2}, and there was no response to any interferants (Knyzhnykova *et al.*, 2018). It can be seen that these biosensors suffer from either sensitivity, selectivity or size issues rendering them unsuitable for neurochemical monitoring. The research carried out by Cordeiro *et al.* in 2015 produced an implantable multiplex micro-biosensor for simultaneous detection of glucose lactate and pyruvate. The pyruvate biosensor in the multiplex system was fabricated using a 1 mm length, 0.2 mm diameter platinum cylinder, it had a pre-implantation sensitivity of 25.9 nA. μM^{-1}. cm^{-2} and there was no response to any interferants (Cordeiro *et al.*, 2015). This research showed that it was possible to develop and deploy a pyruvate biosensor in the *in-vivo* environment. However, this was only a preliminary study in anesthetised animals focused on the development of a multiplex biosensor. The main technique typically used to monitor pyruvate *in-vivo* has been MD with multiple research groups quantifying pyruvate in the ECF as recently as 2019 (Reinstrup *et al.*, 2000; Schulz *et al.*, 2000; Yao, Yano and Nishino, 2004; Gowers *et*

al., 2019). However, MD suffers from a relatively large probe size and poor temporal resolution, both of which can be overcome using a biosensor.

This thesis details the development and characterisation of a new pyruvate biosensor in the *in-vitro* environment followed by the *in-vivo* characterisation of the biosensor in the *in-vivo* environment. Chapter 4 details the work undertaken in order to optimise the sensitivity of the biosensor towards pyruvate. Initially the reliance of pyruvate oxidase on external co-factors in the bulk solution was examined. It was seen that with increasing flavin adenine dinucleotide (FAD) concentration in the enzyme solution to 80 µM resulted in a significant increase in the current response to aliquots of pyruvate. While no significant difference was seen for the same design when FAD was removed from the bulk solution. Thiamine pyrophosphate (TPP) was removed from the bulk solution and no significant change was seen in the response. Following the removal of the reliance on the co-factors in the bulk solution the focus was shifted to the optimisation of the design through choosing an immobiliser, optimising the number of layers, optimising the unit activity in the enzyme solution and the introduction of cross-linkers and stabilisers. The immobilisation matrix utilised was styrene while the optimum number of layers was deemed to be 15 and the unit activity of the enzyme that produced the highest sensitivity was 800 U/mL. Glutaraldehyde (GA), a well-known cross-linker was incorporated into the design which yielded an increase in all kinetic parameters. This was further increased by the introduction of bovine serum albumin (BSA) which provided stability through decreasing direct enzyme cross-linking by the GA. Finally, PEI was introduced which decreased inter-electrode variability. These three components were extensively characterised in terms of concentration and position in the design in order to maximise pyruvate detection. The best design was found to be Pt/Ir (disc) – {Sty – [POx (800 U/mL) + FAD (80 µM)] $_{15}$ + BSA (1 %) + GA (0.25 %) + PEI (2 %)}. It had a sensitivity of 7.16 ± 0.12 ρA/µM (current density of 58.4 ± 1 nA.µM^{-1}.cm$^{-2)}$.The V_{max} and K_m were 24.4 ± 0.5 nA and 1.7 ± 0.1 mM (n = 9) respectively.

Chapter 5 focused on the *in-vitro* characterisation of the biosensor to determine its viability for use in the *in-vivo* environment. The biosensor was examined under the following criteria: temperature, pH, O_2 dependence, shelf-life, stability, interference rejection, limit of detection (LOD) and response time. The initial examination of the biosensors thermal stability yielded poor results due to the thermal denaturation of the enzyme above 30 ^{o}C. To combat this issue

200 mM of sucrose was introduced to the enzyme solution as well as increasing the number of layers of BSA, GA and PEI to 15, as BSA is known to increase thermal stability. This new design was Pt/Ir (disc) – {Sty – ([POx (800 U/mL) + FAD (80 µM) + Sucrose (200 mM)] + BSA (1 %) + GA (0.25 %) + PEI (2 %))$_{15}$} and retained a high sensitivity of 8.24 ± 0.15 (n = 8) at 37 ^{o}C. A pH study was then carried out and it found that increasing pH resulted in a decrease in pyruvate sensitivity but due to the highly regulated nature of pH in the brain it was felt that minimal disruption would be seen. The O_2 dependence of the biosensor was then tested and it was found that it was sufficiently O_2 independent over the physiological range. Shelf-life and stability studies were then carried out with storage at – 20 ^{o}C over a two week period and it was found there was no significant change in sensitivity for the shelf-life study. However, there was a decrease in sensitivity for the stability study. The response on Day 14 of 5.25 ± 0.11 ρA/µM (n = 8) was still relatively large and the decrease seen is most likely due to loss of enzyme activity previously seen with other published sensors (Saurina *et al.*, 1998; Baker *et al.*, 2019). Interferants were successfully eliminated with the introduction of the size exclusion polymer poly-*o*-phenylenediamine (PPD). This layer was electropolymerised onto the working electrode at least 4 hrs prior to any modifications. PPD blocks access of the larger interferents such as AA while smaller molecules such as H_2O_2 can still permeate the layer (O'Neill *et al.*, 2008). With the inclusion of the PPD layer there was no change to the pyruvate response, while there was only a 5 % relative change in current for AA and a 1 % change for L-cystine the rest of the interferants caused negligible changes indicating the biosensor was highly selective to pyruvate. Finally, the LOD was determined to be 0.33 ± 0.172 µM and the response time was deemed to be *ca.* 10 s but was within the mixing time which indicates a potential sub-second response *in-vivo*.

Finally, in Chapter 6 the characterisation of the presented pyruvate biosensor was undertaken in the *in-vivo* environment in the striatum of a freely moving male Wistar rat. Initial experiments were conducted to determine if the composite blank suffered from cross-talk interference from the pyruvate biosensor. Correlation analysis was conducted for the changes in normalised pyruvate currents with respect to the changes in normalised composite blank currents for bi-lateral implantation. The correlation coefficient (0.07389) indicated that cross-talk interference was negligible on the composite blank electrode. The next step was to determine the basal fluctuations in pyruvate associated with sleep/wake cycles. It was seen that

there was an increase in pyruvate during the wake phase and a decrease in pyruvate during the sleep phase which corresponds with what is reported in the literature (Van den Noort and Brine, 1970; Bourdon *et al.*, 2018). From the baseline data an estimate of the ECF concentration of pyruvate was made (197 ± 18 µM). After establishing basal changes, the *in-vivo* characterisation was carried out. Chloral hydrate (350 mg/kg) was administered via an intraperitoneal (i.p) injection to increase basal O_2 levels and determine the O_2 dependence of the biosensor. The differential signal (pyruvate – blank) response showed a non-significant ($t_{(0.04)}$, p = 0.9643) decrease from the pre-injection baseline at the peak O_2 response with the slight decrease possibly attributed to the aesthetic effect, as previously stated pyruvate decreases during periods of sleep. The integrity of the PPD layer was then examined by the administration of sodium ascorbate (0.5 g/kg, i.p). This caused an increase in AA in the brain but no change was seen in the differential signal (pyruvate – blank) indicating the biosensor was highly selective towards pyruvate in the *in-vivo* environment. The next step was to determine if the biosensor was capable of responding to perfusions of pyruvate through a MD probe adjacent to the biosensor. This was achieved by establishing an artificial cerebrospinal fluid (aCSF) baseline and then perfusing 500 mM pyruvate. There was an observed increase in current of 11.3 ± 1.1 % from the aCSF baseline and this peak was reached after *ca.* 20 mins. This demonstrates that the biosensor is capable of detecting pyruvate changes in the local environment. The final step of the characterisation process was to examine the stability of the biosensor over a 2-week period. This was again done via local perfusions through a MD probe. It was found that there was an increase in current of 16.1 ± 2 % from the aCSF baseline for week 1 while there was an observed increase of 11.2 ± 2.8 % in current for week 2. This indicates that the biosensor is capable of detecting relative changes in pyruvate for up to 2 weeks. The 5 % decrease from week 1 to week 2 was significant but not unexpected as biosensors generally suffer from a loss of sensitivity over time due to varying degrees of biofouling (Wisniewski and Reichert, 2000).

Progression of this body of work will include further characterisation work investigating brain hyperthermia by the use of methamphetamine (Brown, Wise and Kiyatkin, 2003) and 3,4-methylenedioxymethamphetamine (MDMA) (Brown and Kiyatkin, 2004) with an implanted thermocouple. Zero-net-flux (ZNF) has previously been used to estimate the ECF concentration of glucose (Lowry *et al.*, 1998) and this technique will be utilised to verify the

ECF concentration of pyruvate. Investigations into the role of pyruvate in brain energy metabolism will also be explored. Various inhibitors will be used to disrupt the normal function of pyruvate in the brain, three have been identified for use in the future. Dichloroacetate (DCA) which prevents the phosphorylation of the pyruvate dehydrogenase complex (PDHC) by inhibiting the action of pyruvate dehydrogenase kinase thus lowering the pyruvate concentration (Colohan *et al.*, 1986). Malonate and Oxamate are both lactate dehydrogenase isoenzyme inhibitors which prevent the synthesis of lactate from pyruvate (Koeppen and Riley, 1987; Miskimins *et al.*, 2014). This may result in an increase in pyruvate and a subsequent decrease in lactate and could be used to investigate the astrocyte-neuron-lactate shuttle (ANLS) theory, proposed by Luc Pellerin and Pierre Magistretti in 1994 (Pellerin and Magistretti, 1994). The ANLS theory hypothesised that upon neuronal activation by glutamate, astrocytes take up glutamate that was presynaptically released through Na^+ dependent glutamate transporters. This results in an increase in intracellular astrocytic Na^+ which induces Na-K-ATPase activity to pump out the extra Na^+. The pumping activity increases the demand for ATP which leads to the uptake of glucose into the astrocyte which undergoes glycolysis and thus produces lactate. The lactate is then transported via monocarboxylate transporters (MCT) into the extracellular space where it is taken up by neighbouring neurons and oxidised in the mitochondria (Schurr, 2006). A better understanding of pyruvate in ANLS/metabolism may help in better understanding the pathology of major neurodegenerative disorders associated with abnormalities in pyruvate metabolism (see Chapter 2, Section 2.6.1). There is also scope for incorporating the biosensor into a multiplex system along with a previously developed O_2 sensor as well as glucose and lactate biosensors developed by the research group to establish a more complete picture of brain energy metabolism in the freely moving animal model.

7.2 References

Baker, K.L., Bolger, F.B., Doran, M.M. and Lowry, J.P. (2019) 'Characterisation of a Platinum-based Electrochemical Biosensor for Real-time Neurochemical Analysis of Choline', *Electroanalysis*, 31(1), pp. 129–136. doi:10.1002/elan.201800642.

Bolger, F. and Lowry, J. (2005) 'Brain Tissue Oxygen: In Vivo Monitoring with Carbon Paste Electrodes', *Sensors*, 5(11), pp. 473–487. doi:10.3390/s5110473.

Bourdon, A.K., Spano, G.M., Marshall, W., Bellesi, M., Tononi, G., Serra, P.A., Baghdoyan, H.A., Lydic, R., Campagna, S.R. and Cirelli, C. (2018) 'Metabolomic analysis of mouse prefrontal cortex reveals upregulated analytes during wakefulness compared to sleep', *Scientific Reports*, 8(1). doi:10.1038/s41598-018-29511-6.

Brown, F.O., Finnerty, N.J. and Lowry, J.P. (2009) 'Nitric oxide monitoring in brain extracellular fluid: Characterisation of Nafion®-modified Pt electrodes in vitro and in vivo', *Analyst*, 134(10), pp. 2012–2020. doi:10.1039/b909005c.

Brown, P.L. and Kiyatkin, E.A. (2004) 'Brain hyperthermia induced by MDMA (ecstasy): modulation by environmental conditions.', *The European journal of neuroscience*, 20(1), pp. 51–58. doi:10.1111/j.0953-816X.2004.03453.x.

Brown, P.L., Wise, R.A. and Kiyatkin, E.A. (2003) 'Brain Hyperthermia Is Induced by Methamphetamine and Exacerbated by Social Interaction', *Journal of Neuroscience*, 23(9), pp. 3924–3929. doi:10.1523/JNEUROSCI.23-09-03924.2003.

Chatard, C., Meiller, A. and Marinesco, S. (2018) 'Microelectrode Biosensors for in vivo Analysis of Brain Interstitial Fluid', *Electroanalysis*, 30(6), pp. 977–998. doi:10.1002/elan.201700836.

Cohen, D. (1972) 'Magnetoencephalography: Detection of the Brain's Electrical Activity with a Superconducting Magnetometer', *Science*, 175(4022), pp. 664–666. doi:10.1126/science.175.4022.664.

Colohan, A.R., Welsh, F.A., Miller, E.D. and Kassell, N.F. (1986) 'The effect of dichloroacetate on brain lactate levels following incomplete ischemia in the hyperglycemic

rat.', *Stroke*, 17(3), pp. 525–528. doi:10.1161/01.STR.17.3.525.

Cordeiro, C.A., de Vries, M.G., Ngabi, W., Oomen, P.E., Cremers, T.I.F.H. and Westerink, B.H.C. (2015) 'In vivo continuous and simultaneous monitoring of brain energy substrates with a multiplex amperometric enzyme-based biosensor device', *Biosensors and Bioelectronics*, 67, pp. 677–686. doi:10.1016/j.bios.2014.09.101.

Dixon, B.M., Lowry, J.P. and O'Neill, R.D. (2002) 'Characterization in vitro and in vivo of the oxygen dependence of an enzyme/polymer biosensor for monitoring brain glucose', *Journal of Neuroscience Methods*, 119(2), pp. 135–142. doi:10.1016/S0165-0270(02)00170-X.

Garguilo, M.G. and Michael, A.C. (1995) 'Optimization of amperometric microsensors for monitoring choline in the extracellular fluid of brain tissue', *Analytica Chimica Acta*, 307(2), pp. 291–299. doi:https://doi.org/10.1016/0003-2670(94)00558-4.

Glover, G.H. (2011) 'Overview of functional magnetic resonance imaging', *Neurosurgery clinics of North America*, 22(2), pp. 133–vii. doi:10.1016/j.nec.2010.11.001.

Gowers, S.A.N., Rogers, M.L., Booth, M.A., Leong, C.L., Samper, I.C., Phairatana, T., Jewell, S.L., Pahl, C., Strong, A.J. and Boutelle, M.G. (2019) 'Clinical translation of microfluidic sensor devices: focus on calibration and analytical robustness', *Lab Chip*, 19(15), pp. 2537–2548. doi:10.1039/C9LC00400A.

İnce, R., Adanır, S.S. and Sevmez, F. (2020) 'The inventor of electroencephalography (EEG): Hans Berger (1873–1941)', *Child's Nervous System* [Preprint]. doi:10.1007/s00381-020-04564-z.

Knyzhnykova, D. V., Topolnikova, Y. V., Kucherenko, I.S. and Soldatkin, O.O. (2018) 'Development of pyruvate oxidase-based amperometric biosensor for pyruvate determination', *Biopolymers and Cell*, 34(1), pp. 14–23. doi:10.7124/bc.00096C.

Koeppen, A.H. and Riley, K.M. (1987) 'Effect of Free Malonate on the Utilization of Glutamate by Rat Brain Mitochondria', *Journal of Neurochemistry*, 48(5), pp. 1509–1515. doi:https://doi.org/10.1111/j.1471-4159.1987.tb05693.x.

Lowry, J.P., O'Neill, R.D., Boutelle, M.G. and Fillenz, M. (1998) 'Continuous monitoring of

extracellular glucose concentrations in the striatum of freely moving rats with an implanted glucose biosensor', *Journal of Neurochemistry*, 70(1), pp. 391–396. doi:10.1046/j.1471-4159.1998.70010391.x.

Miskimins, W.K., Ahn, H.J., Kim, J.Y., Ryu, S., Jung, Y.-S.Y.-S. and Choi, J.Y. (2014) 'Synergistic Anti-Cancer Effect of Phenformin and Oxamate', *PLOS ONE*, 9(1), p. e85576. doi:10.1371/journal.pone.0085576.

Mizutani, F., Yabuki, S., Sato, Y., Sawaguchi, T. and Iijima, S. (2000) 'Amperometric determination of pyruvate, phosphate and urea using enzyme electrodes based on pyruvate oxidase-containing poly(vinyl alcohol)/polyion complex-bilayer membrane', *Electrochimica Acta*, 45(18), pp. 2945–2952. doi:10.1016/S0013-4686(00)00373-X.

Van den Noort, S. and Brine, K. (1970) 'Effect of sleep on brain labile phosphates and metabolic rate.', *The American journal of physiology*, 218(5), pp. 1434–1439. doi:10.1152/ajplegacy.1970.218.5.1434.

O'Neill, R.D. (1993) 'Sensor-tissue interactions in neurochemical analysis with carbon paste electrodes in vivo', *The Analyst*, 4(118), pp. 433–438. doi:10.1039/AN9931800433.

O'Neill, R.D. and Lowry, J.P. (2000) 'Voltammetry In Vivo for Chemical Analysis of the Living Brain', in *Encyclopedia of Analytical Chemistry*. American Cancer Society. doi:10.1002/9780470027318.a0216.

O'Neill, R.D., Rocchitta, G., McMahon, C.P., Serra, P.A. and Lowry, J.P. (2008) 'Designing sensitive and selective polymer/enzyme composite biosensors for brain monitoring in vivo', *TrAC - Trends in Analytical Chemistry*, 27(1), pp. 78–88. doi:10.1016/j.trac.2007.11.008.

Ormonde, D.E. and O'Neill, R.D. (1990) 'The oxidation of ascorbic acid at carbon paste electrodes. Modified response following contact with surfactant, lipid and brain tissue', *Journal of Electroanalytical Chemistry*, 279(1–2), pp. 109–121. doi:10.1016/0022-0728(90)85170-A.

Palmisano, F., Rizzi, R., Centonze, D. and Zambonin, P.G. (2000) 'Simultaneous monitoring of glucose and lactate by an interference and cross-talk free dual electrode amperometric biosensor based on electropolymerized thin films', *Biosensors and Bioelectronics*, 15(9–10),

pp. 531–539. doi:10.1016/S0956-5663(00)00107-X.

Panjan, P., Virtanen, V. and Sesay, A.M. (2017) 'Determination of stability characteristics for electrochemical biosensors via thermally accelerated ageing', *Talanta*, 170, pp. 331–336. doi:10.1016/j.talanta.2017.04.011.

Reinstrup, P., Ståhl, N., Mellergård, P., Uski, T., Ungerstedt, U. and Nordström, C.H. (2000) 'Intracerebral microdialysis in clinical practice: Baseline values for chemical markers during wakefulness, anesthesia, and neurosurgery', *Neurosurgery*, 47(3), pp. 701–710. doi:10.1227/00006123-200009000-00035.

Revzin, A.F., Sirkar, K., Simonian, A. and Pishko, M. V. (2002) 'Glucose, lactate, and pyruvate biosensor arrays based on redox polymer/oxidoreductase nanocomposite thin-films deposited on photolithographically patterned gold microelectrodes', *Sensors and Actuators, B: Chemical*, 81(2–3), pp. 359–368. doi:10.1016/S0925-4005(01)00982-0.

Saurina, J., Hernández-Cassou, S., Fàbregas, E. and Alegret, S. (1998) 'Potentiometric biosensor for lysine analysis based on a chemically immobilized lysine oxidase membrane', *Analytica Chimica Acta*, 371(1), pp. 49–56. doi:10.1016/S0003-2670(98)00310-9.

Schulz, M.K., Wang, L.P., Tange, M. and Bjerre, P. (2000) 'Cerebral microdialysis monitoring: Determination of normal and ischemic cerebral metabolisms in patients with aneurysmal subarachnoid hemorrhage', *Journal of Neurosurgery*, 93(5), pp. 808–814. doi:10.3171/jns.2000.93.5.0808.

Schurr, A. (2006) 'Lactate: The ultimate cerebral oxidative energy substrate?', *Journal of Cerebral Blood Flow and Metabolism*, 26(1), pp. 142–152. doi:10.1038/sj.jcbfm.9600174.

Wagner, H.N. (1998) 'A brief history of positron emission tomography (PET)', *Seminars in Nuclear Medicine*, 28(3), pp. 213–220. doi:https://doi.org/10.1016/S0001-2998(98)80027-5.

Wilson, G.S. and Gifford, R. (2005) 'Biosensors for real-time in vivo measurements', *Biosensors and Bioelectronics*, 20(12), pp. 2388–2403. doi:10.1016/j.bios.2004.12.003.

Wisniewski, N. and Reichert, M. (2000) 'Methods for reducing biosensor membrane biofouling', *Colloids and Surfaces B: Biointerfaces*, 18(3–4), pp. 197–219. doi:10.1016/S0927-7765(99)00148-4.

Yao, T., Yano, T. and Nishino, H. (2004) ‘Simultaneous in vivo monitoring of glucose, L-lactate, and pyruvate concentrations in rat brain by a flow-injection biosensor system with an on-line microdialysis sampling’, *Analytica Chimica Acta*, 510(1), pp. 53–59. doi:10.1016/j.aca.2003.12.062.